Stem Cell Mediated Retinal Repair:

Models and Mechanisms

Thesis submitted for the degree of

Doctor of Philosophy

Wai Siene Ng

APRIL 2017

SCHOOL OF OPTOMETRY AND VISION SCIENCES
CARDIFF UNIVERSITY

Table of Contents

Acknowledgement

The completion of this thesis would not have been possible without the generous support from a large team of people. Firstly, the overall supervision, careers advice and bench work support from both Prof James Morgan from Cardiff Centre for Vision Sciences and Prof Bing Song from School of Dentistry, has been imperative to this thesis. Essential to the experiments; Dr Katie Binley for the pooled data of RGCs for analysis of Sholl profiles for program manual calibration and explant viability experiment as well as help with TUNEL on retinal explants, Dr Jimmy Tribble for help with MATLAB Sholl profiles, Dr Matthew Edmundson for supplying COS-7 cells, Dr Jia Liu and Dr Qian Liu for help with neural stem cell culture, Dr Bangfu Zhu for help with electrotactic cell chamber setup and time-lapse imaging, Dr Gaofeng Zhang for advice on Boyden chamber setup and Katharina Sauberli for help with Western Blots of BDNF. Furthermore, the administrative support of the School of Vision Sciences and the labs at School of Dentistry was much appreciated. Last but not least, my eternal gratitude is given for the love and support from my mother, husband as well as my friends.

Abbreviations

Age related macular degeneration (AMD)

Area Under Curve (AUC)

Basic Fibroblast Growth Factor(bFGF)

Brain-derived Neurotrophic Factor (BDNF)

Bone marrow derived stem cells (BMDSC)

Bovine Serum Albumin (BSA)

Ciliary Marginal Zone (CMZ)

1,1'-dioctadecyl-3,3,3',3'-tetramethyl-indocarbocyanine perchlorate (DiI)

Days Ex-Vivo (DEV)

Electrical Field (EF)

Electroretinogram (ERG)

Embryonic stem cells (ESC)

Epidermal Growth Factor (EGF)

Forward Migration Index (FMI)

Fibroblast Growth Factor (FGF)

Fetal Bovine Serum (FBS)

Forward Migration Index (FMI)

Glial cell derived neurotrophic growth factor (GDNF)

Inner Limiting Membrane (ILM)

Intraocular Pressure (IOP)

Inner Nuclear Layer (INL)

Inner Plexiform Layer (IPL)

Leber's Congenital Amaurosis (LCA)

Luria-Bertani (LB)

Magnetic nanoparticles (MNP)

Neural Stem Cells (NSC)

Nerve Growth Factor (NGF)

Olfactory Epithelium (OE)

Olfactory Ensheathing Stem Cells (OEC)

Outer Limiting Membrane (OLM)

Oligodendrocyte precursor cells (OPC)

Phosphate buffered saline (PBS)

Paraformaldehyde (PFA)

Retinal Ganglion Cell (RGC)

Royal College of Surgeon (RCS)

Retinal Ganglion Cells (RGC)

Retinal Pigment Epithelium (RPE)

Retinitis Pigmentosa (RP)

Abstract

Aim:

I aimed to investigate methods of delivering neuroprotection to the retina: a) using magnetofection (a non-viral transfection technique) in ocular tissue, b) using stem cells as a vector of neuroprotection delivery and c) harnessing galvanotaxis to direct migration of stem cells into the retina.

Methods:

For the recipient test bed of the experiments in my thesis, I used retinal explants from mice. The viability of retinal explants was determined using retinal ganglion cell health as a read-out in the form of Sholl plots. I also explored magnetofection with oscillation as a non-viral technique for neuroprotection delivery in ocular tissue using cornea and retinal explants. Using the galvanotaxis technique, I explored its use in directing neural stem cells in-vitro with and electrotactic chamber and ex-vivo on the retinal explant in a modified Boyden chamber. Finally, I magnetofected neural stem cells to over-express BDNF and directed their migration into the retina using galvanotaxis.

Results:

The retinal explants had a viability of up to 3 days based on the Sholl plots of retinal ganglion cells. Magnetofection with oscillation transfected cornea endothelium and the retinal ganglion cell layer with GFP in the explant models. It also transfected neural stem cells with BDNF-myc. Directed migration with neural stem cells occurred in the electrotactic chamber as well as in the retinal explant model. In the absence of electric field, no migration into the retina occurred. Neurospheres transfected with BDNF-myc also migrated into the retina when exposed to an electric field.

Conclusion:

Within the period of up to 3 days, retinal explants can be used to investigate neuroprotective therapeutic agents using Sholl plots of retinal ganglion cells. Magnetofection with oscillation is a novel non-viral technique for potentially transfecting the eye in the anterior and posterior segment. Neurospheres can be directed to migrate into the retina using an electric field in the ex-vivo model

CHAPTER 1 INTRODUCTION

Retinal degenerative diseases are often incurable, due to damage or atrophy of the retinal layers. In 2014, the WHO Report estimated 39 million people to be blind and 246 million people to have low vision(RNIB, 2002). The annual total costs for sight loss is in the region of £49 billion a year (RNIB, 2002). It has been suggested that via stem cells, replacement of lost cells, delivery of neuroprotection or correction of gene defects maybe the cure to retinal degenerative diseases.

Survival, controlled differentiation, directed migration and integration with accurate synapse formation in the retina are crucial for a stem cell-based retinal repair. The retina is a complex laminar structure with multiple interconnecting circuits. Transplanted stem cells need to migrate and integrate into this sophisticated structure. Therefore, for successful stem cell based therapy to occur, a focus on optimizing directed migration is a priority. In this thesis, I will attempt to direct magnetofected stem cells using an external electrical field to achieve migration from the inner layer of retina to the outer layer of retina.

The delivery of stem cells allow for neuroprotection of inner and outer retina through neurotrophic growth factors inherent with their properties. However, tachyphylaxis can occur and repetitive administration of neurotrophic growth factors is necessary to sustain this effect. To circumvent this, a controlled delivery of intraocular neurotrophic growth factors is needed. Here, I propose to deliver this by transfected stem cells which over secrete neurotrophic factors.

1.1.1 RETINAL STRUCTURE AND CIRCUITRY

The retina consists of a neural layer and the retinal pigment epithelium making up ten layers (see Figure 1.1). The retinal pigment epithelium consists of a single layer of cells from the margin of the optic nerve to the ora serrata [Snell 1998]. The adjacent ends of the retinal pigment epithelium are bound together by tight junctions called the zonula adherens and zonula occludens. These are essential in maintaining the barrier between the retina and the systemic circulation. The retinal pigment epitheliums' functions also include light absorption, participation in turnover of the outer segments of the photoreceptors, and the formation of rhodopsin and iodopsin by storing and releasing vitamin A.

The neural retina consists of three main groups of neurons: the photoreceptors, the bipolar cell and the retinal ganglion cells. There also other important neurons that modulate their activity: the horizontal cells and the amacrine cells [Snell 1998].

The photoreceptors consist of the rods and the cones. The rods are mainly responsible for vision in dim light where else the cones are adapted to bright light and can resolve fine details and colour vision [Snell 1998]. The density of rods and cones varies in different parts of the retina. The rods are absent at the fovea but increases in numbers towards the periphery. The cones are most dense at the fovea and are lesser in numbers in the periphery.

Bipolar cells have a radial orientation with one or more dendrites passing outward to synapse with the photoreceptor cell terminals and a single axon directed inward to synapse with the retinal ganglion cells and amacrine cells [Snell 1998].

Retinal ganglion cells are situated in the inner layer of the retina and form a single layer. Their dendrites synapse with the axons of bipolar cells and amacrine cells. The retinal ganglion cells have a non-myelinated axon that make a right angled turn when they reach the inner surface of the retina and converge at the exit of the optic nerve at the optic disc [Snell 1998].

Müller cells are supporting cells that have long processes extending through almost the whole thickness of the retina. In the outer surface of the retina a dense-staining line traditionally called the outer limiting membrane is formed by the radial processes of the Müller cells between the photoreceptors. At the vitreous surface the neural retina the Müller cell processes have expanded terminations covered by the basement membrane. This is called the inner limiting membrane [Snell 1998].

The retinal circuitry is generated by two streams of visual information: the main vertical pathway (from the photoreceptors to the bipolar cells and from the bipolar cells to the retinal ganglion cells) and the secondary lateral pathway made of local feedback circuits (from horizontal cells back to the photoreceptors [Kamermans 2001] and from the amacrine cells back to the bipolar cells [Kaneko 1987]). The vertical flow is directly involved in sending signals to the brain and the lateral circuits adjust the gain of the pre-synaptic and post-synaptic cells, optimizing signal transmission.

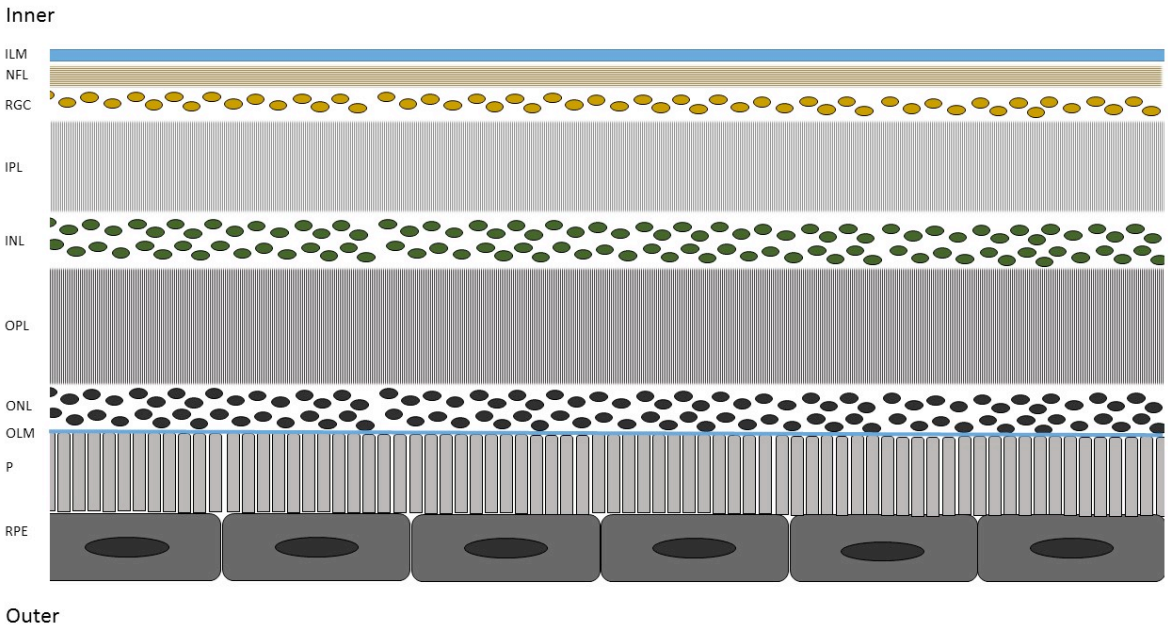

Figure 1.1 Diagram showing the ten layers of the retina: ILM= Inner Limiting Membrane, NFL= Nerve Fibre Layer consists of axons of the retinal ganglion cells that are converging toward the optic disc, RGC= Retinal Ganglion Cell nuclei, IPL= Inner Plexiform Layer consists of the synaptic connections between the bipolar cells, the horizontal cells and the retinal ganglion cells, INL= Inner Nuclear Layer consists of the nuclei of the bipolar cells, the horizontal cells, the amacrine cells and the Müller cells, OPL= Outer Plexiform Layer made of synapses between the terminal synapses of the rod and cone cells, the bipolar cells and the horizontal cells, ONL= Outer Nuclear Layer consists of nuclei from rods and cones, OLM=Outer Limiting Membrane, P=Photoreceptors, RPE= Retinal Pigment Epithelium.

1.1.2 RETINAL DISEASES AND STEM CELL-BASED THERAPY

There has been great interest in stem cell therapy in the retina as it holds the potential to treat a number of blinding diseases which impacts a large proportion of the population. Any retinal disease that results in neuronal loss could potentially be a target for stem cell-based therapy. Diseases that could benefit from stem cell-based therapy so far are age related macular degeneration, retinitis pigmentosa (RP), glaucoma, Staargardt's dystrophy, Gyrate atrophy and Leber's congenital amaurosis(Schwartz et al., 2012, Bull et al., 2009, Lamba et al., 2009, Howden et al., 2011, Tibbetts et al., 2012). However, stem cell based rescue of inner retinal layers i.e. retinal ganglion cells (RGC) in glaucoma, should not be excluded from this list. It has received relatively less attention due to the difficulties of SC as a cell replacement therapy for RGC. Furthermore, the ability of SCs to migrate and integrate into the inner retinal layer is thwarted by physical barriers such as the Inner Limiting Membrane (ILM) (Johnson et al., 2010b). In this thesis, I will attempt to address this by harnessing galvanotaxis with a view of using SCs as a vector for neuroprotective delivery.

1.1.2.1 AGE RELATED MACULAR DEGENERATION

Age related macular degeneration (AMD) is one of the most commonly recorded causes for the certification of blindness and partial sight in the UK (Bunce and Wormald, 2006). The pathogenesis of AMD is the subject of active research. It is thought to have a multifactorial aspect to include age dependence, a complex interaction of metabolic, functional, genetic and environmental factors which create chronic changes in the macula(Nowak, 2006). Two subgroups of AMD exists; atrophic (dry) form and exudative (wet) form, both of which eventually cause disruption and loss of retinal pigment epithelium (RPE) and photoreceptors. Although, treatments for the exudative form works through molecular inhibition of choroidal new vessels (Rosenfeld et al., 2006), the majority still suffer some degree of photoreceptor loss, which is inevitable in the atrophic (dry) subgroup. Theoretically, stem cell derived RPE can replace diseased RPE and is thought to be feasible given that RPE cells do not have to reconnect into a complex synaptic network. Indeed, there have been several on-going phase I/II human clinical trials looking at treating patients with AMD with RPE derived from embryonic stems cells or umbilical tissue(Schwartz et al., 2012).

1.1.2.2 HEREDITARY RETINAL DISEASES

One of the most commonly investigated hereditary retinal diseases in stem cell-based therapy is RP. The prevalence of non-syndromic RP is approximately 1/4000 (Hamel, 2006). It belongs to a group of pigmentary retinopathies that cover all retinal dystrophies presenting with a loss of photoreceptors and retinal pigment clumping mainly in the peripheral retina and a relative sparing of the central retina. There is degeneration of the rods initially followed by the cones, explaining the early symptom of nyctalopia in patients. RP is genetically heterogenous with more than 45 causative genes/loci identified in the non-syndromic RP (Hartong et al., 2006). Currently, there is no therapy at present that stops the evolution of RP and restores vision, although some promising advances have been made in AAV-mediated gene therapy (Ghazi et al., 2016). Stem cell-based therapy aims to replace the lost photoreceptors, or serve as a vector for corrective gene therapy. Indeed, cell replacement in the form of fetal neural tissue and intravitreal autologous bone marrow-derived mononuclear cells transplanted into RP patients has been assessed in an on-going phase I/II clinical trials with promising results (Siqueira et al., 2011, Radtke et al., 2008).

Stargardt's macular dystrophy is the commonest paediatric macular degeneration. It is caused by mutations in the ABCR (ABCA4) gene leading to Defective Rim Protein causing and accumulation of protonated N-retinylidene-PE in the rod outer segments followed by A2-E a by-product of N-retinylidene-PE which is toxic to RPE, resulting in its degeneration along with photoreceptor loss. Clinical trials involving cell replacement with human embryonic stem cell derived RPE have been reported(Schwartz et al., 2012), with three more phase I/II clinical trials on-going.

Leber's congenital amaurosis (LCA) comprises of a group of inherited disorders involving retinal degeneration with severe vision loss noted in early infancy. Most patients will have severe visual impairment throughout childhood, which deteriorates to total blindness by the third or fourth decade of life. There is genetic heterogeneity with LCA and 14 genes have been identified, with considerable overlap in other non-syndromic or syndromic retinal diseases such as RP(den Hollander et al., 2008). There is currently no treatment for LCA but promising results have been reported in phase1-2 trial of gene therapy in humans with RPE 65 mutations (Bainbridge et al., 2015).

The treatment of inherited retinal dystrophies with gene therapy is making good progress, with eight registered on-going clinical trials for LCA (targeting patients with RPE65 deficiency) and two for Stargardt's macular dystrophy. These advances could potentially be a primer for stem

cell-based gene delivery as these studies are viral-based. Stem cell-based gene correction in humans has not yet taken place. For this to occur, repair of a disease causing gene defect will be necessary. With the recent advances of gene therapy, it is hopeful that a stem cell-based gene correction is close. Indeed, in recent years gene-correction of human induced pluripotent stem cell-RPE taken from gyrate atrophy patient, has been demonstrated in vitro (Meyer et al., 2011, Howden et al., 2011). Furthermore, intravitreal implants of encapsulated RPE cell lines genetically modified to secrete CNTF have reported varying degrees of success in patients with RP or geographic atrophy (Birch et al., 2013, Kauper et al., 2012, Zhang et al., 2011b).

Essentially, there is scope for application of stem cell-based therapeutics in this group of patients. Retinal degenerative diseases encompass a large proportion of the visually impaired population that if treated could reduce morbidity and a growing socioeconomic burden.

1.1.2.3 GLAUCOMA

Glaucoma is a common irreversible neurodegenerative disease in which retinal ganglion cells (RGC) are damaged and degenerate, resulting in a characteristic cupping appearance of the optic nerve head and a corresponding pattern of visual field loss. Worldwide, glaucoma affects more than 45 million people and is the second commonest cause of blindness. It remains the second leading cause of blind registration in the UK(Bunce and Wormald, 2006, Quigley and Broman, 2006). Its pathophysiological feature is a combination of impaired axonal transport, oxidative stress and reactive glial changes (Bull et al., 2009). Elevation of intraocular pressure (IOP) is the strongest treatable known risk factor. Hence, treatment has mainly been focused on reduction of IOP. Nevertheless, IOP reduction alone fails to arrest a proportion of glaucoma cases. Novel treatment targeting neuroprotection delivery to surviving RGCs or even RGC replacement has been considered as a therapeutic option. However, stem cell-based therapies for glaucoma have mainly developed around a neuroprotective strategy rather than replacement therapy. This is due to the complex migration and integration transplanted stem cells would have to undertake for successful replacement therapy to take place. The transplants will need to also differentiate into RGC-like cells and generate neurite connections and multiple complex axons not only from within the retina but which must also extend to the optic nerve and project to various parts of the brain. This is a much more complex task than RPE and photoreceptor cell replacement. Attempts at generating RGC-like cells from SC have shown varying degrees of success (Sluch et al., 2015) and migration (Venugopalan et al., 2016). It is still thought to work on a neuroprotective basis rather than replacement (Johnson et al., 2010a, Aoki

et al., 2008, Chen et al., 2010). Indeed, encapsulated NSC-based intraocular administration of CNTF has been reported to protect RGCs in axotomized mice eyes(Flachsbarth et al., 2014). The reasoning behind encapsulation of SC is that it protects the cells from the immune system of the host. During intravitreal implantation, results of SC migration are often low, leaving them on the surface of the inner retina. In this thesis, I aim to deliver BDNF by using stem cells which have been magnetofected to over-express BDNF. Instead of encapsulation, I will attempt to direct their migration into the retina with galvanotaxis to increase their chances of survival.

1.1.3 STEM CELL SOURCES

Stem cells have the ability to self-renew, divide and differentiate into specialized cell types. They are divided into five categories according to their increasing ability to differentiate; unipotent, oligopotent, multipotent, pluripotent and totipotent. Totipotent stem cells have the ability to differentiate into any type of cell in the body and have the ability to create an entire organism. They are derived during development when male and female gametes fuse to form a zygote. Pluripotent stem cells also have the ability to differentiate into all cell types but are not capable of developing a full organism. Multipotent stem cells are able to differentiate into a limited number of cells from a particular tissue-specific group i.e. marrow stem cell produce any blood cell type, oligopotent stem cells are able to differentiate into just a few cell types and unipotent stem cells can only differentiate into a single type of cell. For this thesis, my choice of stem cell source was NSCs as they have well described galvanotaxic properties and are of similar origins to the retina which may influence migration. However, other stem cell sources have been investigated in eyes and a brief overview of them will be described in the next few subheadings.

1.1.3.1 STEM CELL SOURCES FOR RETINAL REPAIR: EMBRYONIC STEM CELL

Embryonic stem cell (ESC)s are pluripotent cells isolated from the inner cell population of day 5-8 blastocysts with indefinite self-renewal capabilities and the ability to differentiate into all cell types derived from the 3 embryonic germ layers. This was first demonstrated in mouse ESCs in 1981, where they were driven into all cell types of the body in vitro and in vivo(Evans and Kaufman, 1981, Martin, 1981). Human ESC was achieved not long after in 1998 (Thomson et al., 1998).

ESCs can differentiate into retina-specific cells in mouse, primate and human ESC(Aoki et al., 2006, Aoki et al., 2008, Haruta et al., 2004, Ikeda et al., 2005, Lamba et al., 2009). Their potential to differentiate and their viability in long term culture makes them a strong candidate for retinal repair(Bi et al., 2009). Retinal neurons, RPE cells, eye-like structures and photoreceptors have been derived from mouse and human ESC(Meyer et al., 2011, Haruta et al., 2004, Eiraku et al., 2011). Most protocols published involve combining defined growth factors such as Retinoic Acid and Taurine, Sonic hedgehog[SHH], Insulin Growth Factor-1[IGF-1], bFibroblast Growth Factor[bFGF], Wnt2b, noggin and Dickkopf-1[dkk1](MacLaren et al., 2006).

Furthermore, ESC have been cultured to produce a three-dimensional neural retina in vitro from mouse ESC(Eiraku et al., 2011). They were cultured with extracellular matrix components to produce optic vesicles, which then underwent dynamic morphogenesis to form bilayered cups. This development of growing a three-dimensional retina in-vitro brings new possibilities of generating artificial retinal tissues sheets rather than simple cell grafting. Early phase I/II trials fetal retinal sheet transplantation have shown that fetal retinal sheet transplantation improved visual acuity in patients with AMD and RP.(Radtke et al., 2008, Radtke et al., 2002). These data suggest that retinal sheets derived from human ESC could deliver a similar treatment effect.

In animal models of disease, ESC-derived RPE has been successfully transplanted with a resultant visual improvement and photoreceptor rescue (Lu et al., 2009). This has translated to phase I/II clinical trials of ESC derived RPE transplanted in patients with Stargardt's and AMD with encouraging visual improvement results in their preliminary data(Schwartz et al., 2012). However, the authors acknowledge that it is unclear whether the visual gains were due to the transplanted ESC, immunosuppression or intervention bias.

Although ESC's pluripotency is attractive, obstacles remain for ESCs clinical application. This includes ethical use, better isolation, identification and differentiation protocols (Osakada et al., 2009), host immune rejection, and the risk of teratocarcinoma.

1.1.3.2 STEM CELL SOURCES FOR RETINAL REPAIR: INDUCED PLURIPOTENT STEM CELLS

Induced pluripotent stem cells (iPSC) are derived directly from adult tissue such as skin fibroblasts and then differentiated into a variety of cell types(Stadtfeld et al., 2008). This avoids the need for immunosuppression and offers the potential to remove ethical issues associated with ESCs.

The process involves reprogramming of adult somatic cells by numerous combinations of transfected genes and small molecules such as K1f4, Sox2, c-Myc and Oct4; a core set of genes for reprogramming (Takahashi et al., 2007). Other reprogramming cocktails use Oct4, Sox2, Nanog, and Lin28 (Yu et al., 2007), or replace a number of the reprogramming factors with closely related proteins(Nakagawa et al., 2008), suggesting multiple possible avenues towards achieving pluripotency from adult somatic cells.

It has been demonstrated that human photoreceptors, RPE and RGC can be derived from iPSCs and survive post transplantation into animal disease models(Buchholz et al., 2009, Carr et al., 2009, Meyer et al., 2009, Lamba et al., 2010a, Hirami et al., 2009, Ohlemacher et al., 2016). In principle, a small tissue sample from a patient such as a skin biopsy could be cultured and reprogrammed into iPSC to derive retinal cells for transplantation. A more realistic and immediate benefit is to use these cells as an accurate disease model for drug screening technologies.

However, the disadvantage of iPSCs is that the patient's inherent genomic error causing the retinal disease will persist in the iPSCs. Indeed, Ohlemacher et al. demonstrated that RGCs cultured from a patient with and inherited form of glaucoma exhibited increase in apoptosis(Ohlemacher et al., 2016). Since this could be rescued by neuroprotective factors the study highlighted the clinical value in hiPSC may lie in its use for pharmacological screening rather than cell replacement therapy(Ohlemacher et al., 2016). To overcome this, the iPSC would have to be repaired by targeted gene editing prior to transplantation back into the patient. A more efficient culture protocol to increase the yield of iPSC in a shorter amount of time also needs to be developed. Furthermore, as adult cells, there are issues on their regenerative abilities given that they are "older" than ESCs, as well as the inherent risk of tumorgenesis.

1.1.3.3 STEM CELL SOURCE FOR RETINAL REPAIR: ADULT STEM CELLS: BONE MARROW DERIVED STEM CELLS

Adult stem cells are present in most organs and tissues such as brain, bone marrow, blood vessels, skin, teeth and heart. They are situated in the tissue [niche] into which they will differentiate. They rarely divide but do so when stimulated producing rapidly diving cells, which can differentiate into all cell types found in the niche.

Bone marrow derived stem cells (BMDSC) are multipotent progenitor cells that are harvested from a heterogenous cell population found in the bone marrow. They have an advantage in that they offer easy access for harvesting and an autologous stem cell source avoiding the need for

immunosuppression. The bone marrow is considered the richest reservoir of versatile stem progenitor cells capable of differentiating into various cell types of the human organism, including photoreceptors(Kicic et al., 2003). Furthermore, there is considerable clinical experience in their use in the treatment of leukaemia.

There are two distinct stem cell populations which can be derived from bone marrow: haematopoietic stem cells and mesenchymal stem cells. Hematopoietic stem cells are multipotent and able to give rise to all blood cell types: monocytes and macrophages, neutrophils, basophils, eosinophils, erythrocytes, megakaryocytes/platlets, dendritic cells, T-cells, B-cells and NK-cells. Mesenchymal stem cells are progenitors of connective tissue cells and have been differentiated into bone, cartilage, fat, muscle, tendon, liver, kidney, heart and brain cells.

It has been proposed that BMDSC may be able to restore retinal function through cellular differentiation, as a paracrine effect and through RPE repair(Siqueira et al., 2010). BMDSC can be aspirated from bone marrow harvested from the superior iliac crest, tibia, femur, thoracic and lumbar spine. Although BMDSCs circulate peripherally in response to RPE damage, this is insufficient to repair retinal damage(Machalinska et al., 2011). Potentially, inducing more BMDSC into peripheral blood may increase their accessibility. Hence, BMDSC delivered intravenously was attempted and showed repair and migration into a laser-induced retinal injury model(Chung et al., 2011). However, they did not determine the cell differentiation and so, the exact mechanism of repair in this injury model is not known. Interestingly, another group who also looked at intravenous delivery of mesenchymal stem cells reported rescue of cone and rod photoreceptors and increase in visual acuity in the Royal College of Surgeons rat model, a recognised animal model for RP(Wang et al., 2010b). They also labelled the infused mesenchymal stem cells and were found not only in retinal ganglion cell layers, inner and outer plexiform layers but also in the lungs, kidneys and liver. The fates of the cells deposited in the extraocular sites were not investigated.

Most groups have looked at intravitreal transplantation of BMDSC rather than intravenous methods of delivery, possibly to minimise off-target effect and maximise impact. Many have used an injury model either through laser application to the retina, ischaemic/reperfusion injury, or mechanical injury to the retina with a hooked needle, to induce BMDSC incorporation into the retina. Direct injection of BMDSC without pre-treatment with some form of injury induction is ineffectiveas the BMDSCs do not migrate into the neurosensory retina(Minamino et al., 2005). Stimulatory signals are required to ensure that injected BMDSC integrate into the retina. It has been hypothesized that inflammatory factors and cytokines from damaged retina

may have a role in directing migration of BMDSC(Li et al., 2006). The SDF-1/CXCR4 axis is one proposed pathway in directing stem cell, as well as the complement component C3a(Li et al., 2006). Once incorporated into the retina, BMDSC have been reported to survive in the eye for up to one year in mice and still express retina nerve cell specific antigens such as rhodopsin, MAP2 and nestin(Minamino et al., 2005).

Adult human peripheral blood mononuclear cells have also been reported to differentiate into retinal neuron-like cells in-vitro and in-vivo(Xian et al., 2016). Post subretinal transplantation in RD1 mice, survival and migration with differentiation into photoreceptor and neuronal markers were present at 6 months, providing another source for SC transplantation in retina.

Indeed, the encouraging results seen in animal models [see Table 1] have prompted human transplantation of bone marrow derived mononuclear cell transplantation in a patient with atrophic retina and optic nerve atrophy, three diabetic retinopathy patients and a glaucomatous optic neuropathy patient(Jonas et al., 2008). Autologous bone marrow derived mononuclear cells were also transplanted into five advanced RP patients by intravitreal injection (Siqueira et al., 2011). They concluded that there was no functional or structural toxicity over 10 months after a single intravitreal injection of these cells. The same group is currently recruiting RP patients for a follow-up Phase II non-randomized open label trial. Also of note, there is one Phase I safety study recruiting patients with RP for treatment with BMDSC in Bangkok, Thailand. Further trials are needed to determine the ideal stage at which RP patients can be transplanted, the effect of pre-treatment with laser, the long term effects of transplanted BMDSC with regards to safety and its effect on other diseases such as glaucoma and diabetic retinopathy given its paracrine and enhanced angiogenic effect.

Reference	Disease model	Route	Type of Bone marrow derived stem cell
(Otani et al., 2004)	rd1 and rd10 mouse model of retinal degeneration	Intravitreal	Adult bone marrow derived lineage negative hematopoietic stem cells
(Li et al., 2009)	Rat injured by ischaemic/perfusion	Intravitreal	Mesenchymal stem cells
(Zhang and Wang, 2010)	Light-damaged rats	Subretinal space	Mesenchymal stem cells
(Tomita et al., 2002)	Mechanical injury of rat retina with hooked needle	Intravitreal	Hematopoietic stem cells
(Wang et al., 2010a)	Mice with laser-induced retinal injury	Intravitreal	Lineage negative hematopoietic stem cells
(Johnson et al., 2010a)	Glaucoma model: Ocular hypertension induced rats by laser to trabecular meshwork	Intravitreal versus intravenous	Mesenchymal stem cells
(Castanheira et al., 2008)	Rats with laser-injured retina	Intravitreal	Mesenchymal stem cells
(Xian et al., 2016)	RD1 mice	Subretinal	Adult human peripheral blood mononuclear cells

Table 1 table showing experimental studies using bone marrow derived stem cell therapy for retinal diseases adapted from [adapted from Siqueira et al. 2010]

1.1.3.4 STEM CELL SOURCE FOR RETINAL REPAIR: ADULT STEM CELLS: NEURAL STEM CELLS

Neural stem cells (NSC) , neural progenitor cells and oligodendrocyte precursor cells (OPC) are multipotent cells with the ability to differentiate into three central nervous system lineages; neurons, astrocytes and oligodendrocytes. They have been isolated from the adult subventricular zone and dentate gyrus of the hippocampus in the central nervous system. Their harvest and preparation are complicated by their deep location within the brain. However, they are highly proliferative and their ability to differentiate into site-specific lineage under the influence of the microenvironment is advantageous.

Most groups have used adult hippocampus-derived neural stem cell [AHSC](Akita et al., 2002, Takahashi et al., 1998, Young et al., 2000). Takahashi et al found that AHSCs will integrate into neonatal rat retina post intravitreal transplantation and adopted the morphology and positions of Muller, amacrine, bipolar, horizontal, and photoreceptor cells(Takahashi et al., 1998). They have also been shown to integrate into a variety of injury models: retinal ischaemia-reperfusion models, genetically-degenerated adult rat retina, mechanically injured rat retina with a hooked needle and retinal ganglion cell depleted mouse retina(Nishida et al., 2000, Kurimoto et al., 2001, Guo et al., 2003, Mellough et al., 2004). Moreover, migration has also been observed in normal adult retina without prior trauma or disease models(Warfvinge et al., 2001). This was demonstrated using a subretinal transplantation method using two different brain-derived precursor cell lines; C17-2 (from postnatal mouse cerebellum) and RN33B(from embryonic rat medullary raphe)(Warfvinge et al., 2001). However, these are not adult-derived stem cells and so a higher integration capability would be expected, and subretinal implantation is in itself a form of trauma due to the induced serous retinal detachment prior to implantation. Although migration and assumed morphology of neurons have been demonstrated, they failed to express retina-specific markers and retinal function had not been tested.

OPCs are highly proliferative and are abundant in the adult central nervous system. They have been shown to deliver a dramatic neuroprotective effect in the trabecular laser glaucoma rat model(Bull et al., 2009). RGC survival, reported in optic nerve axon count was nearly 30% less than controls. However, the protection of retinal ganglion cell death was dependent on inflammatory cell activation of the OPC by Zymosan.

Recently, human neural progenitor cells transplanted subretinally into RCS rats not only survived and migrated into the retina, but also protected photoreceptors from degeneration(Gamm et al., 2007). Gamm et al investigated both neural progenitor cells with and without glial cell derived neurotrophic growth factor (GDNF) transduction. Both managed to

preserve retinal function recorded by ERG waves, optomotor response testing and luminance threshold responses. The protective effect was augmented with genetically modified human neural progenitor cells. These results are encouraging and suggest that neural progenitor cells have potential as a therapeutic option for retinal degenerative disease.

1.1.3.5 ADULT STEM CELLS: OLFACTORY-DERIVED STEM CELLS

The lack of a suitable donor site i.e. one with easy access is a major limitation of utilizing neural stem cells. Recently, the olfactory system has attracted interest due to its regenerative capacity and extracranial location giving it easy access. The olfactory system undergoes active neurogenesis throughout life including the subventricular zone and the olfactory epithelium. Olfactory ensheathing cells (OEC) are glial cells in the nasal mucosa and olfactory bulb that guide and ensheath the axons of olfactory nerve from the nose to the brain. However, harvest of OECs from the olfactory bulb requires highly invasive surgery, which is a major obstacle. Moreover, obtaining sufficient therapeutic quantities of OECs from olfactory bulbs is difficult.

By contrast, olfactory epithelium (OE); located high in the nasal vault, also has a regenerative capacity and is readily accessible form its location in the nasal cavity, allowing for autologous harvest with minimal donor damage. The human OE is located high in the nasal vault. Cultures of OE prepared from fresh postmortem tissue or endoscopic biopsy from patients undergoing sinus surgery have been subcultured to generate neurosphere forming cell lines(Roisen et al., 2001, Winstead et al., 2005). They have been cultured for over 200 passages and can be generated from OE biopsy irrespective of donor age or gender and remain equivalent. So far, no studies have investigated its effect on the retina.

To date, studies have been mainly focused on animal models and OEC. Early work with RGC and OEC was carried out by Sonigra et al (Sonigra et al., 1999). They found that OECs promoted retinal ganglion cell survival and neurite outgrowth in rats in vitro. They considered a number of mechanisms for this result; neurotrophin release, interaction between adhesion molecules on the surface of two cell types and interaction between neuronal integrins or other receptors and matric proteins elaborated by OECs. The lack of evidence for a secretory factor suggested that a neurotrophic mechanism was unlikely neurotrophins. Other groups have confirmed OEC promotes neurite outgrowth in RGC in vitro and in retinal explants (Moreno-Flores et al., 2003, Leaver et al., 2006b). Optic nerve crush models have also demonstrated reduced retinal ganglion cell death following OEC transplantation(Wu et al., 2010, Li et al., 2003).

In disease models, OEC can reduce the gliotic injury response. In the Royal College of Surgeon(RCS) rat; an animal model for RP(Huo et al., 2011), subretinal injection of OEC and

olfactory nerve fibroblasts into 1-month-old RCS rats(Huo et al., 2012) restored recoverin expression, protected retinal outer segments, increased peanut-agglutinin (PNA)-positive cone outer segments, reduced caspase-positive apoptosis and downregulated glial fibrillary acidic protein. Functionally, these changes were associated with the maintenance of the ERG b-wave. In contrast to Sonigra et al, they showed that a mixture of OEC and olfactory nerve fibroblasts secreted nerve growth factor(NGF), brain-derived neurotrophic factor(BDNF) and basic fibroblast growth factor(bFGF). These observations suggest a neurotrophic factor mediated role in maintaining the survival of photoreceptors. Liu et al proposed that OEC and GDNF induce a synergistic effect in promoting the recovery of visual function following optic nerve injury in adult rats(Liu et al., 2010). They showed that intravitreal GDNF alone did not induce axonal regeneration, which was explained by the suggestion that inhibitory factors secreted by glial scars at the late stage of injury, impeded axon growth, therefore GDNF was not able to promote axon regeneration to penetrate glial scars. OEC may have served as a cell bridge, guiding nerve cells to penetrate and grow through glial scars. These encouraging results have promoted further research into OEC use in combination with neurotrophic factor augmentation.

1.1.4 STEM CELL SOURCE FOR RETINAL REPAIR: EYE-DERIVED STEM-LIKE CELLS

In fish and amphibia, retinal stem cells are located in the retinal periphery, the ciliary marginal zone (CMZ) and produce new neurons in the retina throughout life. The CMZ is a transitional region between the neural retina and the iris/ciliary epithelium, and contains retinal progenitor cells that proliferate for a long time. In mammals and birds, stem-like cells have been isolated and characterized from the ciliary marginal zone(Reh and Levine, 1998).

In humans, there is increasing interest the existence or absence of a CMZ-like zone in the adult eye. Nestin positive cells found in adult human retina and epiretinal membrane is suggestive of this(Mayer et al., 2003). Furthermore, the distribution of nestin positive cells in the extreme periphery of the retina suggests that a CMZ-like region exists(Bhatia et al., 2009).

In mammals, the CMZ is analogous to the pigmented ciliary margin in the far retinal periphery where potential stem cells have been cultured in vitro. Neurospheres have been grown from the ciliary epithelium to differentiate into photoreceptors, bipolar cells and Muller glia(Ahmad, Tang and Pham, 2000). However, since the pigmented ciliary margin is non-mitotic and fully differentiated in mammals, cell derived from this area should be regarded as having stem cell potential and that they remain in a quiescent state in vivo (Amato, Arnault and Perron, 2004).

The ciliary epithelium and retina share a common origin and arise from the inner layer of the optic cup. However, in the adult eye they diverge in roles and the ciliary epithelium secretes aqueous humour. Due to their common derivation from the neuroepithelium during embryonic development, it has been thought that perhaps the ciliary epithelium could be a source of stem cells. Neural retinal stem cells have been isolated and grown in vitro from human ciliary epithelium of the pars plana and the pars plicata (Coles et al., 2004). However, when these cells were transplanted into the mouse eye, they showed limited migration into the neural retina and RPE. More recent studies suggest that ciliary epithelium from mouse and human lack stem cell properties(Cicero et al., 2009). Although cells isolated from ciliary epithelium could be induced to express low levels of neuronal markers, they retained their epithelial morphology and failed to differentiate into retinal neurons(Cicero et al., 2009). Furthermore, they demonstrated that ciliary epithelium spheres contain cells with epithelial properties and limited expression of neuronal markers compared to those of neural stem cells(Moe et al., 2009).

Muller glia are the main glial cells in the retina. Radial glia in the brain, function as stem cells in mammalian central nervous system(Merkle et al., 2004). Glial cells may play a neural precursor role in the adult central nervous system(Lawrence et al., 2007). Muller stem cells have been isolated from human retina and have been shown to be capable of proliferating indefinitely in vitro(Lawrence et al., 2007). They have been shown to adopt a neuronal morphology and express markers of postmitotic retinal neurons such as peripherin, recoverin, calretinin and S-opsin. However, they do not migrate well into the subretinal space of RCS rats or neonate Lister hooded rats(Lawrence et al., 2007).

1.1.5 POST-MITOTIC PHOTORECEPTOR PRECURSOR CELLS

Post-mitotic photoreceptor precursor cells can be derived from P1-5 postnatal mouse retina and have been shown to migrated successfully into adult wild type and degenerating mammalian retina(MacLaren et al., 2006). This time range was concurrent with the peak of rod genesis. Although a recovery of light response was reported, it was unclear if true cell connections were being formed within the retina. It is likely that the beneficial effect seen may be from a neurotrophic response. Furthermore, for this to translate to human therapy, cells would have to be derived from fetal tissue in the second trimester, which is ethically problematic, bearing in mind that legally fetal viability is 24 weeks.

1.2.0 PROPOSED MECHANISMS FOR STEM CELL-MEDIATED RETINAL REPAIR

1.2.1 STEM CELL AS CELL REPLACEMENT

Tissue replacement approaches to stem cell therapy in retinal degeneration have consisted of replacing diseased photoreceptors, RPE, and recently the entire retinal layer (Eiraku et al., 2011, Assawachananont et al., 2014).

The replacement of RGCs has received comparatively less attention. The challenge is more daunting as the transplanted cell will not only need to migrate into the correct spatial location within the ganglion cell layer, but also make connections within the retina and generate axons which extend topographically to the optic nerve and brain. Encouraging work has been achieved on generating RGC-like cells for replacement. iPS cells and ESC have been driven towards an RGC-like fate(Parameswaran et al., 2010, Jagatha et al., 2009, Aoki et al., 2008, Chen et al., 2010). However, they have not been able to integrate these cells into the retina as yet.

By contrast, photoreceptor replacement represents less of a challenge. ESC and iPS cells driven towards a photoreceptor fate can be transplanted into the eye to generate mature rods integrated within the retina (Lamba et al., 2009, Lamba et al., 2010b). Transplantation of ESCs into the subretinal space of a mouse model of Lebers congenital amaurosis showed some restoration of photoreceptor function by ERG, as well as structural integration and evidence of local synapse formation within the host outer nuclear layer (Lamba et al., 2009).

RPE replacement aims to re-establish the critical metabolic interaction between itself and the photoreceptor. Autologous RPE grafts have achieved some success in patients, leading to further work on SC derived RPE grafts as a more sustainable source of tissue. ESC(Lund et al., 2006) and BMDSC(Atmaca-Sonmez et al., 2006, Harris et al., 2006) have been identified as sources for RPE replacement.

Although photoreceptor SC replacement therapy has reported functional improvement in vision, it does not exclude the possibility that the transplanted SC had a neuroprotective effect rather than a regenerative effect (Dahlmann-Noor et al., 2010). Furthermore, transplanted photoreceptors or RGCs will be non-topographic in contrast to normal retina.

1.2.2 STEM CELL AND NEUROPROTECTION DELIVERY

Since stem cells are dynamic and underpin neuronal development, they produce neurotrophic factors that influence the growth and maintenance of their own and surrounding tissues via autocrine and paracrine mechanisms. Neurotrophic factors are groups of naturally occurring molecules that support neural cell survival, proliferation, migration, differentiation, growth and function(Ventura et al., 2008). Six biological families of neurotrophic factors directly impact stem cell development: classic neurotrophins (nerve growth factor[NGF](of which brain-derived neurotrophic factor(BDNF) is related to), neurotrophin-3[NT-3], and neurotrophin-4[NT-4]), transforming frowth factor (TGF)-beta family (glial cell line-derived neurotrophic factor [GDNF] and bone morphogenic proteins [BMPs], neurturin, artemin, persephin), cytokine growth factor family (ciliary neurotrophic factor [CNTF], leukaemia inhibitory factor [LIF], cardiotripin-1), epidermal growth factor(EGF) family (EGF, transforming growth factor-alpha[TGF-alpha], neuregulins, neural and thymus-derived activator for ErbB kinases[NTAK]), insulin growth factors (IGF-I, IGF-II and IGF-6) and the fibroblast growth factor family (FGF1, FGF2)(Tuszynski, 2007).

Previous reports have shown that the integration of neural progenitors is greater following transplantation in immature compared with adult recipients(Mellough et al., 2004). West et al examined the effects of manipulating the extrinsic microenvironment of the host retina toward a more developmental-like state(West et al., 2012).They examined the effects of AAV transfected P4 postmitotic photoreceptor precursor with IGF1, FGF2 and CNTF on cell integration into the retina. Interestingly, CNTF overexpression decreased cell integration probably as a result of increased glial scarring. IGF1 significantly increased the levels of integration and FGF2 showed no significant effect. This would suggest adjunctive neurotrophic factor delivery with stem cell transplantation play a role in improving SC integration into retina.

Apart from improved SC integration into the retina, neurotrophic growth factors are known to protect cells in the inner and outer nuclear retinal layers. These will be summarised in the following subchapters.

1.2.2.1 RETINAL GANGLION CELL RESCUE BY NEUROTROPHIC FACTORS

Neurotrophic factor supplementation by gene therapy is a promising strategy to promote retinal ganglion cell survival and axon regeneration post glaucomatous injury models. Gene therapy can be targeted, inducing innate retinal cells to overexpress neurotrophins or modifying stem cells to secrete specific growth factors. BDNF, CNTF, GDNF and FGF-2 have been explored using gene therapy approaches to promote RGC survival and regeneration in these models.

Of all the neurotrophic factors, BDNF is the most potent survival factor for RGCs. They express the BDNF receptor tyrosine receptor kinase B (TrkB)(Perez and Caminos, 1995) and BDNF intravitreal injections have been shown to temporarily slow RGC loss in glaucomatous experiment models(Ko et al., 2001). However, repeated intravitreal injection of BDNF do not provide a clinical solution for a sustained delivery and so the use of viral vectors to deliver a BDNF-expressing gene has been investigated. Adenoviral and adeno associated virus (AAV) vectors have been reported to show a beneficial effect of gene therapy in a glaucoma models(Martin et al., 2003, Di Polo et al., 1998, Leaver et al., 2006a). They have shown RGC survival after optic nerve transection. Indeed, Martin et al reported 32% RGC axonal loss in AAV BDNF treated eyes in comparison to a 52% RGC loss in control eyes(Martin et al., 2003).

CNTF has also been shown to promote RGC survival as well as induce axonal regrowth(Pease et al., 2009, Muller et al., 2007). Vectors including AAV, adenoviral and lentiviral have been investigated to transfer the CNTF gene(van Adel et al., 2003, van Adel et al., 2005). It has also been reported to stimulate RGC survival in experimental glaucoma(Pease et al., 2009, Muller et al., 2007).

FGF-2 gene transfer mediated by AAV has also resulted in increased RGC axon regeneration following optic nerve crush (Sapieha et al., 2003). However, it does not enhance the survival of RGCs but has the ability to induce axon regeneration.

GDNF gene transfer has also been explored via AAV as well as electroporation (Straten et al., 2002, Ishikawa et al., 2005). It also imparted neuroprotection of RGCs following optic nerve transection.

Since neurotrophic factors have a short half-life, there is a need for a sustained growth factor delivery. Stem cell-based delivery of BDNF to the retina has been investigated with promising results. Park et al. transduced MSC (retroviral) with a vector of BDNF, which was successfully transplanted into rat retina (15.7% incorporation rate) by a subretinal injection which

significantly increased BDNF expression post transplantation (Part et al.,2012). Similarly, Harper et al. demonstrated the feasibility of genetically modified MSCs(via a lentiviral vector to express BDNF) to deliver BDNF and attenuate glutamate- and hydrogen peroxide- mediated RGC-5 cell death(Harper et al., 2009). This lead on to in-vivo rat work whereby Harper et al. demonstrated the lentiviral transduced BDNF-producing MSCs provided RGC preservation with higher RGC cell counts and functional improvement, evidenced by enhanced pupillary light reflex and ERG preservation in rats with chronic ocular hypertension(Harper et al., 2011). This was compared with transplantation of MSC-GFP, not sham injections, as intravitreal MSC transplantation alone can also be neuroprotective in experimental glaucoma(Johnson et al., 2010a).

Currently, there is one on-going Phase I study looking at NT-501 CNTF encapsulated cell implant to deliver neurotrophic factors for glaucoma patients(Goldberg, 2016). To date, there are no human clinical trials investigating intraocular neurotrophic factor gene transfer for use in glaucomatous patients, but a phase 1 trial has confirmed the NT-501 CNTF encapsulated cell implant does not result in systemic increase of CNTF(Kauper et al., 2012). Little is known about the long-term effects of sustained neurotrophin levels in the retina, and it has been reported that BDNF and CNTF expression via AAV leads to changes in dendritic structure of transduced RGCs(Rodger et al., 2012). It is necessary to firstly optimize a safe and efficient method of neurotrophic gene delivery, alongside long-term safety studies for prolonged neurotrophic factor expression in the eye as well as systemically.

1.2.2.2 PHOTORECEPTOR RESCUE BY NEUROTROPHIC FACTORS

Basic fibroblast growth factor(bFGF) first showed the progression of photoreceptor degeneration could be slowed down in RCS rats(Faktorovich et al., 1990). Since then, several other neurotrophic factors such as BDNF, GDNF, CNTF have been shown to confer protection of photoreceptors in animal models of photoreceptor degeneration. Interestingly, LaVail et al showed that there were variations between species and transgenic retinal degenerating animal models with regards to their response to neurotrophic growth factors(LaVail et al., 1998), so it is difficult to identify a single neuroprotectant which would work best for all retinal dystrophies and degenerations. Nevertheless, they demonstrated that it was possible for CNTF, BDNF and leukemia inhibitory factor (LIF) to protect photoreceptor degeneration in animal models(*rd/rd*, *nr/nr* and Q344ter mutant rhodopsin mice) with same or similar genetic defects as those in human retinal degeneration(LaVail et al., 1998).

Consequently, Cayouette et al demonstrated that intraocular adenovirus-mediated gene transfer of CNTF in rds/rds mice reduced photoreceptor loss and caused an increase in length of photoreceptor outer segments resulting in a redistribution and increase in retinal rhodopsin content(Cayouette et al., 1998). These morphological changes were accompanied by a significant increase in amplitude of a and b waves in the scotopic ERG. AAV-mediated GDNF expression was also reported to enhance photoreceptor survival in RCS rat and *Prph2* $^{RD2/RD2}$ mice(Buch et al., 2006). These positive results encouraged work on the transduction of stem cells for the prolonged delivery of neurotrophic factors in animal models of retinal degeneration. Cell-based methods of neurotrophin delivery into animal models of retinal degeneration have been reported in Schwann cell lines and ESC into RCS rats and TgNS334ter rats (a rat model of retinal degeneration) exerting a neuroprotective effect on photoreceptor survival for up to 3 months (Lawrence et al., 2004, Gregory-Evans et al., 2009, West et al., 2012, Zhang and Wang, 2010, Zhou et al., 2009b)). These were virally mediated and had overexpression of BDNF or GDNF.

A Phase 2 study demonstrated the safety profile of NT-501 implant secreting CNTF in patients with geographic atrophy from dry AMD over 12 months(Zhang et al., 2011b). The encapsulated cell-based delivery of CNTF has also been shown to protect photoreceptors in *rcd1* canine model of RP(Tao et al., 2002). The clinical translation of stem-cell based neurotrophic delivery has not yet been made for the treatment of RP, though both stem cell transplantation and neurotrophic growth factors are currently in clinical trial. Sustained neurotrophic growth factor delivery is promising but should be applied with caution. Indeed, it has been reported that in *Prph2* $^{RD2/RD2}$ mice, AAV-mediated CNTF therapy or when used in combination with gene replacement therapy, visual function was reduced despite the observed reduction in photoreceptor loss. Furthermore, this deleterious effect was also observed in wild-type mice treated with AAV-mediated CNTF causing up to 50% reduction in b-wave amplitude (Schlichtenbrede et al., 2003). Furthermore, the effects of CNTF suppression of retinal function was reported to be dose-dependent(Buch et al., 2006). Interestingly, in the same study, AAV-mediated GDNF expression did not produce the adverse effects seen with CNTF in rodent models of RP. This highlights that there is still a need to understand the true effects of sustained neurotrophin expression not just through perceived neuroprotection via cell counts, but also through cell morphology and visual function.

Overall, there is evidence to show that neurotrophic growth factors improve photoreceptor survival, but more work is necessary to delineate its safety profiles and a as well as a safe method for sustained intraocular delivery.

1.3.0 STEM CELL MIGRATION INTO RETINA

The potential for stem cell transplantation as a form of treatment in retinal degenerative diseases is a subject of constant research and rapidly progressing. However, it is hampered by barriers preventing migration and integration. Several groups have looked at identifying barriers to migration of grafted cells with variable results as the adult retina is implastic and relatively inhibitory to cellular migration [Johnson 2010]. Most groups have only reported low levels of intraocularly transplanted cells migrating into the retina with the majority remaining as a bolus outside of the neural tissue with low SC survival reports of (0.04% to 8%)(Ballios et al., 2015). Efficacious and successful migration is key to establish the ultimate goal of a stem cell mediated treatment; be it by neuroprotection delivery or cell replacement.

Barriers to stem cell integration into the retina exist across SC types. Most of the studies reporting successful SC integration into retina used a subretinal approach. Table 2 summarises some studies that show migration into the retina post transplantation of stem cells in varying conditions.

Reference	**Cell type**	**Method of transplantation** **+adjunct therapy**	**Host status**	**Migration** **observed (%)**
G Castro 2013	Mouse NPC in growth factor-free culture condition	intravitreal	Mouse with sodium iodate induced retinal degeneration	Yes (N/A)
H Mizumoto 2003	Mouse NPC	subretinal	B6 mice Rds BALB/C mice Pigment dystrophic RCS rats	Yes for all but best for B6 mice (2-10%)
Pearson et al 2012	Rod photoreceptor precursors	subretinal	Adult Gnat1-/- mouse	Yes(16%)
Singhal et al 2008	Müller stem cells	subretinal +Chondroitinase ABC +immune suppression	RCS rats Neonate Lister Hood rat	Yes in Chondroitinase ABC treatment(80%)
Bull et al 2008	Müller stem cells	subretinal intravitreal +immune suppression +erythropoietin +Chondroitinase ABC	Adult rats with laser induced glaucoma model	No for intravitreal and subretinal without adjunct Yes for both methods +EPO or Chondroitinase ABC(N/A)
Canola et al 2007	Retinal stem cells of neonatal DBA2J mice	subretinal intravitreal	Adult wild type Mouse models of retinal degeneration*rd1 or VPP strain)	Yes subretinally in disease model (N/A)
Maclaren et al 2006	Post-mitotic photoreceptor precursors	subretinal	Adult	Yes (N/A)
Lamba et al 2009	Human ES derived retinal cells	subretinal	4-6 week age wild type mice Crx-/- mice	Yes (N/A)

Table 2 Summary of some studies assessing migration of stem cells into retina with varying conditions.

1.3.1 IMPROVING STEM CELL SURVIVAL AND INTEGRATION INTO THE RETINA

Attempts at improving SC survival and integration into retina have targeted delivery methods, immunosuppression and overcoming the physicals barriers i.e. inner limiting membrane (ILM), outer limiting membrane, glial scarring and chondroitin sulfate proteoglycans.

The major obstacle to SC integration is the physical barriers such as ILM and its extracellular matrix. ILM is formed by astrocytes and the end feet of the Müller cells. This barrier has been shown to prevent SC migration with previous failed attempts of intravitreal SC delivery resulting in the cells lining the ILM without penetrating the retina (Johnson and Martin, 2008). Enzymatic removal by alpha-aminoadipic acid digestion (Johnson et al., 2010b)has been reported to increase integration for intravitreal mesenchymal stem cell transplantation. This was enhanced with mechanical peeling of the ILM and correlated positively with the amount of peeled ILM. Disruption of Chondroitin Sulfate proteoglycans with Chondroitinase ABC have also showed improved SC integration (Singhal et al., 2008, Ma et al., 2011).

Biomaterial approaches such as injectable hydrogels like hyaluranon and methylcellulose, biodegradable polymer composite grafts with variable degrees of integration (Ballios et al., 2015, Ballios et al., 2010, Tomita et al., 2005, Pakulska et al., 2012). Materials have also been developed to support the culture of a three dimensional tissue to improve survival of SCs(Eiraku et al., 2011). Indeed, three dimensional sheets of ESC and IPS were also investigated in retinal degenerative eyes with the development of a new ONL(Assawachananont et al., 2014). Biomaterials have been reported to promote stem cell attachment, proliferation and gene expression(Anderson et al., 2004)

Immunosuppression has also been described to improve SC integration mainly due to the inactivation of host microglia. Singhal et al reported increased survival of transplanted Muller stem cells by using triamcinolone(Singhal et al., 2010).

The uninjured retina seems to be very resistant to migration (Chacko et al., 2003). Indeed, induced injury has been shown to facilitate migration into the retina i.e mechanical or laser induced(Nishida et al., 2000). This may explain how subretinal routes seem to show more success with SC migration into the retina.

The source of stem cells also seems to play a role in migration into the retina. In a stem cell transplantation model using retinal explants, MSCs and Müller progenitor cells(hMIO-M1) showed no migration in MSCs but a few hMIO-M1 cells were able to migrate into RGC(Johnson and Martin, 2008). Of note, Maclaren et al found that transplantation of photoreceptor

precursor cells from P1 mice showed not only migration into the ONL and differentiation into photoreceptors post subretinal transplantation(MacLaren et al., 2006). In this thesis, I will attempt to drive NSCs into the inner retina past the ILM by electric field application.

1.4.0 MAGNETOFECTION AND OCULAR USE

INTRODUCTION

Nanotechnology deals with the fabrication and application of nanometer-sized materials. It can be applied across a multitude of fields, but has widespread use in medicine. Research has been driven in the direction of targeting specific organs, tissues and cells for the purposes of targeted drug delivery i.e. in oncological treatment, for enhancing contrast in MRI imaging, for cell transfection and cell transplantation therapy. With stem cells, it has diverse applications; as a gene delivery system in-vitro and in-vivo, in stem cell isolation in vitro, for nano-scaffolds in in-vivo stem cell therapy and bioengineering, for nano-biopolymeric scaffolds, for proliferation and differentiation of stem cells in ex-vivo cultures, as nano-biosensors for stem cells, and in-vivo labelling and tracking of stem cells(Kaur and Singhal, 2012, Smith et al., 2009, Ngen et al., 2015).

The literature on nanoparticle use in ocular tissue is increasing. It has been mainly described in ocular pharmacological delivery and to a lesser extent in gene delivery, retinal vascular imaging and tracking devices, delivering cells to a targeted location and as a shock protein inducer with consequent retinal ganglion cell neuroprotection(Das et al., 1995, Basaran et al., 2010, Durairaj et al., 2010, Shih et al., 2012, Jeun et al., 2011, Yanai et al., 2012).

In pharmacological drug delivery, gatifloxacin, ciprofloxacin, cyclosporine-A, brinzolamide, pilocarpine, 5 -fluorouracil, indomethacin, betaxolol and anti-fungal therapy are among the many drugs that have had nanoparticle-mediated delivery (Hippalgaonkar et al., 2013), (Wu et al., 2013, Pagar and Vavia, 2013, Khan et al., 2013, 2013, Jain et al., 2013, Xu et al., 2013). It has also been used in imaging where the ocular circulation of a rat was shown with monocrystalline iron oxide nanoparticle injection magnetic resonance angiography (Shih et al., 2012). Furthermore, retinal ganglion cell neuroprotection has been demonstrated by the use of superparamagnetic $Mn_{0.5}Zn_{0.5}Fe_2O_4$ particle agents to induce localized heat shock proteins by local magnetic hyperthermia induced by the application of an external magnetic field (Jeun et al., 2011).

Gene delivery literature surrounding MNP use in the eye has been mainly focused on the outer retina. The majority of anterior and posterior segment gene delivery systems are viral based. However, non-viral gene delivery is being actively researched and range from lipofection, electroporation, ballistic transfer and nanoparticle transfer. The appeal of nanoparticles in comparison to the viral approach is that there is a larger cargo limit and a lower risk of inducing an immune response. Nanoparticles can be magnetised or non-magnetised. The non-magnetised DNA nanoparticle use for gene delivery such as CK30PEG nanoparticles, are composed of single molecules of DNA compacted with 10kDa polyethylene glycol-substituted polylysine. They have been shown to drive efficient persistent retinal gene expression (Han et al., 2012a). Mitotic and post-mitotic photoreceptors have been successfully transfected with these DNA nanoparticles as well (Cai et al., 2010). They have been demonstrated to safely and efficiently target RPE and photoreceptors without significant toxicity and mediate improvement in RP animal models (Cai et al., 2010, Han et al., 2012b). Indeed, on direct comparison with adeno-associated virus gene delivery, DNA nanoparticles can drive gene expression on a comparable scale and longevity with adeno-associated viral vectors, although the viral vector was still more efficient per vector genome(Han et al., 2012a).

Magnetofection was designed to enhance the non-viral delivery of genes to targeted cells(Scherer et al., 2002). It utilises magnetic beads and magnetic attraction. The next subheadings will focus on targeted ocular stem cell based gene delivery by magnetofection.

1.4.1 MAGNETOFECTION USE WITH STEM CELLS

Magnetic nanoparticles (MNP) are a class of nanoparticles that can be manipulated by a magnetic field. Its use in stem cell gene transfer has been encouraged due to its safety, its ability to allow for non-invasive stem cell tracking post transplantation, its potential ability to target stem cell delivery to localized areas of injury, and its ability to deliver larger biomolecules(DNA/siRNA) than viral vectors.

So far, neural stem cells, astrocytes, OPCs, MSCs, ESC have been reported to have successful gene delivery with magnetofection for a variety of gene transfers(Adams et al., 2013, Jenkins et al., 2011, Freitas et al., 2013). MNPs have also been used as adjunct to assist in increasing transfection efficiency in combination with viral methods and lipofection(Rieck et al., 2013, Fujii et al., 2010).

Efforts have been placed in its use for iPS preparation. Conventionally, adult cells are transfected, commonly by a viral vector, to express pluripotency related genes(Oct3/4, Sox2, c-Myc, Nanong, LIN28 and KLF4). Indeed, Ruan et al demonstrated the feasibility of using MNPs to transfect adult human fibroblasts with four transcription factor genes; Oct4, Sox2, LIN28, and Nanong (Ruan et al., 2011). Furthermore, they were tagged with fluorescent MNPs to allow for tracking by fluorescent microscopy and MRI.

In this thesis, I will be optimizing the magnetofection technique to transfect NSCs with BDNF-myc to overexpress BDNF. This will then allow me to demonstrate that magnetofected NSCs which have been directed to migrate within the retina can serve as a vector for sustained release neurotrophic growth factor.

1.4.2 MAGNETOFECTION AND GENE DELIVERY IN THE EYE

Research into gene therapy in ocular disease is expanding. Clinical trials include AMD treatment with a viral vector expressing pigment epithelium-derived factor, and promising visual improvement with gene therapy in LCA(Campochiaro et al., 2006, Testa et al., 2013). Most studies utilize viral vectors, as they enter cells easily and are more efficient than other gene delivery vehicles with consequent good expression of secreted proteins. However, they run the risk of immune responses, inflammation and virus integration into the host genome. It is interesting to see that one quarter of the phase 1 clinical trial with AMD patients treated with a viral vector expressing pigment epithelium-derived factor showed signs of intraocular inflammation (Campochiaro et al., 2006). Hence, the pursuit for a non-viral vector for transfecting the retina commenced.

Non-viral transfection methods are safer, more economical and easier to manipulate. MNP-based gene delivery was first demonstrated by Mah, Byrne et al (Mah et al., 2002, Scherer et al., 2002, Plank et al., 2003). It is thought that magnetic fields assist transfection by increasing particle-cell contact, followed by MNP uptake by cellular endocytosis(Plank et al., 2011).

Magnetofection has been shown to improve efficiency of cell transfection and have been used to enhance viral adenoviral transduction(Sapet et al., 2012). Magnetofection gene delivery in the eye has been reported by Prow et al (Prow et al., 2008). They investigated two non-magnetised nanoparticles, poly [cholesteryl oxocarbonylamido ethyl] methyl bis[ethylene]ammonium iodide] ethyl phosphate, chitosan and one MNP in rabbits in-vivo. The MNP had DNA tethered to a magnetic core of iron oxide coated with dectran and bioconjugated to streptavidin.

Interestingly, once the DNA was tethered to the MNP, they were coated with Lipofectamine 2000, therefore the group was essentially investigating two nano-magnetized nanoparticle vectors and one magnetolipofection vector. The results were much in favour of magnetofection as neither non-magnetized nanoparticles were able to deliver the reporter gene to the retina, and only the MNP under investigation was capable of doing so. Moreover, the MNP did not induce inflammation nor showed any major toxic effect on the retina(Prow et al., 2008). Furthermore, the non-magnetized nanoparticle chitosan evoked an unanticipated intraocular immune response in subretinal delivery despite many publications on safe use of chitosan in non-ocular tissue in-vivo (Prow et al., 2008).

1.4.3 MAGNETOPARTICLES AND OCULAR AND STEM CELL TOXICITY

It is essential to not only strive to achieve the highest transfection efficiency level in search of the optimum non-viral vector for gene delivery in the eye, but also to assess the parameters induced by cell toxicity if present.

Studies have approached this by studying MNP clearance in the eye post intraocular injection by using MRI to track MNP biodistribution (Raju et al., 2011, Raju et al., 2012). It was shown that particle size unsurprisingly was linked to clearance time (Raju et al., 2012). The 50-nm MNP cleared more quickly than 4μm MNPs. The MNP under investigation was 4 μm Dynabeads M-450, 37% iron oxide and 50nm MNP 55-59%iron oxide. The long term persistence of micron-scale particles may not be as preferred in future magnetofection plans due to this. No MNP were detected in organs systematically. The same group also reported MNP to be safe for intraocular injection at a single injection dosage volume of 3μl and found no toxicity at histological level(Raju et al., 2011).

Zinc oxide nanoparticles have also been investigated for toxicity in RGC-5 cells(Guo et al., 2013). Zinc oxide is more commonly investigated as anticancer therapy, and has not been used in magnetofection although they can be induced to adopt a ferromagnetic-like behaviour(Garcia et al., 2007). The MNPs under study were about 60nm diameter and cell viability decreased with the increase of culture time and concentrations of zinc oxide. This was accompanied by a concentration-dependent rise in caspase-12 expression levels due to reactive oxygen species overproduction.

More ocular cell toxicity studies need to be run on the many proprietary MNP available, which needs to be validated in the short term as well as post multiple long term exposure periods.

Overall, MNPs seem safe and are a reasonable therapeutic option. Nonetheless, in chapter 4 tissues and NSCs were subjected to cell viability tests to find the highest tolerable concentration of proprietary MNPs that can be used prior to magnetofection studies.

1.4.4 MAGNETOFECTION AND OSCILLATION

Increased efficacy of transfecting stem cells have been reported by deploying MNPs with applied oscillating magnetic fields. This novel technique to enhance magnetofection was first reported in mouse embryonic fibroblasts and human umbilical vein endothelial cells were reported to show improved transfection with MNP in an oscillating magnetic field (Lim and Dobson, 2012). This was also directly compared to lipofection and static magnetofection(Fouriki et al., 2012). Interestingly, some transfection (2%) was observed in the presence of MNP DNA complex in the absence of magnetic field. Increase in transfection efficiency was observed between no magnetic field and both static and oscillating magnetic field conditions. They were also found to be much more efficient than lipofection after 30 minutes but similar in transfection rates after 6 hours. Disappointingly, in this study there was no significant difference between static magnetofection and oscillating magnetofection (22% vs 25% transfected cells), but have suggested the parameters of oscillating frequency (2Hz used in this study) would need to be optimised before any conclusions could be made from this. Further to this, neural stem cell transfection with an applied oscillating magnetic field was found to be maximally statistically significant in increasing transfection levels at 4Hz(Adams et al., 2013). They reported no effect on cell viability, cell number, stem cell marker expression and differentiation profiles of the NSC cultures that were magnetofected. The authors admit that the mechanism for this is not clear. However, they propose that the horizontal magnetic field component stimulates endocytotic activity of the neural stem cell membrane. Hence the observed oscillation dependent increase in transfection.

No studies have investigated gene delivery with magnetofection and oscillation in the eye. In chapter 4, I will investigate this novel technique as a method for gene delivery into ocular tissues. Furthermore, I will use it to transfect the neurospheres which to deliver BDNF in the retina explant in chapter 7.

1.5 GALVANOTROPISM

Galvanotropism is the process whereby cells respond to an extracellular electric field by changing their morphology along the voltage gradient(McCaig et al., 2005). It was first described in small animals such as tadpoles, salmon embryos and crayfish in the 19th century (Miller, 1907). By the 1920s Ingvar et al. showed that neurons in culture directed their growth in response to application of a direct current electrical field(Ingvar). Indeed, many reports of success in vivo and in vitro of EF application improving nerve growth have been published (Borgens et al., 1999, Yao et al., 2008). To date, galvanotaxis has been reported in over thirty animal-derived cell types(Allen et al., 2013) including stem cells(Meng et al., 2012, Feng et al., 2012), neurons(Patel and Poo, 1982), lung cancer cells(Yan et al., 2009), and ocular cells(Pullar et al., 2001, Zhao et al., 2012a).

1.5.1 ENDOGENOUS ELECTRICAL FIELDS, EMBRYONIC GUIDANCES AND WOUND HEALING

In vivo, voltage gradients are maintained by cells across the cell membrane by constantly pumping ion channels across their membrane; the membrane potential. Ion channels constantly pump Na^+, K^+ and Cl^- to establish this. Organs and embryos are surrounded by a layer of cells: the epithelium. This polarised distribution of ion channels gives the transcellular current. This current cannot flow freely into the extracellular space as tight junctions and adherens junctions exist [see figure 1.2]. The apical-basal transcellular current must flow via the paracellular pathway whereby high resistance is encountered at the tight junctions. This resistance leads to a transepithelial potential (TEP) which is positive on the basal side. The TEP is the basis of most endogenous ionic currents in embryos and adults. Values for TEP range within 15 to 60 mV in human bodies (Farboud et al., 2000, Nuccitelli, 2003). In wound healing, when epithelial integrity is compromised, TEP at the wound drops to 0mV, creating a transverse voltage gradient along the epithelium [see figure 1.3]. The wound centre effectively acts as a cathode to orientate tissue and promote wound healing (Song et al., 2004). A similar occurrence is present during embryogenesis in areas of low tight junction resistance along the primitive streak, posterior intestinal portal or at the limb bud in amphibian, chick or mouse embryo (Jaffe and Stern, 1979, Altizer et al., 2001, Hotary and Robinson, 1994).

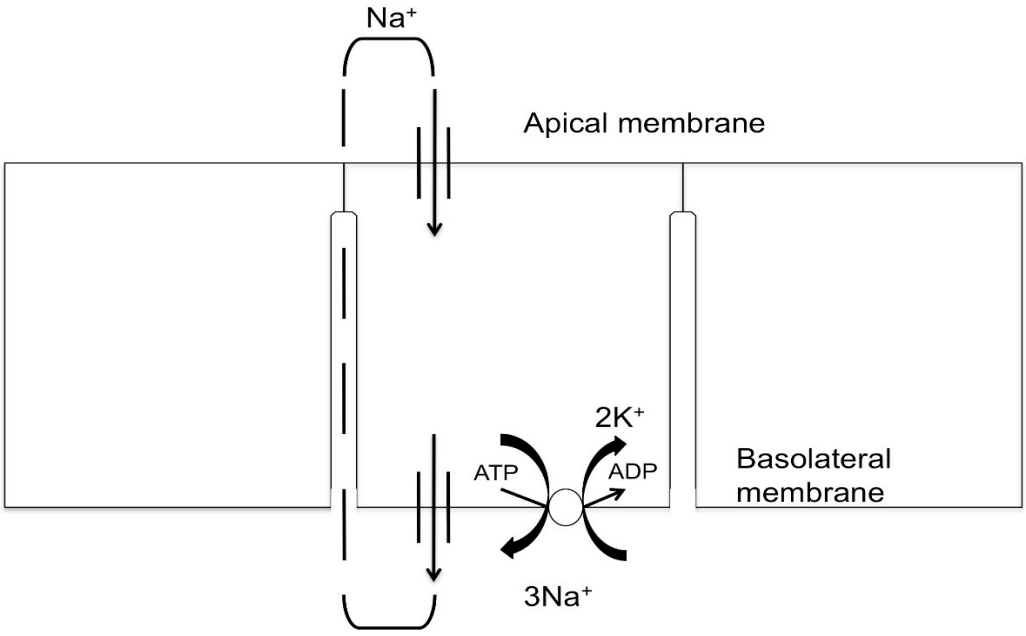

Figure 1.2 Diagram of epithelial cell monolayer with Na+ channels localised on the apical plasma memebrane and K+ channels localised on the basolateral membranes, along with the na+/K+-ATPase. The asymmetric distribution of ion channels generates a transcellular flow of positive current. This current flow generates a transepithelial potential that is positive on the basolateral side of the monolayer. figure adapted from (Nuccitelli, 2003).

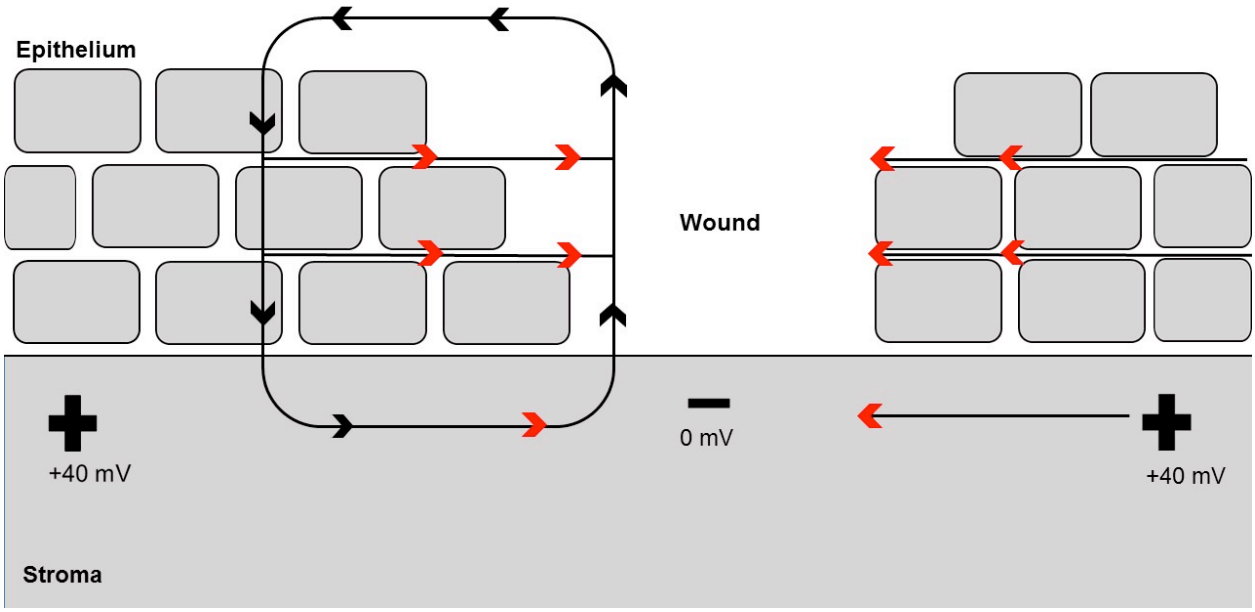

Figure 1.3 This figure shows the transepithelial potential [TEP] difference is 40 mV. When wounded, the TEP collapses to zero at the wound centre, but remains 40 mV distally where ion transport is unaffected. This voltage gradient establishes an electrical field (red arrows) that has a vector parallel to the epithelial surface and the wound centre as the cathode. Furthermore, leakage of Na+ and K+ ions out of the wound down its concentration gradient gives the physiological injury current; as indicate by the black arrows. Figure adapted from(McCaig et al., 2009)

1.4.2. GALVANOTAXIS IN STEM CELLS

As endogenous electrical fields play such an integral role in embryogenesis, it is not surprising that many stem cells and progenitor cells demonstrate galvanotaxis. The literature surrounding galvanotaxis in stems cells mainly focus around NSC or NPC although it has been described in iPS cells, adipose stem cells, mesenchymal stem cells, epidermal stem cells and endothelial progenitor cells (Li et al., 2012, Zhang et al., 2011a, Tandon et al., 2009, Tan et al., 2015, Zhao et al., 2012b).

Although the majority of galvanotaxis reports have shown migrational direction towards the cathode, this is not universally the case. The direction differs depending on cell type, species and can even be culture dependent. For instance, in neurites (rats) migration can be perpendicular to an electrical field(Rajnicek et al., 1992). Human IPS cells migrate to the anode but human ESC migrate to the cathode(Zhang et al., 2011a). Mesenchymal stem cells' response to an electrical field is dependent on number of passages, reversing directionality the higher the passage number (Tan et al., 2015). In NSCs and NPCs, direct current electrical fields guide migration towards the cathode in both adult and embryonic cells which has been shown in rodent and human(Li et al., 2008, Feng et al., 2012, Babona-Pilipos et al., 2011).

NSC migration has been studied for its potential therapeutic use in many neurological diseases such as stroke, Parkinson's and spinal cord injury. Their migratory ability facilitates cell migration into a damaged area. Indeed, electrical fields have been detected around damaged nerves in the spinal cord, suggesting that they play a major role in physiological CNS repair(Borgens et al., 1980, Zuberi et al., 2008). The mode of NSC migration under migratory cues has not been characterized in detail but Arocena et al. observed that they move in sequential short steps by extending protrusions(Arocena et al., 2010).

Migratory guidance cues for NSC other than electrical stimulation such as chemokines (eg. Stromal derived factor-1α/CXCR-4) also exist through chemotaxis; a mechanism differing from electrotaxis, and does not affect electrotaxis (Miller et al., 2008, Aguirre et al., 2005, Meng et al., 2012, Feng et al., 2012). However, biochemical guidance cues are difficult to manipulate and implement due to the complicated chemical gradients existing in vivo with the confounding factor of being less predictable or controllable to target injured tissue.

The interaction of chemical and electrotactic pathway is complex. It is thought to commence through polarized signalling molecules at the cell membrane which induce an asymmetric activation of signalling molecules and cytoskeleton leading to cell migration(Liu and Song, 2014). Molecules and signalling pathways reported to control electrotaxis include calcium and

sodium channels, cAMP, and several kinase cascades such as PI3K/Akt pathway (Mycielska and Djamgoz, 2004, Pullar et al., 2001, Zhao et al., 2006). Figure 1.4 summarises some of the known signalling network in electrotaxis.

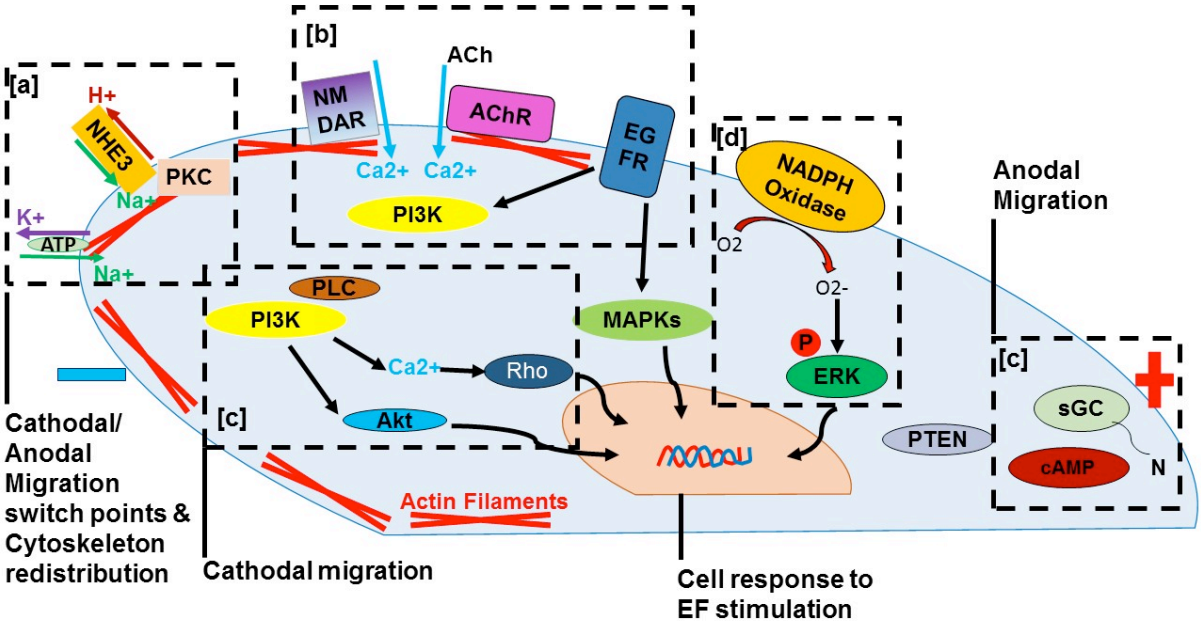

Figure 1.4 Summary of known signalling network in EF stimulated cells; adapted from Liu et al(Liu and Song, 2014). [a] The ion channels NaKA and NHE3 are considered a switch point of the cathodal/anodal migration. When the cell is exposed to EF, NaKA and NHE3 are reported to accumulate at the cathodal/anodal edge of the migration cell, depending on different cell types. This activation induces Na+ and Ca2+ influxes, which lead to formation of the ion gradient along/against the EF direction; ultimately this leads to cell depolarization and cytoskeleton redistribution(i.e actin, tubulin, myosin, etc) through intracellular signalling. NHE3 also induce cytoskeleton redistribution through complex with PKC and tubulin when treated with EF. [b] Cell membrane receptors also contribute towards ion influxes and signalling activation under EF stimulation. AChR and NMDAR both are reported to be activated at the cathodal pole of the EF and play a role in inducing Ca2+ influx and cell depolarization. EGFR may be activated in a ligand-independent manner to trigger downstream MAPKs and PI3K activation. This contributes to cytoskeleton redistribution and cellular responses through Ca2+ influxes and downstream effectors. [c] PI3K/AKT signalling pathway plays an important role in electrotaxis and other cellular responses. Post Ca2+ influxes and cell depolarization, PI3K and downstream effectors are found to accumulate and activate the leading edge of the electrotaxing cell. This plays an important role in EF-induced cathodal migration. The activated PI3K at the leading edge could initiate other cellular responses through Akt of combining with PLC to activate Rho through Ca2+. PTEN has been reported to downregulate at the cathodal side and show more activation at the anodal side. Apart from PI3K, the catalytic domains of sGC with GbpC are also involved in cell migration to the cathodal pole; while the N-domain of sGC and cAMP-activated pathways may contribute to mediate the anodal migration. [d] Other moleculesmay contribute in the signalling transduction during EF stimulation. i.e. NADPH oxidase activated to give superoxide, triggering upregulation of ERK phosphorylation, influencing cell response to EF.

1.5. RETINAL GANGLION CELL MORPHOLOGY: SHOLL ANALYSIS

Sholl analysis was first reported by DA Sholl in 1953 where he described the dendritic organization in the neurons of the cat's visual and motor cortices (Sholl, 1953). It is used to show the complexity of dendritic branching by analysing the number of branches intersecting with a distance from the soma; using a series of concentric spherical shells as co-ordinates of reference(Sholl, 1953). It is well established in neurobiology to quantify and analyse the complexity of neurite morphology. Use of Sholl analysis in the study of retinal ganglion cell morphology is also well reported (Rodger et al., 2012, Kalesnykas et al., 2012, Li et al., 2011, Williams et al., 2010, Gastinger et al., 2008, Qu et al., 2012). When done manually, it is a time consuming and laborious process. Hence, a range of computer-assisted programs have emerged to allow for a simpler method of data acquisition and analysis (Gutierrez and Davies, 2007, Longair et al., 2011, Schmitz et al., 2011).

Sholl analysis has been widely used to quantify RGC morphology. Diabetic morphological changes in RGC have been reported to have an increased density at certain distances from the soma, portrayed as a higher peak in a Sholl profile (Gastinger et al., 2008). Conversely, in optic nerve crush models and eyes subjected to acute IOP elevation a rapid decrease in the Sholl profile is reported(Li et al., 2011, Kalesnykas et al., 2012). Mechanisms exploring retinal ganglion cell degeneration in glaucoma models have also been reported using the area under the curve to analyse Sholl profiles(Qu et al., 2012). Furthermore, a comprehensive analysis of changes in morphology from long-term viral gene therapy included Sholl analysis(Rodger et al., 2012). All of these studies used a computer assisted program for Sholl analysis which was mostly from Image J, or MATLAB(Gastinger et al., 2008, Li et al., 2011, Rodger et al., 2012, Qu et al., 2012). In this thesis, I will validate four of the most commonly used semi-automated Sholl analysis programs against the manual method as it would form the basis of one of my latter experiments where I evaluate RGC morphology in retinal explants.

1.6. RETINAL EXPLANT VIABILITY

Adult organotypic retinal explant culture systems in rodents are well established. Retinal explants have been utilised as an in-vitro ocular stem cell transplantation model, to investigate neuroprotective therapies, pharmacological toxicity and laser retinal applications (Johnson and Martin, 2008; Schlichtenbrede et al., 2009; Wood et al., 2011(Manabe et al., 2002). In-vivo work involves intravitreal injection of drugs of which precise drug concentrations cannot be controlled in comparison to in-vitro studies(Manabe et al., 2002). In-vitro culture of dissociated retinal cells causes loss of its normal morphological features. Retinal explant culture systems allow the maintenance of cell-to-cell interactions in normal cellular architecture and is relatively easy to establish compared to dissociated retinal cell cultures(Zhang, Fu and Barnstable, 2002). Furthermore, it is an easily accessible part of the central nervous system (Becker et al., 1998), not only in ophthalmic research but also as a CNS disease model and development outline (Zhang et al., 2002).

However, use of retinal explants as a therapeutic test platform is critically dependent on the duration of its viability in culture. In rodents this has been reported to be sustained for up to two weeks in adult rats (Johnson and Martin, 2008). Viability extending further than this have also been described in neonatal rodent explants but neonatal biology differs from that of an adult, and in RGC apoptosis is age-dependent(Guerin et al., 2011)

Efforts towards prolonging retinal ganglion cell survival through extrinsic neuroprotective therapies have been promising(Martin et al., 2003). Indeed, adult rat retinal explant culture models have been utilized to screen for potential retinal ganglion cell neuroprotective therapies (Bull et al., 2011, Guerin et al., 2011, Manabe et al., 2002). To assess retinal ganglion cell survival, histological analysis of the retinal ganglion cell layer is often used (Caffe et al., 2001; Johnson and Martin, 2008). Most reports have assessed retinal ganglion cell neuroprotection through nuclei counts in the retinal ganglion cell layer, whereby overestimation of RGC survival is likely to occur(Bull et al., 2011, Guerin et al., 2011) as microglia have been reported to engulf dead RGC especially when labelled with DiI(Thanos, 1991). Measured variables required ex-vivo explants to be cultured for at least 4 days before sufficient cell death had occurred to detect any neuroprotection conferred by therapy(Bull et al., 2011; Froger et al., 2012). Once explanted, histology of the retina is limited by tissue oedema, rapid degeneration of outer segments and thinning of retinal layers (Kaempf et al., 2008). The need to culture explants for 4 days before neuroprotection can be observed is not only time consuming, but imposes the confounding factor of increased inaccuracies with increasing culture time. There is a need for a more sensitive and quicker read-out for reporting neuroprotective effect in RGC.

The cell death/survival of RGC is often taken as an outcome measure. Morphological differences in RGCs in retinal explants over time have not been analysed. In our search for therapeutics that specifically retard retinal ganglion cell death, the window of opportunity for targeting healthy RGC needs to be demarcated. In this thesis, I will determine the viability of the retinal explants by assessing the morphology of RGCs diolistically dyed by DiI. Prior to using retinal explants as my test bed for EF directed migration, it is essential to demarcate its viability as the period of EF application necessary for migration into the retinal explant is unknown.

AIMS AND OBJECTIVES

The main aim of this thesis is to assess methods of delivering neuroprotection to the retina i.e. by magnetofection of ocular tissue or by directing migration of neurospheres into the retina from the inner layer to the outer layer by galvanotaxis, acting as a vector for neuroprotection delivery.

The basis of my experiments will be performed on a retinal explant, a validated organotypic culture method commonly used. In chapter 3, I will outline the explant's viability to include the health of the retinal ganglion cells. This will be performed with Sholl analyses. My choice of a semi-automated Sholl analysis programme will be based on the one that compares best with manual calibration.

In chapter 4, I will explore a non-viral gene transfer technique (magnetofection with oscillation) in ocular tissue such as cornea and retina as a proof of concept for future gene transfer application including the delivery of neurotrophic growth factors. Although viral gene transfer is currently the most efficient, it comes with disadvantages of a limited cargo size, immune reactions and incorporation of genetic material into host DNA. Hence, I opted for a non-viral approach that I will test on ocular tissue (the cornea and the retina) for future in-vivo application and also for transfecting neural stem cells with BDNF-myc prior to directing their migration into the retina.

Several barriers exist to impede stem cell migration into the retina, notably physical barriers of the inner limiting membrane and extracellular matrices. Galvanotaxis in stem cells is widely studied but its use in the retina has yet to be explored. In chapter 5 of this thesis, I will briefly demonstrate and replicate the published galvanotactic properties in neural stem cells. In chapter 6, I will assess the ability of galvanotaxis to direct migration into the retina in an explant model and optimize its parameters for voltage and duration. In chapter 7, I will proceed to demonstrate that magnetofected neurospheres that overexpress BDNF can be directed into the retina by galvanotaxis.

CHAPTER 2 MATERIALS AND METHODS

2.1 ANIMAL HUSBANDRY

Handling and euthanasia of animals were handled in accordance to the regulations formulated by the Home Office of the United Kingdom (Animal Welfare Act 2006) and in compliance with the ARVO Statement for the Use of Animals in Ophthalmic and Vision Research.

2.2 SUMMARY OF FLUORESENCE MICROSCOPY

A summary of laser excitation wavelengths and emission filters used are summarized in Table 3.

Label	Laser Excitation (nm)	Laser Filter Emission (nm)
TOPRO-3	633	630-750
GFP	488	500-550
FITC	488	500-550
DiI	488	500-550
Myc	543	610-720
DAPI	405	440-550
Nestin	543	550-620
Ethidium Bromide	543	550-620
β3-Tubulin	638	655-695

Table 3 Summary of laser excitation and emission filter wavelength settings for confocal imaging of labels used.

2.3 RETINAL EXPLANT CULTURE

2.3.1 PREPARATION OF RETINAL WHOLE MOUNTS

Adult C57BL/6 male and female mice (P36-73) were killed by cervical dislocation. Both eyes were immediately enucleated and immersed in ice-cold HBBS containing penicillin (100 U/mL) and streptomycin (100 µg/mL). A paralimbal circumferential incision was made under an operating microscope to remove the anterior segment, lens and vitreous body. The residual cup of the posterior segment was carefully inverted with fine forceps allowing for the detachment of the retina away from the pigment epithelium. Efforts were made to minimise instrumental contact with the inner retina. The optic nerve head was then severed, separating it from the retina. The retina was segmented into three equal sized pieces and separately transferred onto 30-mm diameter filters (0.4 µm pore, Millipore; Millicell Inc., Cork, Ireland) with the RGC layer facing up (see Figure 2.1).

The filters were placed into a well plate containing 1200µL of retinal explant media. This consisted of a neuronal growth medium (Neurobasal A) supplemented with 2% B27 (Invitrogen Ltd.), 1% N2 (Invitrogen Ltd.), L-glutamine (0.8mM), penicillin (100 U/mL), and streptomycin (100 µg/mL). The culture medium selected was based on Johnson et al 2008 (Johnson and Martin, 2008) which showed superiority of non-serum based media in rodent retinal explant culture viability. Retinal explant culture mediums were maintained at 34^0C and 5% CO^2. Culture media were changed on day ex-vivo (DEV) 1 and daily thereafter.

Figure 2.1 Retinal explant segmented into three placed on filter, retinal ganglion cell layer side up. Scale bar:1mm

2.3.2 DIOLISTIC LABELLING OF RETINAL GANGLION CELLS

Two hundred milligrams of Tungsten (Tu) particles (0.7 μm in diameter Tungsten Microcarriers, Bio-Rad, UK) were spread on a clean glass slide. Two milligrams of 1,1'-dioctadecyl-3,3,3',3'-tetramethyl-indocarbocyanine perchlorate (DiI, Molecular Probes N-22880, Eugene, OR) was dissolved in 200μl of methylene chloride and applied over the tungsten particles on the glass slide. After the methylene chloride had evaporated, the tungsten particles were coated with DiI and formed a thin film across the surface of the glass slide. The dye coated tungsten particles were scraped off with a clean razor blade and the fine powder was funnelled into a clean BioRad tubing. Parafilm was applied to each end and the tubing was vortexed overnight to ensure that particles stuck to the tubing wall and were dispersed throughout the tubing in a uniform manner. This was done in a dark room. A Helios gene gun system (Bio-Rad, Hertfordshire, UK) was used for diolistic labelling of the retinal neurons. The DiI/Tu particles were propelled into the retina at a delivery pressure of 100 psi, held at a set distance of 5cm above the retina through a 3.0 μm filter (BD Falcon ™ 3.0μm Cell Culture Inserts PET Membrane) to block any large clumps of tungsten particles (Figure 2.2).

Figure 2.2 Gene gun positioned 5cm vertically over a retinal explant culture separated by a 3.0micron filter (Falcon BD)

2.3.3 NUCLEAR STAINING AND IMAGE ACQUISITION

After 30 minutes of incubation with dye particles, the retinal explants were fixed in 4% PFA in PBS at room temperature for 10 minutes. For nuclear staining, retinas were washed with PBS, followed by incubation with diluted DNA dye TO-PRO-3 (Invitrogen, Carlsbad, CA) 1:1000 in distilled water for 10 minutes. After a further PBS wash retinal explants were then mounted with an antifade reagent (ProLong Gold, Invitrogen). Image stacks (1µm steps) of RGCs were acquired using a Zeiss LSM 510 confocal microscope (Carl Zeiss Ltd, UK) captured at 20x objective. RGCs were identified based on their morphological appearance based according to Sun et al.(Sun et al., 2002) and the presence of an axon. TO-PRO-3 served as a nuclear counter stain as well as a guide for identification of the retinal cell layers.

2.3.4 PRODUCTION OF SHOLL ANALYSIS AND MANUAL CALIBRATION OF AUTOMATED SHOLL PROGRAMMES

Dendritic complexities were analysed by Sholl analysis profiles. Firstly, RGC image stacks were manually traced in 3D using the FIJI plug-in Simple Neurite Tracer. The RGC axons were identified and excluded from tracings. The tracing produced a Z-compressed 8-bit trace image which was used by all 4 programs under investigation.

FIJI is a distribution of Image J which supplements it by supporting the installation and maintenance of its plug-ins. It is popular due to its robust distribution system for multiple image processing plug-ins and is a non-commercial open access software. Indeed, the FIJI project has achieved international recognition and is used in every major academic research centre throughout the world (Schindelin et al., 2012). Manual calibration of FIJI plug-ins for Sholl analysis has not been performed. MATLAB SYnD(Schmitz et al., 2011), MATLAB Bonfire(Langhammer et al., 2010), MATLAB FastSholl(Gutierrez and Davies, 2007) programs have been scientifically or manually validated. MATLAB is a commercial software, and hence its use is limited by cost.

Individual Sholl profiles were produced for every RGC tracing by the 4 programs under investigation: FIJI plug-in: Simple Neurite Tracer, FIJI plug-in: Bit Map Sholl Analysis, FIJI plug-

in: Ghosh Lab Sholl analysis and Fast Sholl MATLAB script. These four Sholl profiles were then compared with a Sholl profile produced from manual counts which was considered as the gold standard. Sholl profiles produced from manual counts were generated by superimposing overlays of 10μm radius concentric rings centred on the RGC soma and counting the number of dendrites intersecting each concentric ring (see Figure 2.3) up to 500μm.

To reduce single observer bias, two observers (WSN, KB) were used to dissect retinal explants, acquire, trace and manually calibrate RGC images. To quantify observer effects, intraclass correlation coeffeciencies [ICC] using a two-way mixed effect model from average measures were calculated for the two assessors at 95%CI on 10 RGC manual calibrations to show any discrepancies between assessors. Area under the curve [AUC] for all programs including manual counts was calculated. The percentage difference between the AUC for the manual count Sholl profile and the four programs were analysed. Bland-Altman plots were calculated to measure the agreement between the four programs with the "gold standard" manual count Sholl profile. Statistical analysis was carried out by Microsoft Excel (Office 2010) and IBM SPSS statistics (version 20).

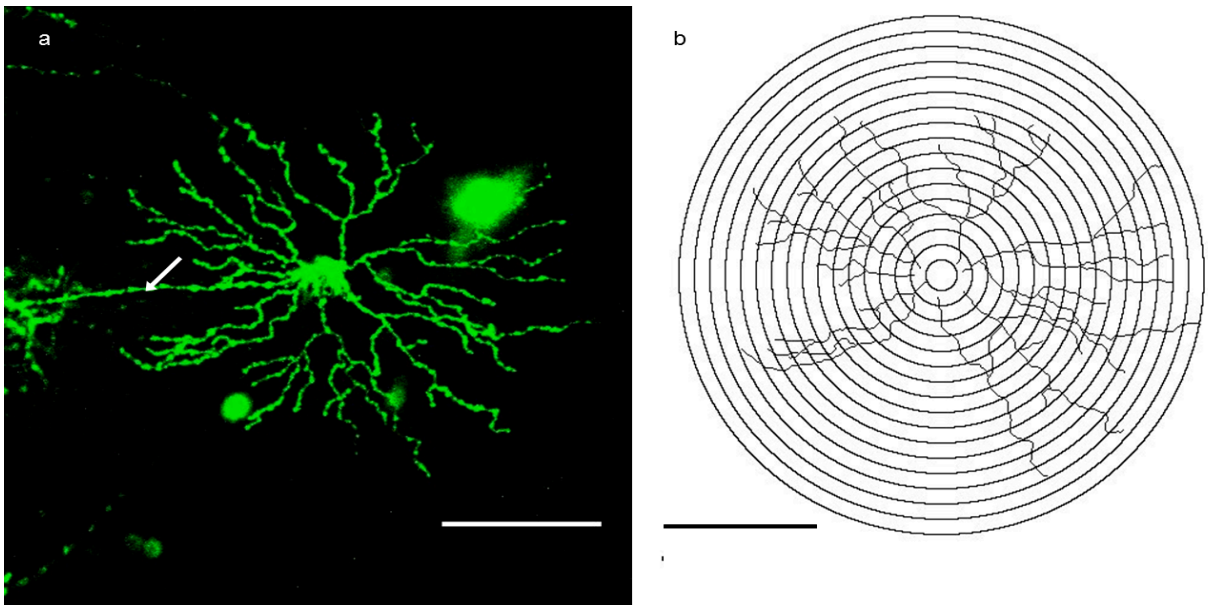

Figure 2.3 A) A confocal image of a DiI stained retinal ganglion cell. Axon shown by white arrow. B) The corresponding manual tracing of retinal ganglion cell in [A] with an overlay of incremental 10 micron radius rings. Scale bar: 100 micron.

2.3.5 RETINAL TISSUE PROCESSING, HISTOLOGY AND IMMUNOHISTOCHEMISTRY

Retinal explants were fixed with 4% PFA for 24 hours at 4^0C. They were then cryoprotected in 30% sucrose for 24 hours at 4^0C before being embedded in OCT, frozen and stored at -20^0C. Cryosections were cut at 14µm and transferred onto microscope slides (Superfrost, Fisher Scientific, Pittsburgh, PA). Sections were stained with nuclear stain Topro-3 (1:1000) before being mounted with antifade reagent (ProLong Gold;Invitrogen). Images were acquired using a Zeiss LSM 510 confocal microscope (Carl Zeiss Ltd, UK) at 20x magnification. Retinal structure was quantified by inner nuclear layer thickness, outer nuclear layer thickness and retinal ganglion cell nuclei per mm. Values were taken from a mean of three areas within a single cryosection sample. Explants were cultured for up to 14 days to assess retinal layer architecture.

2.3.5.1 TUNEL LABELLING

Cryosection samples were washed in PBS for 30 minutes at 37^0C. TUNEL Apoptosis Detection Kit (Merck Milipore, UK) was used according to manufacturer's the instructions. Protein K solution was made by diluting 1:24 PBS. Sections were then covered in diluted Protein K solution for 30 minutes at 37^0C and then washed with distilled water for 2 minutes 4 times. TdT buffer was then incubated with sections. A cocktail of TdT end-labelling cocktail was then made at a ratio of 90:5:5 with TdT Buffer, Biotin-dUTP and TdT respectively. Sections were incubated with 50µl of the cocktail for 60 minutes at 37^0C. The reaction was stopped by immersing sections in TB Buffer diluted in distilled water (1:9) for 5 minutes at room temperature. A wash was then applied with distilled water 4 times for 2 minutes. 50µl of blocking buffer (Blocking Solution diluted 1:3 with PBS) was applied to the sections and incubated at room temperature for 20 minutes. 50µl of Avidin-FITC solution (1:9 dilution with blocking buffer) was incubated with sections for 30 minutes in the dark. Sections were washed with PBS twice over 15 minutes in the dark. The sections were cover slipped and viewed by Zeiss LSM 510 confocal microscope (Carl Zeiss Ltd, UK) captured at 20x magnification under FITC settings. Positive controls were done with the above method using mouse spleen as the test sample.

2.3.5.2 CALCEIN-AM LABELLING OF RETINA EXPLANTS

Retinal explants were labelled with calcein-AM (Biotium, Inc., CA, USA) 10μM in PBS applies as 200μl topical aliquots for 30 minutes at 37^0C. Explants were washed three times with PBS and counterstained with TOPRO-3 prior to mounting. Z-stacked images of 1 micron thickness were captured by Zeiss LSM 510 confocal microscope (Carl Zeiss Ltd, UK) at 20x magnification under FITC settings through the entire GCL at four quadrants of the retina. Cell viability was calculated by counting the average fluorescent cells in a 100 μm^2 square per image frame captured in each quadrant of each explant and described as Calcein-positive cells per mm^2.

2.3.6 BDNF TREATMENT OF RETINAL EXPLANTS

Retinal explants were incubated with 100 ng/ml BDNF (Regeneron/Amgen) diluted in PBS and 0.1% BSA at day 0 ex-vivo for 3 days. Controls had no BDNF treatment but were cultured as per section 2.1.1. for 3 days. Diolistic labelling of RGCs and image capture are as described above. Sholl profiles were analysed and AUCs were calculated using the trapezoidal rule and compared.

2.4 MURINE EMBRYONIC NEURAL STEM CELL (NSC) ISOLATION AND CULTURE

Meninges were isolated from embryonic E12-E14 C57/Bl6 murine cortices into ice cold DMEM/F-12 media containing 1% penicillin-streptomycin. After tissue digestion in accutase at 37^0C for 10 minutes, isolated cells were centrifuged at 1300rpm and resuspended in NSC media (50ml DMEM/F-12 media and 1% penicillin-streptomycin supplemented with 20 ng/ml FGF-basic Recombinant Human (Invitrogen), 20 ng/ml EGF Recombinant Human (Invitrogen) and 1 ml B27 supplement liquid) and incubated at 37^0C, 5%CO2. GFP-positive NSC were produced according to the above method but using GFP transgenic mice (gift from Keele University).

Cells were passaged every 4-5 days with 300 μl of accutase for 3 minutes and kept in 12 mls of media in T25 flasks for culture at 37^0C, 5%CO2. Experiments involving NSCs were taken from P7 up to P25.

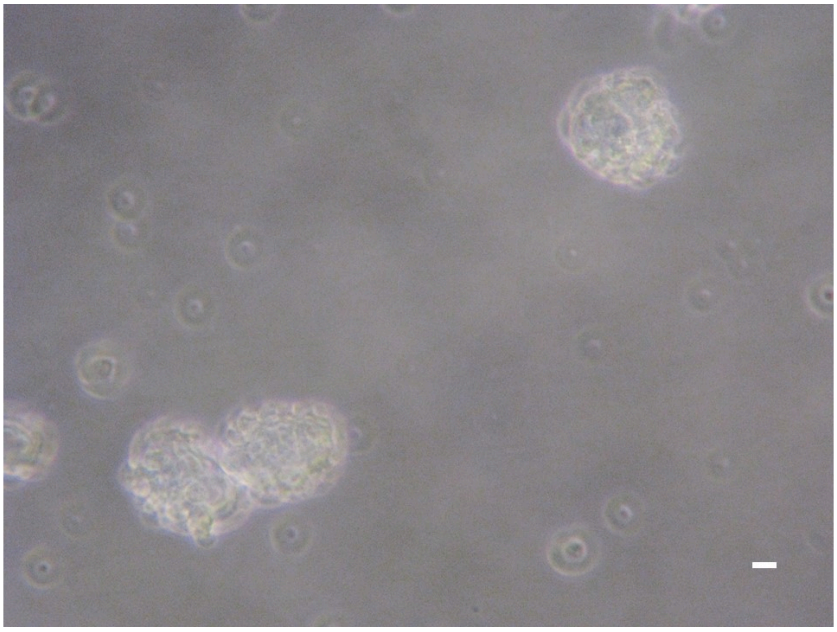

Figure 2.4 Light microscopy showing mouse neurospheres in culture amongst some single cells in media. Scale bar: 100μm

2.5 MURINE CORNEA EXPLANT PREPARATION AND CULTURE

To test magnetofection as a technique of gene delivery in ocular tissue, cornea explants were used to demonstrate its potential use in the anterior segment of the eye. Corneas are easily accessible and its transparent but robust properties make it ideal as a test bed for magnetofection in the anterior segment of the eye.

Corneas were obtained from adult C57Bl6 mice. Animal were killed by cervical dislocation and cornea cups were rapidly dissected out and placed endothelial side up in a well of a 24-well culture plate and immersed fully in 1 mL Dulbecco's modified Eagle's Medium (DMEM) with 25 mM glucose (Invitrogen-Gibco, Rockville, MD), supplemented with 2% fetal bovine serum (FBS), penicillin G (100 U/mL), and streptomycin (100 µg/mL). Half of the culture medium was exchanged daily and incubation was kept at 37^0C and 5% CO2.

2.6 COS-7 CELL CULTURE

COS-7 cells were obtained from a stock cell line in School of Dentistry, Cardiff University. Cells were thawed from N_2 storage in media (DMEM supplemented with 10% Fetal Bovine Serum, 1% glutamine and 1% peniciliin and streptomycin). This was centrifuged at 1500rpm for 5 minutes and the supernatant was discarded. Cells were resuspended in fresh media and cultured in T75 flasks. The media was changed the following day and passaged every 3-4 days after. The passage of cells was performed with 0.25% trypsin (2 minutes) to release adhered COS-7 cells. Media with free-floating cells were then centrifuged at 1500 rpm for 5 minutes and supernatant was discarded. Cells were resuspended in fresh media and cultured in T75 flasks at 37^0C and 5% CO_2.

2.7 PLASMID PREPARATION

2.7.1 TRANSFORMATION REACTION AND MINIPREP

Ten LB agar plates were made with 8g LB agar powder dissolved in 250 ml distilled water in a 500 ml glass dewar. The mixture was heated for 20-30 seconds with a loose lid to allow for all LB agar powder to dissolve in the solution. This was autoclaved for 20 minutes and left to cool

to 50^0C. 500 µl of antibiotics [40 mg/ml ampicillin for CAG-GFP and BDNF-myc plasmid minipreps and 10 µg /ml kanamycin for CBA-GFP plasmid] was added to the LB agar solution. The solution was poured into ten plates to 5 mm thickness and distributed evenly. Agar plates were left to cool with lids slightly off for 20 minutes then flipped to avoid condensation. These are sealed with parafilm and stored at 4^0C.

25 µl of DH5α competent cells and 1µl of plasmid were defrosted on ice for 2 minutes and pipetted out gently. These were mixed together in an autoclaved eppendorf and stood on ice for 30 minutes. A heat shock to allow for plasmid uptake was carried out in by placing the eppendorf in a 42^0C water bath for 30 seconds. 50 µl of Super Optimal broth with Catabolite Suppression (SOC) was then incubated with the mixture for 60 minutes at 37^0C on an orbital incubator shaker. Using a sterilised glass spreader, the solution was plated onto the agar plates, inverted, sealed and incubated at 37^0C for not more than 10-17 hours to prevent excessive colony growth.

LB broth (2g LB Broth base powder dissolved in 100 ml distilled water) was autoclaved for 25 minutes at 120^0C and 200 µl of 40 mg/ml ampicillin was added when cooled. This was split between 10 bottles of T75 culture flasks. Colonies were carefully selected with a 10µl pipette tip and dropped into the prepared culture flasks. The flasks were incubated overnight in an orbital incubator shaker at 37^0C.

5 mls of culture solution was removed and underwent miniprep (Qiagen Spin Miniprep kit, Qiagen Dorking UK) as per manufacturer's instructions. Plasmid solutions were measured for dsDNA concentration using a NanoVue spectrophotometer and a Picodrop Microliter system.

2.7.2 VALIDATION OF GFP PLASMIDS USING COS-7 CELLS

The choice of plasmid for the evaluation of the magnetofection technique was based on validation by lipofection with COS-7 cells. Plasmid DNA encoding CAG promoter, green fluorescent protein (GFP) reporter (Addgene) and plasmid DNA encoding chicken beta actin (CBA) promoter, GFP reporter (Oxford Genetics) was multiplied and purified from Escherichia coli using the Qiaprep Spin Miniprep kit (Qiagen, Dorking, UK) [see figure 2.5 and 2.6 for construct maps].

COS-7 cells were seeded to 90% confluence on a 96 well overnight and transfected with the Lipofectamine® 2000 kit (Life Technologies) as per manufacturer's protocol. 25µl of Opti-MEM® media was used to dilute 1µl of Lipofectamine® 2000 reagent. 1µg of plasmid was diluted in 125µl of Optim-MEM® media individually. Diluted DNA were added to diluted

Lipofectamine® 2000 reagent on a 1:1 ratio and incubated for 5 minutes at room temperature. DNA-lipid complexes were added to COS-7 cells and incubated for up to 3 days with daily media exchange. Images of transfected cells were acquired at 20X objective by DeltaVision Microscopy Imaging System (Image Solutions, Preston) on FITC settings.

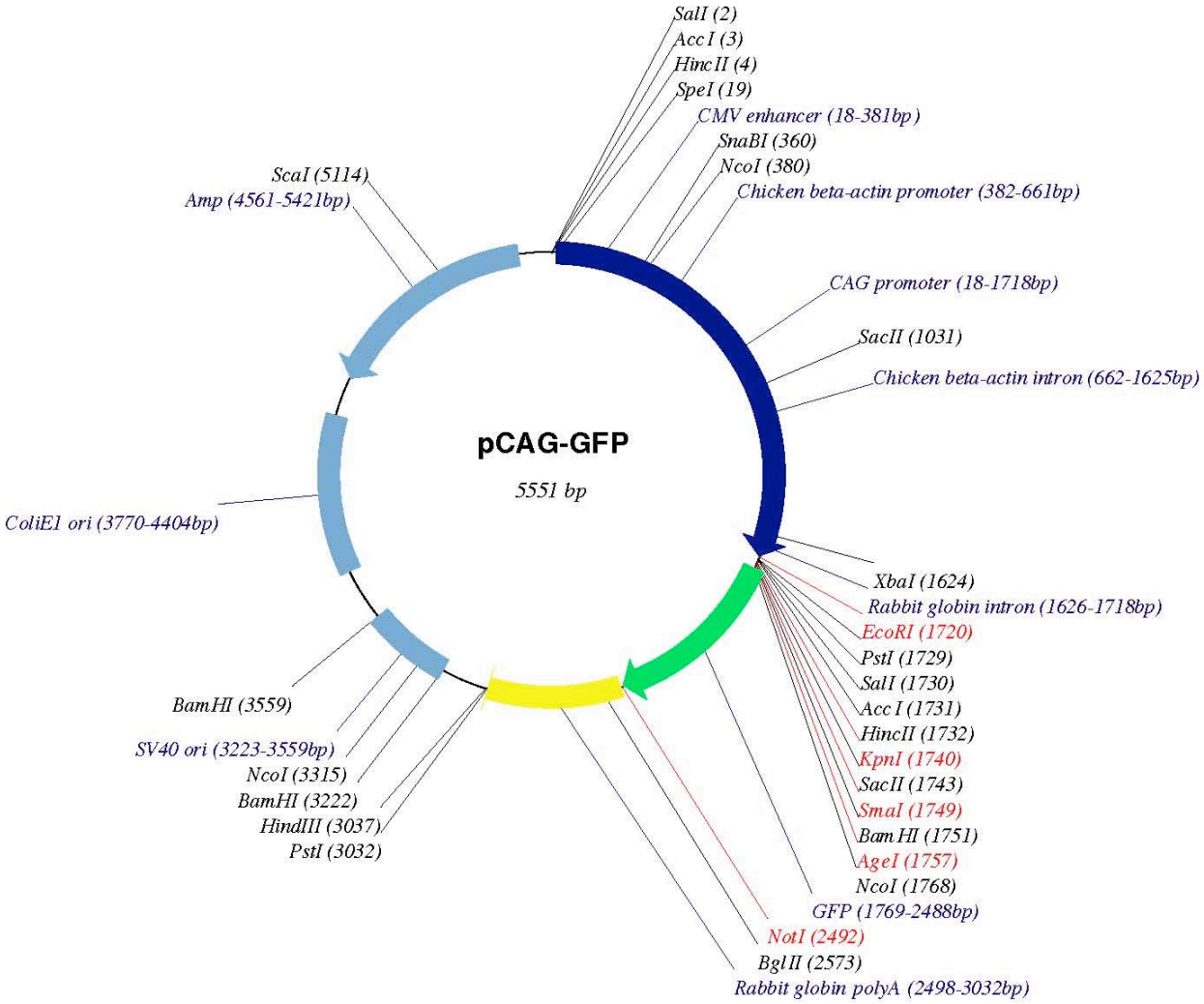

Figure 2.5 Construct map for pCAG-GFP (Addgene)

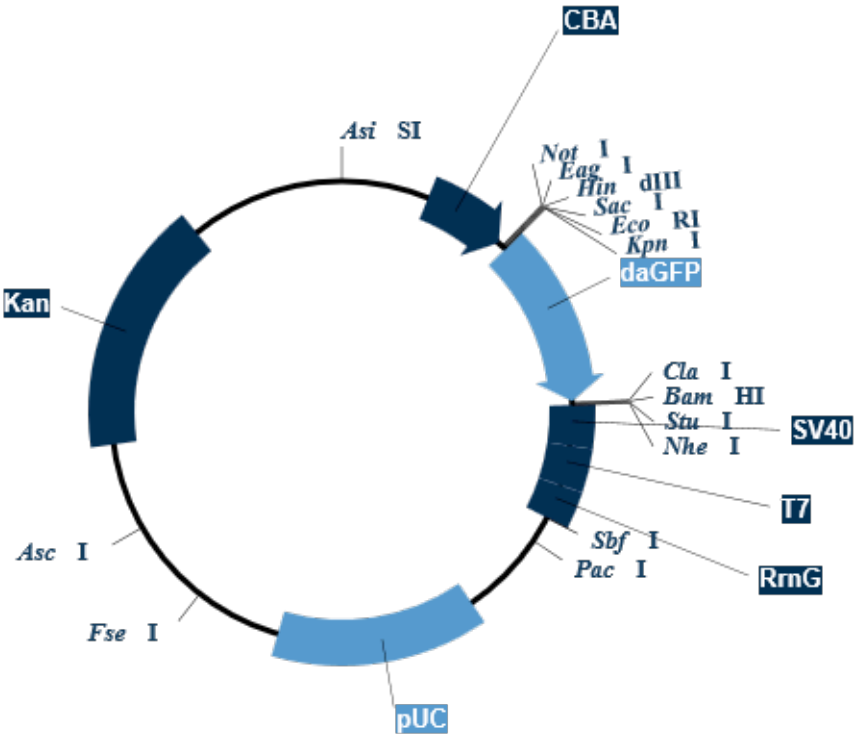

Figure 2.6 Construct map for CBA-GFP (Oxford Genetics)

2.7.3 SEQUENCING OF BDNF-MYC PLASMID

Post transformation and mini prep, BDNF-myc plasmids were sent to CBIB DNA Core[https://dnacore.mgh.harvard.edu/new-cgibin/site/pages/complete_plasmid_sequencing_main.jsp;jsessionid=AA353FB9A13D09A2B9BD3EDD418A8414] as a 35µl alliquot of 70ng/µl in buffer EB solution (10mM Tris-Cl, pH8.5; QIAprep©) at room temperature for sequencing (Figure 2.7 shows construct map for BDNF-myc plasmid).

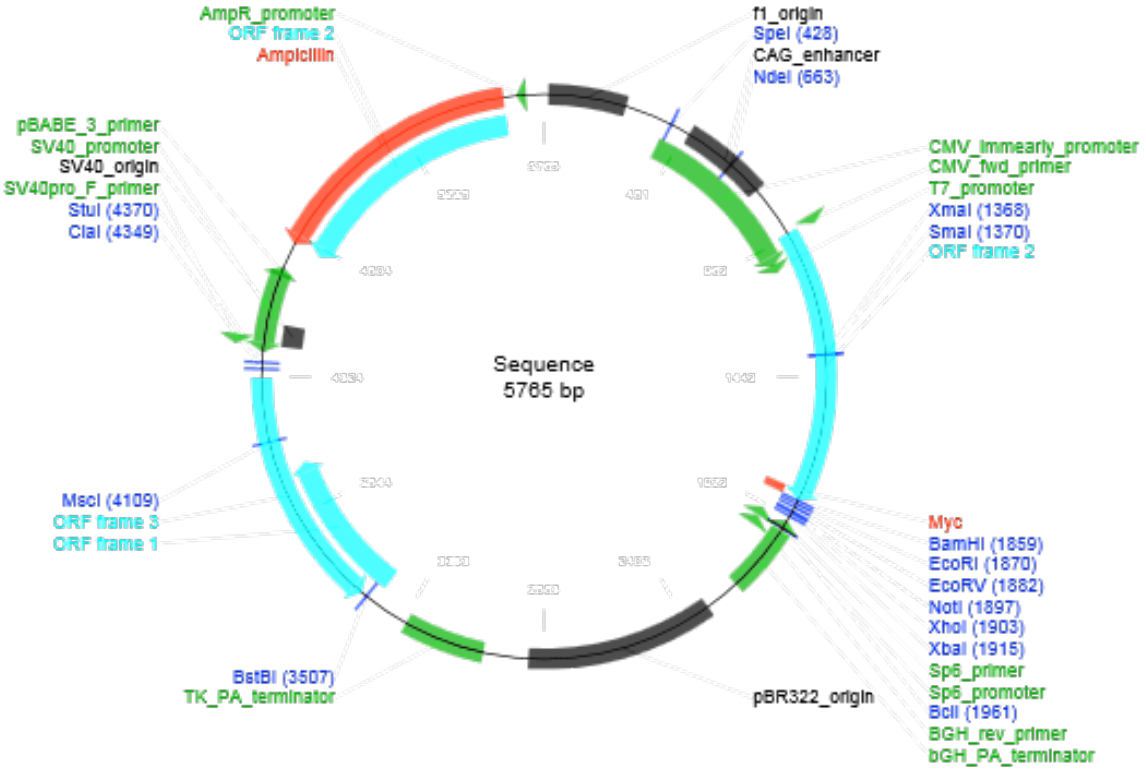

Figure 2.7 Construct map for BDNF-myc plasmid. (gift from Prof Yves-Alain Barde, Cardiff University)

2.7.4 VALIDATION OF BDNF-MYC PLASMID WITH COS-7 CELLS

To validate the plasmids after mini prep, plasmids were validated by COS-7 cell transfection. COS-7 cells are derived monkey kidney tissue. They were used as they are robust and can be cultured easily. These cells were seeded to 90% confluence on a 96 well overnight. COS-7 cells were transfected with the Lipofectamine® 2000 kit (Life Technologies) as per manufacturer's protocol. 25µl of Opti-MEM® media was used to dilute 1µl of Lipofectamine® 2000 reagent. 1µg of BDNF-myc was diluted in 125µl of Optim-MEM®. Diluted DNA was then added to diluted Lipofectamine® 2000 reagent on a 1:1 ratio and incubated for 5 minutes at room temperature. DNA-lipid complexes were added to COS-7 cells and incubated for 24 hours before being processed for myc labelling (see 2.8.7). Controls experiments were cells that were not magnetofected.

2.8 MAGNETOFECTION WITH OSCILLATION

2.8.1 MAGNETOFECTION OF COS-7 WITH CAG-GFP

To prove that the magnetofection technique was applicable to cells, COS-7 cells were transfected with CAG-GFP and CBA-GFP. COS-7 cells were seeded to 90% confluence on a 96 well overnight. Paramagnetic 100nm nTMAG-nanoparticles (nanoTherics Ltd., Stoke-on-Trent, UK) were used as the transfection vehicle. These consisted of a magnetite with a mean core diameter of 65-75nm coated with a positively charged polymer (Zeta potential +23.14mV) in an aqueous suspension. nT-MAG particles and plasmid DNA; (CAG-GFP and CBA-GFP separately), were mixed in serum-free media at room temperature for 15 minutes to form nTMAG-DNA complexes. They were then added to serum-free media of plated COS-7 cells. An oscillating magnetic field of 2Hz was applied from beneath the well using the Magnefect Nano II (nanoTherics Ltd., Stoke-on-Trent, UK) system and a 96 magnet array, compatible with 96 well plates. Cells were left in culture for 3 days and images of transfected cells were acquired at 20X objective by DeltaVision Microscopy Imaging System (Image Solutions, Preston) confocal microscope using FITC settings.

2.8.2 MAGNETOFECTION OF CORNEA EXPLANT WITH CAG-GFP

nT-MAG particles and plasmid DNA; CAG-GFP (Plasmid with better transfection efficiency), were mixed in serum-free media at room temperature for 15 minutes to form nTMAG-DNA complexes. This was then added to serum-free media cornea cultures in a 96 well plate with the corneal endothelium side up. A magnetic field was applied from beneath the well on the epithelial side using the Magnefect Nano II (nanoTherics Ltd., Stoke-on-Trent, UK) system and a 96 magnet array (NdB magnet 0.4T) compatible with 96 well plates [see figure 2.8 for experiment setup]. The magnet applied had an oscillatory horizontal displacement of 2mm distance in a sinusoidal wave form which can be adjusted from 0Hz to 5Hz. Following magnetofection, corneas were cultured in media supplemented with 2% FBS for three days prior to confocal microscopy with daily media exchange. Each experimental condition was triplicated.

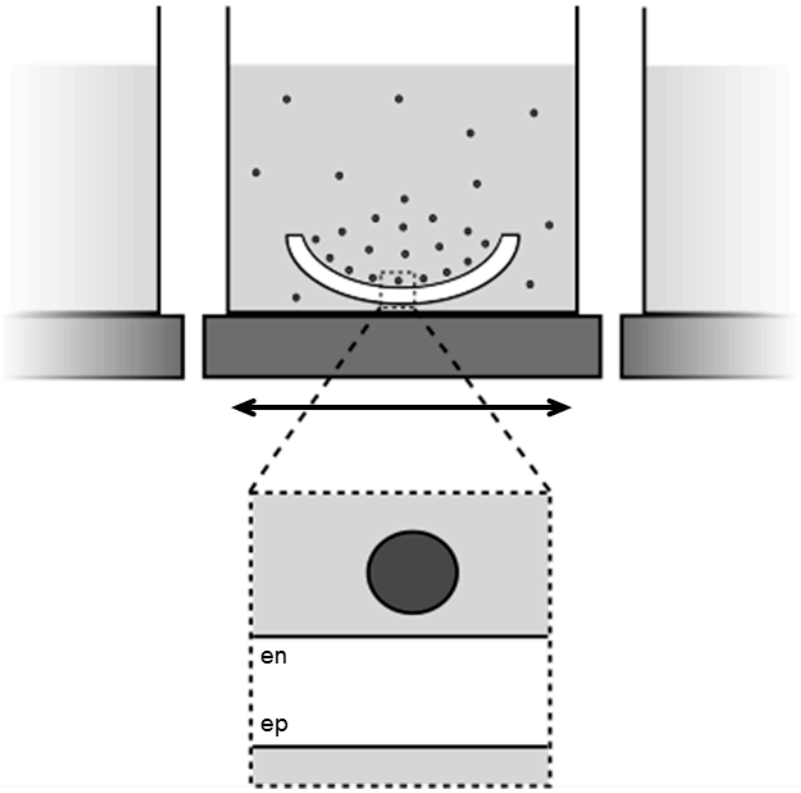

Figure 2.8 Experiment setup with dissected cornea; endothelium (en) side up, immersed in a solution of serum-free media and nTMag-DNA complex with a 2mm horizontal displacement oscillating magnetic field(0.4T) applied from beneath the cornea cup.

2.8.2.1 FLUORESCENCE MICROSCOPY AND DATA ANALYSIS

Following incubation for three days at 37□C and 5% CO2, transfected corneal specimens were fixed in PFA followed by counterstain with TO-PRO 3 (1:1000; Invitrogen) for 10 minutes with three phosphate buffered saline (PBS) washes post-stain. Specimens were then mounted; cornea endothelium side up, on a slide with ProLong Gold AntiFade Reagent (Invitrogen). A confocal laser scanning microscope (Zeiss LSM 510, Carl Zeiss Ltd, UK) was used to capture corneal images at 20x objective for GFP expression at 1µm intervals. The image subtended 394 by 394 µm (512 by 512 pixels, 8 bits per pixel). Control experiments (corneas cultured in nTMag and CAG-GFP complexes in the absence of an external magnetic field) were used to calibrate settings on the confocal microscope in order to reduce background fluorescence. GFP-positive cells were counted manually using the FIJI plug-in, Cell Counter. Transfection efficiency was estimated as the percentage of GFP-positive cells per total cells in the microscopic field. The cornea layers were identified according to change in morphological appearances on TO-PRO stain. Endothelial and epithelial layers were separated by sparsely distributed, larger keratocytes in the stromal layer. The endothelium was seen as a single layer of regularly spaced small cells and epithelium consisted of multilayered, closely spaced sheets of cells.

2.8.2.2 CORNEA TISSUE CRYOSECTION

Corneal explants were fixed with 4% PFA at 4^0C for 2 hours. They were then cryoprotected in 30% sucrose for 24 hours at 4^0C before being embedded in OCT, frozen and stored at -20^0C. Transverse cornea cryosections were performed at 14µm and transferred onto microscope slides (Superfrost, Fisher Scientific, Pittsburgh, PA). The sections were stained with nuclear stain TOPRO-3 before being mounted with antifade reagent (ProLong Gold; Invitrogen). Images were acquired using a Zeiss LSM 510 confocal microscope (Carl Zeiss Ltd, UK) captured at 20x magnification under FITC settings.

2.8.2.3 TUNEL LABELLING

Corneal cryosection slices were thawed at room temperature and allowed to dry for 30 minutes. Sections were then washed with PBS for 30 minutes. TUNEL reaction mixture was prepared by mixing 50 µl Enzyme Solution to 450 µl Label Solution as per manufacturer's instructions, [In Situ Cell Death Detection Kit, Fluorescein (Roche)]. Slides were incubated with Permeabilisation solution (0.1 % TritonX-100 in 0.1 % sodium citrate freshly prepared) for 2 minutes on ice.

TUNEL reaction mixture was then incubated with cryosections for 60 minutes at 37^0C in the dark. It was then washed with PBS thrice before counterstained by TOPRO-3 (1:1000). Positive controls were incubated with DNAse 1 recombinant for 10 minutes prior to incubating with TUNEL reaction solution. Negative controls were incubated in Label solution alone without Enzyme solution. Three images per cornea section was captured. Images were captured with a confocal laser scanning microscope (Zeiss LSM 510, Carl Zeiss Ltd, UK) at 20X objective for TUNEL staining under a FITC channel and for TO-PRO-3 stained nuclei. Apoptotic TUNEL positive cells were calculated as a percentage of total number of nuclei staining positive for TOPRO-3.

2.8.3 MAGENOFECTION OF RETINAL EXPLANT WITH CAG-GFP

Retinal explants cultures were prepared as described in section 2.3.1. A 40 µl solution of 1:1 DNA:MNP ratio of CAG-GFP DNA and nTMag was incubated at room temperature for 20 minutes. This was then added to retina media to make up 800 µl which was then added to the upper chamber of the culture insert. A magnetic field was applied from beneath the well using the Magnefect Nano II (nanoTherics Ltd., Stoke-on-Trent, UK) system and a 6 magnet array (NdB magnet 0.4T) compatible with the 6 well plates.]. The magnet applied had an oscillatory movement of 1Hz and was applied for 30 minutes. At the end of the magnetofection, the 800µl of DNA-MNP complex solution was removed and the retinal explant was allowed to culture for 48 hours at 37^0C and 5% CO2 before being fixed with PFA 5%. They were then counterstained with TO-PRO 3 (1:1000; Invitrogen) for 10 minutes followed by three phosphate buffered saline (PBS) washes post-stain. Specimens were then mounted; RGC side up, on a slide with ProLong Gold AntiFade Reagent (Invitrogen). A confocal laser scanning microscope (Zeiss LSM 510, Carl Zeiss Ltd, UK) was used to capture corneal images at 20x objective for GFP expression at 1µm intervals. The image subtended 394 by 394µm (512 by 512 pixels, 8 bits per pixel). Control experiments (retinal explants cultured normally without DNA or an external magnetic field) were used to calibrate settings on the confocal microscope to reduce background fluorescence. GFP-positive cells were counted manually using the FIJI plug-in, Cell Counter. Transfection efficiency was estimated as the percentage of GFP-positive cells per total cells in the microscopic field. The retinal layers were identified according to change in morphological appearances on TO-PRO stain. RGC and INL were separated by a space of IPL with sparse cells present.

2.8.4 MAGNETOFECTION OF NSC WITH PLASMIDS [CAG-GFP AND BDNF-MYC]

NSCs were plated onto laminin coated 96 well at $16x10^3$ cell density in 100µl of media (50 ml DMEM/F-12 media and 1% penicillin-streptomycin supplemented with 20 ng/ml FGF-basic Recombinant Human (Invitrogen), 20 ng/ml EGF Recombinant Human (Invitrogen) and 1 ml B27 supplement liquid) overnight. MNP-DNA complexes were made by combining DNA plasmids to nTMag in an Eppendorf for 15 minutes in the investigated DNA:MNP ratios. The magnefect-nano II was set to the oscillatory parameters under for 30 minutes and the 96 well plate is secured onto the magnet array. The magnetofection experiment was setup in a 37^0C and 5% CO_2 incubator. At the end of the experiment, the media was exchanged for fresh media. For the detection of CAG-GFP transfection, images were acquired at 48 hours for GFP-positive cells at 20X objective by Delta Vision Elite System confocal microscope.

For the detection of BDNF-myc transfection, images were acquired following fixation and anti-myc detection by immunohistochemistry at 48 hours [see 2.8.7]. Myc positive immunofluorescent images were captured at 20x objective with a Leica SP5 inverted confocal microscope. Control experiments consisted of NSCs that had not been magnetofected.

2.8.5 LIVE/DEAD ASSAY OF NEURAL STEM CELLS/NEUROSPHERES

Ethidium homodimer-1 is a commonly used cell viability stain and has been used in cytotoxicity studies [Papadoulos 1994]. It works on the principle that cell death disrupts cell membrane integrity. Ethidium homodimer-1 enters cells with damaged membranes and upon binding to nucleic acids produce a bright red fluorescence in dead cells. It is excluded by intact plasma membrane of live cells.

NSC-GFPs were plated overnight at 37^0C and 5% CO2 on laminin coated Falcon ™ 8 chamber Culture Slides in 400 µl of media and at 1.5x105 cell density. Ethidium homodimer-1 from LIVE/DEAD© Viability Cytotoxicity Kit (Thermo Fisher Scientific) was diluted with PBS to 0.5 µM. The media from plated cells were removed and replaced with 100µl of diluted Ethidium homodimer-1 for 30 minutes at room temperature. Positive controls cells were killed with 70% Ethanol for 10 minutes prior to staining with Ethidium homodimer-1. Negative controls consisted of live cells. All cells were washed with PBS followed by counterstaining with DAPI (Vectashield antifade mounting medium with DAPI; Vector) for 10 minutes before being cover

slipped, sealed with nail polish and inverted for viewing under a Leica SP5 inverted confocal microscope captured at 20x magnification.

2.8.6 NESTIN LABELLING

NSCs under investigation in 8µm pore size filter (BD Falcon) from the modified Boyden Chamber experiment in section 2.7.1, were fixed in 4% PFA for 30 minutes. The filter sheet was cut out from its well and placed on to a slide. The borders of the filter were lined with grease to create a well. Cells were then covered with 5% BSA for an hour and washed with PBS. Anti-nestin rabbit monoclonal antibody (Sigma) was made up to a 1:100 concentration with PBS and 0.1% Triton X. NSCs were incubated with this solution overnight at 4^0C. NSC were then washed with PBS 3 times every 10 minutes. Secondary antibodies (Goat Anti-rabbit IgG Alexa Fluor 555; Invitrogen) were made up to 1:600 with PBS and incubated with NSCs at room temperature for 1 hour before being washed with PBS 3 times at 10 minute intervals. Cells were counterstained by DAPI (Vectashield antifade mounting medium with DAPI; Vector) for 10 minutes before being cover slipped and viewed under a Leica SP5 inverted confocal microscope.

2.8.7 MYC LABELLING

NSCs transfected with BDNF-myc were fixed in 4% PFA for 30 minutes at room temperature. After a PBS wash, cells were exposed to 5% BSA for an hour at room temperature. After another wash with PBS, primary antibodies [1:100 mouse monoclonal anti-c-myc antibodies (Abcam©) diluted with PBS and 0.1%Triton-X], were incubated with NSC overnight at 5^0C. Cells were washed with PBS before being exposed to secondary antibodies (1:500 Anti-mouse Alexa Fluor 594; Invitrogen diluted in PBS) for one hour at room temperature. After a PBS wash thrice at 10 minute intervals, cells were counterstained by DAPI (Vectashield antifade mounting medium with DAPI; Vector) for 10 minutes before being cover slipped and viewed under a Leica SP5 inverted confocal microscope. Control experiments absent of magnetofection were used to calibrate settings on the confocal microscope in order to reduce background fluorescence from low levels of endogenous myc.

2.8.8 COATING OF SLIDES AND PLATES WITH LAMININ

Laminin (Life Technologies) is made to 10 µg/ml in balanced salt solution. 200 µl of laminin solution is added to a 24 well chamber or 100 µl to a Falcon TM 8 chamber Culture Slides per cell culture vessel and left to set under a fume hood for 1 hour. Laminin solution is then removed and washed with PBS thrice before being left to dry under the hood for 15 minutes. Laminin coated chambers are used to plate NSC on the day of preparation.

2.9 GALVANOTAXIS IN NSC

2.9.1 ELECTROTAXIS ASSAY FOR HORIZONTAL NEUROSPHERE MIGRATION

A well-known electrotactic chamber commonly used in our lab for assessing NSC motility was assayed according to Song et al. (Song et al., 2007). Electrical fields were applied in electrotactic chambers(Zhao et al., 1996) consisting of two strips of 0.5mm thick cover glass 10mm apart glued in parallel to the bottom of a petri dish with Dow Corning high vacuum grease. A 70µl solution of $5x10^5$ ml^{-1}density neurospheres and Matrigel (Corning®Matrigel®Matrix) were plated in the resulting space between these strips covered by a roof consisting of a cover slip. Care was taken so as not to trap air bubbles within the plated liquid matrigel-neurosphere solution. Agar-salt bridges (filled with Steinberg's solution gelled with 2% agar) were used to connect silver to silver chloride electrodes in beakers of Steinberg's solution to reservoirs of 1000µl culture medium at either side of the chamber. The pH of this was kept stable by adding HEPES to the medium (1:40 concentration). Organisation of the electrotactic chamber is shown in Figure 2.9. The final dimensions of the chamber through which current was passed were 22 mm by 10 mm by 0.5 mm. For consistency in chamber size setup, a paper template with the measurements was placed beneath the petri dish to aid in accurate cover glass placement.

In order to detect cell migration over time, images of each marked out NSC were obtained every 5 minutes over 2 hours by a DeltaVision Microscopy Imaging System (Image Solutions, Preston) at 37^0C. Control experiments were run and imaged in the same conditions for 2 hours but in the absence of EF.

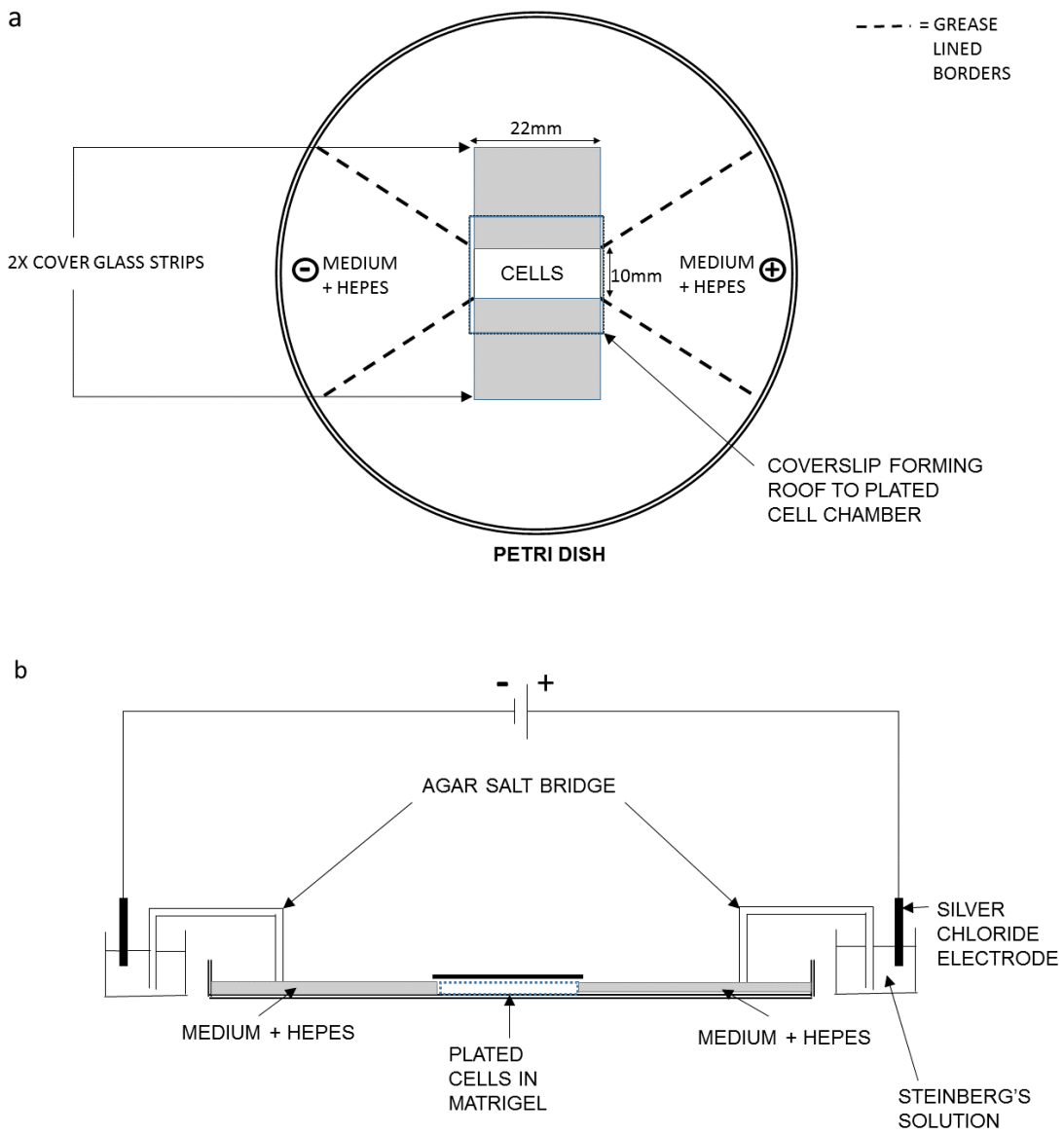

Figure 2.9 a: experimental setup of electrotactic chamber in petri dish viewed from above. b: side-on view of experimental setup including a dc power supply attached to silver chloride electrodes isolated from the culture chamber but connected via agar salt bridges.

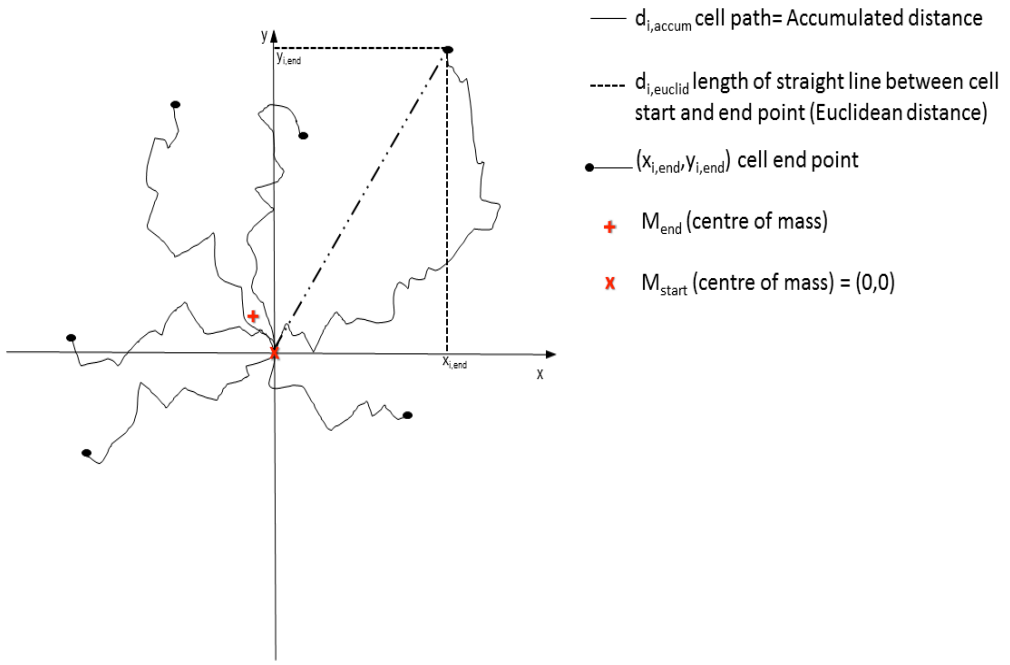

Figure 2.10 Definitions used in the 2D trajectory plots. "I" is the index of different single cells. The first cell has the index "1", the last one "n" ($1 \leq I \leq n$).

2.9.1.1 CHEMOTAXIS AND MIGRATION TOOL DEFINITIONS

For data analysis, cell migration of each individual cell was mapped out manually by tracking the centre of the neurosphere using the FIJI plugin, Manual Tracking.

Average cell migration velocity, directness, distance travelled (euclidean and accumulated) [see figure 2.10], centre of population and parallel Forward Migration Index (FMI) were calculated via a FIJI plugin, Chemotaxis and Migration tool.

Definitions of directedness, centre of population, forward migration index were taken from Chemotaxis and Migration Tool Version 1.01 manual (Ibidi, 2016) .

2.9.1.2 DIRECTEDNESS

Directedness (Semmling et al., 2010) is calculated by comparing the Euclidean distance to the Accumulated distance, representing a measurement of the directedness of cell trajectories(Yuki Asano). The values are always positive. It is not a direct parameter for judging migration, but can be a used to characterize the straightness of migration. (see figure 2.10)

$D_i = d_{i,\,euclid}/d_{i,accum}$

D_i = Directedness of one single cell

$d_{i,\,Euclid}$ = Euclidean distance

$d_{i,accum}$ = Accumulated distance

$D = 1/n \sum^{n}_{i=1} D_i = 1/n \sum^{n}_{i=1} d_{i,Euclid}/d_{i,accum}$

Averaged directedness of all cells

2.9.1.3 CENTRE OF POPULATION

Centre of Population is defined as the averaged endpoint of all cell endpoints (Asano Y). It can be either positive or negative; depending on the direction of which the group of cells has drifted. (see figure 2.10)

M_{start} = (x=0, y=0)

Centre of Population at the beginning of the experiment is located at the point of origin.

$M_{end}= 1/n \sum^{n}_{i=1} (x_{i,end}, y_{i,end})$

$x_{i,end=}$ X cell end point

$y_{i,end=}$ Y cell end point

2.9.1.4 FORWARD MIGRATION INDEX

Forward migration index (FMI) represents the efficiency of the forward migration of cells and how they relate to the direction of both axes(Foxman et al., 1999). FMI values can be positive or negative, depending on the direction in which the cell population has drifted. FMI values only make sense when a taxis effect is expected under the following conditions: they can be parallel to, or perpendicular to the x and y axes but not in 45^0angles. Strong taxic effects are characterized by a high FMI (can be positive or negative value). FMI values parallel to the x axis were reported in this case.

$Y_{FMI}= 1/n \sum^{n}_{i=1} y_{i,end}/d_{i,accum}$

$X_{FMI}= 1/n \sum^{n}_{i=1} x_{i,end}/d_{i,accum}$

2.9.1.5 RAYLEIGH'S TEST

Rayleigh's test is a statistical test run by the software to test if the data was significantly inhomogenously distributed in any direction when p was <0.05. It is a test used in cell migration and chemotaxis and has been shown to correlate with centre of population and forward migration index (Zantl and Horn, 2011, Pepperell and Watt, 2013). The greater the displacement of centre of population and forward migration index, the more negative the p value of the Rayleigh's test.

2.9.2 PLATING NEUROSPHERES WITH MATRIGEL

Matrigel (Corning®Matrigel®Matrix) was thawed from frozen on ice. Once thawed, this was diluted to 1:50 with media containing neurospheres of $5x10^5$ ml^{-1} density and plated to prevent Matrigel from solidifying as it reaches room temperature.

2.9.3 MODIFIED BOYDEN CHAMBER FOR ASSESSING VERTICAL DIRECTION OF NEUROSPHERES

A modified Boyden chamber system from Widera et al.(Widera et al., 2004) was used to test if vertical migration of NSC (which represents penetration into tissues) can be directed by an electric field. The upper chamber consisted of a cell culture insert with a pore size of 8µm (BD Falcon) filled with 1 ml of $1.6x10^4$ NSC and the lower chamber was a 24-well cell culture plate filled with NSC media devoid of cells. Platinum wires electrodes connected to a DC power supply are applied; cathode in the lower chamber and anode in the upper chamber (see figure 2.11 and 2.12). The voltage dial supplied was adjusted according to the parameters investigated on a DC power supply. The actual voltage in the Boyden chamber was measured across the chambers with a voltage meter TES 2700 multimeter at the beginning and end of the experiment. The current supplied remained unchanged throughout for all experiments as measured by the TES 2700 multimeter. Experimental conditions were kept at 37 ^{0}C and 5% CO2 throughout by an incubator.

The filter was removed at the end of the experiment and the upper side of the filter was washed with PBS x 3 and scraped with a cell scraper before being fixed with 4% PFA. Cell migration was quantified by counting all migrated cells in each filter. All experiments were performed in triplicates. Immunofluorescent images were captured at 20 x objective under GFP settings by fluorescent microscopy (Olympus AX70). The number of cells in each filter frame [3mm x 2.5mm] was counted using FIJI plugin, Cell Count and compared with controls (no electrical field exposure). Statistical analysis was performed by t-test using SPSS 20.0.

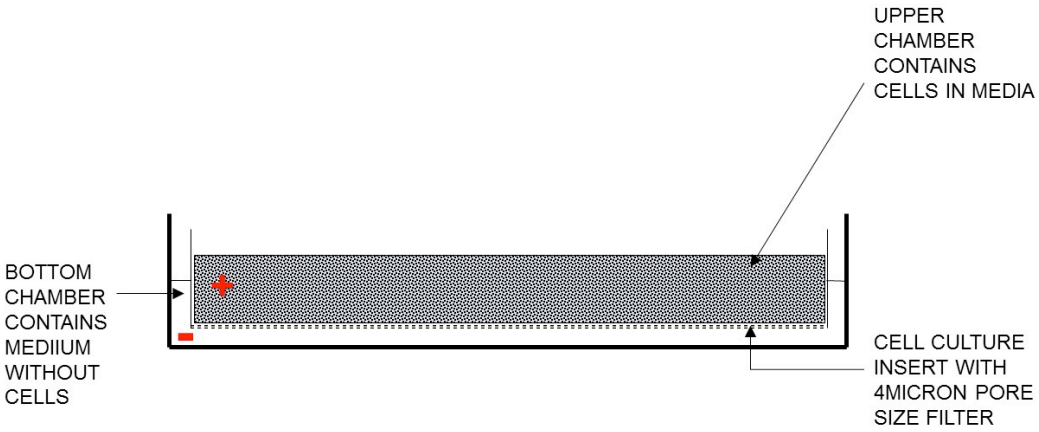

Figure 2.11 A cross sectional illustration of the modified Boyden chamber setup to assess vertical migration of cells directed by electric field application. Plus and minus symbols indicate the anode and cathode platinum wire electrodes which were applied. The anode is in the upper chamber and the cathode is in the bottom chamber.

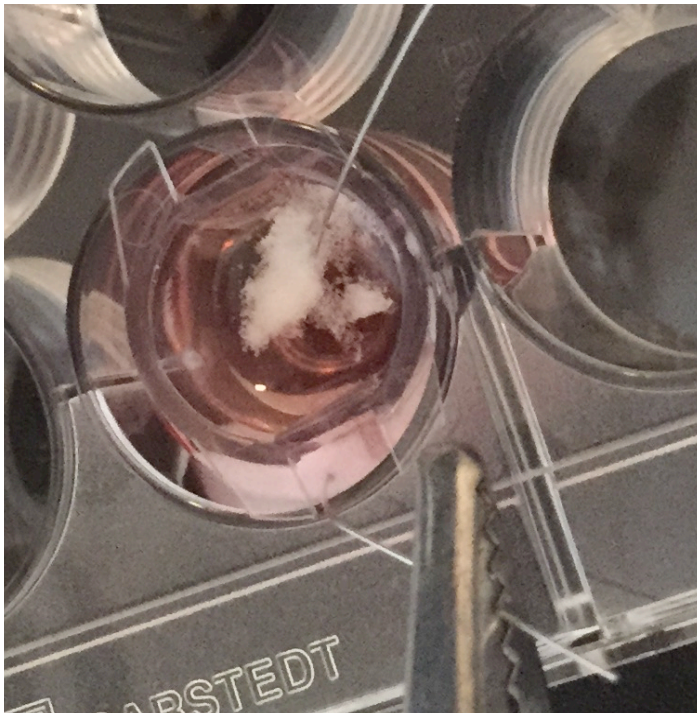

Figure 2.12 Photo of modified Boyden chamber setup with a 24 well culture plate. The crocodile clip at the top is attached to the anode of the DC supply and a platinum wire immersed in the upper chamber and the crocodile clip at the bottom is attached to the cathode and a platinum wire immersed in the lower chamber

2.9.4 MODIFIED BOYDEN CHAMBER SETUP WITH RETINAL EXPLANT

To test if neurospheres can be directed by an electric field vertically into a retinal explant i.e. from inner layer to outer layer, a modified Boyden chamber similar to 2.7.1 was set up to include a retinal explant (see figure 2.13-2.16). This was placed RGC face up on a 4µm pore 6 well filter (BD Falcon) and lined with high vacuum grease (Dow Corning©) so that the filter surface uncovered by retina would be covered in grease, grossly separating the upper chamber from the lower chamber. The upper chamber was filled with 2000µl of NSC-GFP at a density of approximately 8-12x10^5 cell density. The lower chamber consisted of 1400µl of retina culture media devoid without any cells. Platinum wires electrodes are connected to a DC power supply and submerged in medium; cathode in the lower chamber and anode in the upper chamber. Care is taken to ensure the anode wire is submerged but not in contact with the retinal explant. The Boyden chamber experiment is performed at 37^0 with 5% CO2 throughout. The voltage dial supplied was adjusted according to the parameters investigated. The actual voltage in the Boyden chamber was measured across the chambers with a voltage meter TES 2700 multimeter at the beginning and end of the experiment. The current supplied was unchanged throughout for all experiments.

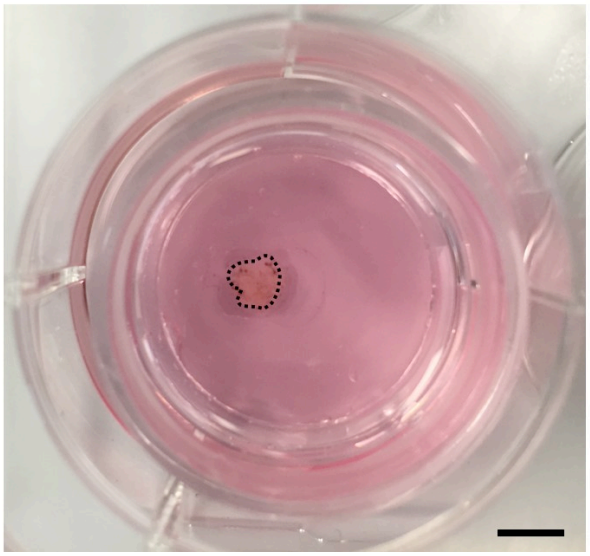

Figure 2.13 Modified Boyden chamber viewed from above. Retinal explant with retinal ganglion cell layer face up on a 4µm pore filter of UPPER chamber, lined by high vacuum grease. Lower chamber consists of 1400µl media. The retinal explant is outlined by black dots. Scale bar: 1mm

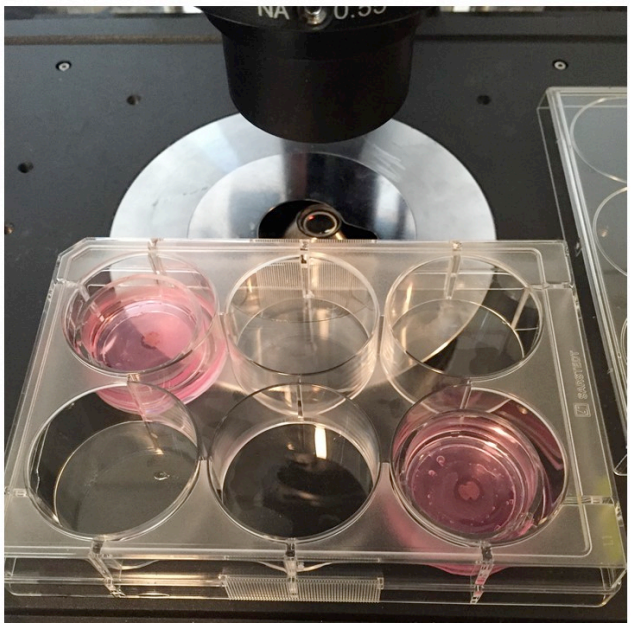

Figure 2.14 Two retinal explants in modified Boyden chambers with upper chamber filled with 2000µl NSC-GFP at 8-12x105 cell density in 6 well.

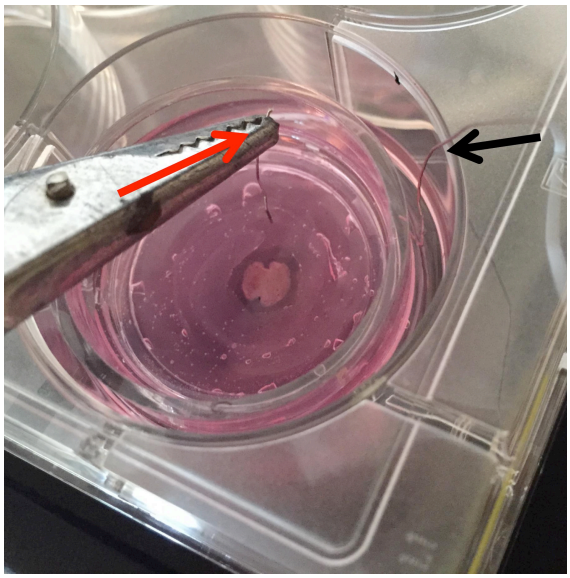

Figure 2.15 A platinum wire attached to a crocodile clip applying the cathode (black arrow) to the lower chamber and the anode (red arrow) to the upper chamber. The cathode wire is submerged in media but does not touch the retina.

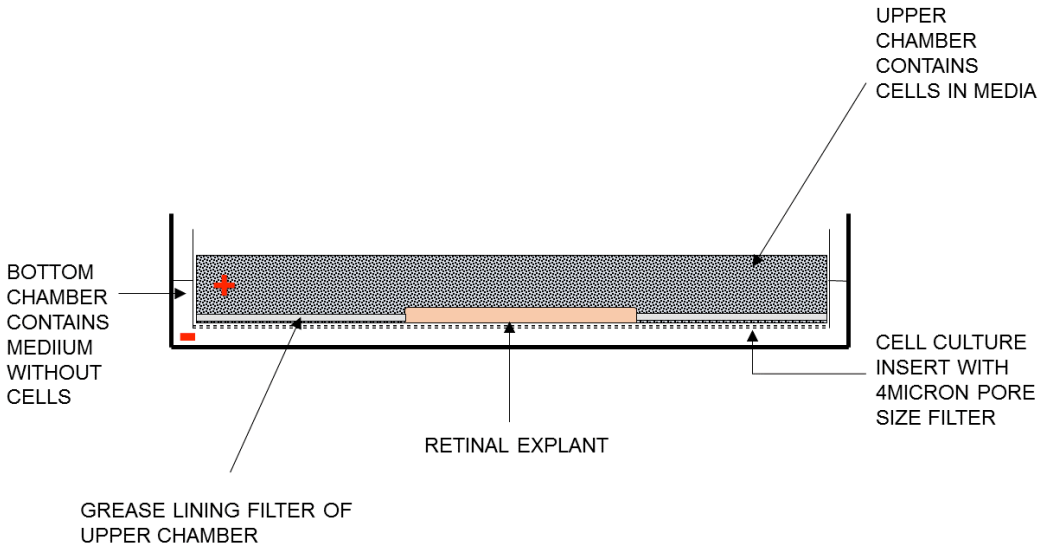

Figure 2.16 Diagramatic representation of a cross sectional view of the modified Boyden chamber with retinal explant laid on the upper chamber filter base, surrounded with grease.

2.9.4.1 RETINAL TISSUE PROCESSING, IMAGING AND ANALYSIS

Following exposure to an electrical field, the retinal explants were fixed in 4% PFA for 30 minutes. The explant along with its underlying filter was excised from the upper chamber and placed on a microscope slide followed by a PBS wash. Retinal explants were stained with nuclear stain TOPRO-3 (diluted in distilled water to 1:1000) before being mounted with antifade reagent (ProLong Gold; Invitrogen). Images were acquired using a Zeiss LSM 510 confocal microscope (Carl Zeiss Ltd, UK) captured at 20x magnification and 1µm interval slice Z stacks. The image subtended at 394 by 394µm (512 by 512 pixels, 8 bits per pixel). Nuclear staining allowed for identification of retinal layers based on the changes in morphology of cell nuclei. Control experiments were used to calibrate settings on the confocal microscope in order to reduce background fluorescence.

To identify any penetration of NSC-GFP into the layers of the retina, firstly I needed to identify the separate layers of the retina. The slices consisting of Retinal Ganglion Cell Layer (RGC), Inner Nuclear Layer (INL), Outer Plexiform Layer (OPL) and Outer Nuclear Layer (ONL) were identified based on the nuclear staining morphology. (see Figure 2.17) RGC was the superficial layer of cells with a single layer of larger nuclei. This was followed by the INL which is a smaller multi-layered nuclei. These layers are separated from the ONL by the OPL which is a space with sparse cells. The ONL is multi-layered with smaller nuclei. Anything above RGC layer was taken as the Inner Limiting Membrane (ILM).

Once the layers are known, an NSC-GFP is then selected using the "Select" tool in FIJI. This demarcates an area around the NSC assessed which is present throughout the layers of the retinal stack images. The average fluorescence density of the selected cell area for each slice of the stack was then recorded. (Figure 2.18).

To standardize the retinal layers, each layer was divided into percentages. Fluorescence density was reported for each tenth of a percentage depth of the retinal layer.

AUC of fluorescence for all retinal layers was calculated using the trapezoid method. To detect any change in the spread of fluorescence which was taken as migration between the layers, the proportion of fluorescence within the three layers was calculated i.e. Proportion of fluorescence in IPL (%) = (AUC of fluorescence in IPL / AUC of fluorescence in ILM+RGC+INL+OPL+ONL) X 100. This identifies any shift in the spread of fluorescence within the retina. Statistical analysis was performed using a Kruskall-Wallis test for non-parametric data and independent sample t-

test or ANOVA for multiple comparisons for parametric data. Data was explored by normality tests Shapiro-Wilk and $p>0.05$ was taken as parametric data. Analysis was performed with SPSS Version 20.0. Bonferroni or Tukey post-hoc correction was also applied to account for multiple comparison and $p<0.05$ was taken as significant.

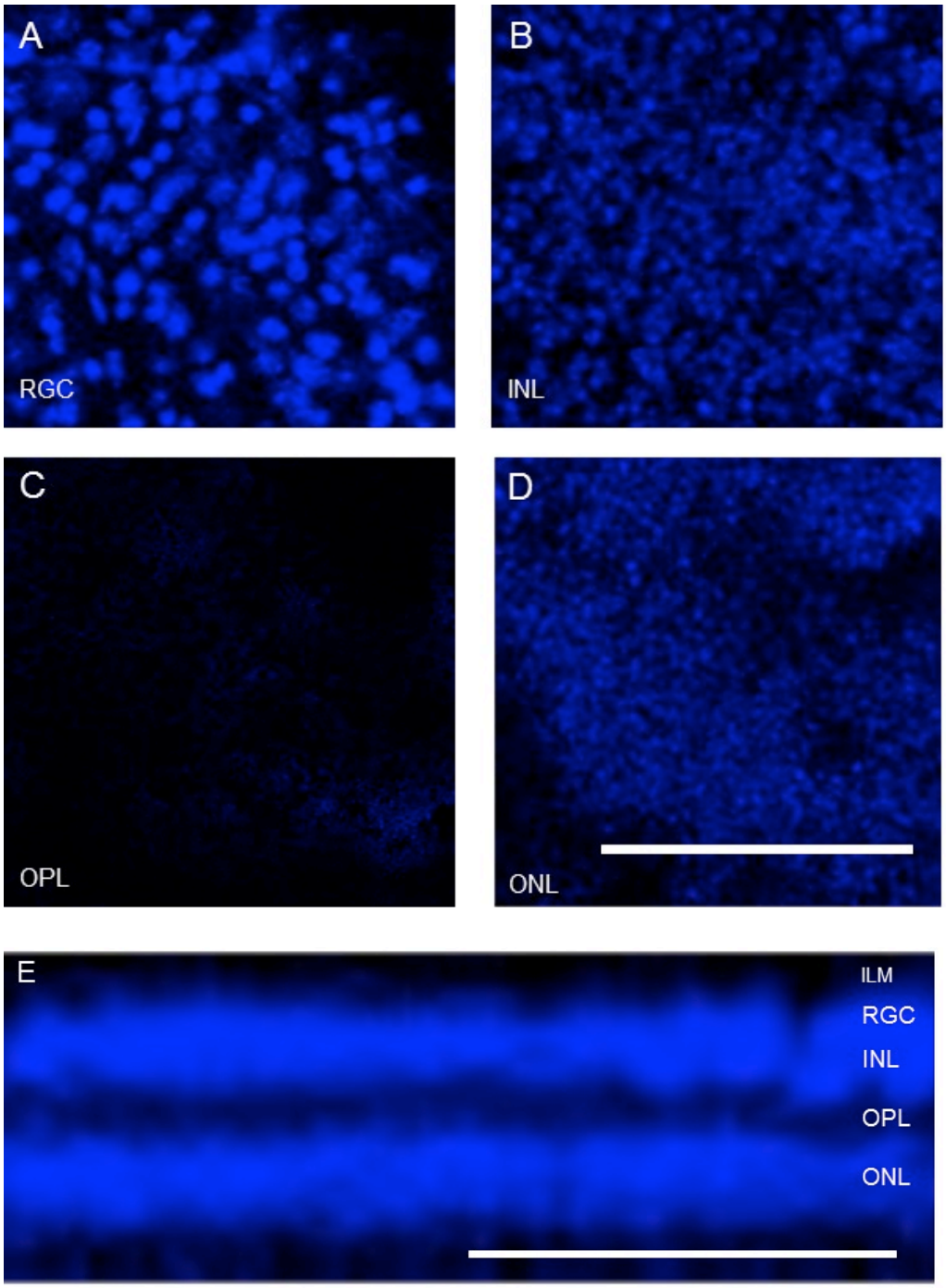

Figure 2.17 Images A-D shows the nuclear stained confocal images of each retinal layer where the nuclear morphology is used to identify each layer. A=RGC, a single layer of larger nuclei cells, B=INL, a multilayer pf smaller nuclei, C=OPL, a space separating the INL from the ONL, D=ONL a multilayer of small nuclei. E is an orthogonal view of the nuclear stained confocal image of the retinal layers. ILM=Inner Limiting Membrane, RGC=Retinal Ganglion Cell, INL=Inner Nuclear Layer, OPL=Outer Plexiform Layer, ONL=Outer Nuclear Layer. Scale bar: 100µm

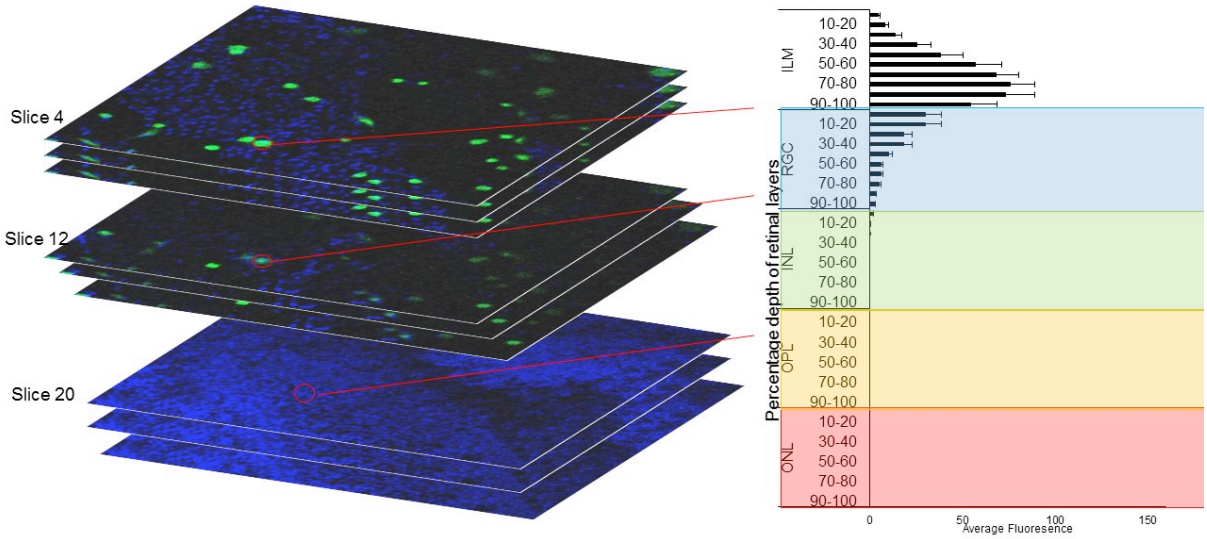

Figure 2.18 Shows a selected circular area (in red) consisting of NSC-GFP. This selected area remains the same as is selected throughout the retinal stack. The average fluorescence density for each slice within the selected area is recorded for each percentage depth of the retinal layer to produce the graph to the right.

2.10 WESTERN BLOT FOR BDNF

Magnetofected NSCs were centrifuged at 15000rpm at 4^0C for 10 minutes. As much supernatant was pipetted off as possible and discarded. The pellet was lysed with 100µl of Lysis Protein solution: RIPA buffer + 0.1%SDS (sodium dodecylsulfate) + 0.1M DTT (dithiothreitol) 2.4µl + Protease Inhibitors (Sigma Phosphatase inhibitor 12µl, Sigma Protease Inhibitor 12µl, Aminohexanoic acid 6µl, Aprotinin 1.2µl, Phenantroline 1.2µl, 0.1M) (see Appendix 1). Pellet and lysis solution were vortexed every 5 minutes and kept on ice for 30 minutes. It was then centrifuged at 15000rpm for 5 minutes at 4^0C. Supernatants were collected into separate eppendorfs and kept on ice.

Protein quantification was performed with a Pierce ™ BCA Protein Assay Kit (Thermo Scientific©). Nine standards of known concentrations were made with Bovine Serum Albumin (BSA); 0.2 mg/ml, 0.15 mg/ml, 0.10 mg/ml, 0.075 mg/ml, 0.05 mg/ml, 0.025 mg/ml, 0.0125 mg/ml, 0.0062 mg/ml and 0.0 mg/ml (blank with water). 100µl triplicates of each standard was placed into a 96 well. Samples were diluted to 1 in 50 with water and 100 µl of each was placed in the 96 well. BCA solution was made up according to manufacturer's guideline; 50 to 1 Reagent A to Reagent B. 100 µl of BCA solution was added to triplicates of BSA standards and samples. The 96 well plate was incubated at 37 ^{0}C for 30 minutes. The plate was then analysed in a spectrophotometer (FLUOstar Omega) and a line of best fit is produced from an average of the standards and blanks using the Omega-Data Analysis. Based on this a calculated protein concentration in µg/ml is produced.

Protein sample solution at a total volume of 27 µl was then prepared for loading onto gel. 30 µg of sample protein is added to 6 µl NuPAGE LDS Sample Buffer, 2 µl DTT, and the residual amount in Lysis Buffer (approximately 5-10 µl depending on protein sample volume). A positive control of 75 picograms of rBDNF was also included.

Protein sample solution was heated for 10 minutes at 70^0C.

The running buffer (800 ml) was prepared using MOPS/SDS Running Buffer 20X diluted to 1X with ddH20. Precast NuPAGE 4-12% Bis-Tris Gel (Invitrogen©) was removed from bad and rinsed with ddH20. Tape from the back of the gel was peeled off and the comb was carefully removed. Wells were washed out with running buffer using a Pasteur pipette. 25 µl of sample solution were gently pipetted to fill each well; care is taken to prevent air bubbles or spillage

into adjacent wells. Novex© Mini-cell (Invitrogen) apparatus was set up as per manufacturer's instructions. Buffer chamber was filled up with 200 mls of running buffer and checked for leaks. The remainder of the running buffer was added to the lower buffer chamber if no leak is present. The sample was run at 120V for 70 minutes.

1x NuPage Transfer Buffer was made from 100ml 10x NuPAGE Transfer Buffer mixed with 200 ml methanol and 700 ml ddH20 (pH7.2). A 7x8cm Amersham™ Protram™ Nitrocellulose 0.2 µm pore size blotting membrane (Life Science) was soaked with this for 5 to 10 minutes. Blotting pads (extra thick blot filter paper, Bio-Rad) and two pieces of manufacturer recommended filter paper was also pre-soaked in transfer buffer. After electrophoresis was complete, the gel cassette was cracked open with a blunt edged knife to expose the polyacrylamide gel. This is soaked in transfer buffer and the stacking gel containing the wells is removed with a knife. One piece of the pre-soaked filter paper is placed on the transfer unit, ensuring no trapped air bubbles were present. The pre-soaked membrane is then placed on top of the filter paper, ensuring no air bubbles were trapped. Transfer buffer was used to wet the surface of the gel and placed on the membrane. Any air bubbles trapped between the membrane and gel was rolled out using a clean pipette. Finally the second piece of filter paper was placed on the transfer unit, once again ensuring no trapped air bubbles were present. The cassette was then placed into the chamber of the unit with a -20^{0}C ice pack to prevent over-heating and was then run at 80v for 60 minutes.

Blocking solution was prepared with 3% BSA, 3% ECL Prime ™ blocking agent (GE Healthcare) and 100 mls of TBST. Once transferred, the membrane was washed with TBST for 2 minutes. 10 mls of blocking solution was placed onto the membrane in a black covered box and placed on a shaker for 1 hour. Blocking solution was then removed and 1:2000 primary antibodies of mouse anti-BDNF (Icosagen) was added and incubated with the membrane overnight at 4^{0}C.

The membrane was washed thrice with TBST every 15 minutes. Secondary antibodies of anti-mouse HRP 1:7500 (Promega) was incubated with the membrane for 1 hour.

This was then washed thrice with TBST and LumiGLO Reserve Chemiluminescent Substrate® (KPL) solution every 20 minutes.

The membrane was then immersed in 1.5 µl of LumiGLO solution for 1 minute. Development of the membrane was processed with a Bio-rad ChemiDoc™ MP System for chemiluminesence detection. Images were processed via Image Lab™ v5.0 software.

For the internal control, the membrane was washed thrice with TBST every 10 minutes and incubated with β_3Tubilin anti-mouse (Biolegend) 1:10000 for 1 hour. It was then washed thrice

with TBST every 15 minutes and incubated with 1:5000 anti-mouse Alexa Fluor 647 secondary antibodies. Image acquisition was captured with a Bio-rad Camera, Imager ChemiDoc™ MP Version 5.0 for 0.369 seconds of exposure time. Pierce staining was used to show the presence of proteins. MemCode™ Reversible Protein Stain kit (Thermo Scientific) was applied as per manufacturer's instructions.

CHAPTER 3 RETINAL GANGLION CELL VIABILITY IN RETINAL EXPLANTS

OBJECTIVES

- To determine which automated Sholl program should be used for analysis by comparing several well-known programs against manually produced Sholl profiles
- To determine duration of retinal explant viability inclusive of RGC health by assessing Sholl profiles

3.1 INTRODUCTION

Adult organotypic retinal explant culture systems in rodents are well established and have been used as an in-vitro ocular stem cell transplantation model, to investigate neuroprotective therapies, pharmacological toxicity and laser retinal applications(Johnson and Martin, 2008, Schlichtenbrede et al., 2009, Wood et al., 2011). In-vivo studies have involved intravitreal injection of drugs of which precise drug concentrations are difficult to control in comparison to in-vitro studies(Manabe et al., 2002). In-vitro cultures of dissociated retinal cells causes loss of its normal morphological features. Retinal explant culture systems maintain cell-to-cell interactions present in intact tissues. However, use of retinal explants as a therapeutic test platform is critically dependent on the duration of its viability in culture. In rodents this has been reported to be sustained for up to two weeks in adult rats (Johnson and Martin, 2008).

Efforts towards prolonging retinal ganglion cell survival through extrinsic neuroprotective therapies have been promising(Martin et al., 2003). Indeed, adult rat retinal explant culture models have been used to screen for potential retinal ganglion cell neuroprotective therapies (Bull et al., 2011, Guerin et al., 2011, Manabe et al., 2002). To assess retinal ganglion cell survival, histological analysis of the retinal ganglion cell layer is often used (Caffe et al., 2001, Johnson and Martin, 2008). Most reports have assessed retinal ganglion cell neuroprotection through nuclei counts in the retinal ganglion cell layer, whereby overestimation of RGC survival is likely to occur(Bull et al., 2011, Guerin et al., 2011) as microglia have been reported to engulf

dead RGC especially when labelled with DiI(Thanos, 1991). In this chapter I will quantify dendritic complexities of RGC in retinal explants over time by Sholl analysis as a more sensitive and efficient marker for retinal ganglion cell survival in comparison to retinal ganglion cell count densities. I will determine the duration for which RGCs maintain the integrity of their dendritic trees that will be the basis for my thesis.

Experimental Design

As retinal explants will act as a test bed for NSC galvanotaxis from inner nuclear layer to outer nuclear layer, duration of explant viability especially its inner nuclear layer consisting of RGCs, needs to be determined. Sholl profiles were analysed to determine RGC health in retina explants. To determine which automated Sholl program should be used for analysis, four programs (FIJI plug-in: Simple Neurite Tracer, FIJI plug-in: Bit Map Sholl Analysis, FIJI plug-in: Ghosh Lab Sholl analysis and Fast Sholl MATLAB script) were compared to manually produced Sholl profiles of RGC diolistically labelled with DiI (See chapter 2.3.2). RGC Sholl profiles were then analysed for up to 3 days to determine its health in retinal explant culture. Retinal explant viability was also assessed; for apoptosis by TUNEL staining, living cells by Calcein-AM staining and architecture by nuclear staining, for up to 14 days.

3.2 RESULTS

3.2.1 MANUAL CALIBRATION OF SHOLL ANALYSIS

Both RGCs and amacrine cells were stained with DiI using the gene gun method. RGCs were identified based on their morphological appearance according to Sun et al.(Sun et al., 2002) and the presence of a definite axon (see figure 3.1). TOPRO-3 served as a nuclear counter stain as well as guided identification of retinal cell layers to ensure the cell identified was in the correct layer. Sixty two RGC images from 25 retinas were acquired and analysed. Figure 3.2 demonstrates the mean of the cumulative Sholl profiles of all 62 RGC images [Wai Siene Ng=38, Katie Binley=24] produced by the four programs under scrutiny in comparison to that produced manually; taken as gold standard. The FIJI plug-in: Simple Neurite Tracer correlated best with that of the manual Sholl profile. Fastsholl MATLAB script, Ghosh Lab and FIJI plug-in: Bitmap Sholl programs undercounted dendritic intersections. Not only were FIJI plug-in: Bitmap Sholl and Ghosh lab undercounting dendrites the most, but they also correlated similarly to each other in Sholl production with a second erroneous peak further away from the soma centre at around 250μm (see figure 3.2). The calculated percentage difference of each program compared to manual plots are shown in Figure 3.3. ICC for the two assessors (Wai Siene Ng and Katie Binley) used for manual count of dendritic intersections ranged from 0.942-0.988 showing excellent agreement levels.

Bland-Altman plots for all four programs are shown in Figure 3.4 with some suggestion of the presence of systematic errors in the FIJI plug-in: Bitmap Sholl, indicated by large limits of agreement (shown in dotted line, see figure 3.1) in the plots and a random arrangement of data points.

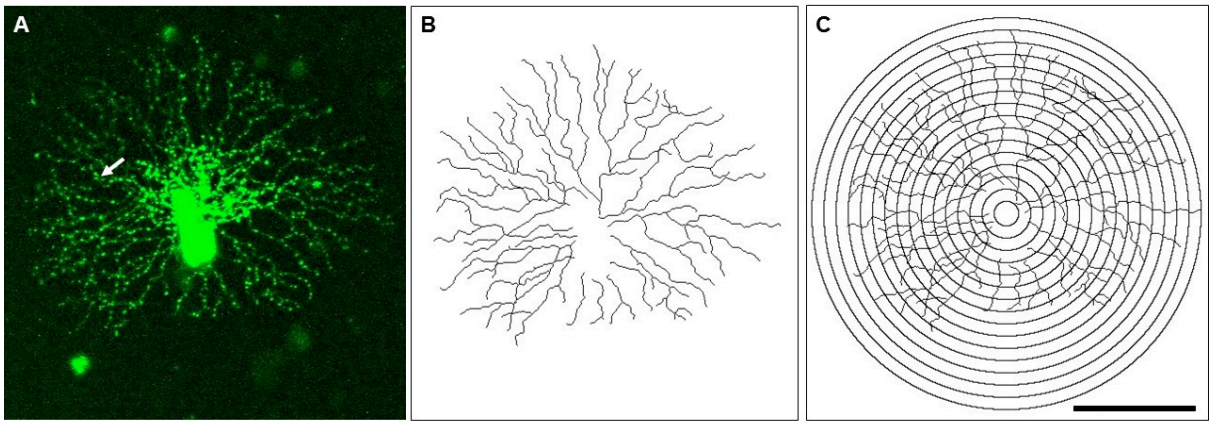

Figure 3.1 A) Confocal image of DiI stained RGC with corresponding tracing (B) and overlay of 10um incremental radius ring tracings for manual count of dendritic intersections (C). White arrow represents axon of RGC. Black scale bar represents 100 microns.

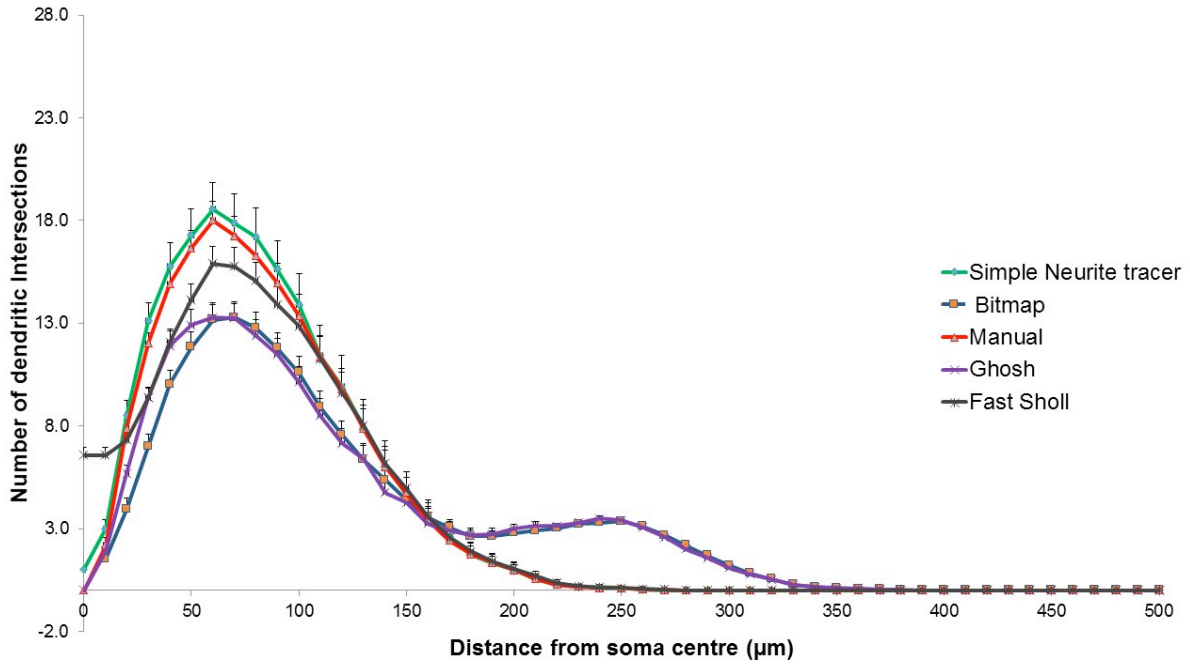

Figure 3.2 Sholl plots produced by; FIJI: Simple Neurite Tracer, Fast Sholl MATLAB script, FIJI Bitmap Sholl and Ghosh lab compared to the gold standard manually produced Sholl plot (red). N=62 Error bars represent SEM.

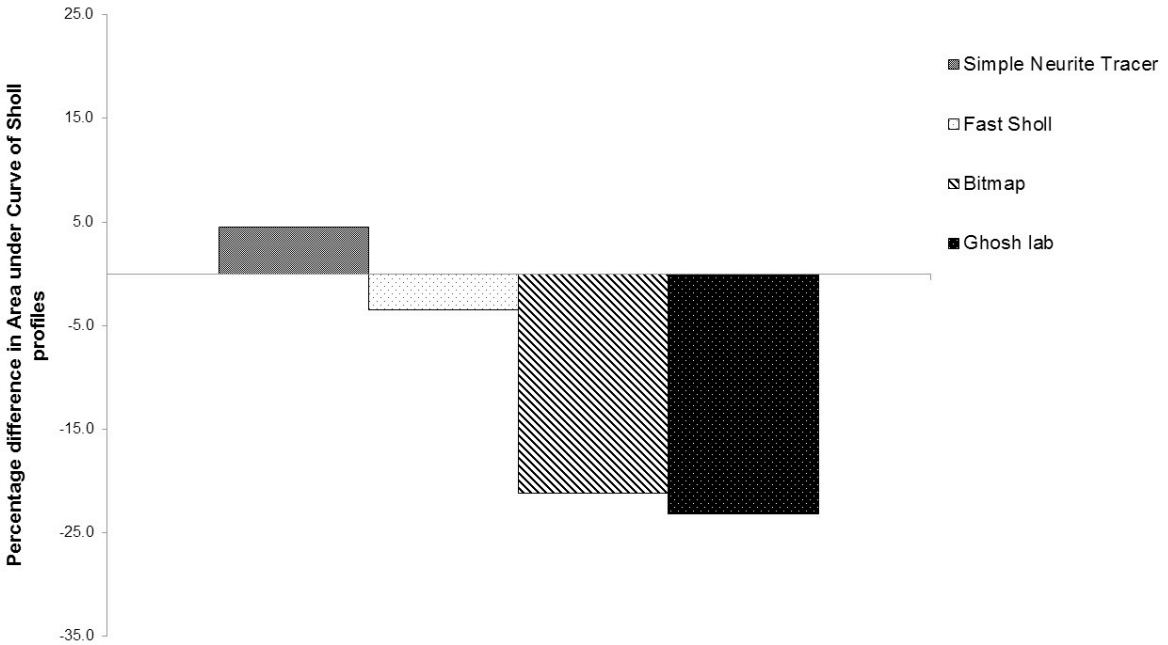

Figure 3.3 Bar chart showing calculated percentage difference for area under curve of Sholl profiles from assessed automated Sholl programs; FIJI: Simple Neurite Tracer, Fast Sholl MATLAB script, FIJI Bitmap Sholl and Ghosh lab, in comparison to area under curve for Sholl profiles produced by manual count.

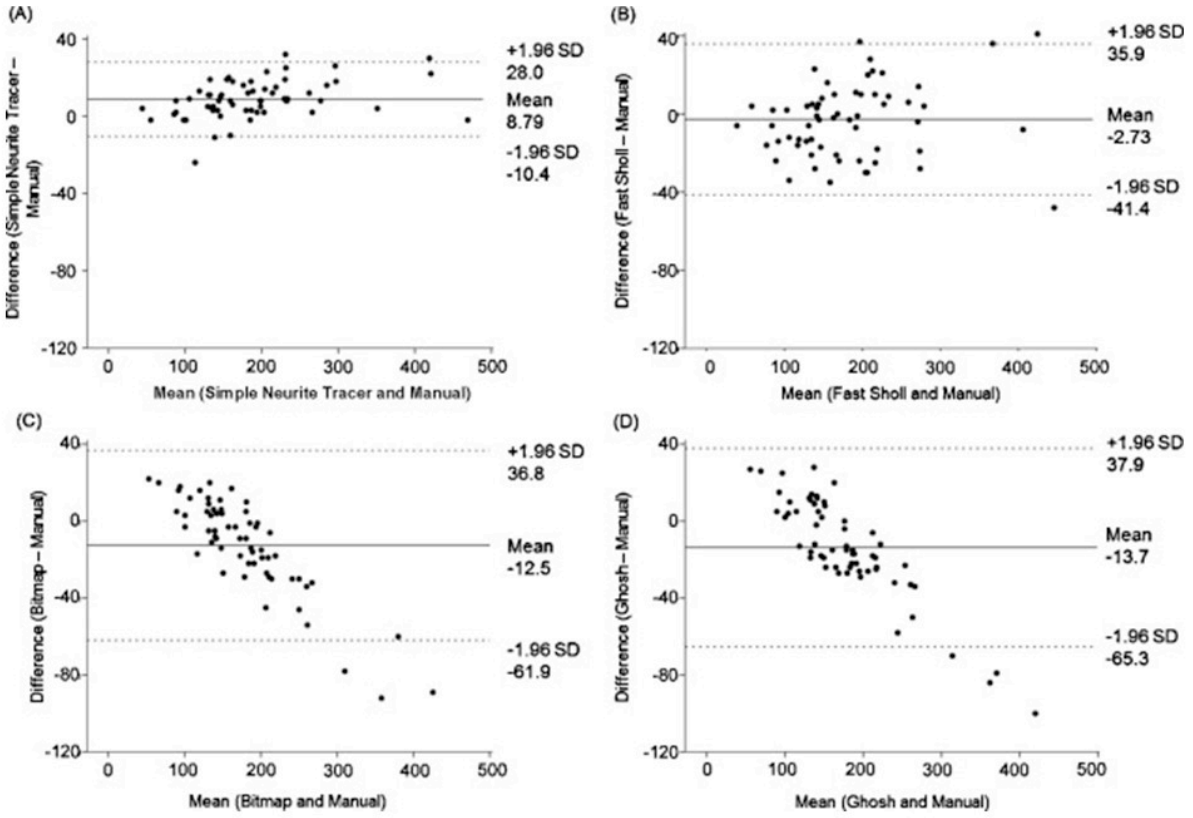

Figure 3.4 Bland-Altman plots comparing total intersections for FIJI: Simple Neurite Tracer, Fast Sholl MATLAB script, FIJI: Bitmap Sholl and Ghosh lab to Manual Sholl analysis. The difference in total number of intersections between each method for each cell is plotted against the average number of total intersections for the two methods for each cell. (n=62) 95% Limits of agreement are shown in dotted lines.

3.2.2 RETINAL EXPLANT VIABILITY

3.2.2.1 SHOLL ANALYSIS

A total of 174 RGCs from 50 retinas were acquired and analysed by the semi-automated programme FIJI: Simple Neurite Tracer. Fourty three RGCs were captured immediately post enucleation (day 0) [Wai Siene Ng=37, Katie Binley=6], 21 RGCs 6 hours ex vivo [Wai Siene Ng=15, Katie Binley=6], 32 RGCs on days ex-vivo 1 (DEV1) [Wai Siene Ng=24, Katie Binley=8], 42 on DEV2 [Wai Siene Ng=8, Katie Binley=34] and 36 on DEV3 [Wai Siene Ng=26, Katie Binley=10]. Figure 3.7 displays the Sholl profiles produced by the mean of RGCs analysed on all 5 time endpoints. By day 4, there were no definite RGCs identifiable. Examples of RGC from retinal explants captured at different time endpoints are shown from figure 3.5. The AUC of Sholl profiles from day 0 to DEV3 decreased with increasing culture time [see figure 3.8]. Two-tailed paired sample T test at 95%CI showed a significant difference between Day 0 vs 6 hours ex-vivo ($p=0.011$), Day 0 vs DEV 1($p<0.001$), Day 0 vs DEV 2($p=0.001$) and Day 0 vs DEV3 ($p<0.001$).

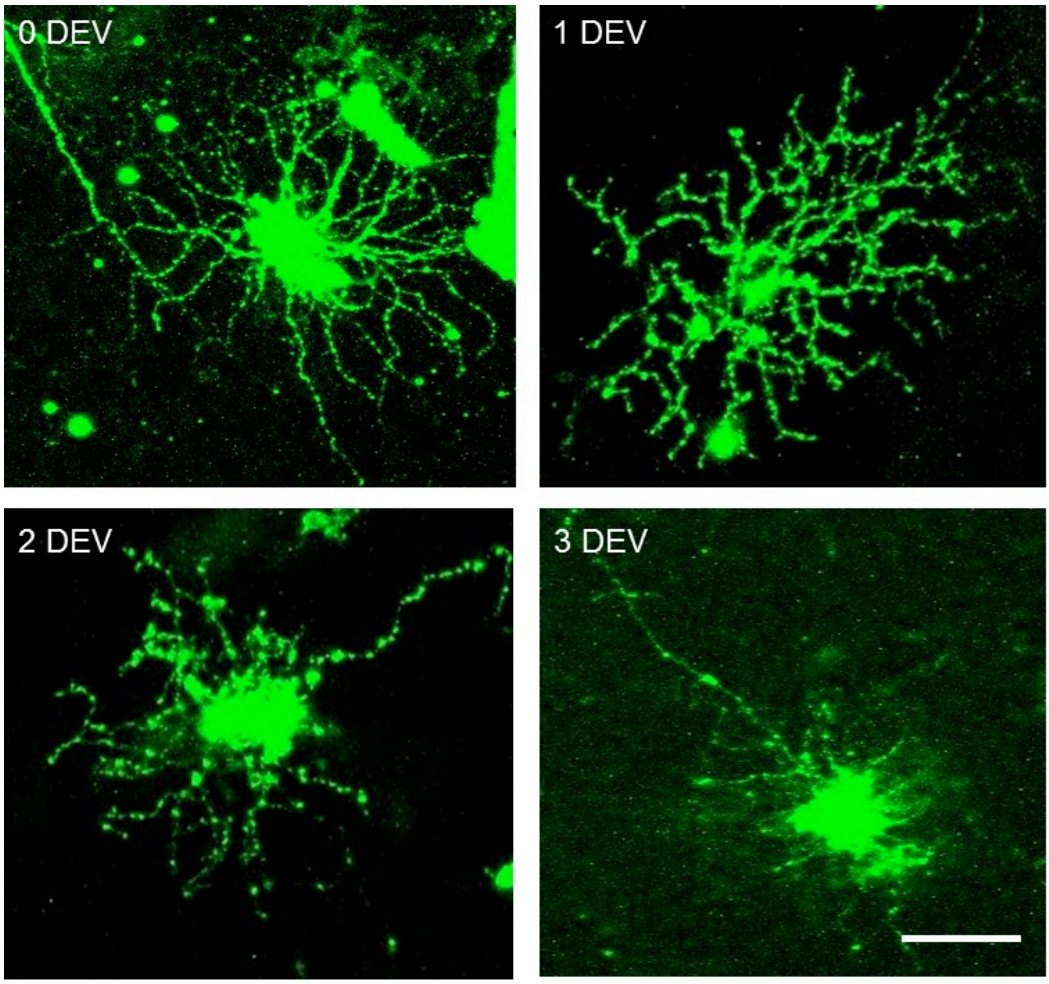

Figure 3.5 Retinal Ganglion Cells (RGC) stained with DiI confocal image at 0 days ex-vivo (DEV), 1 day ex-vivo, 2 days ex-vivo and 3 days ex-vivo. RGC from DEV1 shown still maintains its dendritic complexity while RGC from DEV2 and DEV3 show truncated dendrites with reduced branching complexities. RGC at DEV3 shows a faint axon with markedly truncated dendrites. DEV4 showed no identifiable RGCs. Scale bar represents 100µm.

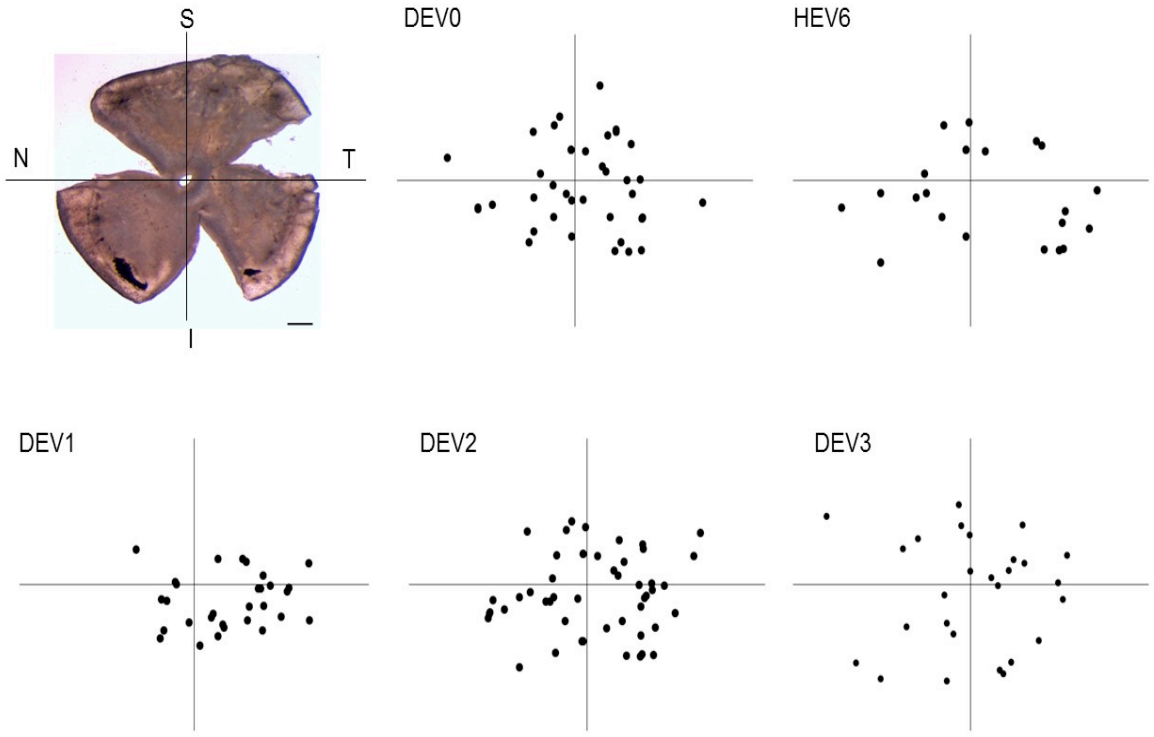

Figure 3.6 Scatter plots of RGC position on retina for days ex-vivo 0 to 3 showing random labelling of RGC. On the X axis N=nasal, T= temporal, and on the y axis S=superior, I=inferior. Optic nerve head is represented at 0, 0 coordinates. Scale bar: 100µm.

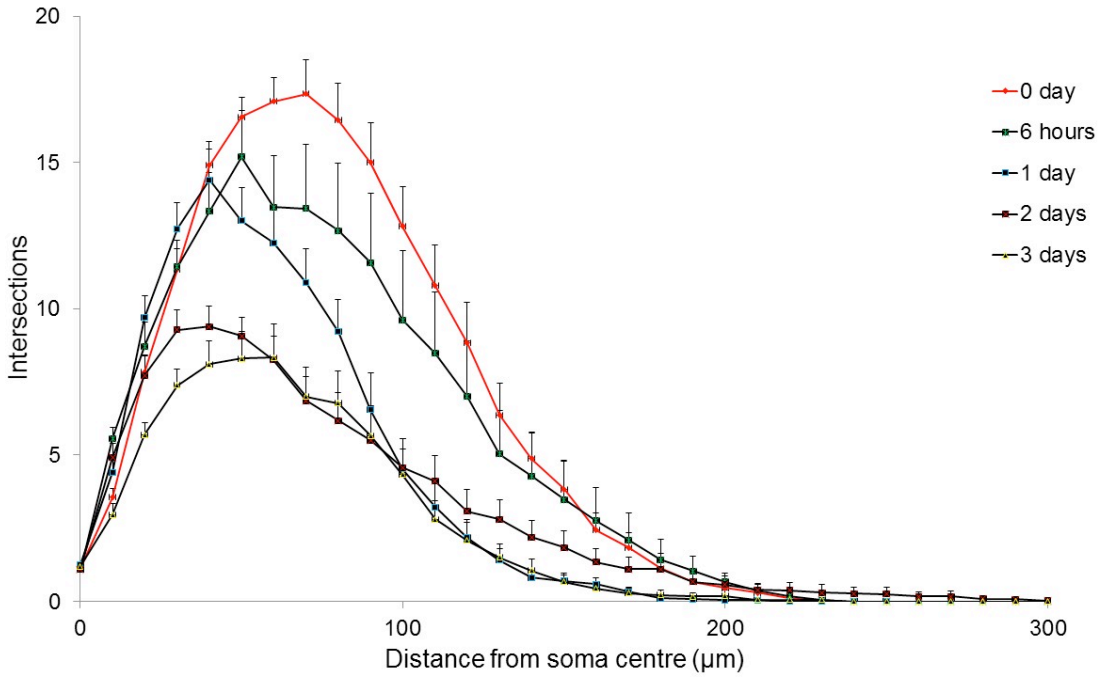

Figure 3.7 Sholl profiles of RGCs from retina explants cultured for 0 days (red) [n=43], DEV6 hours [n=21], DEV1 [n=32], DEV2 [n=42] and DEV3 [n=36] ex-vivo. Error bars shown in SEM.

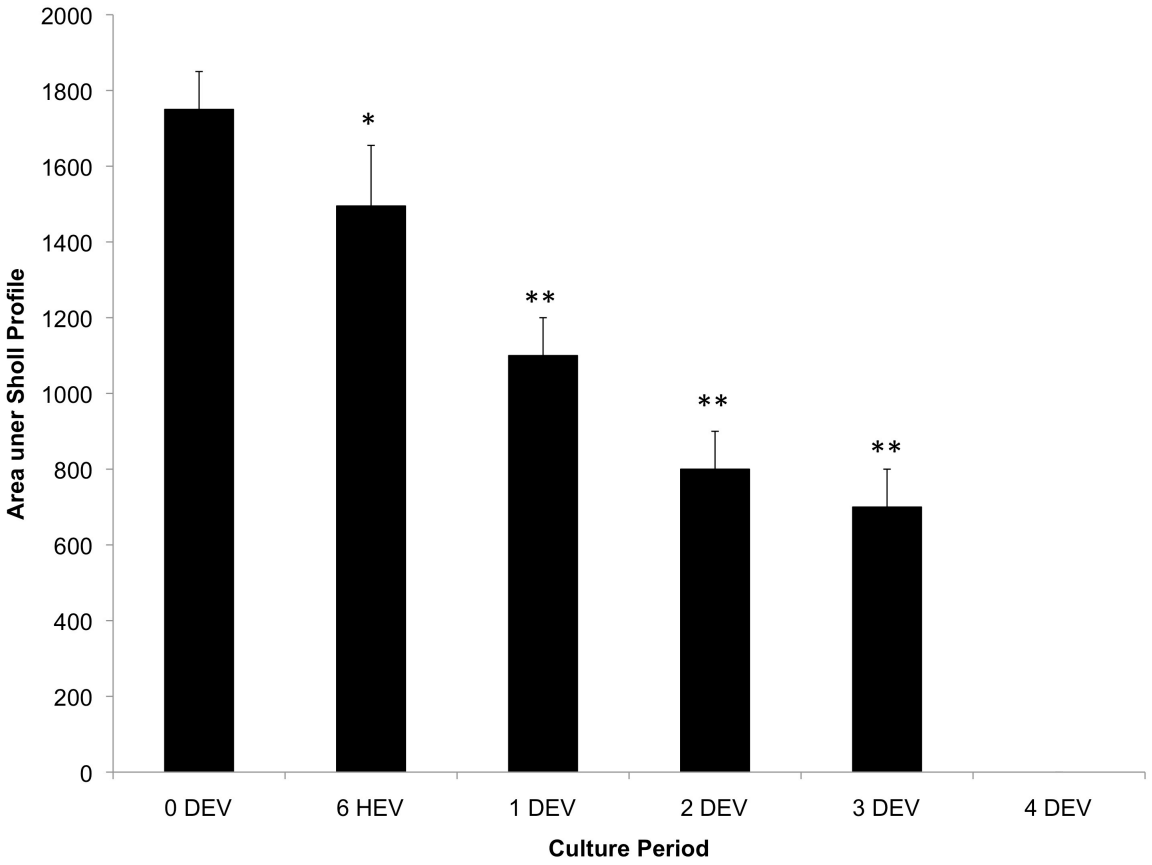

Figure 3.8 Bar chart showing AUC for Sholl profiles of RGC from retina explants culture for 0 days, 6 hours, 1 day, 2 days, 3 days and 4 days ex-vivo. No RGCs were identified on DEV4 to produce a Sholl profile. Error bars shown in SEM. *=p<0.05, **=p<0.01 post Bonferroni correction when compared with 0 days ex-vivo.

3.2.2.2 RETINAL CELL ARCHITECTURE: NUCLEAR STAINING

Nuclei structural integrity for ganglion cell layer (GCL), inner nuclear layer (INL) and outer nuclear layer (ONL) up to 14 days are described in Figure 3.9. Ganglion cell layer nuclei started out high at Day 0 but halved by DEV 3 and stayed similarly low but still present, even at DEV14 ($p=0.007$ at DEV14). Inner nuclear layer thickness surprisingly increased as culture period extended ($p=0.016$ at DEV14), whereas outer nuclear layer thickness increased initially at DEV3 but decreased thereafter but this was statistically insignificant.

3.2.2.3 APOPTOSIS DETECTION BY TUNEL STAINING

All layers were positive for TUNEL staining at 14 DEV. In GCL 14 DEV showed the most TUNEL positive staining, but in ONL and INL layers TUNEL staining was shown to occur from DEV7 (see Figure 3.10). There were no statistically significant differences shown.

3.2.2.4 LIVE CELL DETECTION BY CALCEIN-AM LABELLING

Retina explants showed abundant Calcein-AM staining in the GCL on DEV0 as well as DEV 14. There was a slight reduction in average number of Calcein positive cells per mm^2 and this was statistically significant ($p=0.022$) (Figure 3.11).

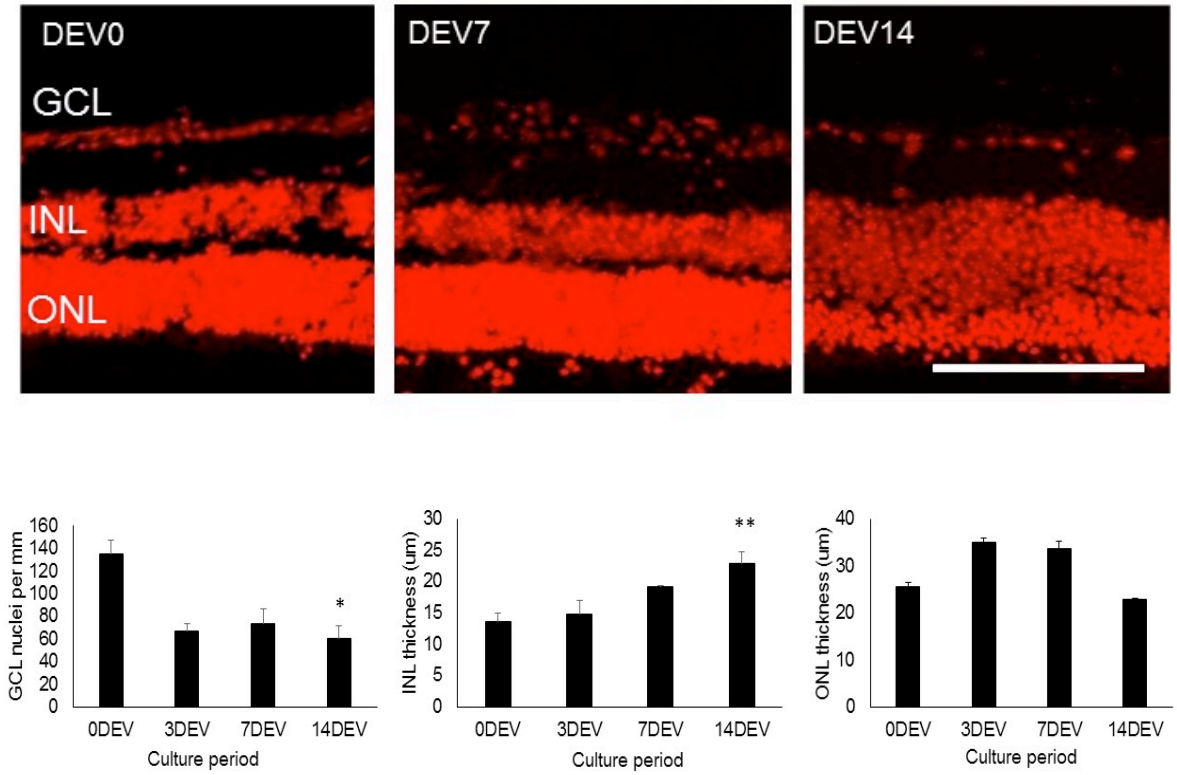

Figure 3.9 Top three confocal images of nuclei stained with TOPRO-3 from cryosections of retinal explants at 0 days ex-vivo, 7 days ex-vivo and 14 days ex-vivo. GCL=Ganglion Cell Layer, INL=Inner nuclear Layer, ONL=Outer Nuclear Layer. White scale bar represents 100 microns. Bottom bar charts show GCL layer nuclear counts (n=4), INL thickness (n=3) and ONL thickness (n=3) from retinal explant cryosections up to 14 days ex-vivo. Error bars shown in SEM. *=$p<0.05$, **=$p<0.01$ post Bonferroni correction compared to 0 DEV

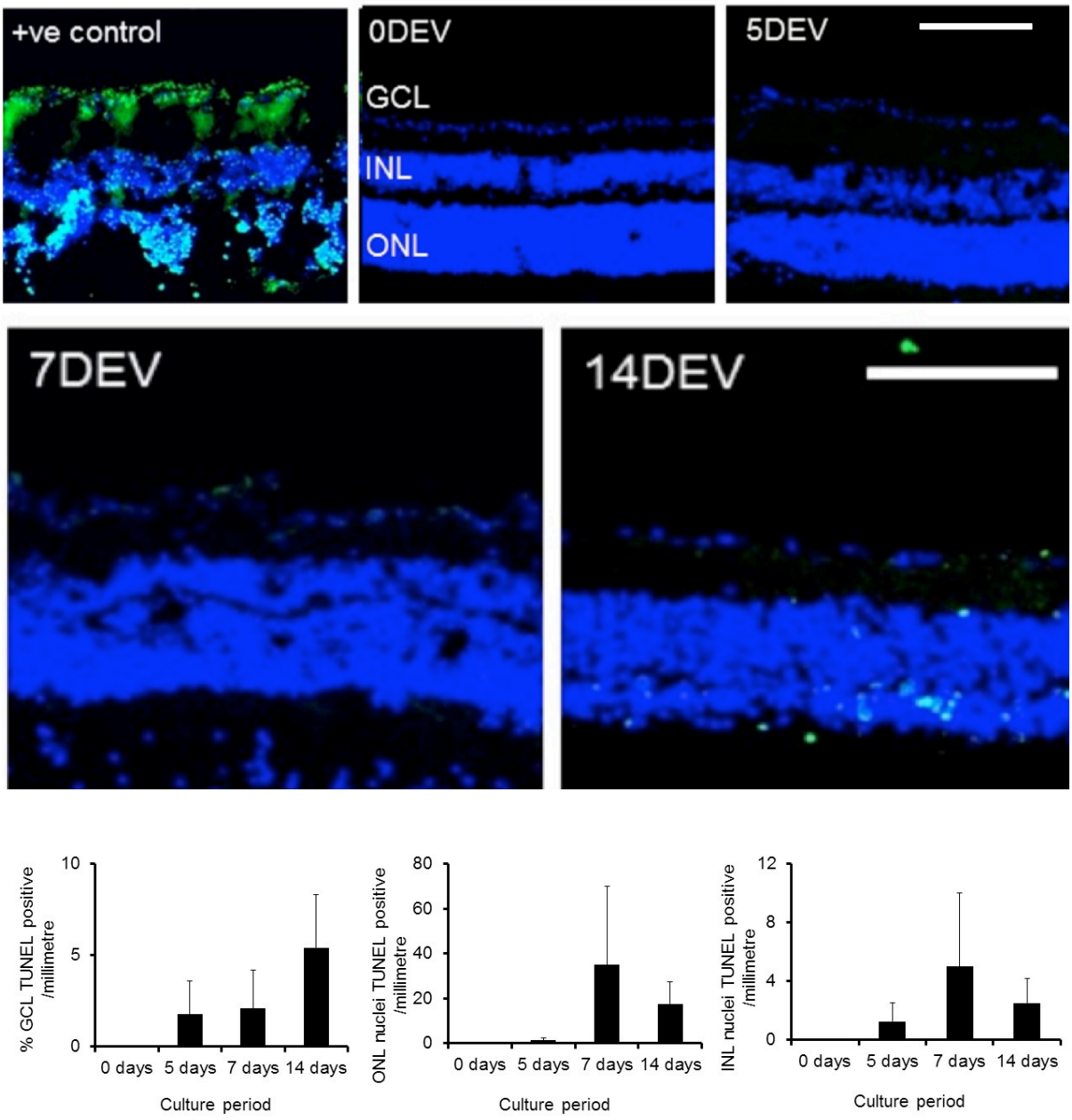

Figure 3.10 Confocal images above demonstrate cryosection images of retinal explants at 0, 5, 7 and 14 DEV stained with TOPRO-3(blue) for nuclei and TUNEL(green) for apoptosis. GCL=Ganglion Cell Layer, INL=Inner nuclear Layer, ONL=Outer Nuclear Layer. Scale bar=100 microns. Bar charts show percentage of TUNEL positive cells per mm, number of TUNEL positive nuclei in ONL and number of TUNEL positive nuclei in INL from retinal explant cryosections up to 14 days ex-vivo. Error bars shown in SEM.

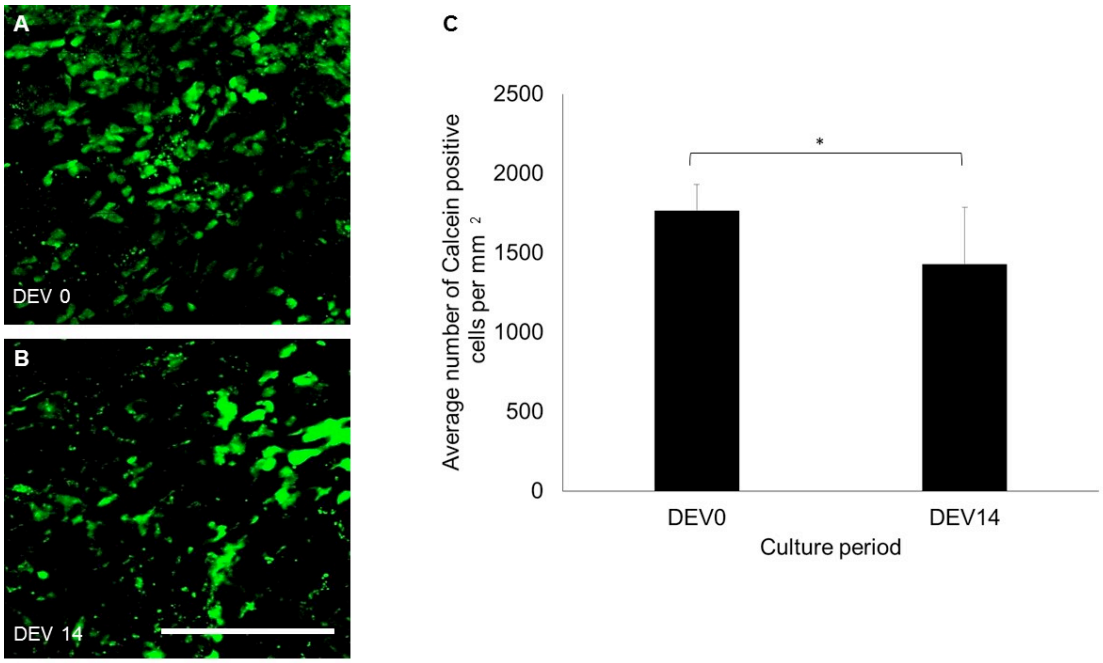

Figure 3.11 Confocal images A-B show Calcein-AM positive cells captured of 1 micron slice images in Ganglion Cell Layer of retinal explant on DEV 0 and DEV 14. Scale bar: 100µm. C) Bar chart showing reduction in the average number of Calcein-positive cells per mm^2 from DEV 0 and DEV 14 (n=8). Error bars represent SEM. *=$p<0.05$

3.3 DISCUSSION

The generation of a Sholl profile is a two stage process in our experiments. Firstly, tracing of the neuron; or in this case the RGC dendrite defines the position of all the dendrites. In the second stage the programs under scrutiny would be run based on the tracings previously produced, to generate a Sholl profile.

In this chapter I calibrated 4 programs to the "gold standard" manual Sholl profile. The FIJI plug-in: Simple Neurite Tracer emerged as the best program out of the 4 in correlation with manual calibration. Fastsholl MATLAB script, FIJI plug-in: Ghosh Lab and FIJI plug-in: Bitmap Sholl programs undercounted dendritic intersections with FIJI plug-in: Bitmap Sholl and FIJI plug-in: Ghosh lab undercounting dendrites the most. As Bitmap and Ghosh lab analysis may lead to undercounting, caution especially in retinal ganglion cell analysis should be taken as this would give a false effect on neuroprotective agents.

Furthermore, an erroneous second lesser hump further away from the soma centre at about 200 microns radius was observed. At first I thought that perhaps a maximum radius limit larger than the dendritic field may cause the algorithm to perform a reverse count of intersections back towards the soma. Efforts to eliminate this by adjusting the maximum limit of radius diameter failed to address this. When readings obtained from a blank image was analysed with Ghosh lab and Bitmap and subtracted from the Sholl analysis of interest, the second peak was removed. This is because FIJI produces a rectangular boundary on the bitmap canvas resulting in the generation of the artefact in the Sholl profile. In order to remove this error, future analyses using these programs should be run with blank image subtraction or an increased canvas size image so that the image outline does not interfere with readings.

The Fastsholl MATLAB script had been manually calibrated(Gutierrez and Davies, 2007) and so correlated well compared to the manual with only a slight undercount [AUC 3.5% below manual count]. Gutierrez et al. acknowledge that in their efforts towards achieving efficiency; using terminal points and branching points to predict the number of intersections at set ring diameters, it is possible that any dendrites which meander and intersect the ring more than once or even extend backwards to the soma, would result in a slight overestimation(Gutierrez and Davies, 2007).

As two assessors was used, Intraclass correlation coeffecient analysis was performed to highlight any inter observer variability in dendrite tracing given that reduced reproducibility and human error with manual neurite tracings have been reported(Meijering et al., 2004). To curb this, a semi-automated neurite tracer plug-in available on FIJI; Simple Neurite Tracer was used ((Longair et al., 2011). Indeed, excellent correlation of nearly 100% between the two tracers was observed (ICC 0.942-0.988).

Overall, the FIJI plug-in: Simple Neurite Tracer would be recommended as the program of choice for Sholl analysis of RGC. Its advantage in being open-source overcasts the commercially available Fast Sholl MATLAB though comparable in accuracy. Having a semi-automated tracing algorithm within the Simple Neurite Tracer plug-in facilitates the generation of a Sholl profile. The experiment highlights the need for calibration of Sholl analysis plug-ins available on FIJI prior to commencing analysis. This could possibly contribute to surprising results such as observing no difference in AUC for Sholl profiles of RGC treated with or without viral mediated gene therapy despite the presence of other morphological changes(Rodger et al., 2012) and in Kalesnykas et al. observing no significant decrease in dendritic structure for experimental glaucoma eyes despite the detection of terminal axon and soma loss(Kalesnykas et al., 2012).

Retinal explants cultured in this lab showed that using diolistics, RGC structure could be identified for up to 3 days ex-vivo. Thereafter, staining of cells were few and if present were indistinguishable from amacrine cells due to the absence of an axon. Prior to this study, there has been no detailed morphological quantification of RGC in retinal explant culture over time. Sholl analysis of RGC identified a significant decrease in dendritic complexity from Day 0 to Day 3. Indeed, the AUC had halved by Day 2 ex-vivo. From the Sholl analysis, it is interesting to note that dendritic complexity was decreasing further away from the soma first and maintaining complexity closer to the soma. It is possible that dendrite loss was occurring distal to the soma first as these were more vulnerable in comparison to those closer to the soma, or that larger RGC were dying faster than smaller RGC. This was similarly observed in Manabe et al. whereby retrograde labelling of RGC with DiI in the superior colliculus, followed by its cell count during retinal explant cultures, found a shift from the size of the fluorescent retinal ganglion cell spot size gradually over 10 days(Manabe et al., 2002). They commented that this was akin to dying of larger RGC first in comparison to smaller ones.

It seems that RGC dendritic complexity is lost, prior to RGC nuclei loss. Johnson et al. had reported explants viability of up to 2 weeks, our data shows that the health of RGCs and perhaps other underlying cells are compromised much earlier than reported (Johnson and Martin, 2008). Although their rat retinal explant culture system was very similar to retina explant

cultured in this lab, these differences in reported explant viability highlights the fact that in retinal explant use, the health of the target cell under investigation i.e. RGC in this thesis, needs to be taken into account. Reliance on retinal architecture and immunohistochemistry alone is insufficient to confirm RGC health. In this chapter, it is demonstrated that although retinal architecture was intact with very low levels of TUNEL staining at up to 14 days explant culture, and positive Calcein-AM labelling at 14 days, when RGCs are viewed directly and quantified by Sholl profile, their health is visibly compromised by day 3 of explant culture. Hence, should any therapeutics be tested after 3 days; by which dendropathy was at a severe extent, no difference would be detected in retinal ganglion cell morphology and possibly function.

Moritoh et al. concurred with results in this chapter as they managed to keep adult rat and mouse retina viable up to 4 days(Moritoh et al., 2010). They tested viability by demonstrating structure by ballistic transfer and function by patch clamp testing. They conducted a particle-mediated ballistic transfer of EGFP into the rat and mouse retinal explants, and showed mouse retina showed less viability when compared to rats and observed more pathological morphologies in their dendrites, such as swelling and thicker dendrites. Unfortunately, they did not quantify retinal ganglion cell morphology but suggested that this would be important in indicating the health of cultured retina (Moritoh et al., 2010). It is worth noting that the culture system of this group differs slightly from ours in that the culture media contained horse serum whereas ours did not, and that the use of rotary shaker was applied in their experiments.

It has been reported that in glaucoma, early changes in retinal ganglion cell dendritic structure precedes soma shrinkage and suggests dendritic abnormalities precede degeneration of other retinal ganglion cell compartments (Morquette and Di Polo, 2008). This agrees with this chapter's findings of dendritic complexity detection of up to 3 days only but a retinal ganglion cell nuclei count viable for up to 2 weeks. It is therefore imperative that a more detailed analysis of retinal ganglion cell morphology is used in tandem with other markers in the search for retinal ganglion cell neuroprotection.

Indeed, Bull et al. have highlighted that viability varies between not only labs but between experimenters (Bull et al., 2011). In this chapter, I was able to demonstrate and replicate their results of retinal architecture integrity up to 14 days with low amounts of TUNEL positive staining.

In summary, a duration of up to 3 days has been delineated for screening of retinal ganglion cell neuroprotection in retinal explants by quantifying dendritic complexities with Sholl profiles. This parameter allows for a quicker throughput for screening neuroprotective drugs as there is no need to wait until day 4 as previously suggested (Bull et al., 2011). It should also be noted

that quantifying retinal morphology is emphasised in retina viability experiments and not solely reliant on retinal ganglion cell nuclear counts as it may be an overestimate.

CHAPTER 4 MAGNETOFECTION

OBJECTIVES

- To explore and optimise the magnetofection parameters for transfection by using cornea as a test bed and retina as a proof of concept for future applications
- To optimise parameters for magnetofection of NSCs to achieve transfection efficiency without toxicity

4.1 INTRODUCTION

Gene therapy has revolutionized the treatment of many ocular diseases with a number of agents in clinical trials (Moreno-Montanes et al., 2014, MacLaren et al., 2014). Most treatments have targeted retinal and optic nerve disease using adeno-associated virus (AAV) viral vectors which are well tolerated in the eye. The AAV2 serotype remains the most popular for gene delivery since it is well tolerated (Sharma et al., 2010b, Sharma et al., 2010a). However, its small DNA cassette limit of 4.8Kb can limit its use of delivering large genes. Efforts have been made to overcome this to some extent by trans-splicing and/or recombination(Ghosh et al., 2011) but this can result in lower transfection efficiencies (Lai et al., 2010, Allocca et al., 2008). In view of these considerations, there has been a concerted effort to develop non-viral method for gene transfer such as electroporation, sonoporation, ballistics, and chemical facilitation (He et al., 2010, Sonoda et al., 2006, Bauer et al., 2013, Nguyen et al., 2002).

MNP transfection has been developed commercially as a non-viral gene delivery agent(Plank et al., 2011, Dobson, 2006) particularly for cells (e.g. neurons) that are difficult to transfect. MNPs have also been used in the eye to deliver genes to cells in the retina and vitreous of rabbits in-vivo with no reported toxic effects (Prow et al., 2008).

While magnetic fields can be used to restrict the distributions of MNP, the modulation of the magnetic field can be used to control the degree of transfection. MNP uptake occurs via cellular endocytosis (Plank et al., 2011) which can be enhanced by oscillating magnetic fields although

the exact mechanism for this is unclear (Adams et al., 2013). In this chapter, the use of a non-viral method of transfection; magnetofection with oscillation was explored.

Experimental Design

Firstly, I needed to identify an efficient plasmid to test transfection efficiencies of the magnetofection technique. I selected COS-7 cells as they are a robust cell line and chose lipofection which is a well-known efficient non-viral transfection method to test the plasmid transfection efficiencies. To explore the magnetofection non-viral technique for future ophthalmic use, I tested it on cornea explants as well as retinal explants. Finally, I optimized the parameters for NSC transfection and established the safest concentration of MNP for NSC with Ethidium Bromide Live/Dead assay.

4.2 RESULTS

4.2.1 VALIDATION OF PLASMIDS WITH LIPOFECTION OF COS-7 CELLS: CBA-GFP, CAG-GFP, BDNF-MYC

Initially a commonly used plasmid CBA (chicken beta actin) promoter with GFP reporter was tested. However, this yielded low plasmid concentrations in mini prep [0.04-0.07 µg/ml] and consequently very low transfection efficiency; only one cell in culture plate (Figure 4.1). Hence, CAG (cytomegalovirus enhancer, chicken beta-actin promoter, rabbit beta-globin gene intron and green fluorescent protein reporter) GFP reporter was tested, which yielded better plasmid concentrations and positive transfection (see figure 4.2).

The two plasmids were then tested with magnetofection in COS-7 cells with varying DNA:MNP concentrations at 2Hz 30 minutes as recommended by manufacturers as these parameters have reported successful magnetofection of NSCs(Adams et al., 2013). No transfection was seen with CBA-GFP but was present in CAG-GFP plasmid (Table 4, Figure 4.3). Hence, the CAG-GFP plasmid was selected for the following magnetofection experiments.

The plasmid BDNF-myc (CAG promoter, BDNF expression with myc reporter tag) was also validated by lipofection in COS-7 cells. Anti-myc staining was present in magnetofected COS-7 cells post lipofection (figure 4.4).

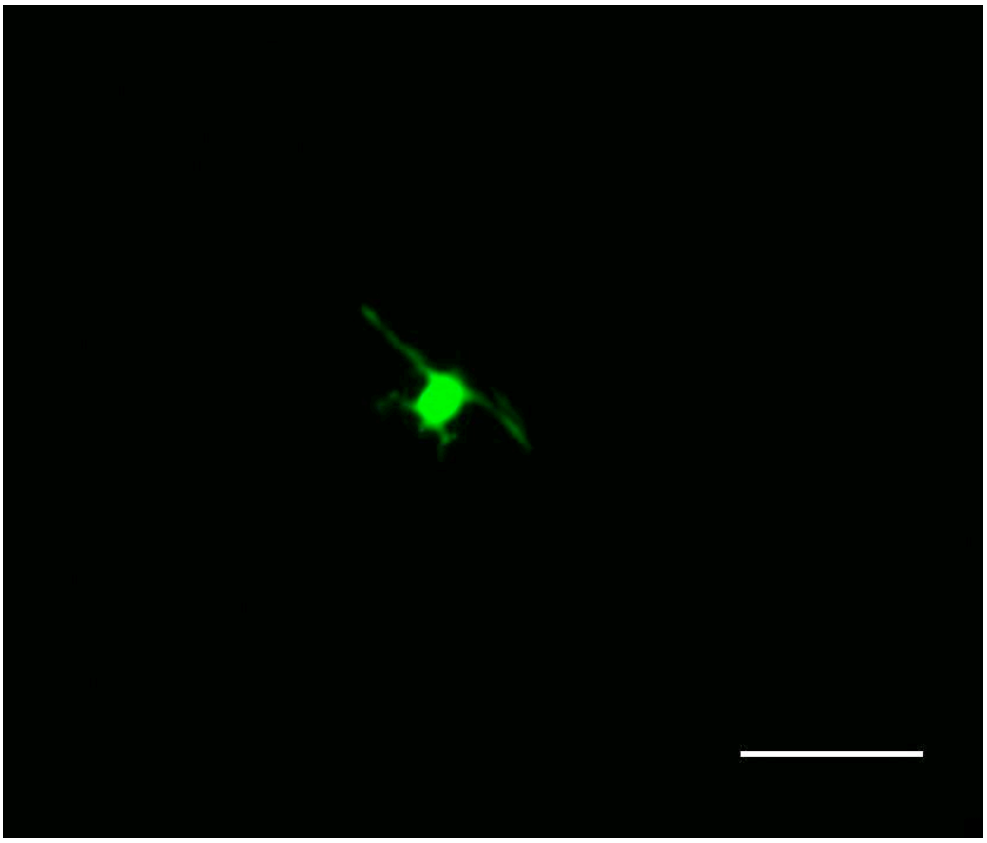

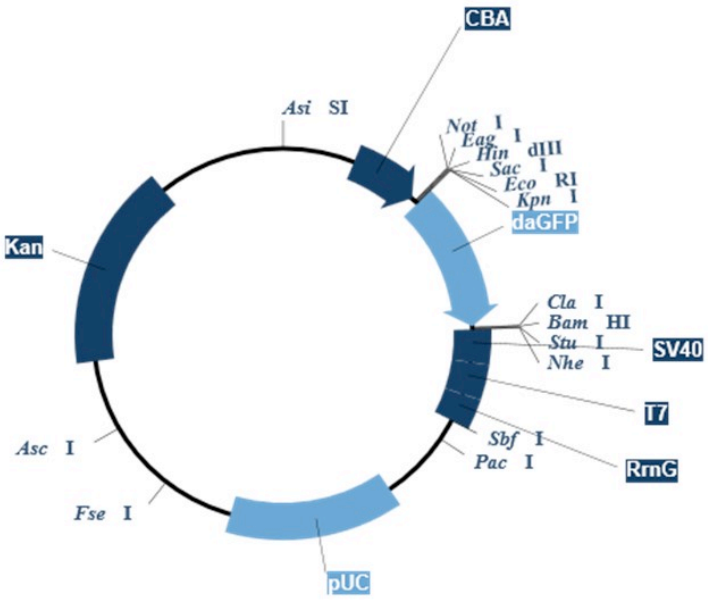

Figure 4.1 Fluorescent image of one GFP-positive COS-7 cell 24 hours post lipofection of COS-7 cells with CBA-GFP [construct map shown] (Oxford Genetics). Scale bar: 100µm.

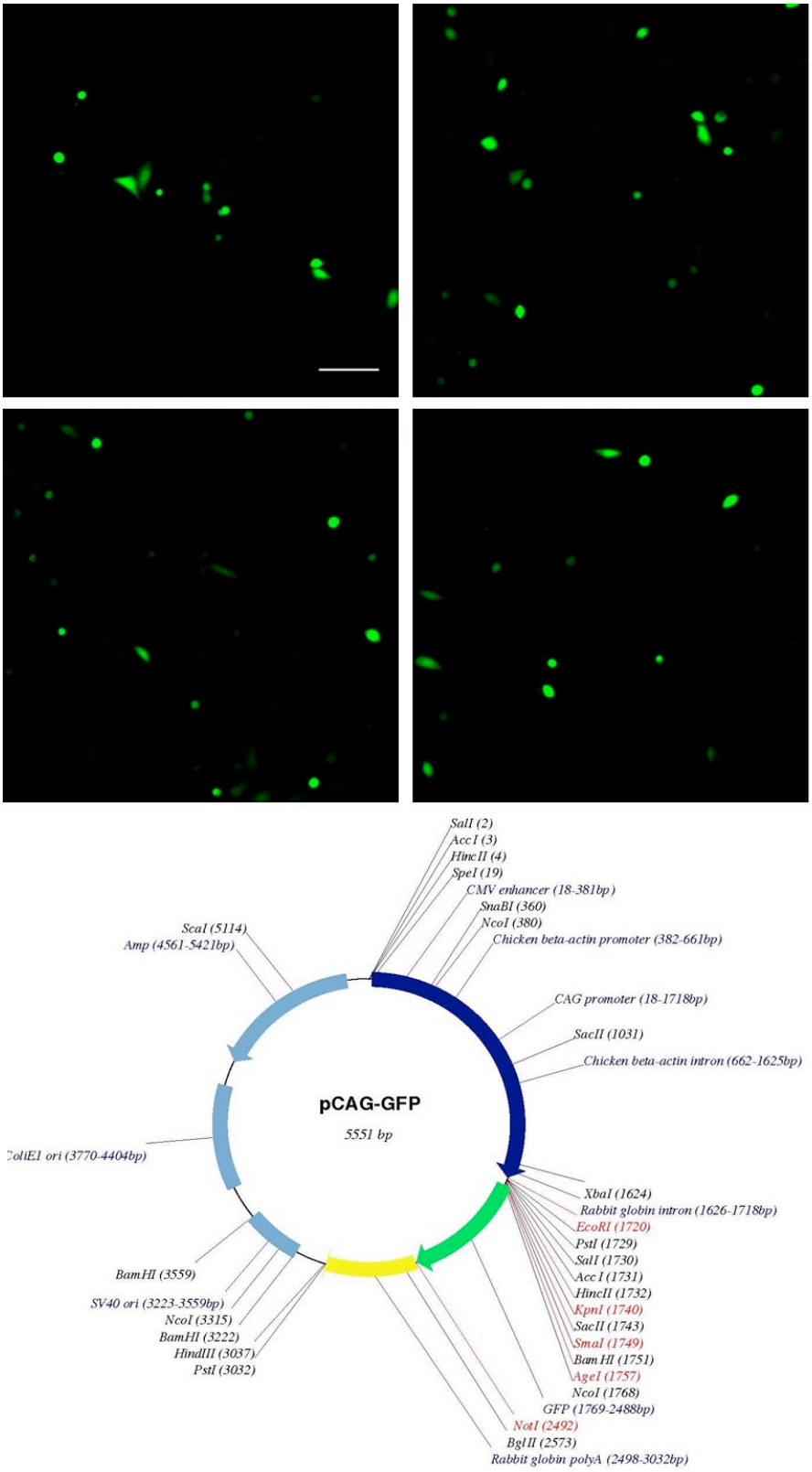

Figure 4.2 Fluorescent images of GFP-positive COS-7 cells 24 hours post lipofection with CAG-GFP [construct shown] (Addgene). Scale bar: 100µm.

DNA:MNP ratio	Plasmid	GFP Positive Cells
1:2	CAG-GFP	Present
1:1	CAG-GFP	Present
3:2	CAG-GFP	Absent
1:2	CBA-GFP	Absent
1:1	CBA-GFP	Absent
3:2	CBA-GFP	Absent
Control	nil	Absent

Table 4 shows presence or absence of GFP-positive cells in varying DNA: MNP ratio of the two plasmids tested with magnetofection in COS-7 cells.

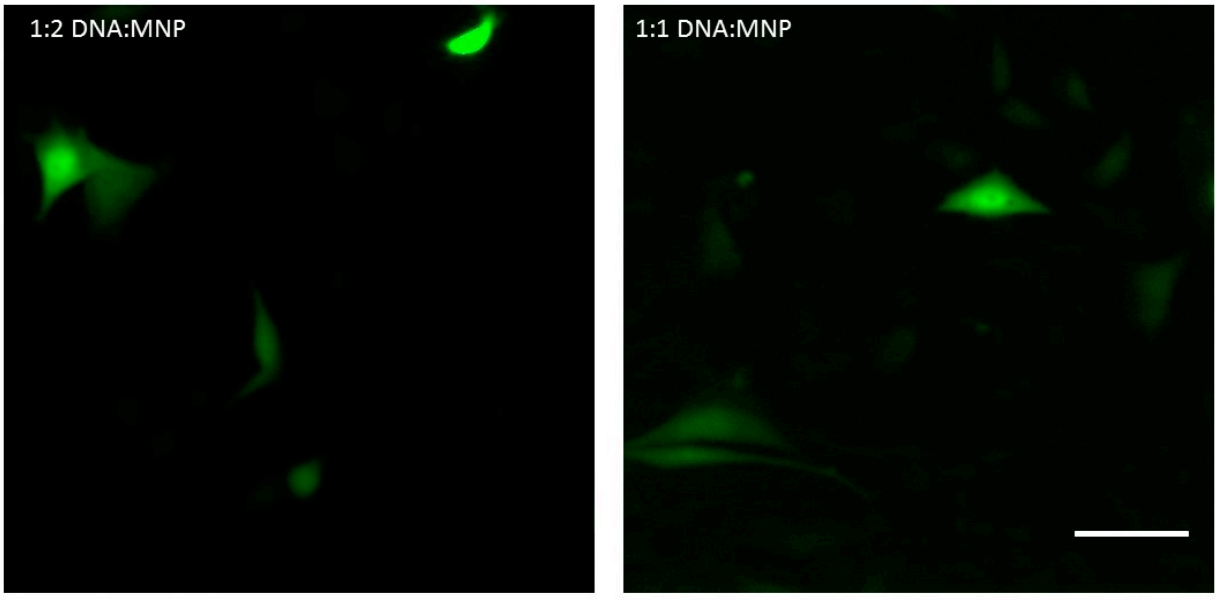

Figure 4.3 Confocal images showing GFP-positive COS-7 cells 24 hours post magnetofection at 2Hz for 30 minutes with CAG-GFP plasmid. Scale bar represent 50 microns.

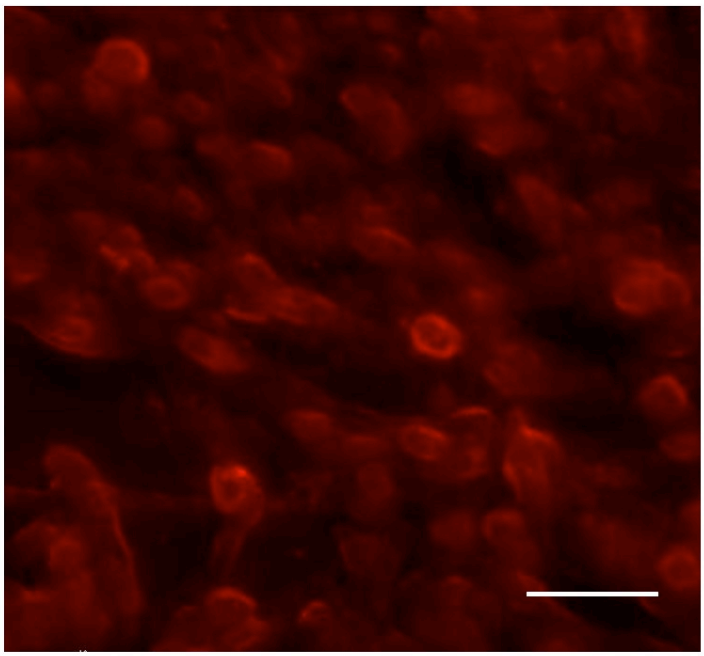

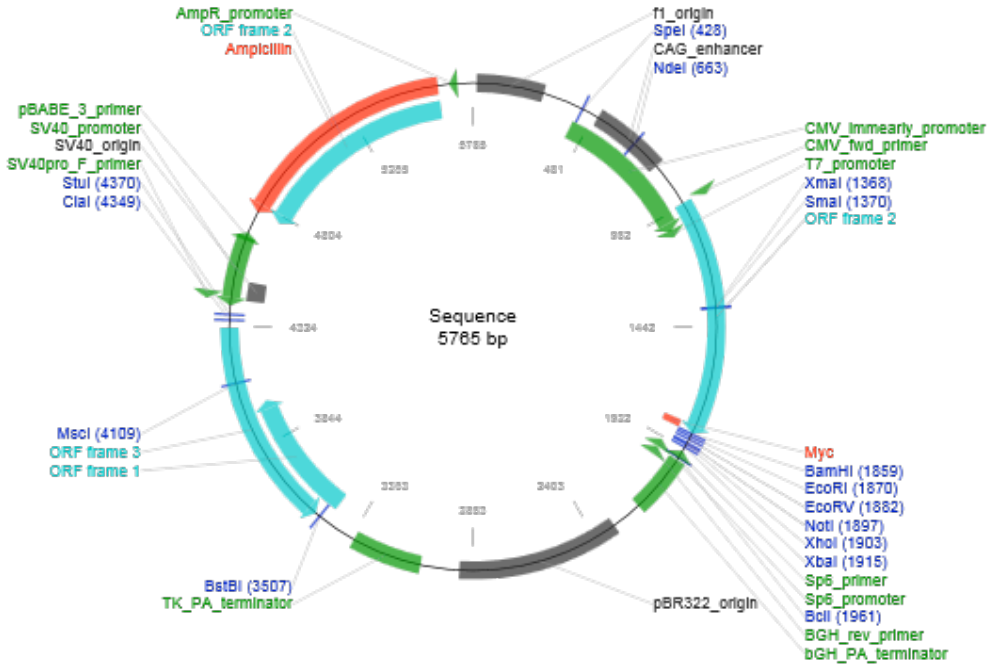

Figure 4.4 Fluorescent image of COS-7 cells positive for anti-myc staining 24 hours post lipofection with BDNF-myc plasmid. [Construct map shown](Gift from Prof Yves-Alain Barde, Cardiff University). Scale bar: 50µm.

4.2.2 CORNEAL MAGNETOFECTION AS A TEST BED FOR IN-VIVO MAGNETOFECTION

Magnetofection with GFP was present in cornea explants and was restricted to the endothelium layer. No endothelium transfection was observed in control experiments or in the absence of an external magnetic field [Figure 4.5]. The distribution of GFP-positive cells when the oscillatory magnetic plate was applied to corneas with endothelium side up is shown in figure 4.6 demonstrating transfection limited to the endothelium. The converse pattern was seen when corneas were placed epithelium side up with transfection limited to the epithelium and no transfection observed in the endothelial [Figure 4.5 and 4.6]

Transfection efficiency of a range of DNA: MNP combinations were investigated i.e. 1:2(0.4µg DNA: 0.8µl MNP), 1:1(0.4µg DNA: 0.4µl MNP) and 3:2(1.2µg DNA: 0.8µl MNP). The highest DNA: MNP (3:2) ratio resulted in the highest GFP-positive endothelial cell counts ($p= 0.05$).

When magnet application times were analysed, conditions with less than 15 minutes magnet application were not associated with any transfection. A statistically significant increase was observed in GFP-positive endothelial cell count with increasing duration of magnetic field exposure; from 15 minutes to 60 minutes magnetofection ($p=0.048$). Longer durations was not investigated as this would not be clinically translatable.

The highest yield for positive GFP endothelial cells was seen at 1 Hz. We noted that transfection efficiency declined above 1Hz $p=0.027$ (Figure 4.7). We noted some stromal transfection at 4Hz oscillation suggesting that increasing oscillation may have a role to play in increasing the depth of tissue transfection.

Conditions yielding the highest average endothelial transfection efficiencies were 3:2 DNA: MNP ratio, 1Hz oscillation and 30 minutes duration of magnetic exposure (23.3% range: 10.6% to 30.9 %) followed by 3:2 DNA: MNP ratio, 2Hz oscillation and 60 minutes duration of magnetic exposure (14.5% range: 12.2%-18.9%).

Toxic effects of MNPs in cornea explants was explored. Control corneas cultured without MNPs showed minimal TUNEL staining in the epithelium and keratocyte (see Figure 4.8). Corneas incubated with MNP for 24 hours showed similar minimal positive signals in the epithelium and keratocyte. Statistical analysis showed no difference between the two groups ($p=0.99$). No TUNEL staining of endothelium was detected.

Statistical analysis was performed with Mann Whitney-U test with Bonferroni correction.

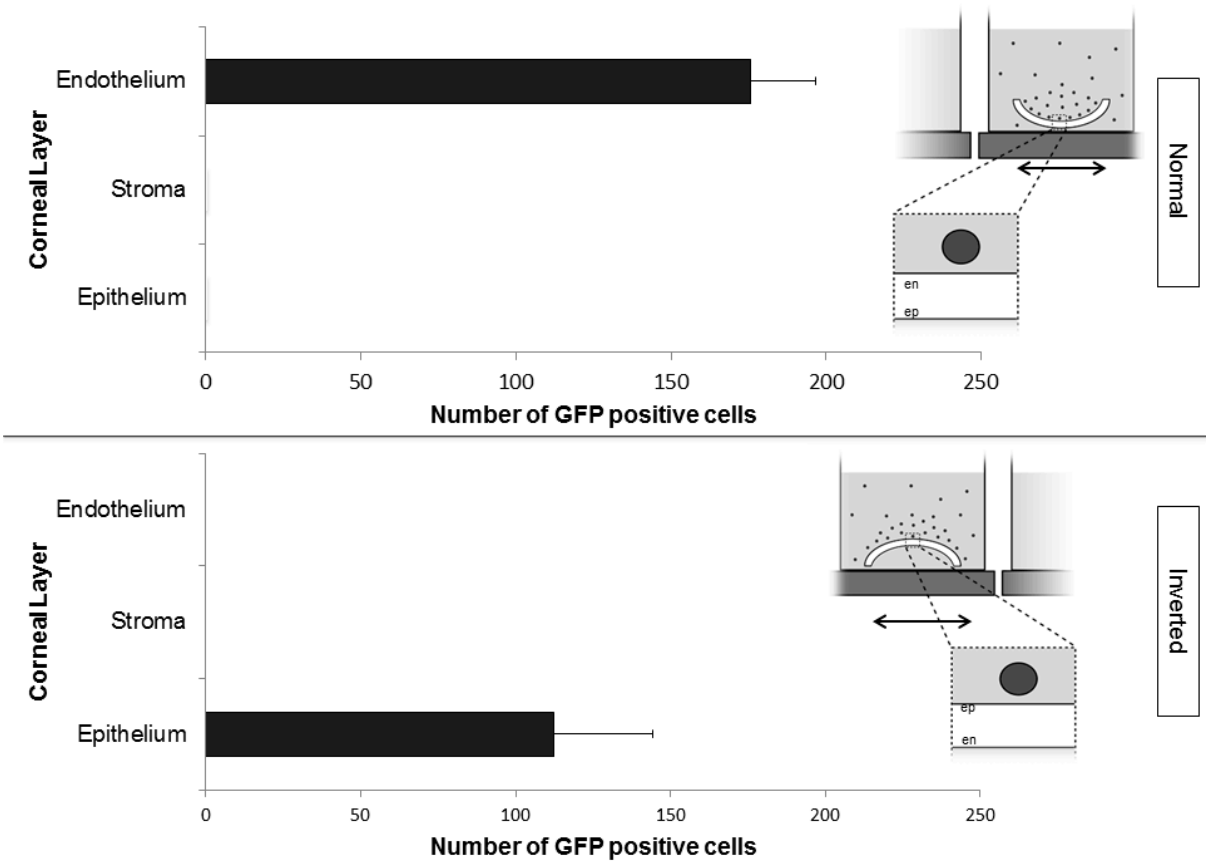

Figure 4.5 Transfection is dependent on cornea cup orientation. Top bar chart demonstrating GFP positive cells present only in endothelium, layer for normal experiment setup at 2Hz horizontal oscillation, 3:2 DNA: MNP ratio for 30 minutes. Bottom bar chart demonstrating GFP positive cell counts present only in epithelium layer for inverted experiment setup at 2Hz horizontal oscillation, 3:2 DNA: MNP ratio for 30 minutes. Experimental setup for each bar chart is shown in cartoon on the right of bar charts. Error bars show SD. Endothelium=en, epithelium=ep.

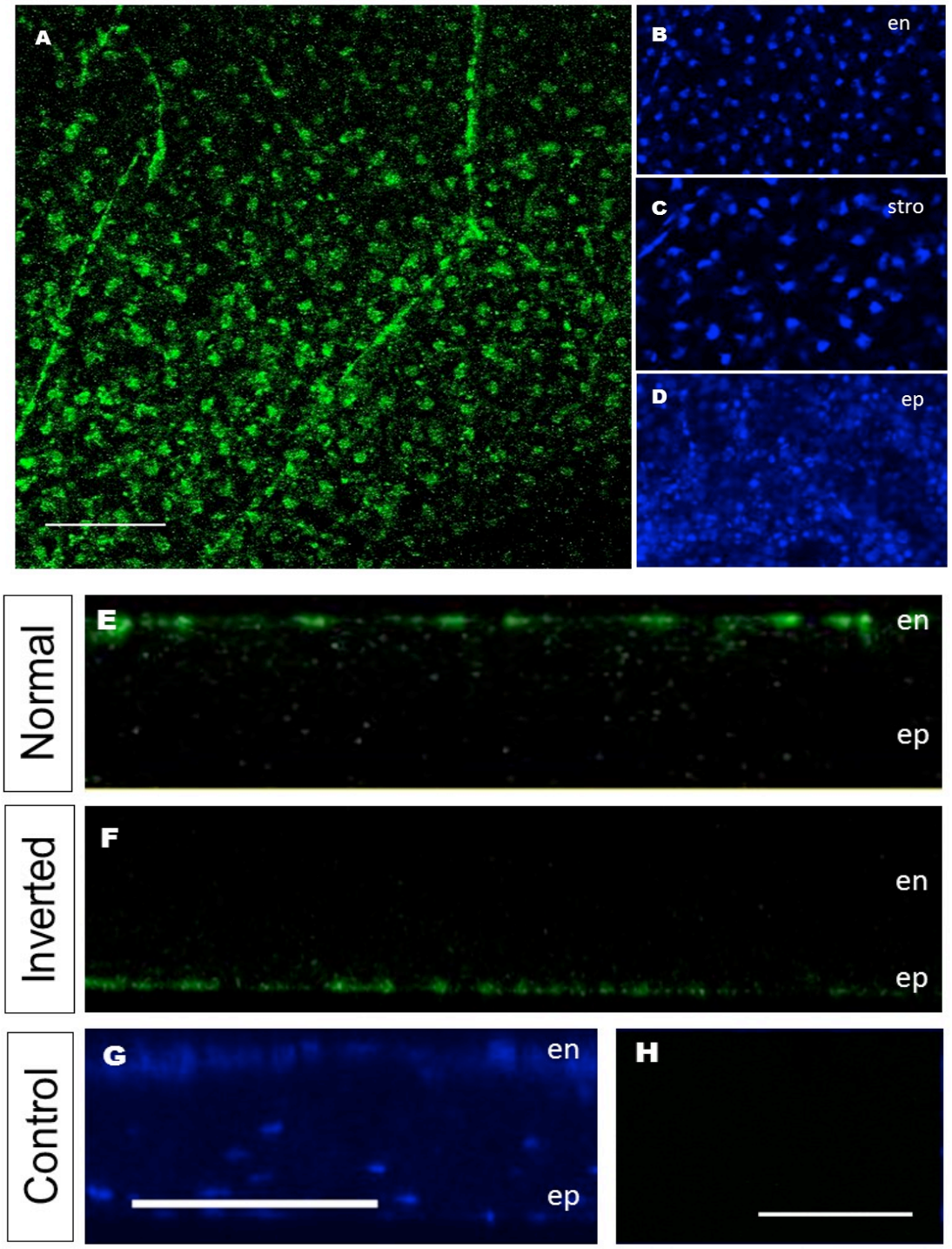

Figure 4.6 (A) endothelial cells exhibiting GFP in cornea (green) [1µm image stack] with corresponding orthogonal view (E). Images were obtained 3 days post CAG-GFP magnetofection of cornea. (B,CD) show 1um thick image slices of nuclear stained (blue) cornea allowing for identification of corneal layers: endothelium [en] single layer of regularly spaced small cells, stroma [stro] multilayers of larger irregularly spaced cells (forms the majority of the cornea) and epithelium [ep] multilayered, closely spaced sheets of cells. (F) Orthogonal view of transfected epithelium in an inverted cornea cup [epithelium side up] experiment setup. (G, H) Control corneas not exposed to magnetic field showing no transfection in endothelial cells [1µm image stack [H]]. (G) shows absence of GFP transfection throughout layers of cornea in corresponding orthogonal view with nuclear stain (blue).en=endothelium, ep=epithelium. Scale bar=100 microns

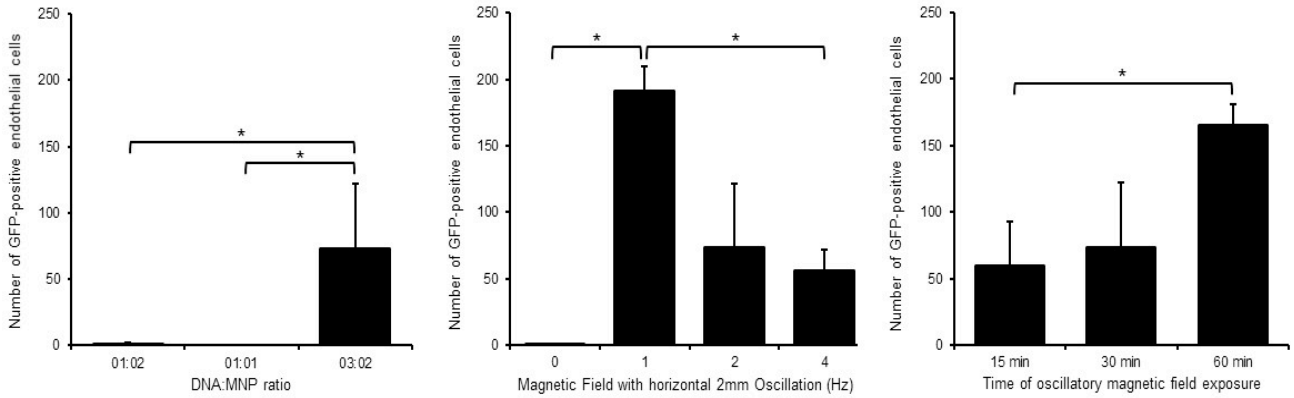

Figure 4.7 Oscillation, DNA: MNP ratio and duration of magnetofection affects transfection efficiency. (a) effect of increasing DNA:MNP ratio 1:2, 1:1 and 3:2 on transfection (2Hz, 30 minutes magnetofection [n=4]. (b) effect of increasing the frequency of field oscillation (1Hz, 2Hz and 4Hz) on transfection (3:2 DNA:MNP ratio, 30 minutes magnetofection [n=9]. (c) effect of duration of magnetic field exposure (15, 30, 60 minutes) on transfection (2 Hz, 3:2 DNA: MNP ratio. [n=6]. *P=0.05 post Bonferroni correction Error bars show SEM.

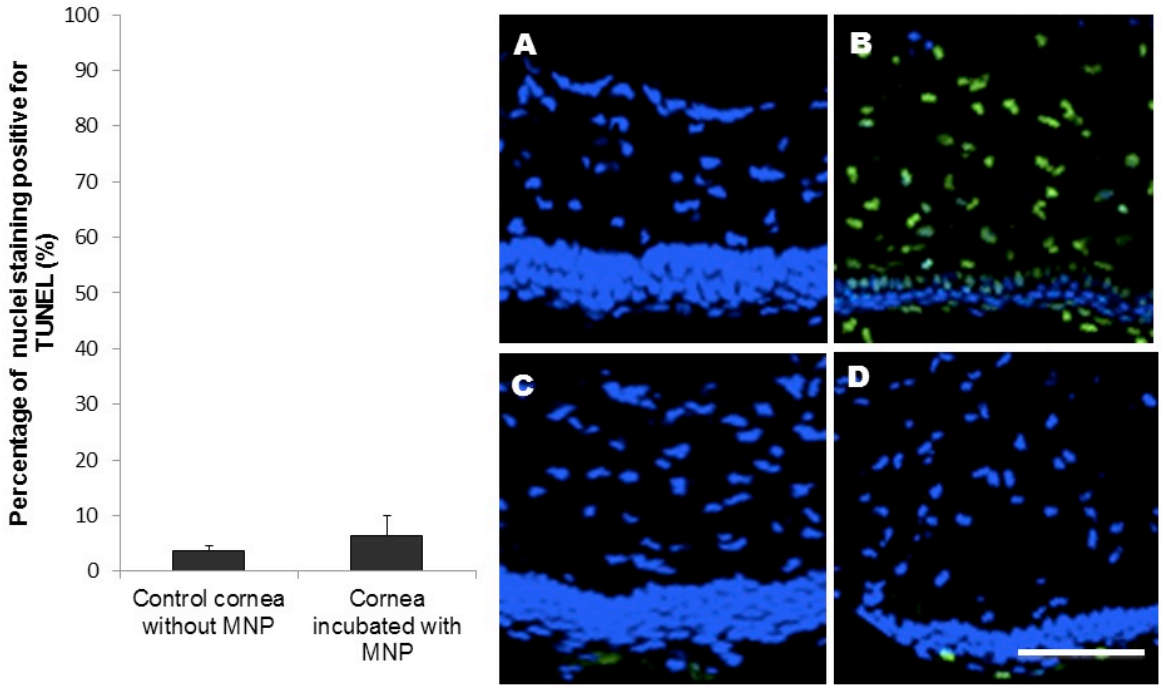

Figure 4.8 MNP incubated with cornea showed no significant toxicity. Bar chart on left shows no statistically significant difference in percentage of nuclei staining positive for TUNEL. Error bars represent SEM. Images to the right are of fluorescence microscopy post TO-PRO nuclear stain (blue) and TUNEL stain (green) of cornea cryosections; A] negative control, B] positive control, C] control cornea cultured without MNP, D] cornea incubated for 24 hours in 1µl of MNP. Scale bar: 100µm.

4.2.3 OPTIMIZATION OF MNP CONCENTRATIONS FOR NSC VIABILITY

Concentration levels of MNP ranging from 0.5µl MNP ml^{-1}(0.2µl MNP in 400µl media) to 2 µl MNP ml^{-1}(0.8µl MNP in 400µl media) were assessed for toxicity on NSC cell viability. Ethidium Bromide staining was absent in concentrations lower than 1 µl MNP ml^{-1} (0.4µl MNP in 400µl media) (Figure 4.9, 4.10). Levels above this also showed decreased ability of NSC to adhere and plate on laminin overnight.

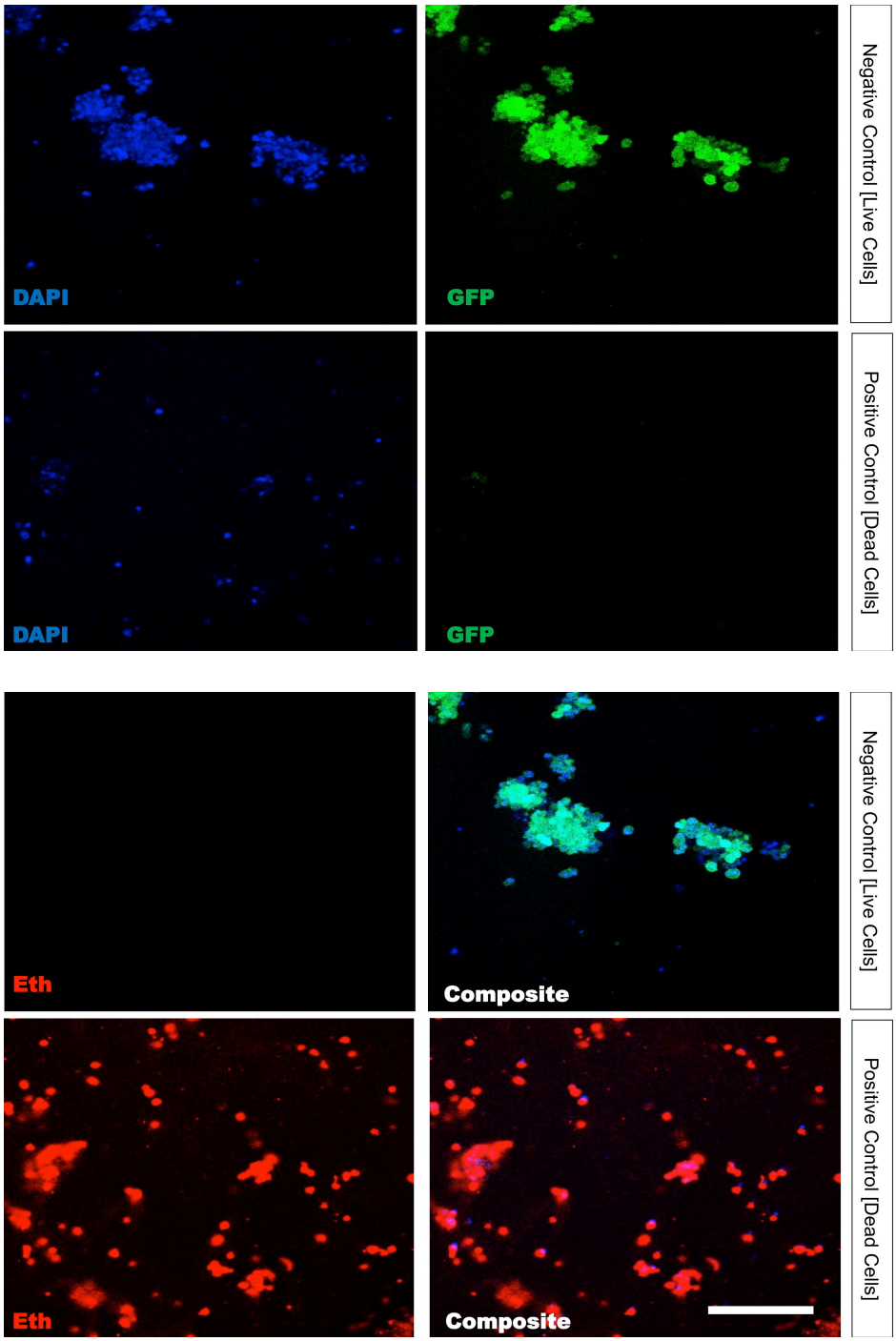

Figure 4.9 Confocal fluorescence imaging showing negative and positive controls for Live/Dead assay of NSC-GFP. Cell death stains positive with Ethidium Bromide (Red), Live=GFP (green) and Nuclei staining with DAPI (blue). Scale bar :100 microns.

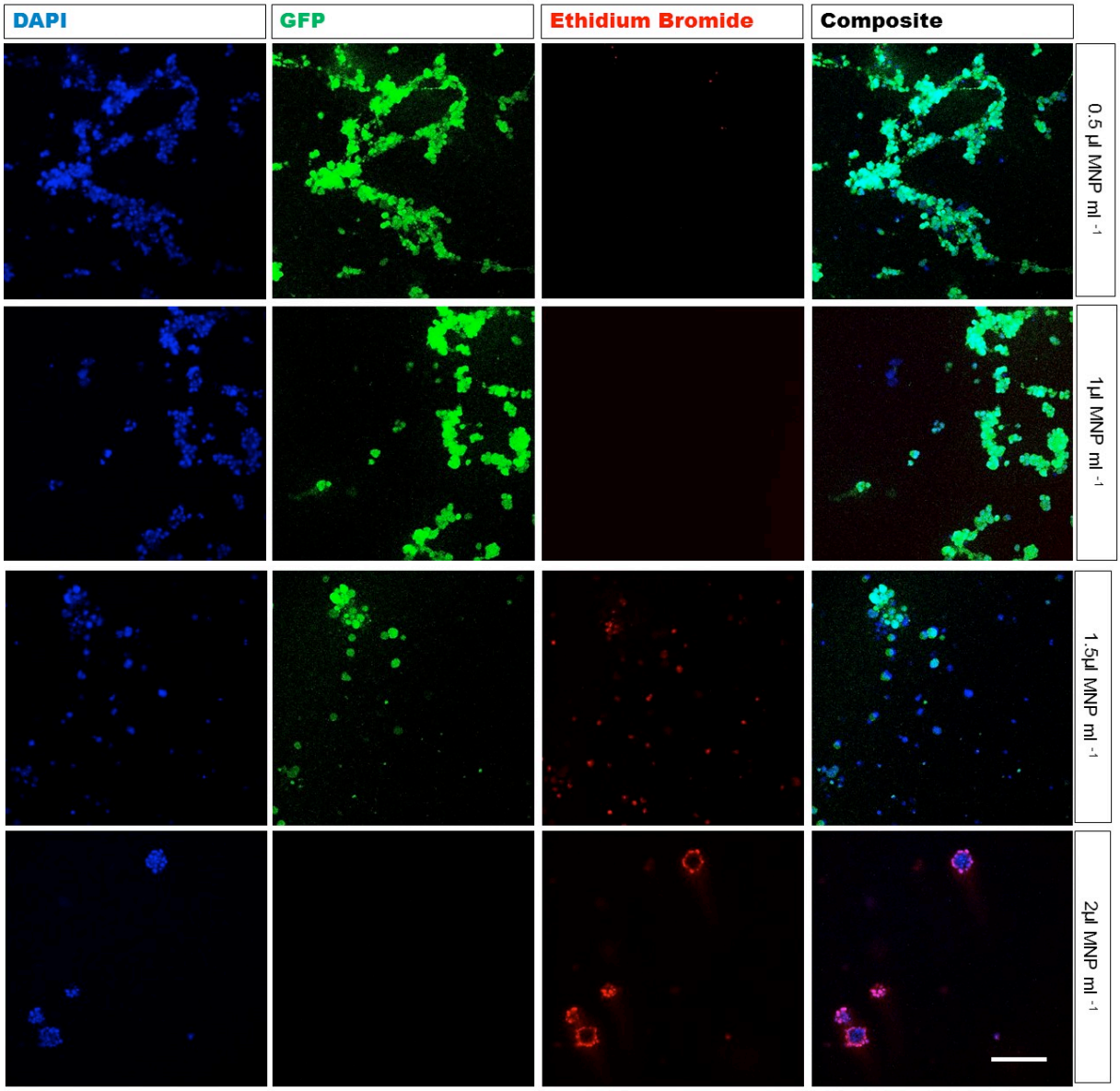

Figure 4.10 Confocal fluorescence imaging showing Live/Dead assay of GFP neuroshperes post 24 hour MNP incubation at various concentrations. Cell death stains positive with Ethidium Bromide (Red), Live=GFP (green) and Nuclei staining with DAPI (blue). At 0.5 and 1 ul MNP per ml, GFP is strongly present with absent red Ethedium Bromide staining indicating good viability at these concentrations. At concentrations higher than this, red staining from Ethidium Bromide is seen. In the neurosphere clusters for 2ul MNP per ml concentration, NSC on the outer part of the neurosphere is staining red where else the inner part of the neurosphere has yet to stain red but GFP is absent. Scale bar in white represent 100 microns.

4.2.4 MAGNETOFECTION OF NSC WITH GFP

Based on the NSC Live/Dead assay, a concentration of 1 µl ml^{-1} of MNP was used in the following experiments to magnetofect NSC with CAG-GFP. Magnetofection of NSC occurred with CAG-GFP with all the DNA:MNP ratios tested. However, only DNA: MNP ratio of 2:3 and 1:1 demonstrated statistical significance when compared to controls for average green fluorescence intensity (see figure 4.13). There was an increase in fluorescence seen from 24 hours to 72 hours post magnetofection (figure 4.11 and 4.12).

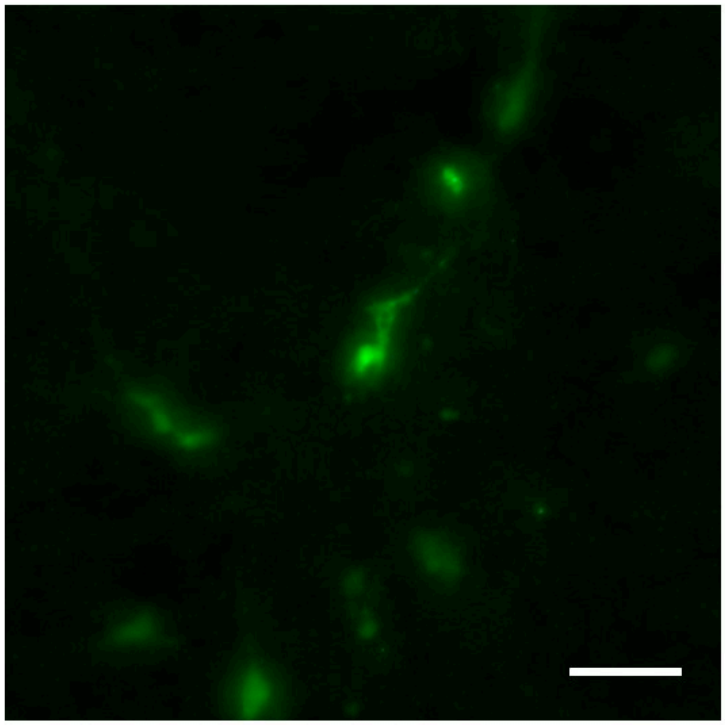

Figure 4.11 Confocal images of GFP-positive NSC 24 hours post magnetofection at 2:3 DNA: MNP ratio for 30 minutes at 2Hz oscillation. Scale bar 100 microns.

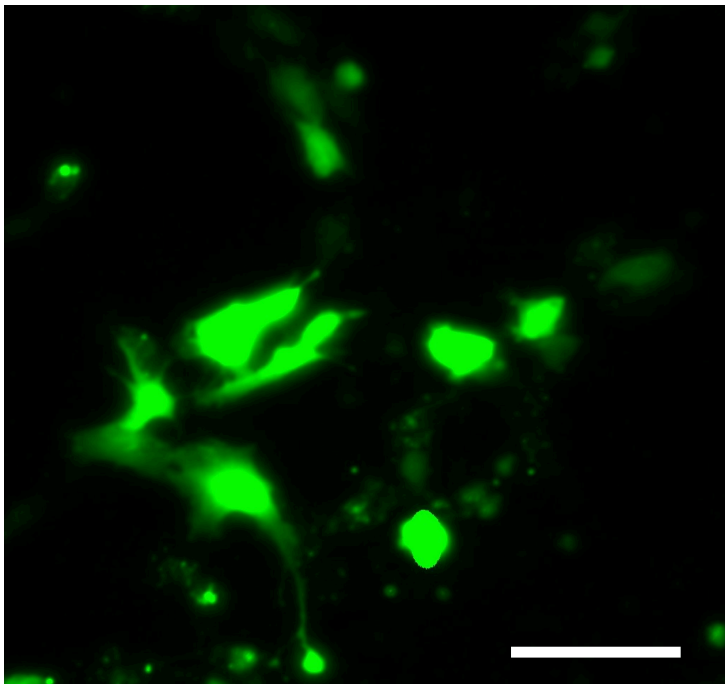

Figure 4.12 Confocal images of GFP-positive NSC 48 hours post magnetofection at 2:3 DNA: MNP ratio for 30 minutes at 2Hz oscillation. Scale bar: 100μm

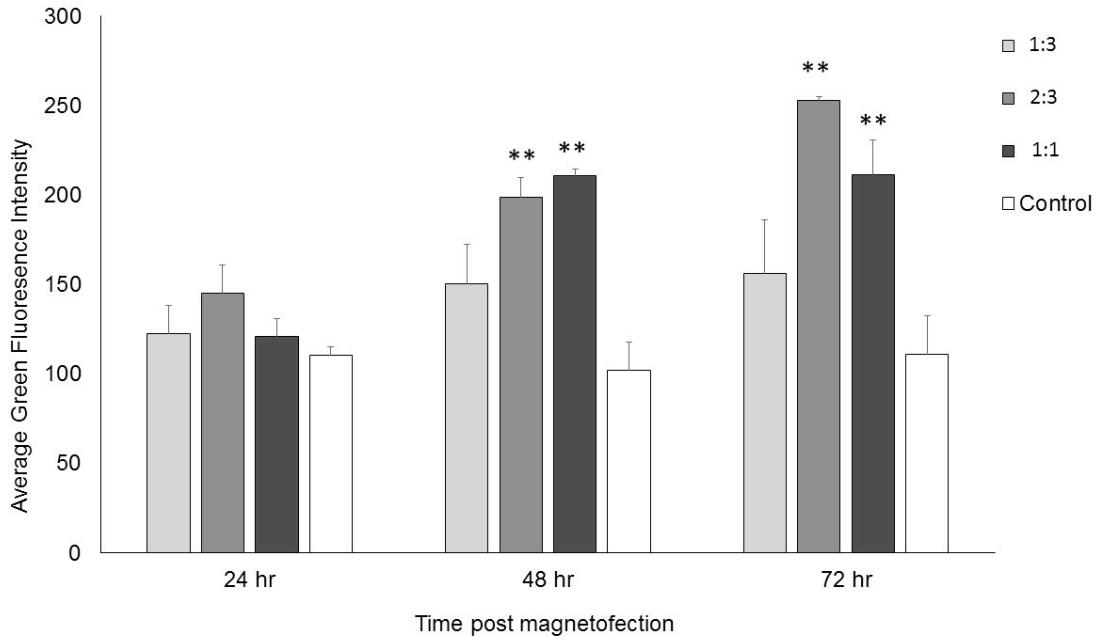

Figure 4.13 Bar chart demonstrating average green fluorescence channel intensity recorded over time for magnetofected NSC with 1:3, 2:3 and 1:1 DNA: MNP ratios. Error bars represent SEM. **=p<0.01 post Bonferroni correction compared to controls.

4.2.5 MAGNETOFECTION OF RETINAL EXPLANTS

Following successful magnetofection in the cornea explants, I then applied the magnetofection technique to assess its suitability for future in-vivo application in the posterior segment. Retinal explants were transfected at 1:1 DNA: MNP ratio, 1Hz magnetofection oscillation and for 30 minutes. This condition was chosen based on the cell viability and optimization results from 4.2.3 and 4.2.4 on NSC and neurosphere magnetofection as retina consists of neural tissue and is likely to be comparable. Fourty eight hours following magnetofection GFP-positive cells were present in the RGC layers but were absent in the INL (figure 4.14). The calculated transfection efficiency was 23.8%. Control explants were cultured for 2 days without DNA, MNP or magnetic field exposure and showed no GFP-positive cells (figure 4.15).

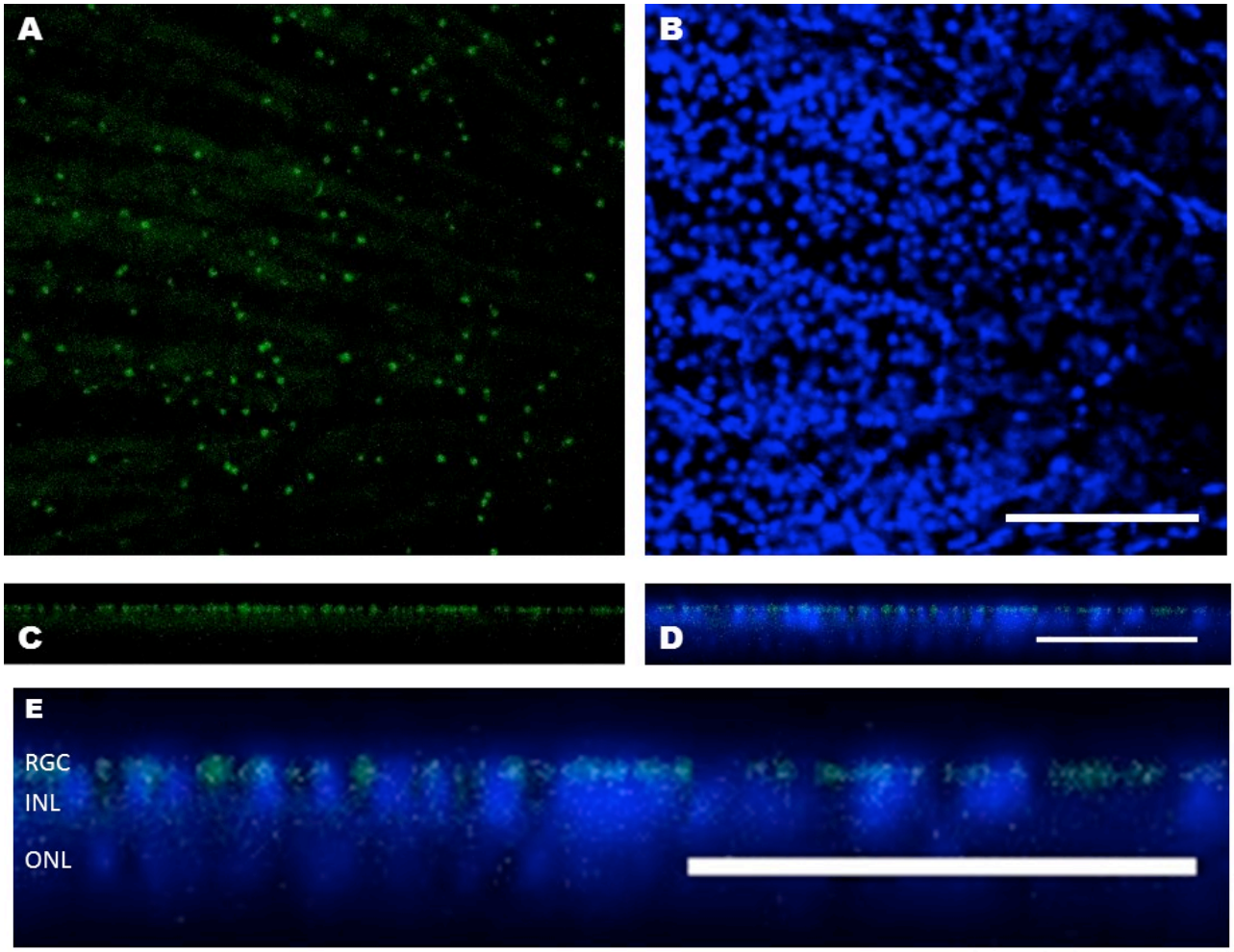

Figure 4.14 A) Confocal image of GFP-positive cells(green) in RGC layer (1 micron image stack) with corresponding nuclear staining (B) (blue), and the corresponding orthogonal views (C=GFP positive cells only, D=composite of GFP-positive cells and stained nuclei) 48 hours post magnetofection. E= orthogonal view of retinal explant showing GFP positive cells in RGC and absence of GFP in ONL. F= bar chart showing average transfection efficiency of 23.8%. Retinal explants were magnetofected at 1Hz oscillation for 30 minutes with 1:1 DNA: MNP ratio. (n=7) Error bars=SEM. Scale bar: 100µm.

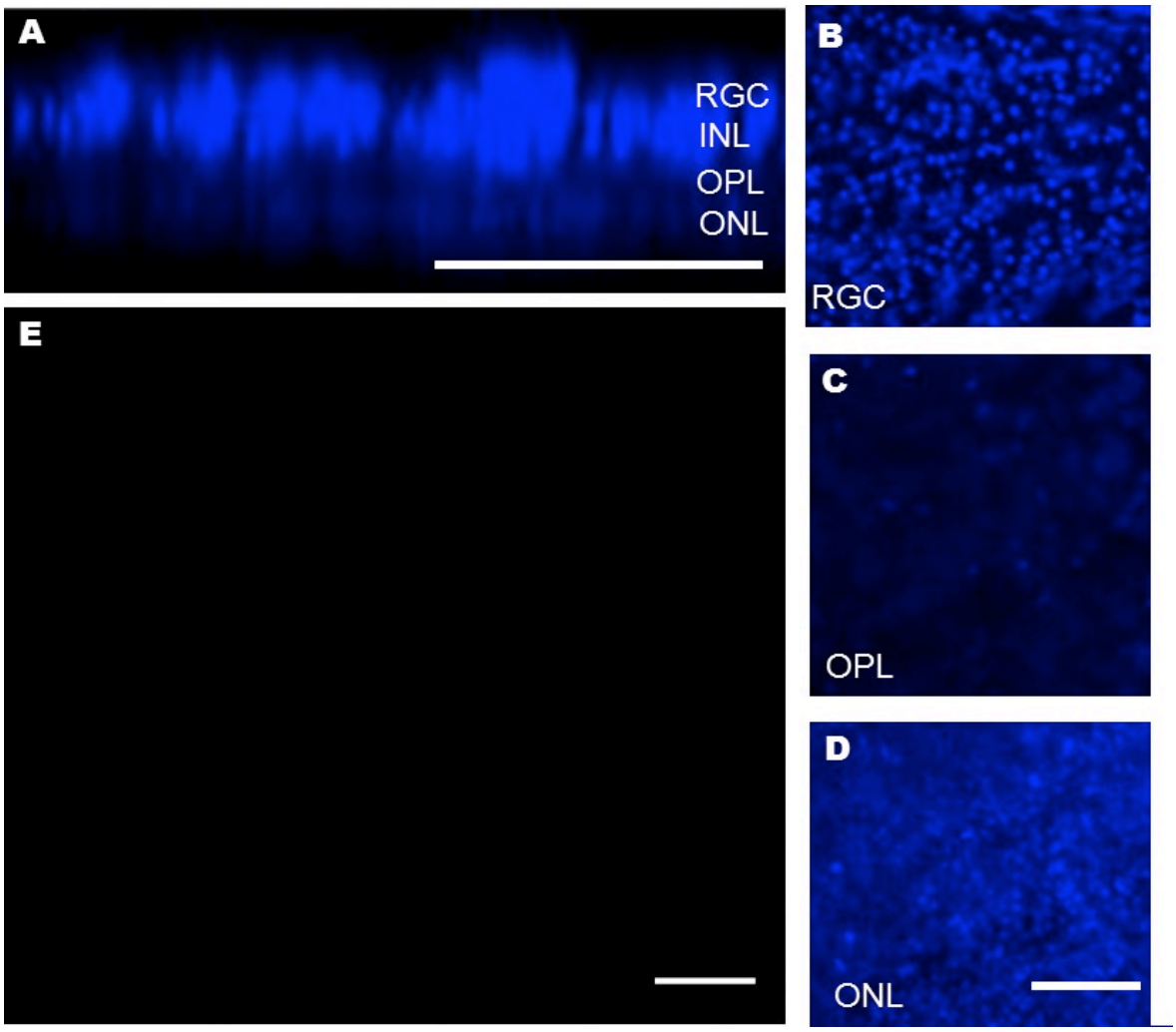

Figure 4.15 A= an orthogonal view of a control retinal explant showing absent GFP positive cells. B,C,D = 1 micron thick image slices of nuclear stained (blue) retina for identification of retinal layers: RGC=Retinal Ganglion Cell Layer OPL=Outer Plexiform Layer (layer of space in between RGC, INL and OPL consisting of sparse cells, INL=Inner Nuclear Layer, ONL=Outer Nuclear Layer.E= Z stack of a control retina showing absence of GFP transfection throughout the layers of the retina. Scale bar: 50µm

4.3 DISCUSSION

Successful magnetofection has been reported in neural stem cells in various publications (Sapet et al., 2011, Adams et al., 2013, Jenkins et al., 2011, Pickard et al., 2011, Pickard et al., 2015). The results in this chapter replicates this in neurosphere cultures. Although MNPs have been shown to have an excellent safety profile (Moysidis et al., 2015,Pickard et al., 2015), my initial pilot studies revealed unhealthy appearances of NSC post magnetofection at higher DNA to MNP concentrations. However, studies vary in the types of MNPs used. Indeed, Adams et al. used a higher MNP concentration of 70 µl MNP ml^{-1} [3.5µl MNP in 50µl NSC and media], but this was using NeuroMag which is an MNP manufactured for neuron transfection(Adams et al., 2013). In this chapter, a maximum concentration of up to 1 µl ml^{-1} of NtMag MNP was well tolerated by NSC as demonstrated by the Live/Dead assay. Furthermore, DNA:MNP ratios were optimized at 2:3 and 1:1 for magnetofection of NSC with nTMag, a lower MNP dose in comparison to Adams et al. Indeed, Sapet et al. who used NeuroMag also found cell death in transfected cells in higher concentrations of MNP NeuroMag i.e. more than 32 µl MNP ml^{-1} [1.6 µl in 50 µl] and ultimately used a DNA:MNP ratio of 1:1 for their experiments.

The cornea is an ideal candidate for evaluating future applications of magnetofection in-vivo. It is accessible, optically clear, avascular and a site of immune privilege. Furthermore, new insights into molecular pathology of several corneal dystrophies has revealed targets that are suited to a gene therapeutic approach, such as utilizing an siRNA against the mutant allele of keratin K3 or K12 in the anterior corneal stroma as therapy for Meesmann epithelial corneal dystrophy(Gillespie et al., 2014, Liao et al., 2011). The cornea can be easily subjected to external magnetic fields to guide and retain MNPs within a region of interest. To date, these studies have been undertaken at a cellular level. In this chapter, we demonstrated the potential for the manipulation of an external magnetic field in controlling the location and degree of corneal transfection.

A significant finding in the cornea experiments is that transfection did not occur in the absence of magnetic field oscillation. This was unexpected as magnetofection has been shown without oscillation (Adams et al., 2013,Pickard et al., 2015,Lee et al., 2008) . Gene transfer for magnetic nanoparticles may be easier in cells cultures; the cornea consists of a more robust structure abundant with collagen fibres, which could resist particle penetration. Interestingly, neurospheres also showed no transfection when a static magnet with no oscillation was applied with NeuroMag (Adams et al., 2013). The key to these contradicting results may lie in the variable MNPs used and hence needs to be taken into account with magnetofection application. In our study, the introduction of an oscillatory magnetic field coupled with a DNA-MNP complex

yielded optimum endothelial transfection at 1 Hz without the need of a tissue traumatizing intervention such as pretreatment with a stromal injections, de-epithelialization, or surgical flaps. Further increases in the oscillation frequency resulted in a reduction in endothelial transfection.

Much of the work on the application of gene transfer to endothelium has focused on strategies to improve outcome of corneal graft survival prior to transplantation(Kampik et al., 2012). Donor cornea can be treated prior to transplantation to transfer genes such as bcl-xL and p35 to improve endothelial cell survival (Fuchsluger et al., 2011) and the application of MNP is particularly suited to this approach where the transfection of non-endothelial layers is not required. Furthermore, the modulation of immunomodulatory genes to donor cornea endothelium can delay allogeneic rejection (Bauer et al., 2006). In-vitro treatment of endothelium cells prior to transplanting them onto the posterior corneal surface can potentially remove the effects of unwanted off-target effects.

Localised gene delivery to cornea is ideal for treatment of stromal scars. In-vivo injection of viral vector suspension into the anterior chamber transfects not only endothelium, but keratocytes at the site of injection and trabecular meshwork(Bainbridge et al., 2001). It also presents an attractive method for the targeted transfection of the trabecular meshwork given the ease with which magnetic particles can be drawn to this for the experimental elevation of intraocular pressure.

Other non-viral methods for corneal gene transfer such as electroporation while effective, can cause significant corneal damage(Blair-Parks et al., 2002). Magnetic nanoparticles have been reported as safe and non-toxic as demonstrated in in-vivo studies with retinal transfection in rabbit eyes (Prow et al., 2008). MNPs have recently been tested on corneal endothelial cells in vitro and have shown no short- or long-term change in viability or identity (Moysidis et al., 2015). Moysidis et al. showed no difference between transendothelial electrical resistance of MNP loaded cells and untreated cells, indicating their ability to form tight junctions between cells were not affected(Moysidis et al., 2015). This agrees with the findings in this chapter whereby TUNEL staining after 24 hours of MNP nTMag incubation with cornea showed no difference to that in untreated cornea.

Furthermore, following the optimum parameters used in cornea magnetofection, I magnetofected retinal explants as a proof of concept for future in-vivo experiments. In this chapter, the RGC layers were transfected with GFP and had a transfection efficiency of 23%, similar to other non-viral techniques. Gene therapy of retinal diseases such as RP and LCA are rapidly progressing with human clinical trials using recombinant AAV(Bainbridge et al., 2008,

Weleber et al., 2016) paving the way for the future application of magnetofection within the retina. However, the magnetofection technique is more technically challenging as it is less accessible. A subconjunctival magnet may need to be temporarily sutured into place on to the sclera for magnetofection to occur (30 minutes in this chapter). Future work into optimizing its parameters to shorten the duration of magnet exposure would make it simpler for clinical translation.

Use of MNP for gene delivery is also a clinically viable option as they are already FDA approved for MRI contrast agents (Thorek et al., 2006). Studies have shown that MNPs do not alter stem cell survival, migration, differentiation and electrophysiological characteristics (Dunning et al., 2004, Bulte et al., 1999, Guzman et al., 2007).Viral gene transfer limited by its cassette size, technical complexity and safety concerns need to be replaced by a safe and efficient non-viral option for clinical translation. In this chapter, I demonstrated the potential for magnetofection as a non-viral vector for gene delivery in NSC and in restricted tissue layers in the eye. In the latter part of this thesis, I will explore the use of magnetofection as a non-viral method for gene transfer of neurospheres to deliver neurotrophins in the retina.

CHAPTER 5 DIRECTING NEURAL STEM CELLS INTO THE RETINA BY GALVANOTAXIS

OBJECTIVES

- To determine if NSC is susceptible to directed migration by electrical field application in the horizontal plane.
- To determine if electrical field can direct NSC migration in a vertical plane

5.0 INTRODUCTION

Neural Stem Cells and directional migration

Endogenous electrical fields (EF) play an important role in the development of the CNS, with endogenous currents detected in many developing systems(Jaffe and Stern, 1979, Hotary and Robinson, 1994) and the disruption to growth i.e. failure of neural tube closure, when endogenous EFs were disrupted (Hotary and Robinson, 1994). EFs used to direct stem cell migration to areas of injury such as in spinal cord injury is currently explored (Song et al., 2004, Meng et al., 2012). The aim would be to promote functional recovery of the neural tissue by providing neurotrophic support or aiding endogenous regeneration. In ophthalmology, degenerative diseases such as dry AMD and glaucoma may benefit from long term neurotrophic growth factor delivery using stem cells as a vector. However, they need to be directed to migrate and integrate within the retina where chances of survival maybe higher and the delivery of neurotrophins is closer to the area of damage.

5.1 DIRECTED MIGRATION OF NEUROSPHERES IN A HORIZONTAL PLANE BY ELECTRIC FIELD APPLICATION

5.1.1 INTRODUCTION

Prior to any attempts at directing NSC migration into retina, proof of galvanotaxis in the NSCs cultured in the lab was essential. Galvanotaxis in NSCs is often reported in the form of single cells (Feng et al., 2012). In this experiment, the electrotactic chamber was applied to NSCs in the form of neurospheres 3 days post passage to assess for galvanotaxis. The rationale for this is that in spinal cord injury models where most of NSC transplantation work is reported, transplantation of NSCs are often in the form of neurospheres rather than dissociated cells(Cheng et al., 2015, Okano et al., 2003). Improved survival and integration has been reported in transplantation of injured rat spinal cord using whole versus dissociated neurosphere transplants(Mothe and Tator, 2005). The theory behind this is that the neurosphere microenvironment i.e. cell-cell contact, neurotrophin secretion (Ourednik et al., 2002) is optimum for its survival.

Experimental Design

Electrotactic chambers that have been widely used in various papers to assess the effect of EF on different cell types were used (Meng et al., 2012, Zhao et al., 2015, Li et al., 2014). [See 2.7.1 for material and methods). Briefly, it consists of plated NSC with matrigel in a chamber of 10mm x 22mm x 0.5mm where a DC current is applied. Cell migration was imaged by a time-lapse microscope fitted with a motorized stage. Based on previously established protocols within the lab, and studies which have reported galvanotaxis with a range of up to 500mV/$^{mm-1}$ in rat NSCs (Meng et al., 2012), EFs of 125mVmm^{-1}(total EF 2.75V [125mVmm^{-1} x 22mm^{2}]) and 250mVmm^{-1} (total EF 5.5V [250mVmm^{-1} x 22mm^{2}]) were evaluated. For data analysis, the FIJI plugin: Chemotaxis and Migration Tool was used to produce cell migration velocity, directness, centre of population, Forward Migration Index parallel to the x axis, Rayleigh's test of uniformity and a trajectory plot for cell migration was created (for definitions please refer to 2.9.1.1).

5.1.2 RESULTS

Neurospheres exhibit electrotaxis with directed migration towards cathode

Trajectory plots for control 0v, 2.75V (125mV mm^{-1}) and 5.5V (250mV mm^{-1}) are shown in figure 5.1. The neurospheres showed galvanotactic response for two hours with migration towards the cathode as previously reported (Meng et al., 2012). Centre of population was x:17.8, y:18.2 for controls, x:21.9, y:22.0 for 2.75V (125mV mm^{-1}) and x:45.8, y:46.2 for 5.5V (250mVmm^{-1}).

Forward Migration Index parallel to the x-axis was highest for 5.5V (250mV mm^{-1}) at 0.761, followed by 0.447 at 2.75V (125mV mm^{-1}) and 0.122 for controls. When aligned over time, neurospheres from 5.5V (250mV mm^{-1}) population showed a significant centre of population displacement increase early on in the experiment in comparison to controls ($p<0.001$). A significant but smaller response was observed in the 2.75V (125mV mm^{-1}) population ($p=0.04$) (see figure 5.2).

The directedness of the 2.75V (125mV mm^{-1}) population and 5.5V (250mVmm^{-1}) population showed a statistically significant difference in directedness $p=0.005$ for 2.75V (125mV mm^{-1}) and $p<0.001$ when compared to controls (see figure 5.3). Distances travelled for both accumulated and euclidean were statistically significant when compared to controls [$p=0.012$ for accumulated distance in 2.75V (125mV mm^{-1}), $p=0.006$ for Euclidean distance in 125mVmm^{-1}2.75V (125mV mm^{-1}), $p=0.018$ for accumulated distance in 5.5V (250mV mm^{-1}) and $p<0.001$ for Euclidean distance in 5.5V (250mV mm^{-1})] (see figure 5.4). Neurospheres displayed increasing velocity of migration as voltage increased; $p=0.012$ for 2.75V (125mV mm^{-1}) and $p<0.001$ for 5.5V (250mV mm^{-1}) (see figure 5.5). The Rayleigh's test revealed $4.86x10^{-9}$ and $1.42x10^{-9}$ for 2.75V (125mV mm^{-1}) and 5.5V (250mV mm^{-1}) populations showing an inhomogeneous distribution of cell end points with respect to circular distribution.

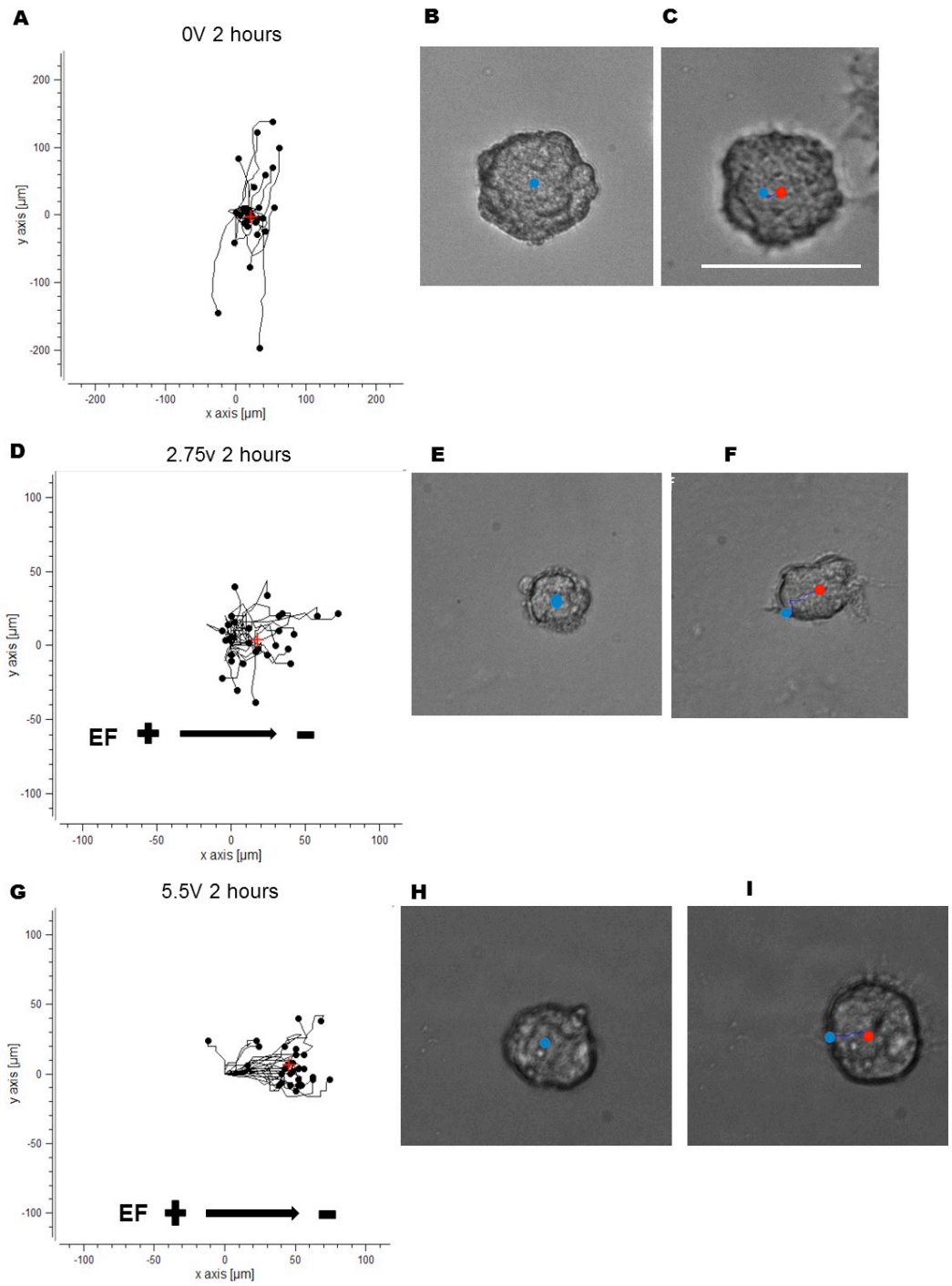

Figure 5.1 (A) trajectory plot of neurospheres imaged over 2 hours with no EF [n=29]. (B) and (C) show neurospheres at the start (B) [blue dot marks beginning centre point for cell] and end(C) of experiment [red dot marks centre point for cell at the end of experiment. Blue line illustrates the path of the cells centre point from start to end]. (D) trajectory plot of neurospheres exposed to 2.75V ($125mVmm^{-1}$) for 2 hours [n=45] ;(E) and (F) show neurospheres at the start (E) and end (F) of the experiment. (G) trajectory plot of neurospheres exposed to 5.5V ($250mVmm^{-1}$)for 2 hours [n=29] (H) and (I) show neurospheres at the start (H) and end (I) of the experiment. Red cross in A, D and G represents the centre of population for the group of cells at the end of the experiment. Scale bar: 100 microns.

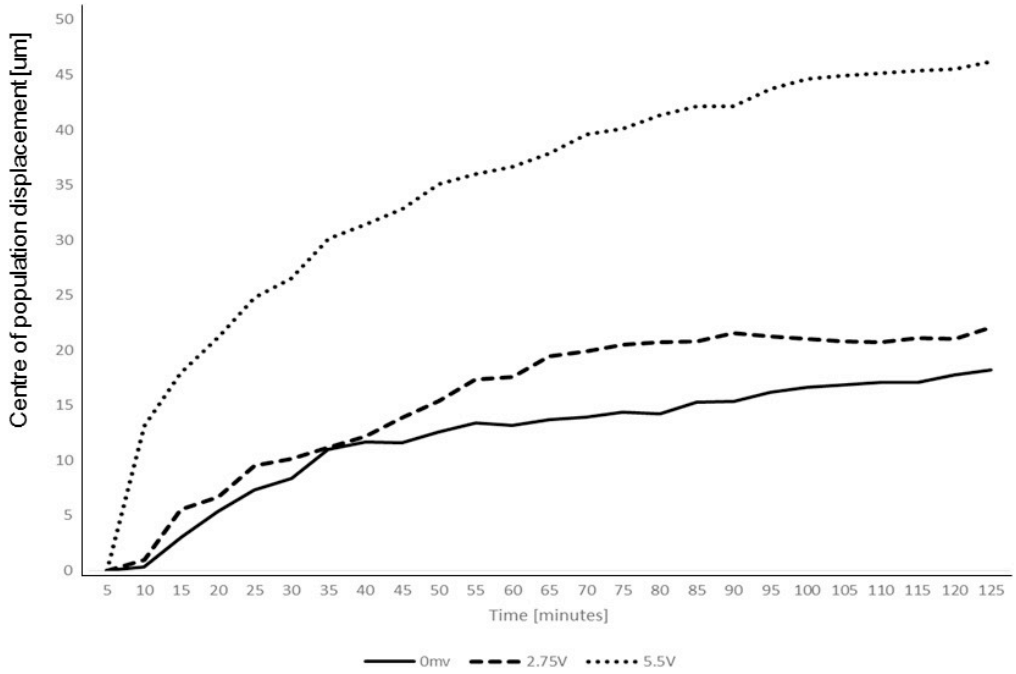

Figure 5.2 shows the displacement of the centre of population for each group [control, 2.75V ($125mVmm^{-1}$) and 5.5V ($250mVmm^{-1}$) group of cells] parallel to the x axis over 2 hours.

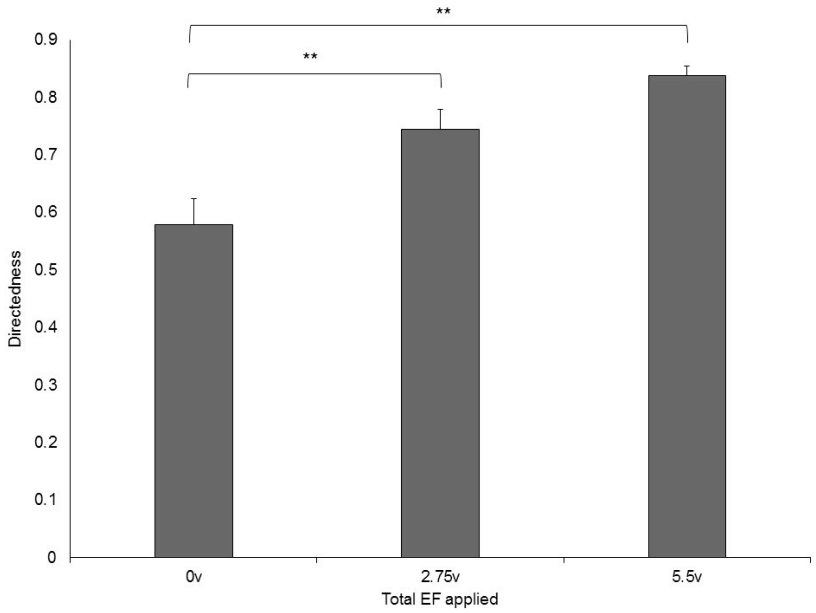

Figure 5.3 Bar chart showing directedness of cell migration for control, 2.75V (125mVmm^{-1})and 5.5V (250mVmm^{-1})experiments. ** = p<0.01 post Bonferroni Error bars=SEM

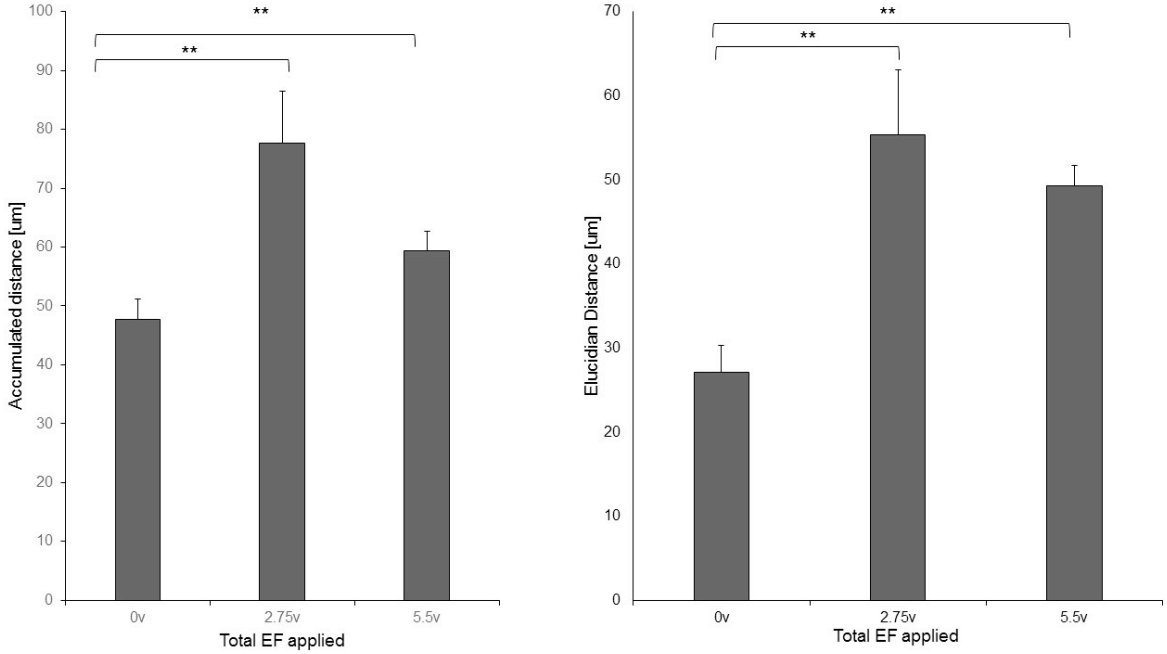

Figure 5.4 Bar charts showing accumulated and euclidean distances of neurosphere migration for control, 2.75V (125mVmm^{-1}), 5.5V (250mVmm^{-1}) experiments .** = p<0.01 post Bonferroni Error bars=SEM

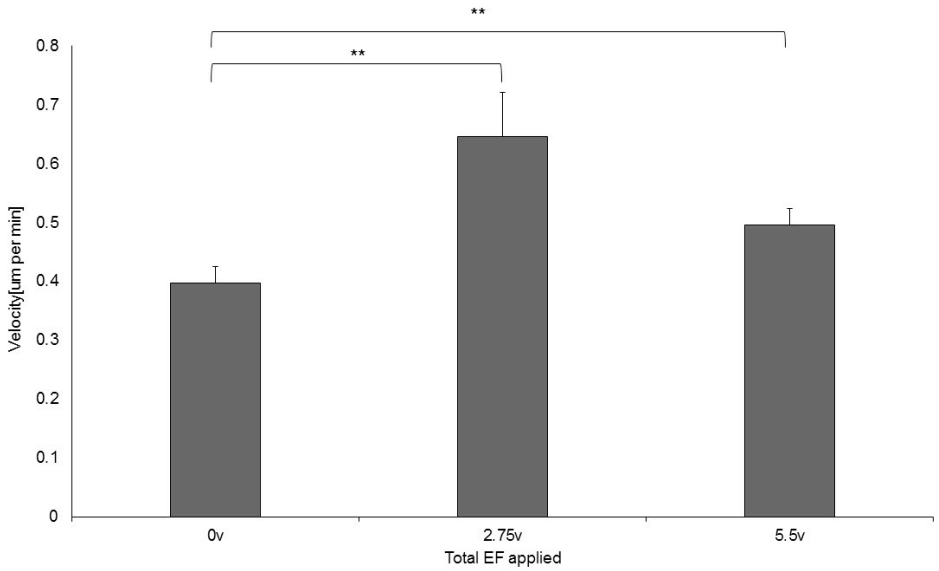

Figure 5.5 Bar chart showing average velocity of migration of cells in microns per minute for control, 2.75V (125mVmm^{-1})and 5.5V (250mVmm^{-1})experiments. ** = $p<0.01$ post Bonferroni. Error bars=SEM

5.2 DIRECTED MIGRATION OF NEURAL STEM CELLS IN A VERTICAL PLANE BY ELECTRIC FIELD APPLICATION

5.2.1 INTRODUCTION

To assess directed vertical migration of NSC by electric field, a conventional assay used in cell migration research; Boyden Chamber a.k.a transwell assay, was employed(Boyden, 1962). Although more often used in chemotaxis migration studies, it has been applied to investigate electrotaxis in lymphocyte cells(Lin et al., 2008).

Experimental design

The modified Boyden chamber consisted of upper and lower chambers separated by a filter with a pore size of 8µm. The upper chamber was filled with NSCs of the same cell density for all experiments. (See 2.9.3 for Boyden chamber set up details). Electric fields of 2.5V (1.47mv/mm^3), 5V (2.94mv/mm^3) and 10V (5.88mv/mm^3) were investigated based on cell viability studies showing cell death at above total EFs of 15V (10.7mV/mm^3). The electric field was applied across the Boyden chamber by placing two platinum electrodes connected to a DC power supply to the top and bottom well of the Boyden chamber; cathode in the lower chamber. Cells migrating from the upper to lower chamber would be captured on the filter mid migration and hence could be counted. The filter pore size of 8 µm was used as it provided enough resistance to show number of cells vertically migrating from upper to lower chamber. An initial pilot study of 4µm filters showed that this was too small for migration to occur and for NSC to be captured within the filter (Figure 5.6). Effect of increasing time of electric field exposure was also investigated at 20, 40, 80 and 180 minutes at 5V (2.94mv/mm^3). Cells present within the filter area captured were counted and compared to controls.

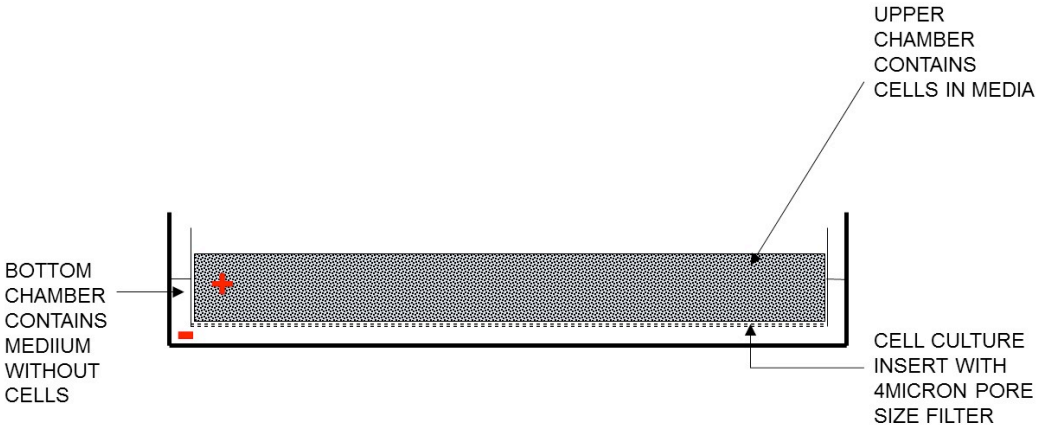

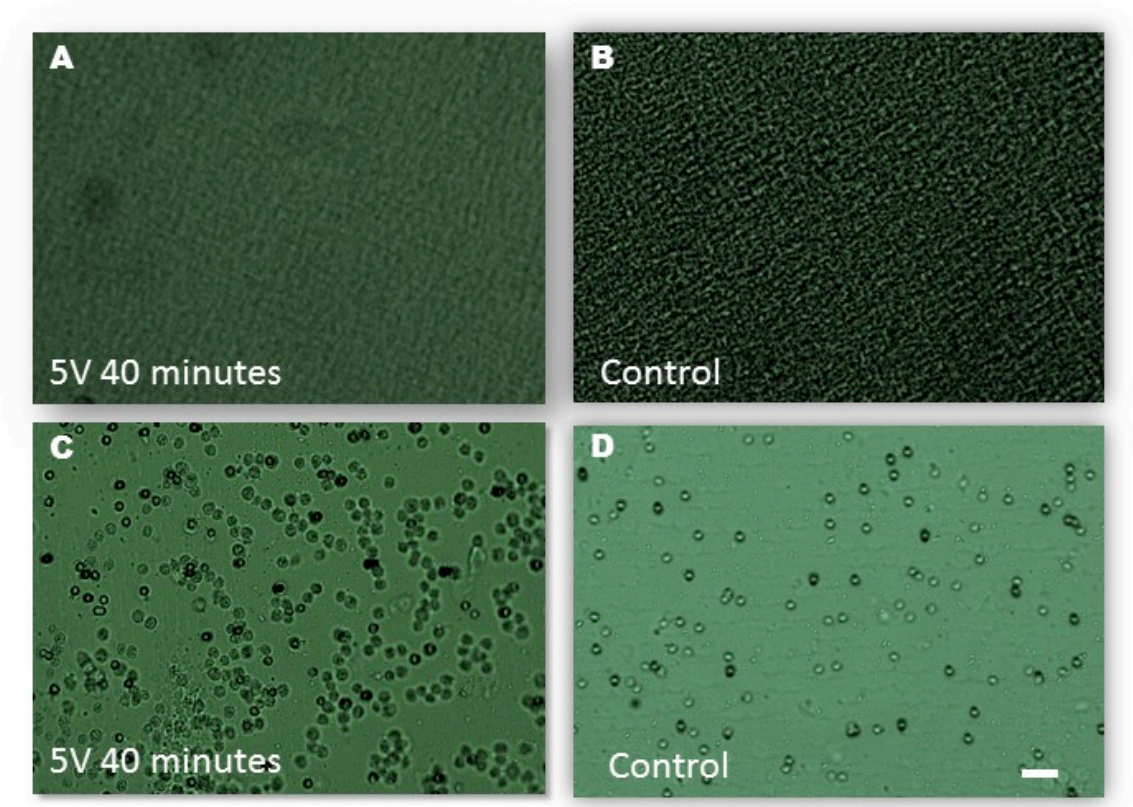

Figure 5.6 Illustration of modified Boyden chamber experiment setup shown above. Images showing NSCs absent in 4micron filter (A,B) vs 8micron filters(C,D). Scale bar: 100µm

5.2.2 RESULTS

Neural stem cells displayed migration in a vertical plane in the presence of an electric field

The number of NSC counted within the filter were significantly more in 2.5V (1.47mv/mm^3), and 5V (2.94mv/mm^3) experiments in comparison to controls p=0.045, p=0.047(figure 5.7). This increased as voltage was increased to 5V (2.94mv/mm^3) but decreased thereafter. Cells counted in the 10V (5.88mv/mm^3) experiment were not statistically significant when compared to controls [figure 5.7].

Prolonged EF exposure at 5V (2.94mv/mm^3) showed an increase in the number of cells counted within the filter from 20 minutes to 80 minutes. This effect tailed off after 180minutes (see figure 5.8). Durations of EF exposure longer than 20 minutes were statistically significant in comparison to controls (40minutes p=0.013, 80minutes p=0.045, 180minutes p=0.047).

To ensure cells counted in filter were indeed NSC, they were stained for anti-nestin. (figure 5.9)

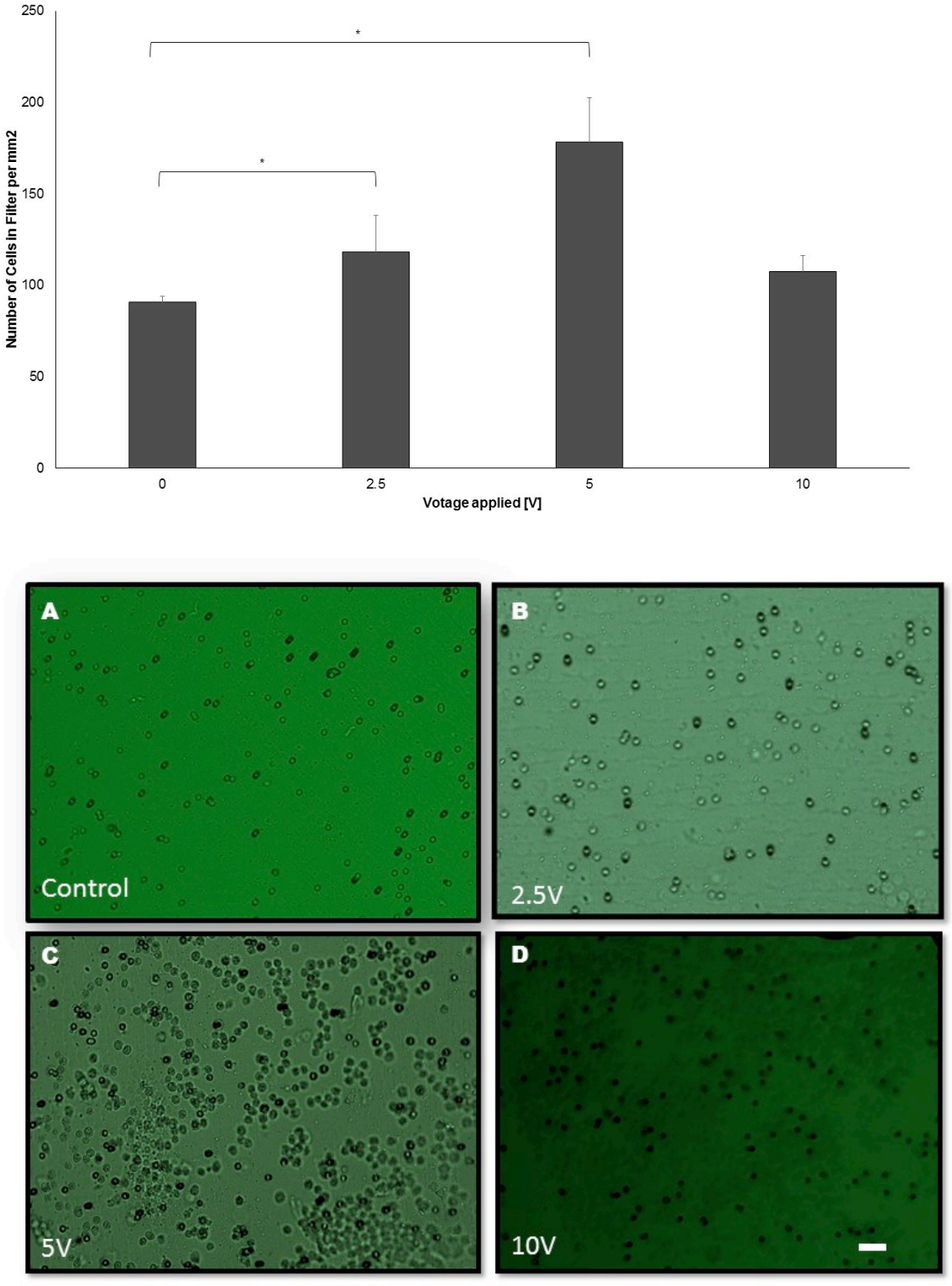

Figure 5.7 Barchart above shows effect of voltage on number of cells counted in filter. *=$p<0.05$ (A) shows cells in filter of control, (B) for 2.5V (1.47mv/mm^3), (C) for 5V (2.94mv/mm^3) and (D) for 10V(5.88mv/mm^3), for 40 minutes. Scale bar: 100µm

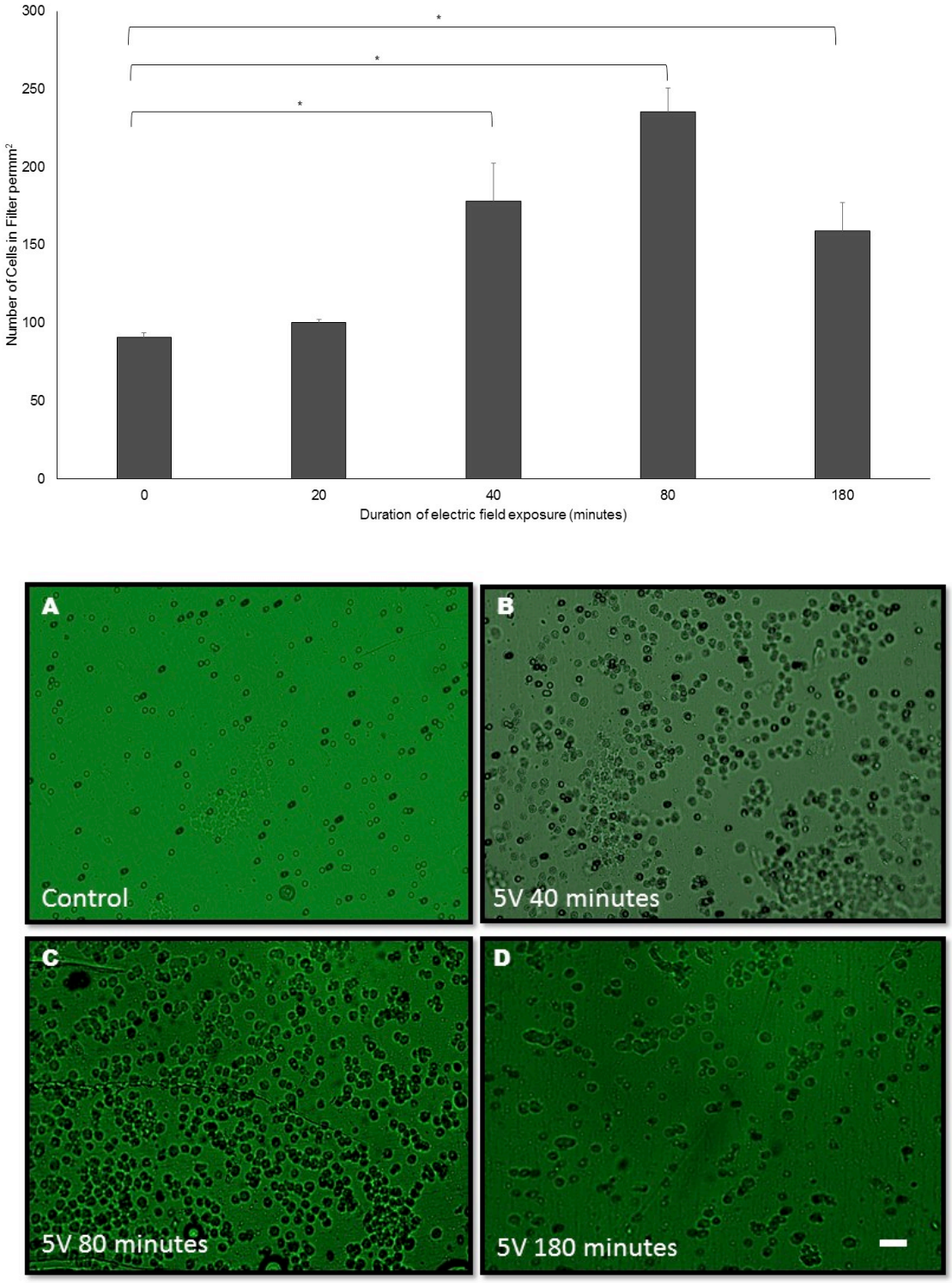

Figure 5.8 Barchart above shows effect of increasing electric field exposure duration at 5V on cells counted per mm^2 in filter. *=$p<0.05$ (A) shows cells in filter of control, (B) 5V ($2.94mv/mm^3$) for 40minutes, (c) 5V ($2.94mv/mm^3$) for 80 minutes and (d) 5V ($2.94mv/mm^3$) for 180 minutes. Scale bar: 100µm

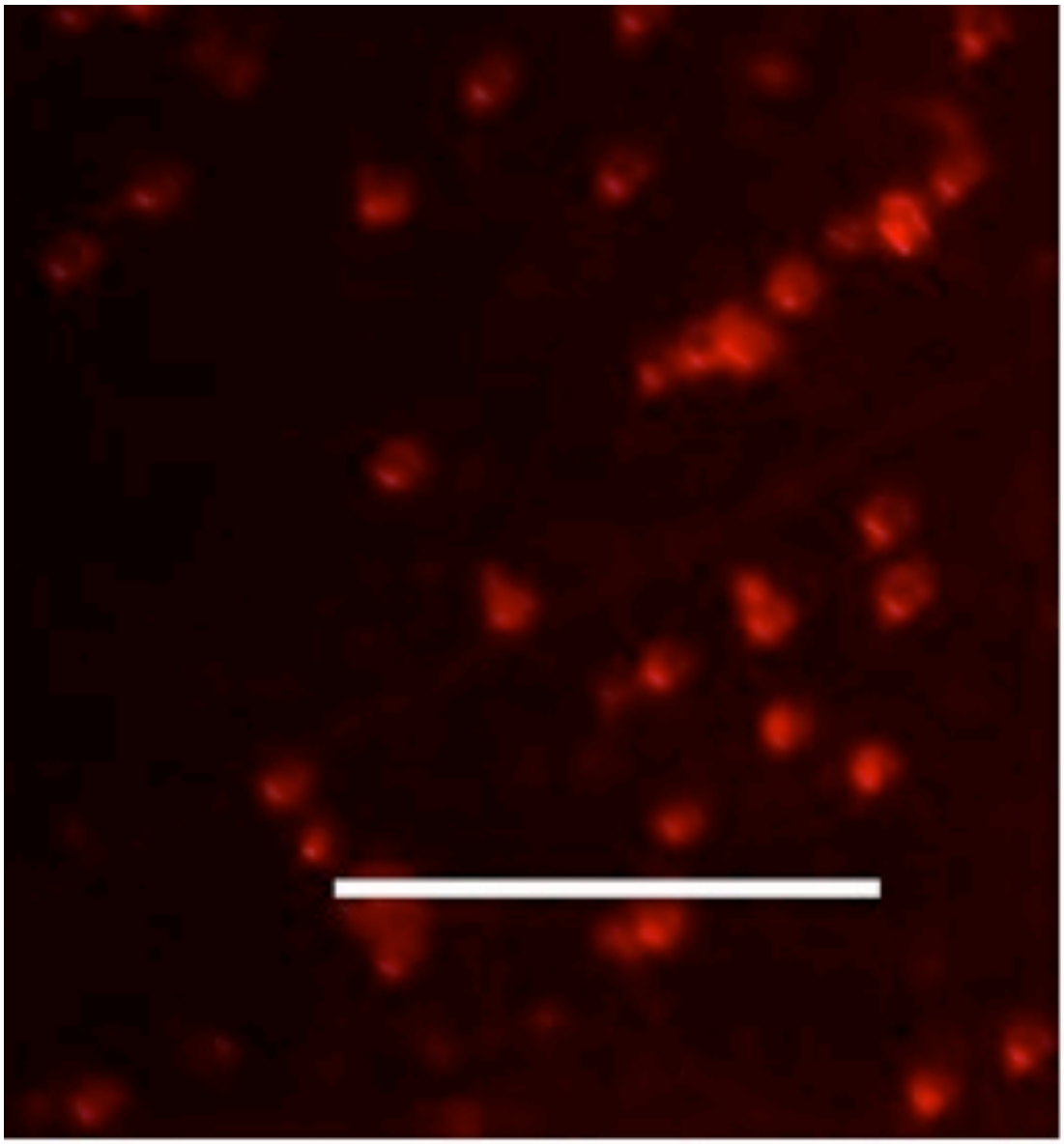

Figure 5.9 Neural stem cells in filter staining positive for nestin (red) following 5V(2.94mv/mm^3) exposure for 40minutes. Scale bar 50 microns

5.4 DISCUSSION

The application of EF directing stem cell migration is a promising field especially in spinal cord injury (Yao et al., 2016). The presence of endogenous EF and the changes in embryonic growth with its disruption indicates the importance of galvanotaxis in normal embryonic development (Hotary and Robinson, 1992). Several studies have demonstrated that an applied EF directs migration of NSC in vitro towards the cathode(Li et al., 2014), as replicated in this chapter for cultured neurospheres. FMI which represents the efficiency of forward migration with relation to the x axis (towards the cathode) was highest for 250mVmm^{-1} and directedness, accumulated distance and euclidean distance were all significantly higher than controls for both EF voltages applied, suggesting the straightness of the cells' migration character was higher than controls (Yuki Asano). In depth analysis of the neurospheres' migration characterisation was not analysed as the focus of this chapter was to direct the neurospheres vertically into the retina and an abundance of work has been published in this respect (Meng et al., 2012, Babona-Pilipos et al., 2012, Li et al., 2014, Zhao et al., 2015).

Although migration of the neuropheres occurred towards the cathode as expected, there was an unexplained anomaly in the control experiments whereby a small proportion of the neurospheres were migrating parallel to the x-axis in the negative as well as positive axes. The majority stayed undirected, but this anomaly cannot be explained as experiments were triplicated and conditions were kept as similar to each other as possible. It may have been that there was an error with the stage of the microscope on the day of the experiment, but nevertheless this did not seem to affect the results of our analyses on comparison with the test variables.

Having demonstrated galvanotaxis characteristics in the NSC-GFP cultured, it was necessary to show that migration towards cathode would also occur in a vertical manner as so far, there has been no work demonstrating this. Vertical migration of stem cells has been published in chemotaxis protocols using Boyden chambers but not for assessing galvanotaxis (Durbec et al., 2008). The use of Boyden chamber with EF has been shown for lymphocytes and hence a modified version of this was used to assess NSC (Lin et al., 2008). The results of this chapter shows vertical migration of NSC from upper to lower chamber occurs when an EF is applied with the cathode in the lower chamber. The migration was affected by voltage and duration of EF application, with 5V (2.94mv/mm^3) for 80 minutes resulting in the highest number of cells migrating within the filter. It is hard to determine if the use of platinum wire electrodes would have altered electrolytes within the media enough to cause a chemical gradient contributing to the taxic response. I chose platinum electrodes as they are one of the most inert metals and has

been used in another published experiment to show migration [Lin et al., 2008]. Future experiments should address this by including a non-metal form of electric field delivery.

Differentiation following prolonged DC electrical stimuli has been shown to induce SC differentiation towards a certain lineage (Thrivikraman et al., 2014, Chang et al., 2016). Durations of up to 48 hours were reported to induce NSC to neurons, astrocytes and oligodendrocytes (Zhao et al., 2015). Although durations of EF application were only investigated up to 180 minutes, NSCs were stained with nestin to ensure differentiation had not taken place post EF exposure and that their stem cell properties remained.

CHAPTER 6 DIRECTED MIGRATION OF NEURAL STEM CELLS FROM INNER TO OUTER LAYER OF THE RETINA BY GALVANOTAXIS

Objective

To determine if exposure to an electrical field can direct NSC migration into the retina from the inner layer to the outer layer.

6.1 INTRODUCTION

Replacing lost cells or delivering neuroprotection with stem cells may repair a degenerative retina and improve visual function. Transplanted stem cells (SC) need to migrate, integrate and hence survive into these sophisticated layers of the retina for effective cell transplantation; and these are interlinked (Ma et al., 2011). So far, efforts have been placed on subretinal delivery whereby migration would have to occur from outer to inner layer of the retina with a resultant localised retinal detachment as part of the delivery process(MacLaren et al., 2006). This approach may better target outer retinal diseases like AMD and RP but would be unlikely to be effective in inner retinal diseases like glaucoma. Furthermore, even though some studies have reported functional restoration after subretinal transplantation (Pearson et al., 2012), most studies have relatively low survival rates ranging from 0.04% to 8% (Ballios et al., 2015). Techniques to improve stem cell delivery to inner retina needs further development as the majority of SC remain in the vitreous body (Johnson et al., 2010a) or at best are adherent to the vitreal surface of the retina when delivered intravitreally. The barrier to this technique is primarily a physical one consisting of the inner limiting membrane, extracellular matrix of the inner basal lamina and microglia(Johnson et al., 2010b, Singhal et al., 2008). Research into improving this have included biomaterial approaches, vitrectomy prior to intravitreal delivery of SC (Jayaram et al., 2014), mechanical peeling of the ILM(Johnson et al., 2010b), enzymatic degradation(Johnson et al., 2010b, Singhal et al., 2008) and manipulation of microglia. Of note, SC augmented to overexpress GDNF reported some integration with intravitreal delivery (Gregory-Evans et al., 2009). This will be discussed and investigated in Chapter 6.

In this chapter, I used an electric field to direct migration of NSCs vertically past the physical barriers of the inner retina into the inner nuclear layer of the retinal explants similar to Chapter 5 where the barrier was a filter.

Experimental Design

In chapter 3, I validated the retinal explants cultured in this lab and confirmed their maximum viability term with the inclusion of healthy RGCs would be for 3 days. This was performed to identify the therapeutic window for retinal explants as the duration of EF field exposure to NSC and retina to demonstrate migration was not yet known.

In brief, a modified Boyden chamber was set up with the retinal explant laid RGC face up on the filter of the upper chamber and the NSCs in media filled the upper chamber (figure 6.1).

Effect of voltage was investigated at 5V (1.47mv/mm^3), 10V (2.94mv/mm^3) and 15V (4.41mv/mm^3) for 60 minutes. Higher voltages [20V(5.88mv/mm^3) and 100V(29.4mv/mm^3)] were trialled but resulted in cell death. The voltages under investigation were applied across the Boyden chamber by placing two platinum electrodes connected to a DC power supply to the top and bottom well of the Boyden chamber; cathode in the lower chamber. Effect of duration of EF application on migration was examined at 5V (1.47mv/mm^3) for 60 minutes, 90 minutes and 120 minutes, at 10V (2.94mv/mm^3) for 30 minutes, 60 minutes and 90 minutes, as well as at 15v (4.41mv/mm^3) for 15 minutes 30 minutes and 60 minutes. To assess if the maximum voltage and EF duration of exposure did not result in cell death, cells were stained with Ethidium Bromide following 15V and 60 minutes of EF exposure.

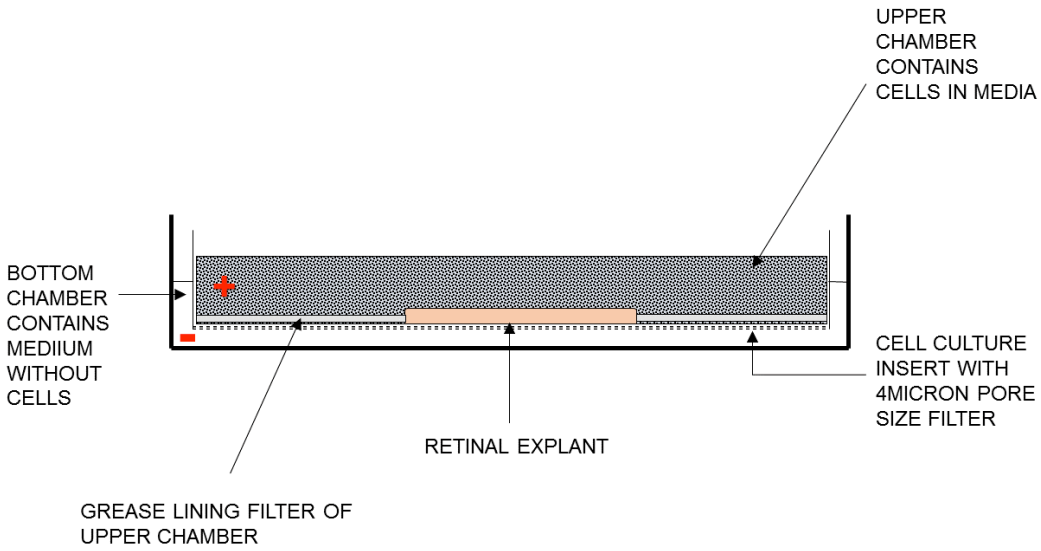

Figure 6.1 Illustration of modified Boyden chamber setup with retinal explant, RGC facing up laid in the upper chamber. Red cross represents the anode charged platinum wire placed in the upper chamber, and the red negative sign represented the cathode charged platinum wire placed in the bottom chamber

6.2 RESULTS

Effect of voltage of EF on migration of neurospheres from inner retinal layer to outer retinal layer

The average fluorescence from NSC-GFP present within retinal layers for 5V (1.47mv/mm^3), 10V (2.94mv/mm^3) and 15V (4.41mv/mm^3) for 60 minutes are shown in Figure 6.2. Migration occurred for all voltages applied, mostly within the RGC and to a lesser extent the INL. Control experiments with no electric field showed no migration.

15V (4.41mv/mm^3) for 60minutes appeared to have the highest proportion of fluorescence within the INL with a corresponding reduction in fluorescence within the RGC layer. However, there seems to be a generally lower fluorescence for the 15V (4.41mv/mm^3) experiment.

Hence, I looked into the duration of EF application to optimize migration as well as cell viability studies to see if the low fluorescence was due to cell death.

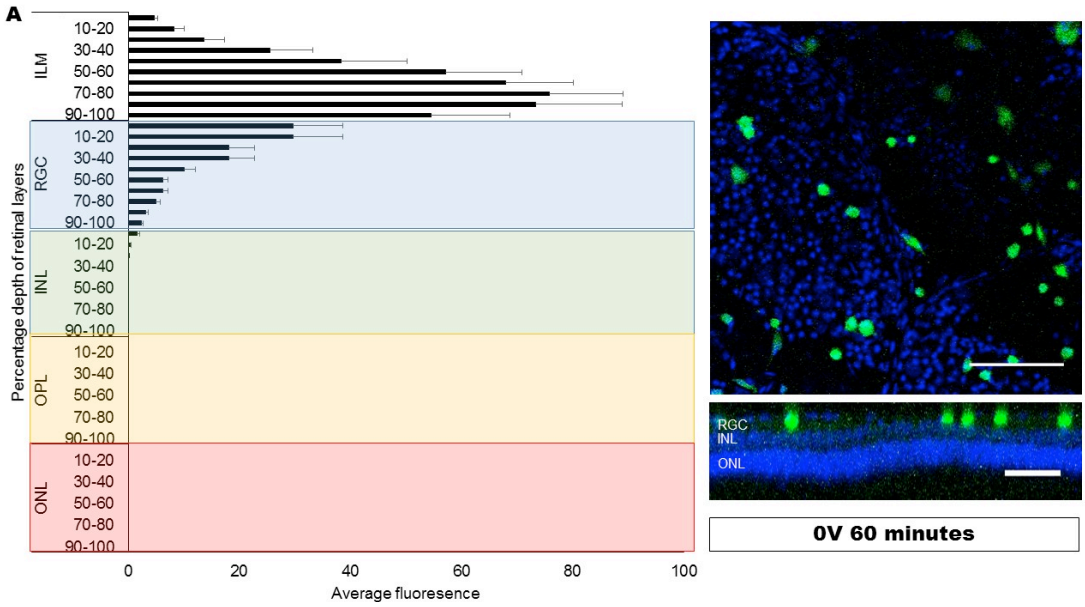

Figure 6.2 (A) Bar chart shows average fluorescence density through retinal layers (RGC layer blue, INL green, OPL yellow, ONL red) in controls 0V 60 minutes [n=13] experiment. ILM=Inner Limiting Membrane, RGC=Retinal Ganglion Cell Layer, INL=Inner Nuclear Layer, OPL= Outer Plexiform Layer, ONL=Outer Nuclear Layer. Error bars =SEM. Image in the upper right shows z stack from confocal microscopy of 1 micron slice in RGC layer. Blue= TOPRO-3 nuclear stain, Green=NSC-GFP cells. Image in lower right shows orthogonal stack of retina showing NSC-GFP lying within RGC layer. Scale bar: 100µm.

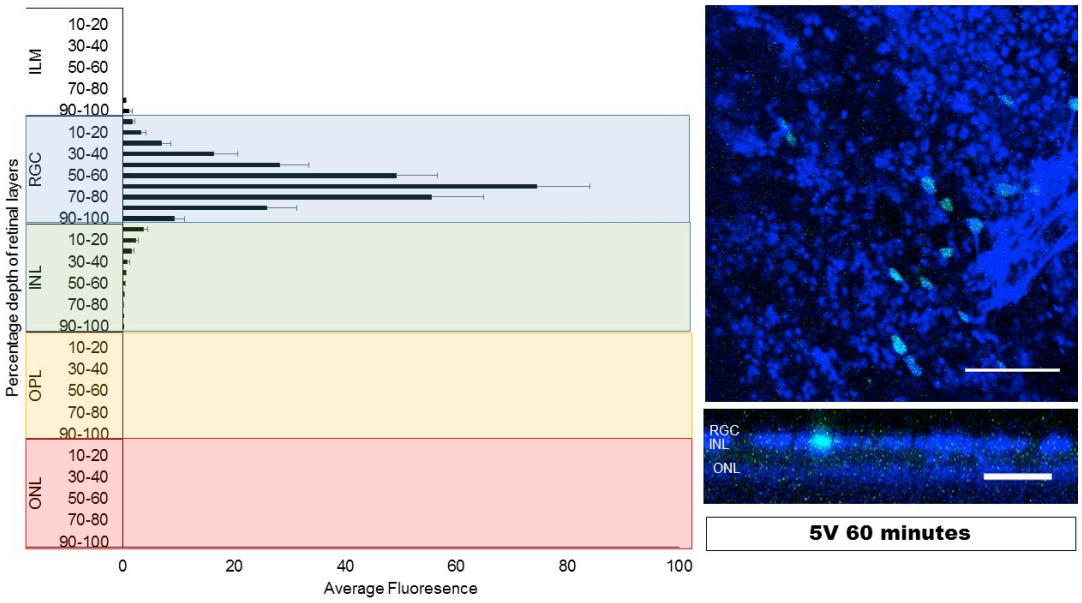

Figure 6.2(B) Bar chart shows average fluorescence density through retinal layers (RGC layer blue, INL green, OPL yellow, ONL red) in 5V (4.41mv/mm^3) 60 minutes [n=19] experiment. ILM=Inner Limiting Membrane, RGC=Retinal Ganglion Cell Layer, INL=Inner Nuclear Layer, OPL= Outer Plexiform Layer, ONL=Outer Nuclear Layer. Error bars =SEM. Image in the upper right shows z stack from confocal microscopy of 1 micron slice in RGC layer. Blue= TOPRO-3 nuclear stain, Green=NSC-GFP cells. Image in lower right shows orthogonal stack of retina showing NSC-GFP lying within RGC layer. Scale bar: 100µm.

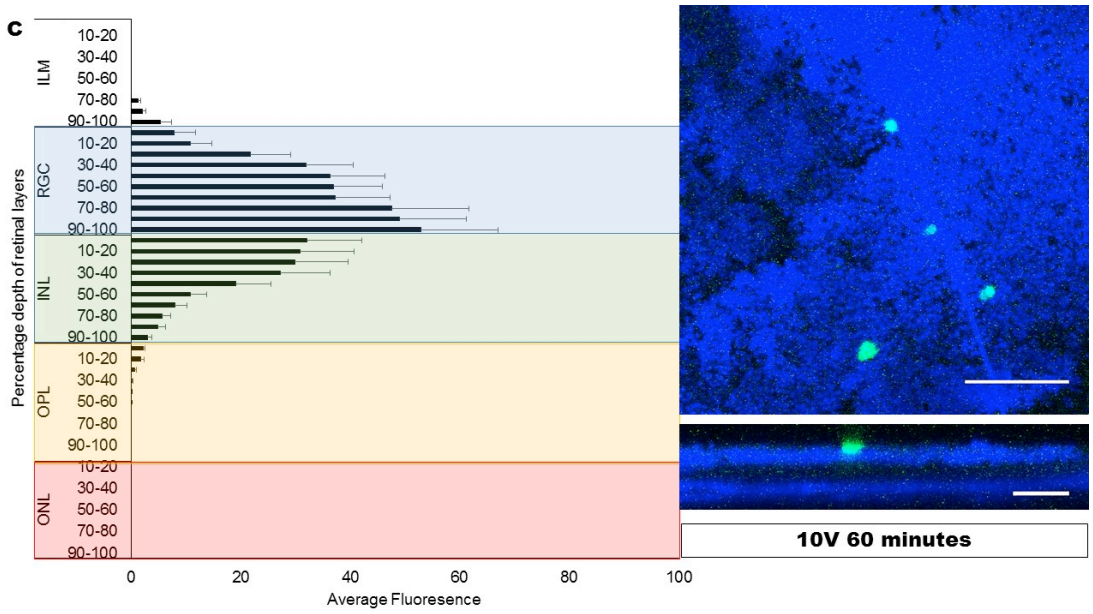

Figure 6.2(C) Bar chart shows average fluorescence density through retinal layers (RGC layer blue, INL green, OPL yellow, ONL red) in 10V(2.94mv/mm^3) 60 minutes [n=19] experiment. ILM=Inner Limiting Membrane, RGC=Retinal Ganglion Cell Layer, INL=Inner Nuclear Layer, OPL= Outer Plexiform Layer, ONL=Outer Nuclear Layer. Error bars =SEM. Image in the upper right shows z stack from confocal microscopy of 1 micron slice in RGC layer. Blue= TOPRO-3 nuclear stain, Green=NSC-GFP cells. Image in lower right shows orthogonal stack of retina showing NSC-GFP lying within RGC layer. Scale bar: 100µm.

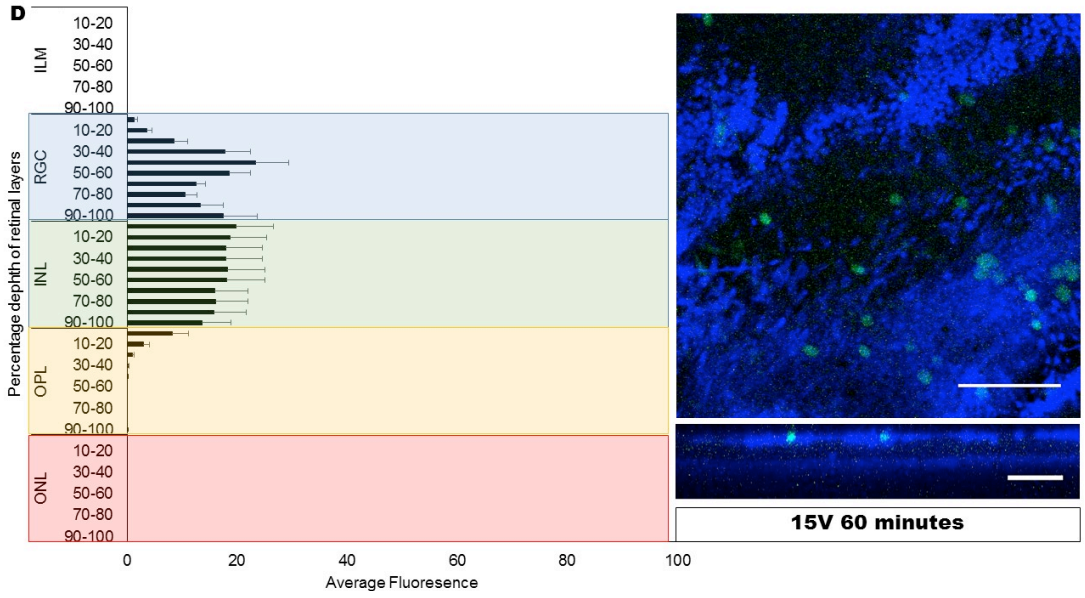

Figure 6.2(D) Bar chart shows average fluorescence density through retinal layers (RGC layer blue, INL green, OPL yellow, ONL red) in 15V (4.41mv/mm^3) 60 minutes [n=16] experiment. ILM=Inner Limiting Membrane, RGC=Retinal Ganglion Cell Layer, INL=Inner Nuclear Layer, OPL= Outer Plexiform Layer, ONL=Outer Nuclear Layer. Error bars =SEM. Image in the upper right shows z stack from confocal microscopy of 1 micron slice in RGC layer. Blue= TOPRO-3 nuclear stain, Green=NSC-GFP cells. Image in lower right shows orthogonal stack of retina showing NSC-GFP lying within RGC layer. Scale bar: 100µm.

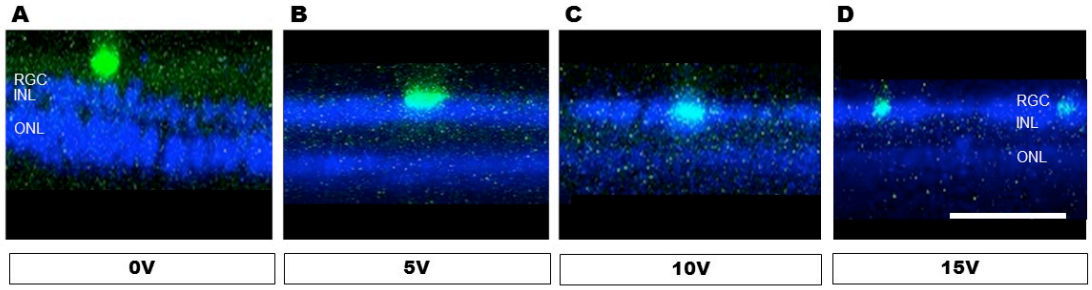

Figure 6.3 Orthogonal view of retinal images captured on confocal microscopy. Blue=TOPRO-3 nuclear stain, Green= NSC-GFP cell. A: Control 0v for 60 minutes; NSC-GFP sitting on top of RGC layer in Inner Limiting Membrane (ILM), B: 5V (1.47mv/mm^3) for 60 minutes, C: 10V (2.94mv/mm^3) for 60 minutes, D: 15V(4.41mv/mm^3) for 60 minutes. RGC=Retinal Ganglion Cell Layer, INL=Inner Nuclear Layer, ONL=Outer nuclear Layer. Scale bar: 50µm.

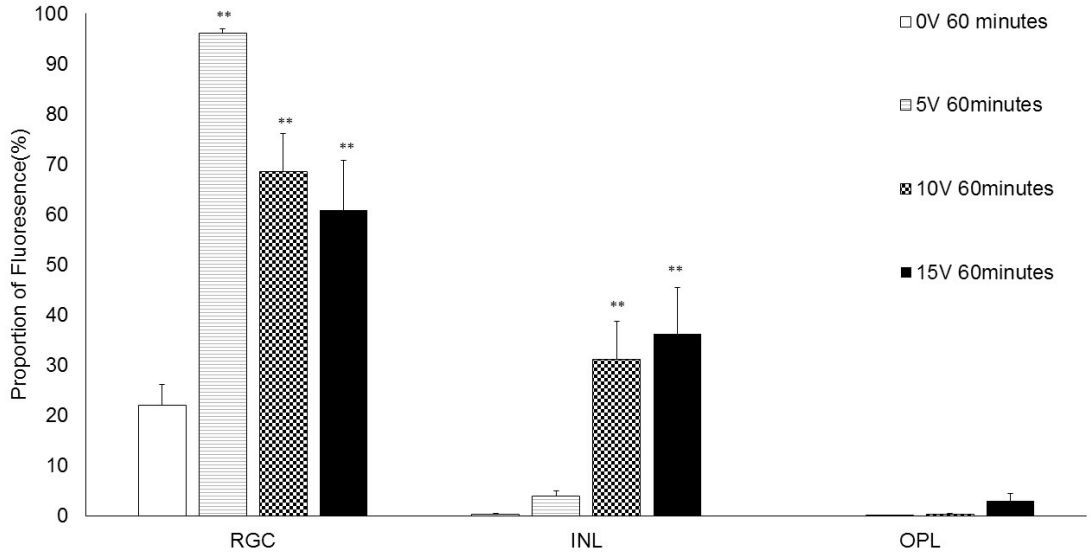

Figure 6.4 Bar chart showing the spread of fluorescence in the retina layers as a proportion of the total fluorescence. Retinal ganglion cell=RGC, inner nuclear layer=INL and Outer plexiform layer=OPL. Error bars =SEM. **=p<0.01, *=p<0.05

Effect of EF exposure duration on migration of neurospheres into retina from inner to outer retinal layer

At 5V (1.47mv/mm^3), a longer duration of EF application showed a trend towards increased migration into INL, although this was not statistically significant. A drop in proportion of fluorescence was seen in the RGC which is accompanied by an increase in INL fluorescence when 5V (1.47mv/mm^3) was used at 120 minutes in comparison to 60 minutes (p=0.029)(see figure 6.5 and 6.6).

At 10V (2.94mv/mm^3) the duration of EF application which showed the most INL migration was at 60 minutes (p=0.004 when compared with 30 minutes) (see figure 6.7 and 6.8).

At 15V (4.41mv/mm^3) more integration was seen in the INL at a shorter duration of exposure. 15V (4.41mv/mm^3) applied for 15 minutes showed the highest proportion of fluorescence within the INL (p=0.011 15v (4.41mv/mm^3) 15 minutes compared to 15V (4.41mv/mm^3) 60 minutes) (see figure 6.9 and 6.10). Fluorescence within the OPL was also detected (see figure 6.10).

To assess cell viability post EF exposure, NSC-GFP neurospheres following 15V EF exposure for 60 minutes were stained with ethidium bromide. No staining was observed (see figure 6.11). NSC-GFP neurospheres post 15V (4.41mv/mm^3) 90 minute exposure stained positive for Ethidium Bromide (figure 6.12)

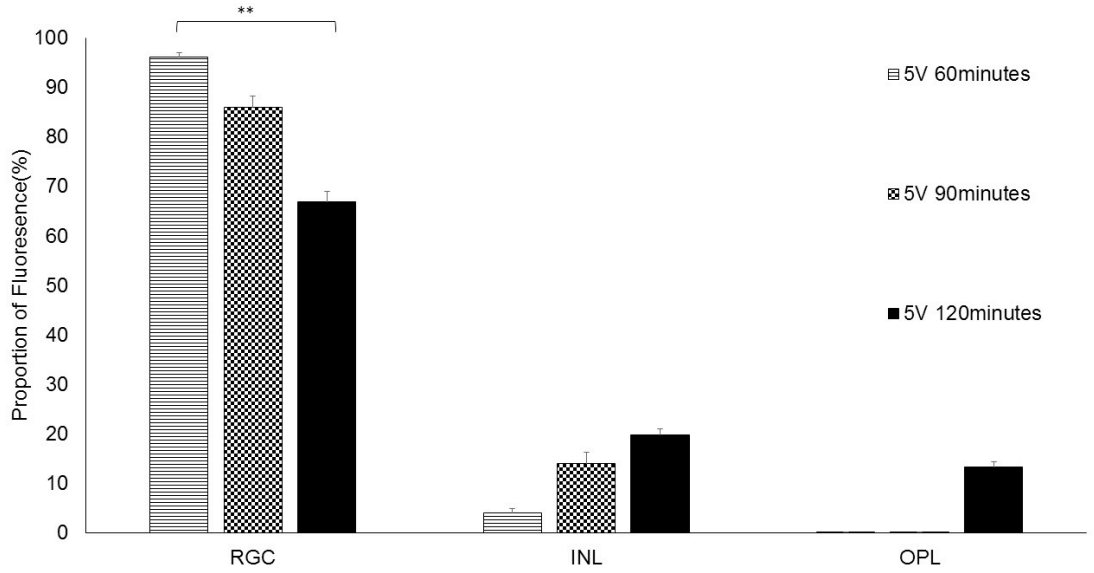

Figure 6.5 A) Bar chart showing proportion of fluorescence within retinal layers; retinal ganglion cell(RGC), inner nuclear layer(INL) and outer plexiform layer(OPL) run at 5V (1.47mv/mm^3) 60 minutes, 90 minutes and 120 minutes Error bars =SEM. **=p<0.01

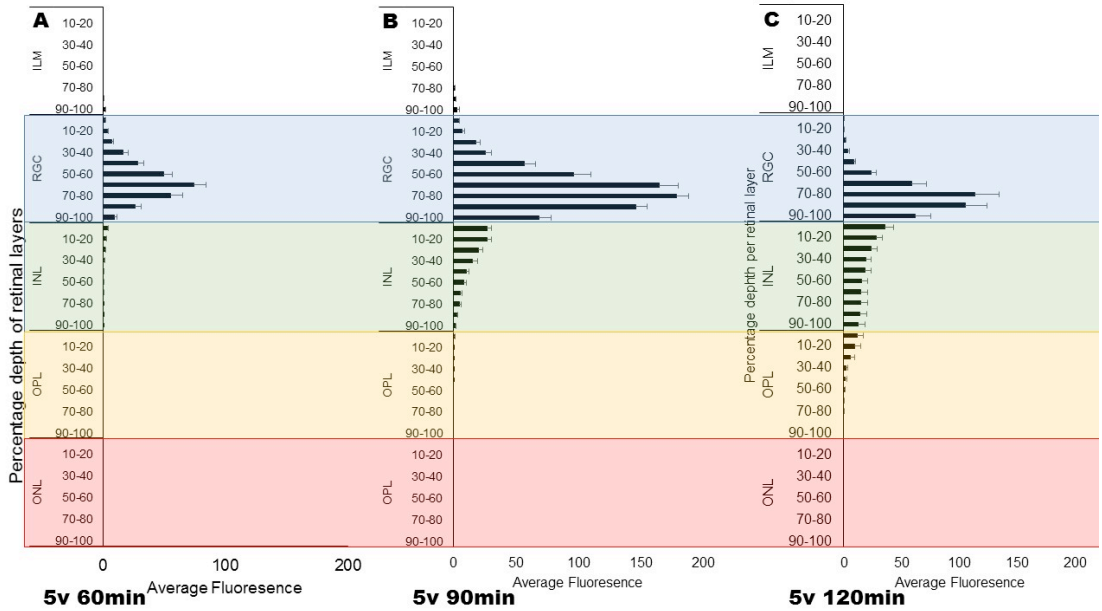

Figure 6.6 Bar charts showing average fluorescence density through retinal layers (RGC layer blue, INL green, OPL yellow, ONL red) in A) 5V(1.47mv/mm^3) 60 minutes [n=19], B) 5V(1.47mv/mm^3) 90 minutes [n=12] and C) 5V(1.47mv/mm^3) 120 minutes [n=16]. ILM=Inner Limiting Membrane, RGC=Retinal Ganglion Cell Layer, INL=Inner Nuclear Layer, OPL= Outer Plexiform Layer, ONL=Outer Nuclear Layer. Error bars =SEM.

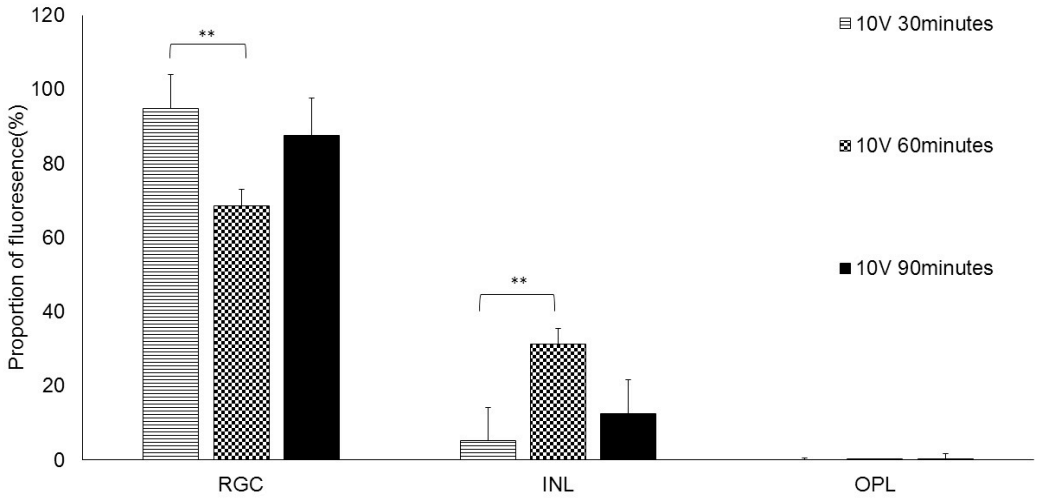

Figure 6.7 A) Bar chart showing proportion of fluorescence within retinal layers; retinal ganglion cell(RGC), inner nuclear layer(INL) and outer plexiform layer(OPL) run at 10V (2.94mv/mm^3) 30 minutes, 60 minutes and 90 minutes. Error bars =SEM. **=p<0.01

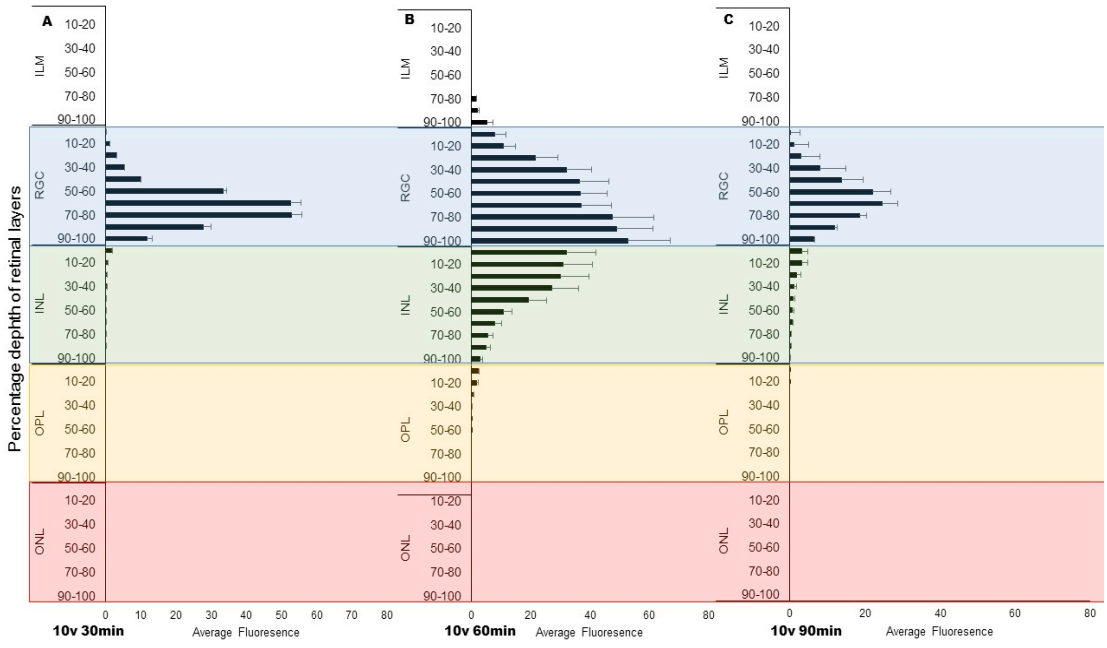

Figure 6.8 Bar charts showing average fluorescence density through retinal layers (RGC layer blue, INL green, OPL yellow, ONL red) in A)10V(2.94mv/mm^3) 30 minutes [n=8], B)10V(2.94mv/mm^3) 60 minutes [n=19] and C)10V(2.94mv/mm^3) 90 minutes [n=8]. ILM=Inner Limiting Membrane, RGC=Retinal Ganglion Cell Layer, INL=Inner Nuclear Layer, OPL= Outer Plexiform Layer, ONL=Outer Nuclear Layer. Error bars =SEM.

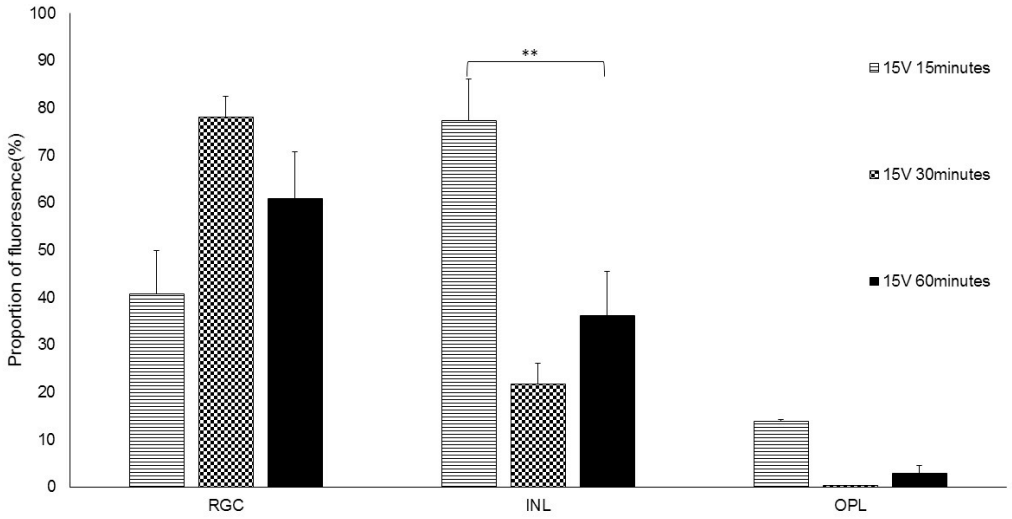

Figure 6.9 A) Bar chart showing proportion of fluorescence within retinal layers; retinal ganglion cell(RGC), inner nuclear layer(INL) and outer plexiform layer(OPL) run at 15V(4.41mv/mm^3) 15 minutes, 30 minutes and 60 minutes. Error bars =SEM. **=p<0.01

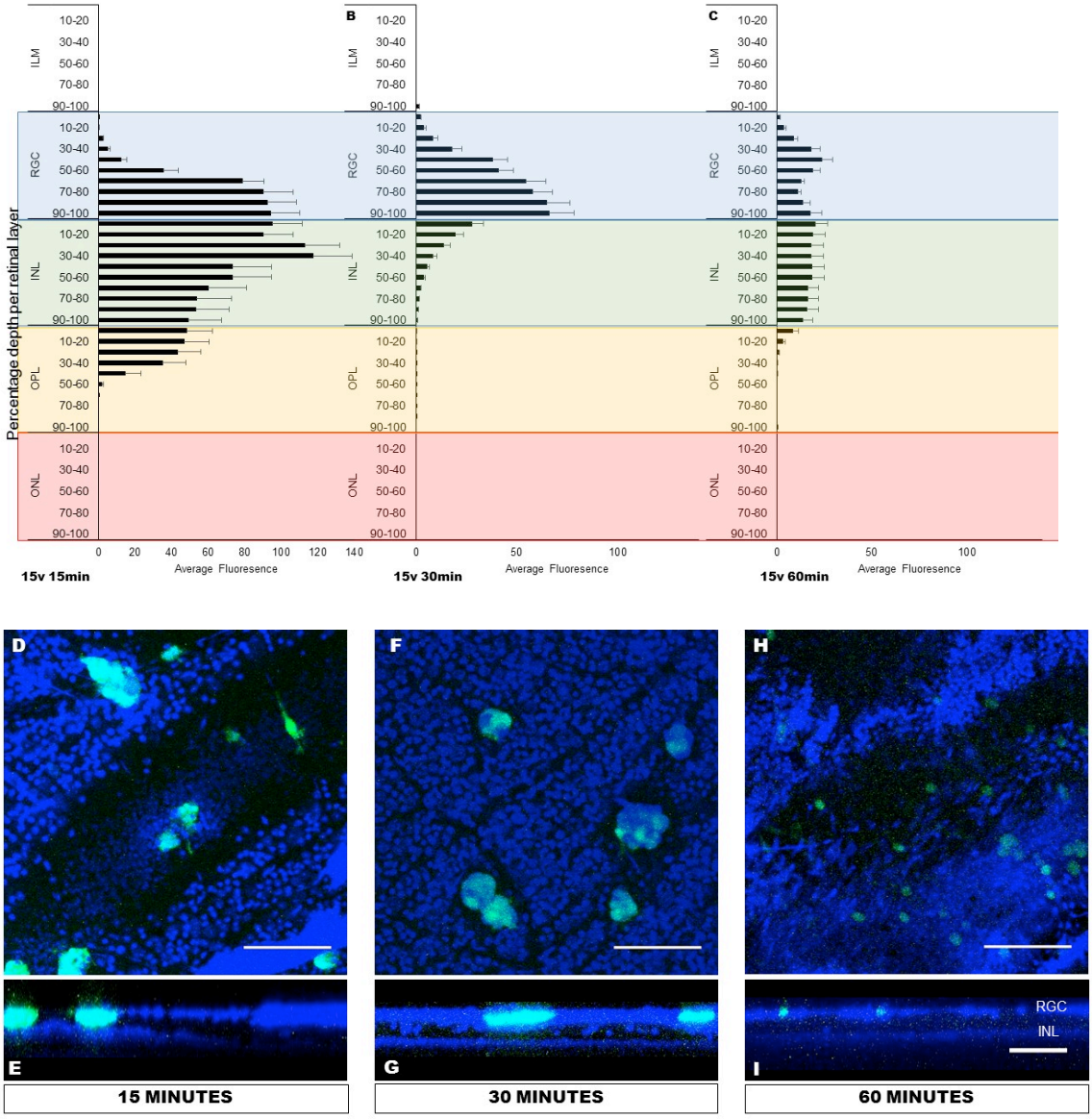

Figure 6.10 Bar charts showing average fluorescence density through retinal layers (RGC layer blue, INL green, OPL yellow, ONL red) in A)15V(4.41mv/mm^3) 15 minutes [n=11], B)15V(4.41mv/mm^3) 30 minutes [n=14] and C)15V (4.41mv/mm^3) 60 minutes [n=16]. ILM=Inner Limiting Membrane, RGC=Retinal Ganglion Cell Layer, INL=Inner Nuclear Layer, OPL= Outer Plexiform Layer, ONL=Outer Nuclear Layer. Error bars =SEM. Images D,F,H shows a z stack from confocal microscopy of 1 micron slice thickness in the retina at 15V (4.41mv/mm^3) for (D) 15 minutes, (F) 30 minutes and (H) 60 minutes. Blue= TOPRO-3 nuclear stain, Green=NSC-GFP cells. Images E, G and I shows their corresponding orthogonal Z stack of slices. Scale bar: 100µm.

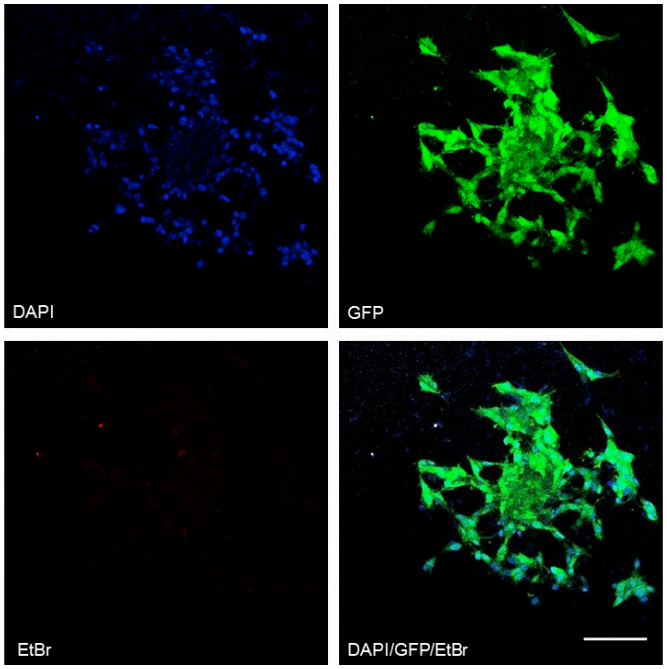

Figure 6.11 Images of NSC-GFP post 15V(4.41mv/mm^3) 60 minutes EF exposure showing no staining with Ethidium Bromide. Scale bar: 100µm

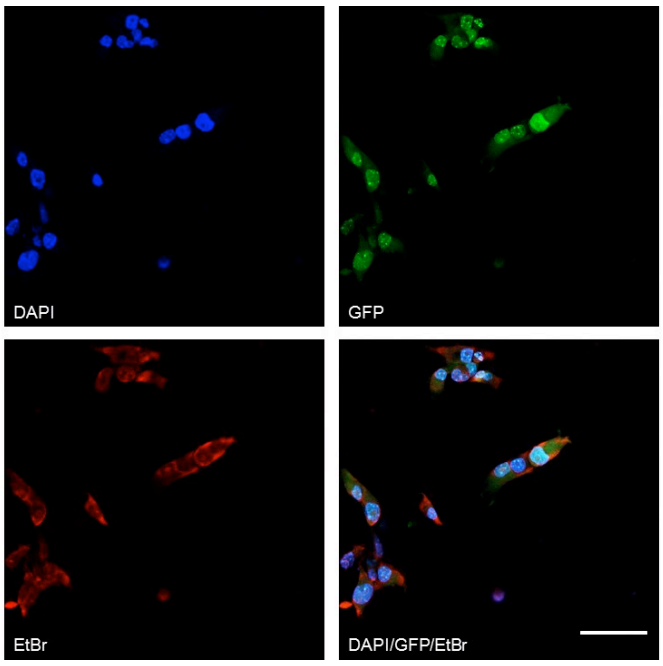

Figure 6.12 Images of NSC-GFP post 15V(4.41mv/mm^3) 90 minutes EF exposure showing positive stain for Ethidium Bromide. Scale bar: 100µm

6.3 DISCUSSION

Success in transplantation of SC into retina has been achieved mainly by using the subretinal technique, whereby a focal retinal detachment is induced prior to SC transplantation, risking damage to the retinal structures (Ong and da Cruz, 2012, Pearson et al., 2012, MacLaren et al., 2006). Intravitreal delivery is a much simpler procedure but leads to poor or no integration unless its environment is manipulated i.e. by mechanical retinal injury (Nishida et al., 2000) or peeling of the ILM (Johnson et al., 2010b). The majority remains as a clump on the retina surface, the ILM or to a small proportion within the RGC layer (Johnson and Martin, 2008). This is demonstrated well in orthogonal slices of the retina in the control group (Fig 6.2A and 6.3A). Upon application of EF, NSC-GFPs were shown to migrate into the INL from the surface of the RGC layer. The proportions of total GFP expression within the retina was shown to increase in the INL layer in comparison to the controls when EF was applied. The experiment with 15V for 15 minutes resulted in the best condition for migration of NSC GFP into INL and ONL. So far, migration of NSCs by EF application in explants have only been demonstrated in explants of spinal cord but not retina (Meng et al., 2012, Fujino et al., 2004). This study provides a proof of principle for harnessing galvanotaxis to direct NSCs past the physical barrier of ILM into the retina after an intravitreal injection.

The EF voltage needed optimization to induce cell migration without causing cell death. Viability tests following EF exposure was determined by Live/Dead assay (GFP/Ethidium Bromide) and its upper limits were shown to be at 15V (4.41mv/mm^3) and 90 minutes. Hence, variables below this limit were examined. As expected, voltage and duration of EF application affected migration into INL. It was encouraging to see that only a short duration of 15 minutes was needed to induce the best result as clinically this would be a tolerable length of time for patients to endure.

The fluorescence measurements should be interpreted with caution as it only gives a gross indication as to migration within the layers of the retina. However, this method is fast, simple and allows for an objective measure. To account for variation in fluorescent intensities of each cell, the proportion of fluorescence within the retinal layers was calculated i.e. Proportion of fluorescence in INL (%) = (AUC of fluorescence in INL / AUC of fluorescence in RGC+IPL+INL) X 100. This identifies any shift in the spread of fluorescence within the retina. In controls, most of the fluorescence is recorded above the RGC layer, but this decreases as voltage is applied which indicates NSC migration. In 15V (4.41mv/mm^3) experiments fluorescence appeared to decrease as the duration of EF application was prolonged. This may be due to the NSCs becoming less healthy as voltage is increased, but not dead as ethidium bromide staining was absent. It could

also be argued that the GFP is more spread out towards the inner retina as the neurospheres are migrating into the INL. When EF at 15V (4.41mv/mm^3) was applied for a shorter duration (15 minutes), there is a definite increase in the proportion of fluorescence in the INL and ONL.

At 5V (1.47mv/mm^3) a trend to increased fluorescence within the INL was observed but longer durations were not investigated as they would be not be clinically translatable and may affect NSC viability.

Given that the voltage and duration of application needs to be optimized, this should be performed on in-vivo animal studies as endogenous EFs need to be accounted for, along with immunological and host retinal tissue response as it has been shown that EF causes RPE cells to migrate and orientate towards the cathode (Sulik et al., 1992). In-vivo studies on rat brain using transcranial direct current stimulation to direct migration of engrafted NSC has been performed but results were hard to interpret as xenograft-induced inflammation occurred (Keuters et al., 2015).

Electrical stimulation in CNS repair has been widely studied, and as a technique is suitable for clinical application as it has been well established e.g. in deep brain stimulation, electroconvulsive therapy and transcranial direct current stimulation(Huang et al., 2015). Translation of EF application to direct NSC migration into the retina with intravitreal injection could occur by electroacupunture with platinum needles; a technique researched in spinal cord injury of rat models(Geng et al., 2015), or by introduction of scleral electrodes imitating transcranial direct current stimulation (Keuters et al., 2015). In-vivo studies using these techniques in animal models would be essential to establish if EF directed migration is strong enough to overcome the current physical barriers of intravitreal SC transplantation such as the ILM, the vitreous body and the propensity for SCs to adhere anterior to the equator of the retina(Gregory-Evans et al., 2009) possibly due to vector currents from aqueous production and vitreous fluid dynamics(Stocchino et al., 2007).

CHAPTER 7 GALVANOTAXIS DIRECTED MIGRATION OF NEURAL STEM CELLS MAGNETOFECTED TO OVEREXPRESS BDNF AS A VECTOR FOR NEUROTROPHIC GROWTH FACTOR DELIVERY IN TO THE RETINA.

Objectives

- To magnetofect NSC with BDNF-myc.
- To assess the effect of magnetofected NSC-BDNF on migration in retinal explant.
- To assess the effect of magnetofected NSC-BDNF on EF directed migration in retinal explant.
- To show RGC neuprotection by BDNF application from Sholl analysis

7.1 MAGNETOFECTION OF NSC-GFP WITH BDNF-MYC

Introduction

Neurotrophic growth factors are essential to the survival of CNS neurons. Indeed, research surrounding its use to rescue neurons and increase their survival are abundant.(Beltran, 2008). Several groups have looked into long term delivery solutions for treatment of degenerative diseases in the eye such as glaucoma, AMD and RP (Cayouette et al., 1998, Kauper et al., 2012, Leaver et al., 2006a, Tao et al., 2002). A phase II clinical trial for slow release encapsulated neurotrophic growth factors in human eyes have started (Goldberg, 2016). Increasingly, stem cells are looked upon as a vector for delivery of neurotrophic factors(Park et al., 2012a). Park et al describe using virally transduced mesenchymal stem cell to over-express BDNF. They used this as a vector for BDNF delivery into the rat retina(Park et al., 2012b). They report integration of about 15% of transplanted SC via the subretinal method following the creation of a retinal detachment bleb. However, they were not successful with the intravitreal method of delivery as SCs remained clustered in the vitreous cavity with no incorporation into the retina. In this final chapter, a non-viral method of magnetofection will be used to firstly transfect NSC-GFP with BDNF tagged with myc for identification purposes, followed by EF application to direct SC and overcome failure of SC integration into retina from inner layer to outer layer. This will form a

proof of principle for EFs use in directing SC and aiding delivery of neurotrophins into the retina.

Furthermore, neurotrophins have been reported to play an integral role in neural stem cell migration and differentiation(Teng et al., 2011). Indeed, BDNF has been shown to induce migration of Multipotent Astrocytic Stem Cells in Boyden chamber assays(Douglas-Escobar et al., 2012). BDNF induced migration of ventricular progenitor cells have also been shown in developing mouse cerebral cortex (Ohmiya et al., 2002). Prior to directing NSC with EF into retina as demonstrated in chapter 5, it is necessary to determine if BDNF overexpression of magnetofected NSC itself will cause directed migration in the absence of EF.

The introduction of BDNF-secreting stem cells in cell cultures and in vivo models has been shown to promote RGC survival (Harper et al., 2011, Harper et al., 2009). To identify the effect of BDNF delivery onto RGC dendritic atrophy of cultured retinal explants, Sholl analysis was used to assess for RGC health. As per results in chapter 3, explants were cultured for 3 days as identifiable RGCs were showing maximum atrophy and a shift in Sholl profile by that stage, prior to being indistinguishable from amacrine cells on day 4.

Experimental Design

NSC-GFP were magnetofected with BDNF-myc at variable DNA:MNP ratios (1:2, 1:1 and 3:2) and variable oscillatory frequencies (0Hz, 2Hz, 4Hz, 5Hz) to assess for optimum transfection conditions. Details of magnetofection experimental setup is described in 2.6.3. Magnetofected NSC were plated on to laminin coated 8 well chambers and cultured for 48 hours. Chambers were then processed and imaged for Myc, DAPI and GFP (see 2.6.7). Transfection efficiencies were reported as a percentage of counted Myc-positive cells out of counted DAPI-positive nuclei per captured image frame (1024x1024 pixel, 300μmx300μm). Presence of BDNF protein was confirmed by Western Blots.

Based on results from 6.1, NSC-GFP cells were magnetofected as described in 2.6.3 at 1:2 DNA:MNP ratio, 5Hz oscillation frequency and for 30 minutes. They were then allowed to culture normally as per section 2.2 for 2 days. Magnetofected NSC were returned to 12 mls of media in a T25 flask. 2 mls of media with a cell density of about 5×10^4 ml^{-1} of magnetofected NSC was taken from this and placed into the upper chamber of the modified Boyden chamber on top of the retina explant. Details of this is described in 2.7.2. Experiments in 6.2 were not exposed to electric field.

7.1.2 RESULTS

Non-viral transfection of NSCs-GFP with BDNF-myc using magnetofection was achieved (figure 7.1). Highest average transfection efficiency was achieved at 5Hz magnetic plate oscillation frequency and 1:2 DNA:MNP ratio (97.2% [17.5myc positive cells/18 DAPI stained cells]) n=8. Lowest average transfection efficiency was observed at 1:1 DNA:MNP ratio 4Hz magnetic plate oscillation frequency (19.4% % [1.17myc positive cells/6 DAPI stained cells]) n=8 (figure 7.2).

DNA:MNP ratios were analysed for each magnetic plate oscillatory frequency group and showed no statistically significant difference.

Overall, transfection efficiencies seemed to be higher in 5Hz experiments (figure 7.4). When analysed with different ratios, there was a trend showing an increase in magnetic plate oscillatory frequency increased transfection efficiency. This was more pronounced in the 3:2 DNA:MNP ratio experiments (5hz vs 0Hz p=0.031) (figure 7.4). In the 1:2 DNA:MNP ratio group, this was also observed, with 5Hz achieving highest efficiencies which was significant in comparison to 2Hz (p=0.029). However, this was not significant when compared to 0Hz. For the 1:1 DNA:MNP ratio group, no statistically significant difference was observed.

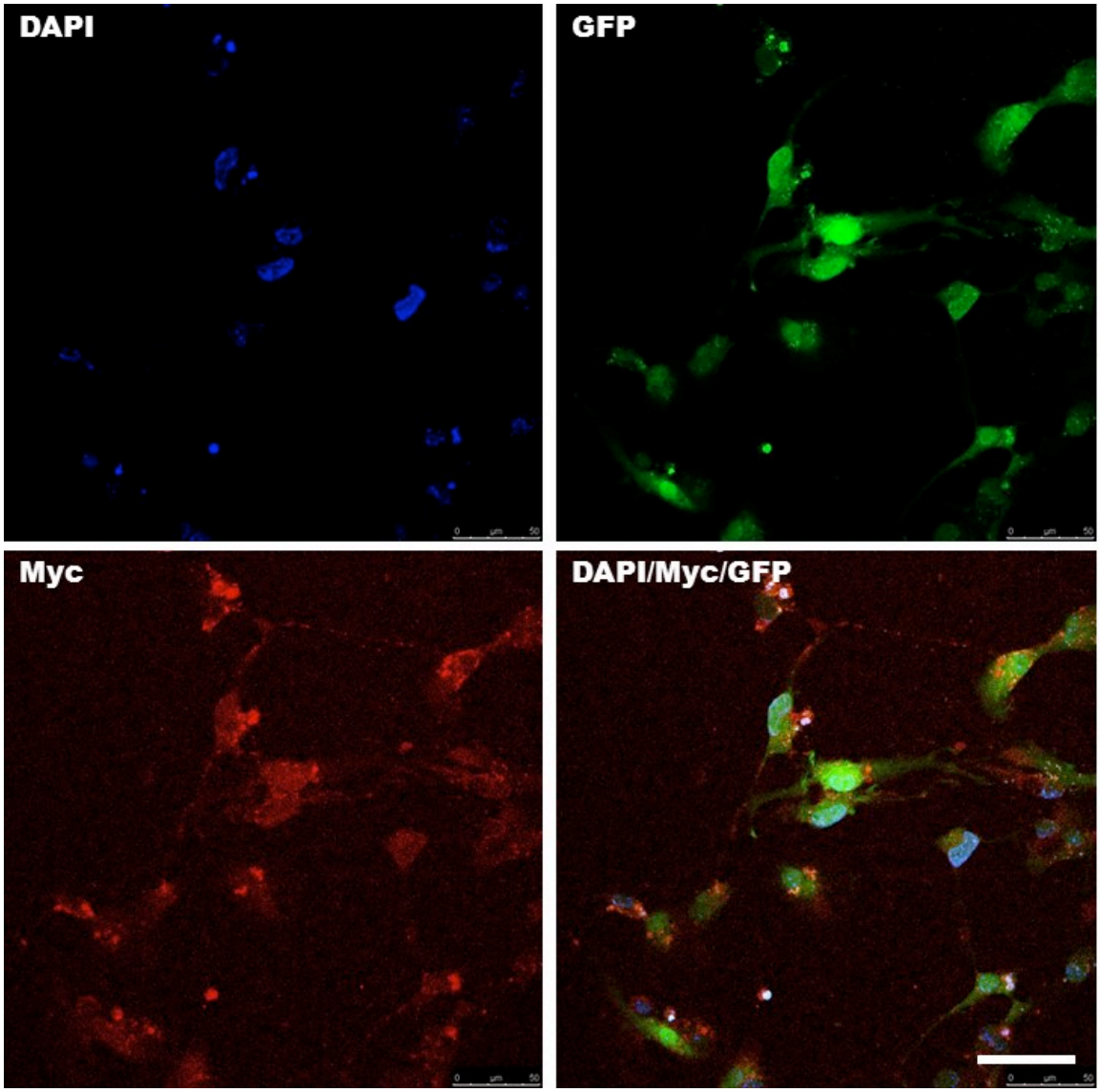

Figure 7.1 Confocal imaging of NSC-GFP cells 2 days post magnetofection with BDNF-myc of 3:2 DNA:MNP ratio at 5Hz oscillatory frequency for 30 minutes. Blue shows DAPI nuclear stain. Green shows GFP fluorescence. Red shows anti-myc positive staining; tag for BDNF. Composite shown in bottom right. Image shows high transfection with calculated transfection efficiency of 100% (19myc positive cells/19 DAPI nuclei stained). Scale bar: 50 microns

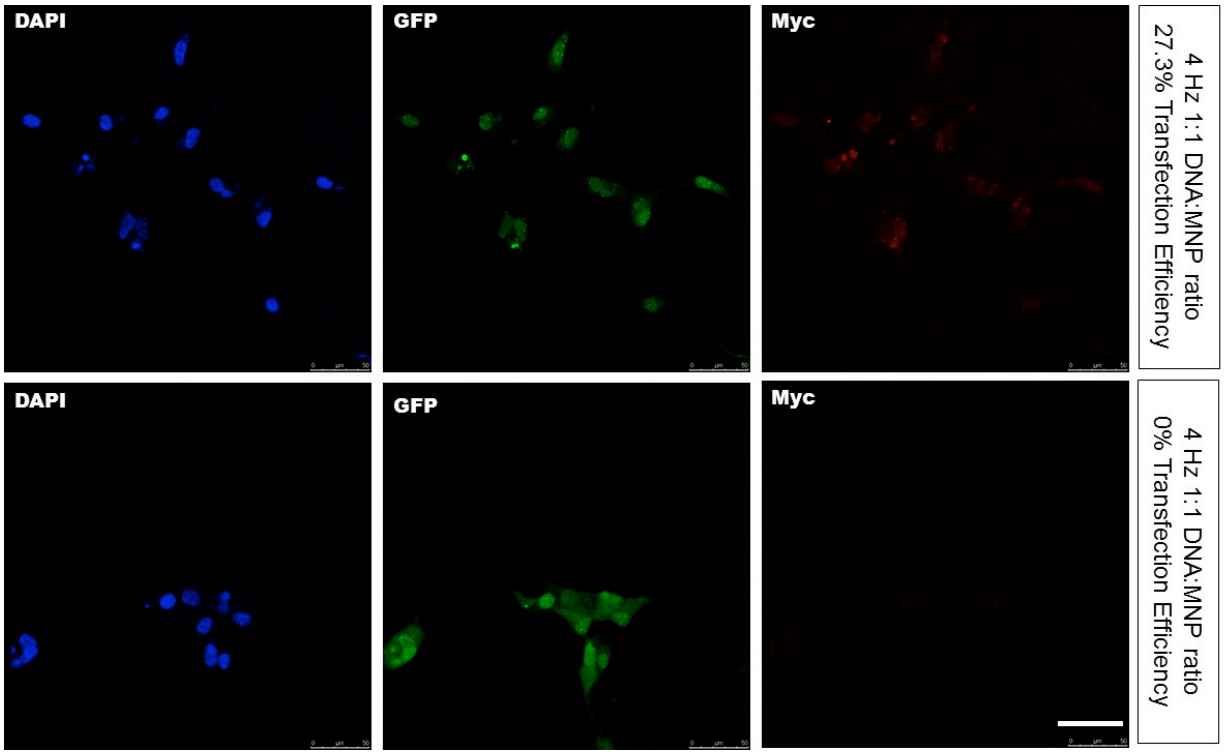

Figure 7.2 Confocal imaging of NSC-GFP cells 2 days post magnetofection with BDNF-myc of 1:1 DNA:MNP ratio at 4Hz oscillatory frequency for 30 minutes. Blue shows DAPI nuclear stain. Green shows GFP fluorescence. Red shows anti-myc positive staining; tag for BDNF. A range of low transfection efficiencies is shown. Top row shows calculated transfection efficiency of 27.3% (3myc positive cells/11 DAPI nuclei stained). Bottom row shows 0 transfection. Scale bar represents 50 microns.

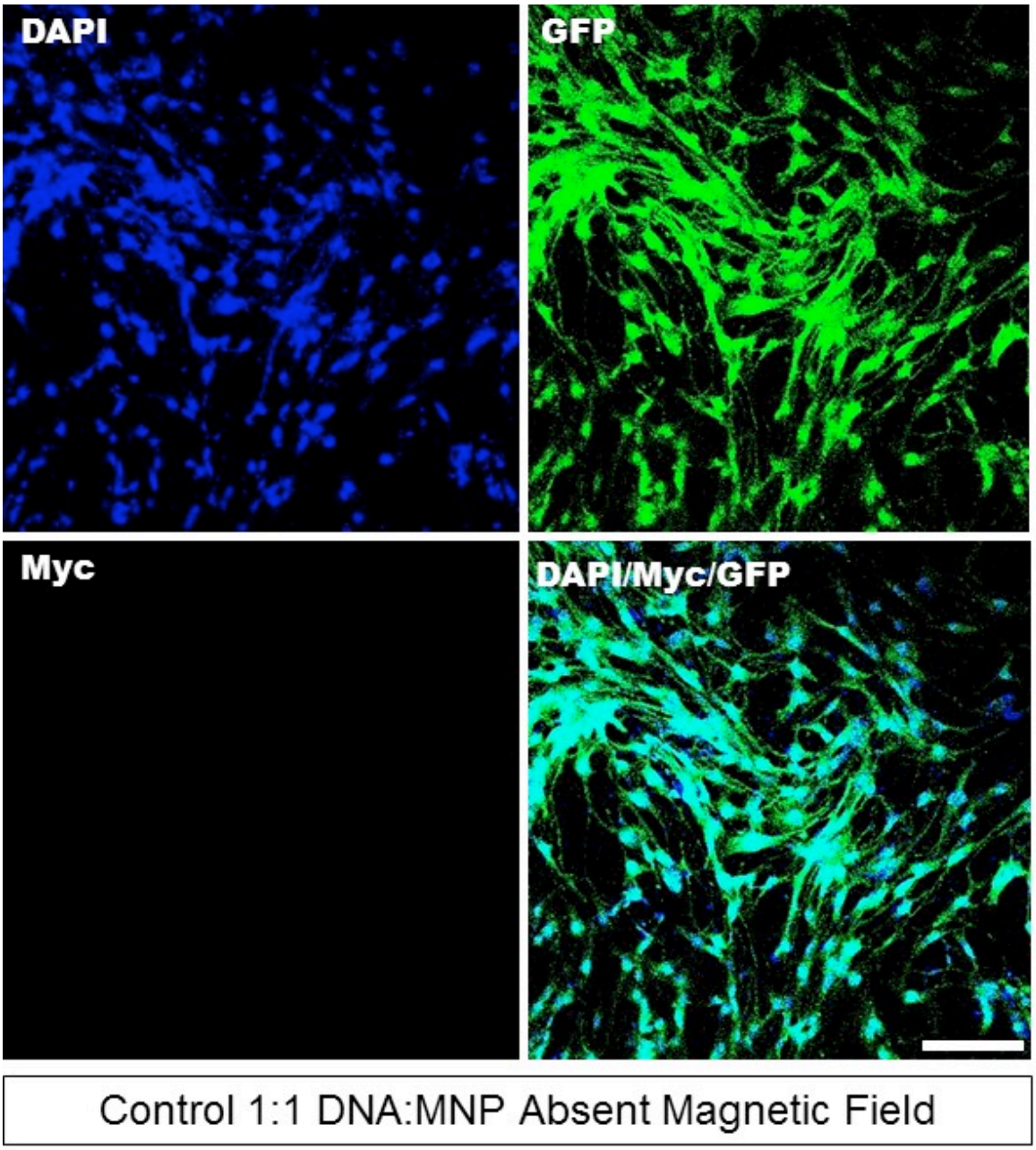

Figure 7.3 Confocal imaging of Control NSC-GFP cells 2 days post exposure to BDNF-myc of 1:1 DNA:MNP ratio without magnetic field exposure. Blue shows DAPI nuclear stain. Green shows GFP fluorescence. Red shows anti-myc staining; tag for BDNF. Composite shown in bottom right. Scale bar: 100 microns

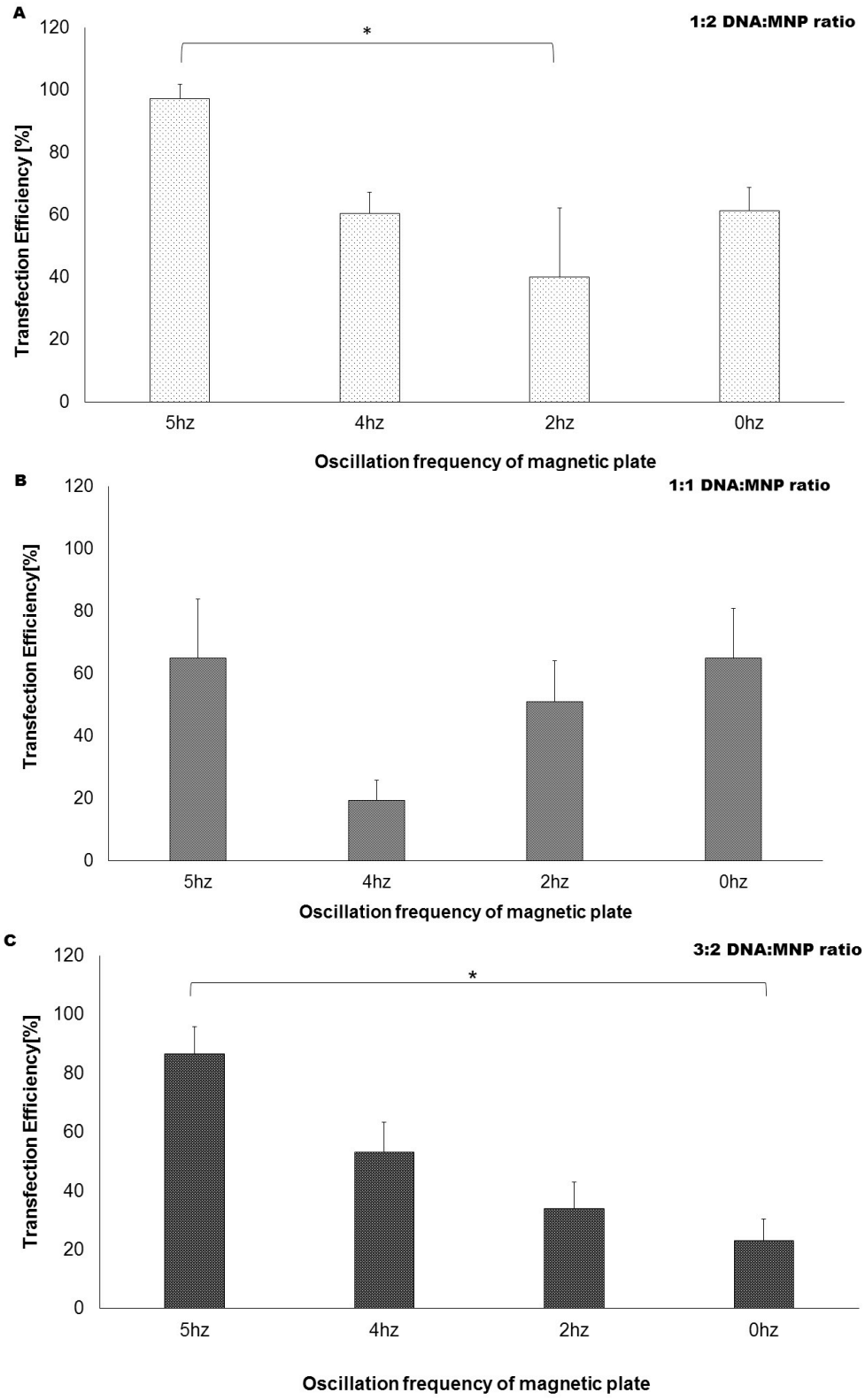

Figure 7.4 Bar chart A shows transfection efficiencies in 1:2 DNA:MNP ratio for varying magnetic plate oscillatory frequencies (n=3-8 image frames) [* p=0.029]. Bar chart B shows transfection efficiencies in 1:1 DNA:MNP ratio for varying magnetic plate oscillatory frequencies [n=8]. Bar chart C shows transfection efficiencies in 3:2 DNA:MNP ratio for varying magnetic plate oscillatory frequencies (n=8) [* p=0.031]. Error bars: SEM.

Western Blots demonstrate BDNF protein presence in magnetofected NSC

Western Blots (WB) for NSCs 48 hours post-magnetofected in 5Hz 1:2, 1:1 and 3:2 DNA:MNP ratios as well as 2Hz 1:2, 1:1 and 3:2 DNA:MNP ratios were performed (figure 7.5). To show presence of protein bands in the samples, Pierce staining was used (see figure 7.6). BDNF was detected at 5Hz 1:2 and at a weaker level, 1:1 DNA:MNP conditions. Negative control (NSC 2 days post passage, without magnetofection) showed no detectable band for BDNF.

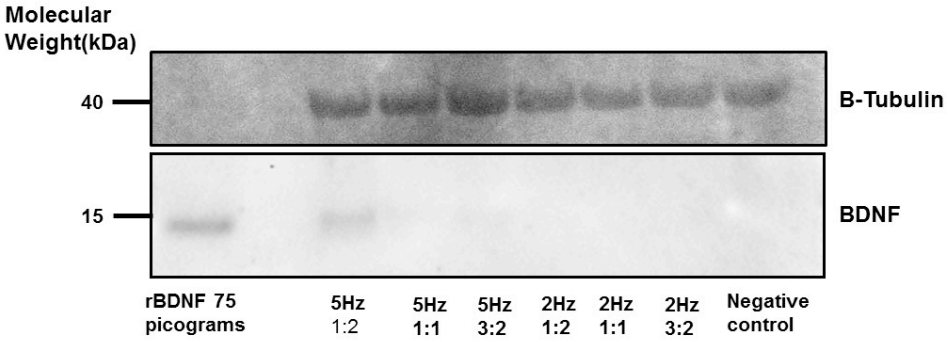

Figure 7.5 Western Blot of BDNF protein for positive control, 5Hz 1:2,1:1 and 3:2 DNA:MNP ratios and 2Hz 1:2, 1:1 and 3:2 DNA:MNP ratios. Positive control was 75 picograms of rBDNF and negative control had NSC with no magnetofection. Internal control was shown with βIII-Tubulin.

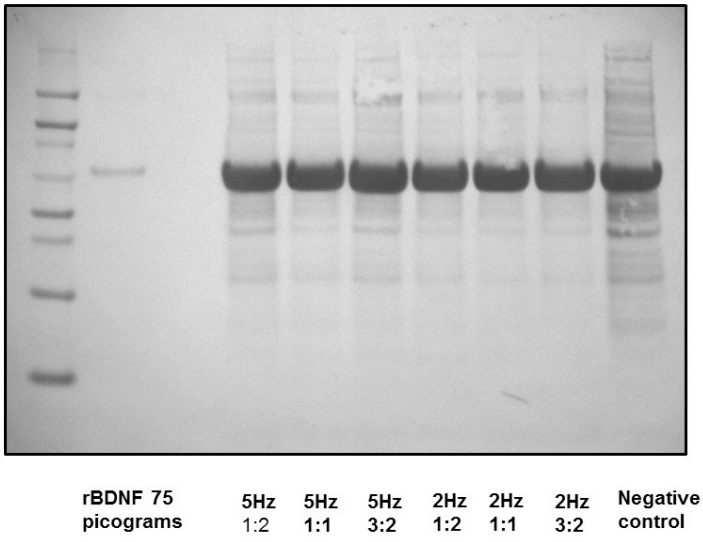

Figure 7.6 Pierce staining of membrane in figure 6.5 confirming presence of protein bands in lanes.

7.2 MIGRATION OF MAGNETOFECTED NSC-GFP WITH BDNF-MYC INTO RETINA DID NOT OCCUR IN THE ABSENCE OF ELECTRIC FIELD

There was no demonstrable difference in fluorescence migration into IPL between magnetofected stem cells with BDNF-myc compared with control (figure 7.7). Fluorescence proportion also did not show any statistically significant shift into the RGC layer when compared to control [p=0.99] (figure 7.8).

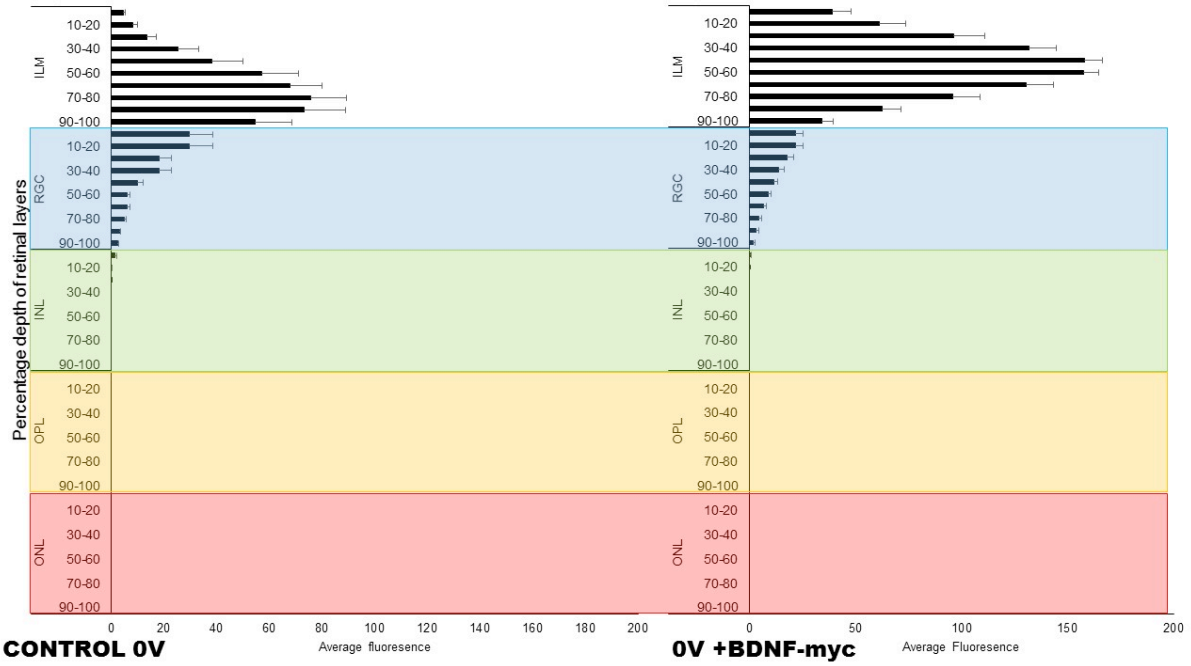

Figure 7.7 Bar chart shows average fluorescence through retinal layers (RGC layer blue=retinal ganglion cell, INL green=inner nuclear layer, OPL yellow=outer plexiform layer, ONL red=outer nuclear layer, ILM white=inner limiting membrane) in controls; 0V 60 minutes [n=13] on the left and NSC magnetofected with BDNF-myc with no electric field application for 60 minutes on the right [n=8]. Error bars: SEM.

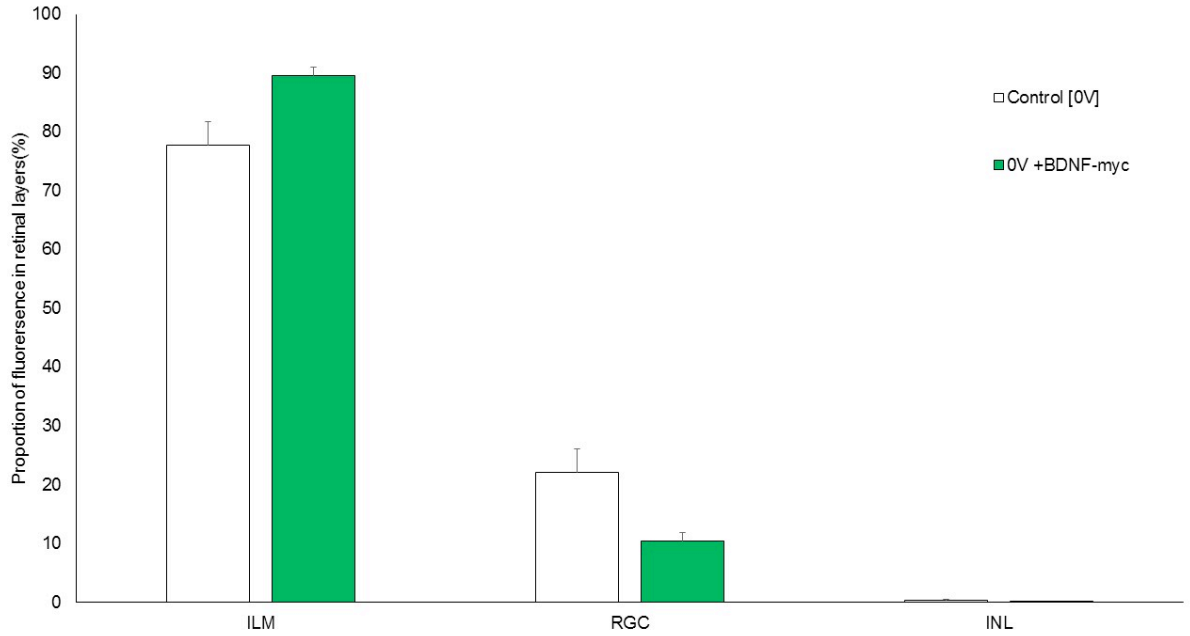

Figure 7.8 Bar chart showing proportion of fluorescence in inner limiting membrane (ILM), retinal ganglion cell layer (RGC), inner nuclear layer (INL) for control with 0V and magnetofected NSC with BDNF-myc with 0V. Error bars: SEM

7.3 MAGNETOFECTED NSC-GFP WITH BDNF-MYC SHOWED AUGMENTED DIRECTED MIGRATION INTO RETINA WHEN EXPOSED TO ELECTRIC FIELD

NSC migration was observed with increased fluorescence in INL and OPL when magnetofected NSC-GFP with BDNF-myc was exposed to 15V (4.41mv/mm^3) of EF for 60 minutes ($p<0.001$) (figure 7.9 - 7.11). There is a visible shift in the average fluorescence recorded from the inner layer to the outer layer as seen when controls were compared with 15V (4.41mv/mm^3) 60minute exposed BDNF-myc neurospheres (Figure 7.10)

Figure 7.11 illustrates no migration seen in controls with 0V and no migration in controls with BDNF-myc magnetofected neurospheres and absent electric field but migration into the RGC layer and INL for 15V (4.41mv/mm^3) 60 minutes and deeper migration into OPL in BDNF-myc magnetofected neurospheres with 15V (4.41mv/mm^3) exposure.

In comparison to 15V (4.41mv/mm^3) 60 minutes and 15V (4.41mv/mm^3) 15 minutes, the magnetofected NSC-GFP with BDNF-myc showed a statistically significant increase in the proportion of fluorescence in the OPL layer ($p<0.001$) (Figure7.12 - 7.13) with a corresponding increase in the INL layer and decrease in the RGC layer.

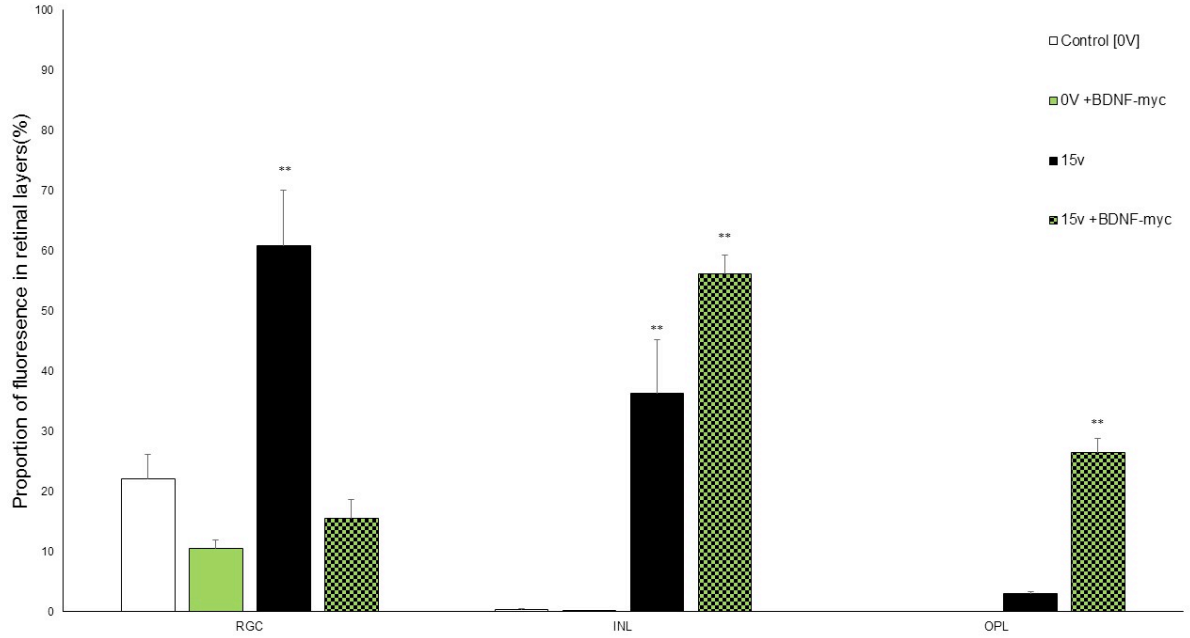

Figure 7.9 Bar chart showing proportion of fluorescence within retinal layers; retinal ganglion cell(RGC), inner nuclear layer(INL) and outer plexiform layer(OPL), run at 15V(4.41mv/mm^3) 60 minutes with NSC-GFP without magnetofection(n=16), 15V(4.41mv/mm^3) 60 minutes run with magnetofected NSC-GFP with BDNF-myc(n=9), Magnetofected NSC-GFP without electric field application for 60 minutes(n=8) and controls consisting of 0V, non-magnetofected NSC-GFP for 60 minutes(n=13). Error bars: SEM. **=p<0.01 when compared against control.

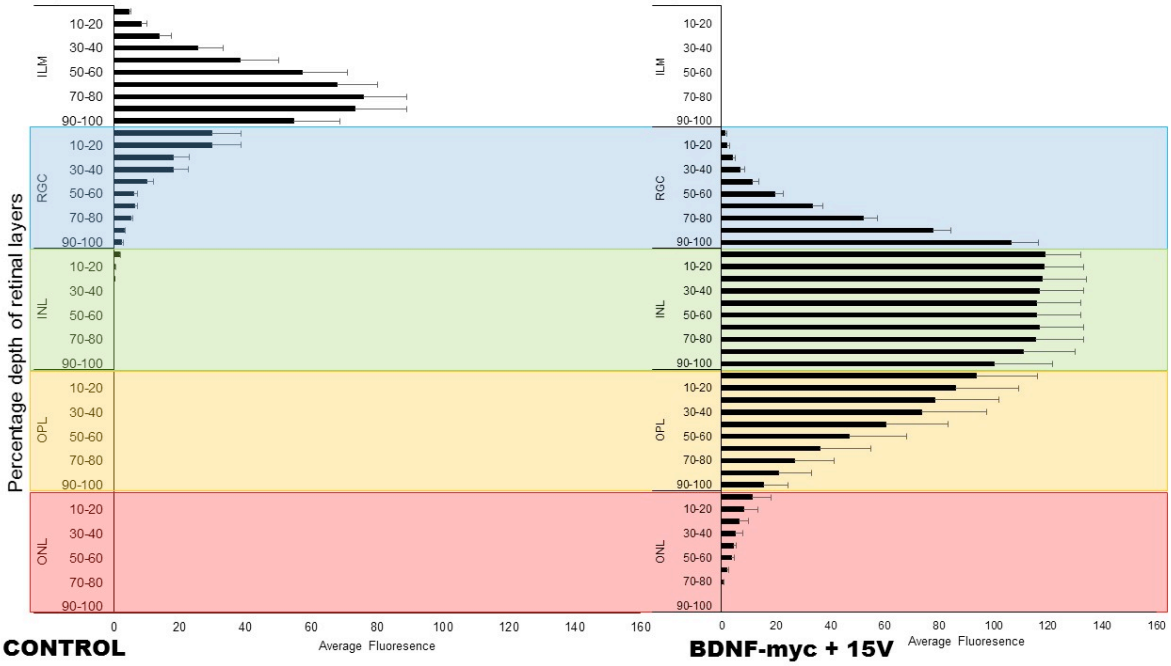

Figure 7.10 Bar chart shows average fluorescence through retinal layers (RGC layer blue=retinal ganglion cell, INL green=inner nuclear layer, OPL yellow=outer plexiform layer, ONL red=outer nuclear layer, ILM white=inner limiting membrane) in controls; 0V 60 minutes [n=13] and NSC magnetofected with BDNF-myc and exposed to 15V(4.41mv/mm^3) electric field application for 60 minutes [n=9]. Error bars: SEM.

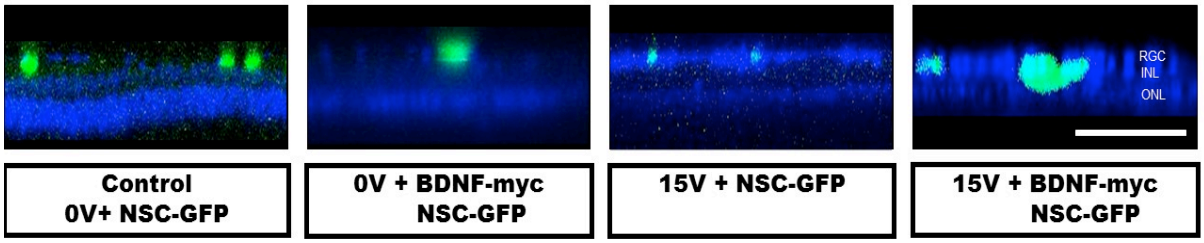

Figure 7.11 Confocal image slices of orthogonal Z stacks of retina showing NSC-GFP neurospheres lying on top and some within the RGC layer in controls and magnetofected NSC-GFP neurospheres with BDNF-myc in the absence of electric field application. 15V(4.41mv/mm^3) 60 minute experiments show NSC-GFP neurospheres migrating into RGC and INL. Magnetofected NSC-GFP-BDNF-myc exposed to 15V for 60 minutes show a deeper migration into the OPL. Blue= TOPRO-3 nuclear stain, Green=NSC-GFP cells. Scale bar: 100 microns. RGC= Retinal Ganglion Cell layer, INL = Inner Nuclear Layer, OPL=Outer Plexiform Layer, ONL=Outer Nuclear Layer.

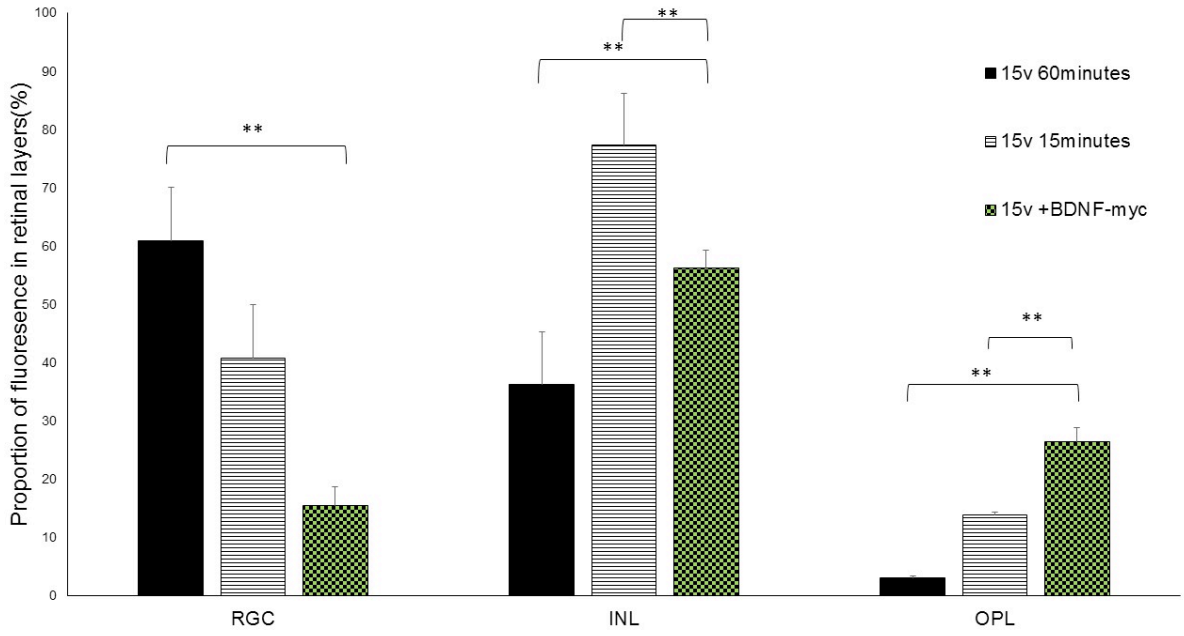

Figure 7.12 Bar chart showing proportion of fluorescence within retinal layers; retinal ganglion cell(RGC), inner nuclear layer(INL) and outer plexiform layer(OPL), run at 15V (4.41mv/mm^3) 15 minutes and 60 minutes with NSC-GFP without magnetofection(n=11,n=16) and 15V (4.41mv/mm^3) 60 minutes applied to magnetofected NSC-GFP with BDNF-myc(n=9), Error bars:SEM. **=p<0.01

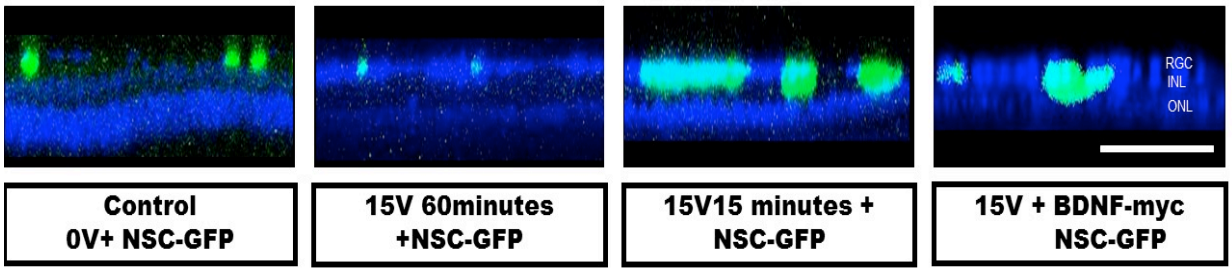

Figure 7.13 Confocal image slices of orthogonal Z stacks of retina showing NSC-GFP neurospheres lying on top RGC layer in controls. 15V (4.41mv/mm^3) 60 minute experiments show NSC-GFP neurosphere within RGC and INL. 15V 15 minutes NSC-GFP and 15V (4.41mv/mm^3) 60minutes magnetofected NSC-GFP-BDNF-myc show migration into the OPL. Blue= TOPRO-3 nuclear stain, Green=NSC-GFP cells. Scale bar: 100 microns. RGC= Retinal Ganglion Cell layer, INL = Inner Nuclear Layer, OPL=Outer Plexiform Layer, ONL=Outer Nuclear Layer.

7.4 BDNF DELIVERY CONFERS NEUROPROTECTION OF RGC IN RETINAL EXPLANT

RGC without BDNF application showed more dendritic pruning and loss of dendritic branching.

Sholl analysis of 3 days ex-vivo shows a higher peak in retinal explants treated with BDNF indicating retention of dendritic integrity in comparison to those not treated. There was an increase in AUC of Sholl profiles for retinal explants cultured in BDNF on DEV3 compared to DEV3 alone (See figure 7.14) which was statistically significant at p=0.038.

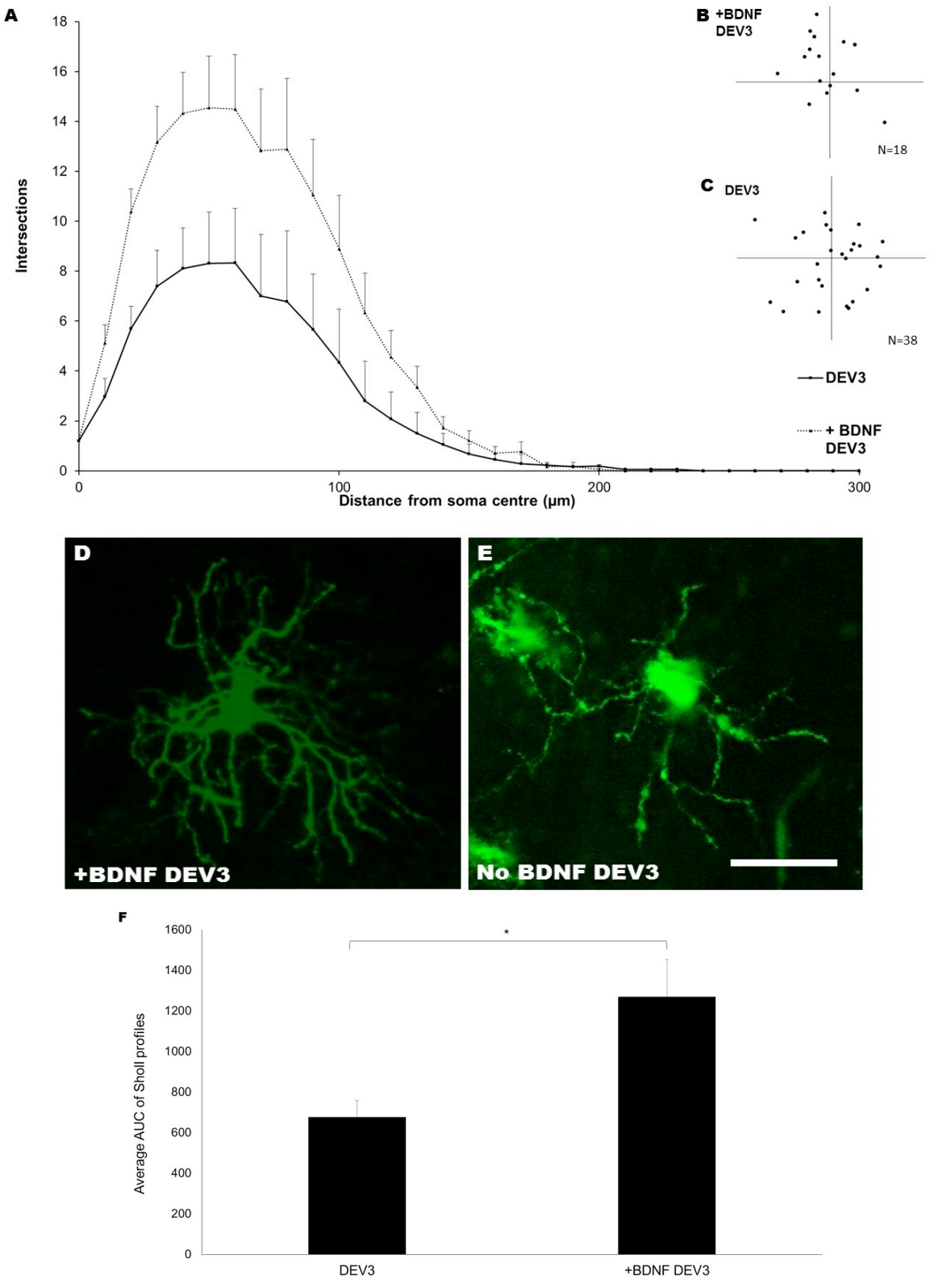

Figure 7.14 A: Graph above shows Sholl analysis of retinal explants on DEV3 with and without BDNF application with corresponding RGC coordinates scatter plots (B,C). Figures (D,E) below are confocal images of DiI labelled RGCs captured on DEV3 with and without BDNF application. F: Bar chart on the right shows AUC of Sholl profiles of RGCs on DEV3 with BDNF (n=18) and without BDNF application (n=38). *=p<0.05 Error bars: SEM

7.5 DISCUSSION

In the first section of this chapter I demonstrated magnetofection of NSC-GFP neurospheres with the BDNF-Myc plasmid with increasing calculated transfection efficiencies proportionate to the oscillatory frequencies of the magnetic plate. The upper limit of frequency under investigation was 5Hz as it was limited by the Magnefect Nano II (nanoTherics Ltd., Stoke-on-Trent, UK) device used. This effect was consistent with several studies who reported an improvement in the transfection efficiency using oscillating magnet arrays in human lung epithelial cells, human cardiac progenitor cells, oligodendrocyte cell precursors and neural stem cells in suspension. (Lim and Dobson, 2012, Subramanian et al., 2013, Jenkins et al., 2011, Adams et al., 2013). Transfection levels of up to ten fold in comparison to static fields have been described, even when compared with lipid-based agents. (Lim and Dobson, 2012). It is suggested that the additional horizontal motion introduced to the particles through oscillation of the magnet array; on top of its primary perpendicular force, enhances transfection(Dobson, 2006).

As this chapter focuses mainly on demonstrating an example of the benefits of EF directed neurospheres into the retina i.e. as a vector for neurotrophin delivery in this case, BDNF quantification was not carried out but is demonstrated by Western Blot, which also confirmed 5Hz to be the optimum oscillation frequency for BDNF expression. The use of myc labelling was utilized as it would facilitate calculation of transfection efficiency as well as being a commonly reported tag for BDNF (Matsumoto et al., 2008, Orefice et al., 2013, Di Polo et al., 1998).

Ratios of DNA:MNP in NSC magnetofection have been reported to vary with optimum levels achieved at a 1:1 ratio (Pickard and Chari, 2010, Pickard et al., 2011). This was investigated but I could not demonstrate any statistically significant difference for DNA:MNP ratios. Transfection was seen to occur in all three variables investigated; 1:2, 1:1 and 3:2 DNA:MNP ratios. Hence, for experiments assessing magnetofected NSC and migration into retinal explants, a DNA:MNP ratio of 1:2 was used which is the variable with the best myc transfection efficiency achieved.

Other conditions did not have detectable amounts of BDNF by western blot, but did not necessarily mean an absence of protein as the levels can be very low. A true quantification can be performed in future experiments either by optimizing the Western Blot for BDNF, or utilising ELISAs instead.

Following magnetofection of neurospheres with BDNF-myc, migration of NSCs into the retina was observed in experiments where EF application was present but not in its absence. As BDNF

is often reported to have an effect on SC migration (Ohmiya et al., 2002), it was necessary to isolate if magnetofected NSCs with BDNF would induce migration into the retina. Indeed, NSCs virally transduced to overexpress BDNF has been shown to migrate and differentiate into neural cells in rat retina but was delivered by a subretinal route (Zhou et al., 2009a). It differs in that a subretinal approached seems to be more successful in general when compared to intravitreal routes whereby migration from inner to outer layer is necessary. Ex-vivo work is also incomparable to in-vivo work and hence, future in-vivo experiments with this experimental condition should be repeated i.e. migration of NSC-BDNF intravitreal injection in the absence of EF.

Based on a rough estimate of the average thickness from ILM to OPL of about 30μm, the rate of migration achieved by the magnetofected BDNF-myc neurospheres in my thesis would be 60μm/hour (1μm per minute), which was comparable to the migration rate in another study looking at mouse neural precursor cells (7 days post-passage neurospheres) exposed to direct current electric field whereby rates of up to 1.22μm per minute were observed [Babano-pilipos et al. 2011]. The neurospheres this paper were shown to move as a group towards the cathode in Matrigel, and it is possible the neurospheres in this thesis are moving as a mass from the inner layer to the outer layer of the retina [Babano-pipilos et al.2011 Supp Movie S6]

Effect of the myc tag itself as a variable needs to be taken into consideration. Myc is well known for its role in tumorigenesis when overexpressed. In knockout of c-myc or N-myc genes of mouse NSC, impairment of overall brain growth occurs alongside decreased migration of NSC (Wey and Knoepfler, 2010). Overexpression and c-myc knock out studies for rat neurospheres show that myc genes play a crucial role in NSC function (Nagao et al., 2008). Therefore, it was reassuring that no migration of NSC was observed when NSC-BDNF-myc were placed on retina explants in the absence of EF. Future in-vivo studies could utilise PCR or ELISA techniques to demonstrate and quantify BDNF levels, removing the need for the use of a myc tag.

There was improved migration of magnetofected NSC-BDNF in comparison to non-magnetofected NSCs exposed to EF. Galvanotaxis of embryonic and neural progenitor cells has been shown to be dependent on the PI3k/Akt pathway, of which BDNF-TrkB has a downstream activation of (Meng et al., 2011). This could explain the enhanced effect on migration observed when galvanotaxis in the presence of BDNF overexpression occurs in the ex-vivo model. EGF and FGF-2 are growth factors linked with electrotaxis (Zhao et al., 1996, Zhao et al., 1999) but BDNF's role in electrotaxis has yet to be described. Interestingly, accelerated and increased expression of BDNF and TrkB mRNA in electrical stimulation of rat femoral motorneurons has

been reported (Al-Majed et al., 2000). Whether asymmetry of BDNF receptors in NSC occur in response to EFs; inducing migration, like in EGF, is yet to be determined (Zhao et al., 1999).

The process of magnetofection necessitates NSC uptake of magnetic nanoparticles which may theoretically cause magnetically guided migration into the retina with an EF induced magnetic field. Zhang et al have reported a magnetic targeting cell delivery system whereby bone MSC; modified to express neurotrophin-3, were labelled with superparamagnetic iron oxide nanoparticles and directed with a 0.57T magnet(Zhang et al., 2016). Indeed, magnetized mesenchymal SC with MNP have been used to target migration to retina using a gold plated neodymium iron boron magnet placed within the orbit (Yanai et al., 2012). Although in this chapter magnetic field directed migration of magnetofected NSC is unlikely (as the EF induced magnetic field is probably too small and negligible) future experiments could address this by assessing the strength of the EF induced magnetic field if present and its effect on SC migration. Theoretically MNPs should also be oxidised by the cell over time, therefore the duration of MNP presence in NSCs also needs to be determined. In future, to establish if the magnetofection process itself is a cause for increasing cell migration and to determine if BDNF truly augments migration, migration studies to include controls using NSC magnetofected with just –myc or no plasmid should be included.

Finally, to show neuroprotection of RGCs via BDNF overexpression in retina is plausible, Sholl analysis of RGCs post BDNF application on retina explants showed a delay in dendritic atrophy and retention of RGC branching. Although it is already known that BDNF confers neuroprotection for RGCs this serves as confirmation that BDNF attenuates dendritic degeneration in the ex-vivo model used. RGC neuroprotection conferred by BDNF have been described mainly by cell counts, RGC dendritic field area or axon counts (Nakazawa et al., 2002, Feng et al., 2016) but there are increasing reports of Sholl analysis use for RGC morphology assessment in neuroprotection therapy (Johnson et al., 2016, Binley et al., 2016). Indeed, the neuroprotective effects on Sholl seen in this chapter agrees with that in Johnson et al. whereby BDNF application in addition to CNTF have been reported to significantly reduce dendritic loss when AUC of Sholl was compared to non-treatment. BDNF delivery via directed migration of magnetofected NSC is therefore a viable treatment option for diseases with early RGC loss such as glaucoma.

CHAPTER 8 GENERAL DISCUSSION

In summary, this thesis has shown in an ex-vivo organotypic culture model, NSC can be directed by galvanotaxis to migrate into the retina from inner layer to outer layer; implying the possibility of NSC as a vector for neurotrophin delivery to RGC.

As the recipient bed for NSC directed migration was the retina, the organotypic retinal explant culture system was employed. Variations between labs and reported culture viability instigated its need for validation prior to transplantation of NSC. I validated the retinal explant culture model for not only retinal architecture and immunohistochemistry, but also for viability of RGC cells. I showed that current methods for assessing RGC for neuroprotective therapy using cell counts and axon counts can overestimate cell viability. However, it is reassuring to see Johnson et al. ; who used Sholl analysis, agree that RGCs in mouse retinal explants begin to degenerate after 3 days in a time-lapse of Thy-1 YFP mice(Johnson et al., 2016). Although the results in Chapter 3 suggest a 3 day therapeutics window period for future investigation, degeneration was witnessed by day 1. As the authors point out, this may be due to their use of Thy1-YFP labelling selecting for healthier RGCs as Thy-1 is downregulated in in states of cell stress (Howell et al., 2011, Guo et al., 2010).

The transplantation of BDNF-overexpressing SCs to provide neuroprotection in RGCs is not a new concept and is often virally mediated as transfection efficiency is nearly 100% with this method. However, the disadvantages of viral transduction remain. Hence, for a better safety profile to improve chances of clinical translation, a non-viral method; magnetofection, known to transfect well in NSC without compromising stemness or viability(Adams et al., 2013) was used. I also explored the use of magnetofection in a 3D tissue form which has not yet been explored. The successful transfection of the endothelium in the cornea and the RGC layer in the retina will provide proof of concept for its application in vivo. In chapter 4, I showed the transfection of whole cornea tissue which can be controlled to restrict transfection to select corneal layers without off-target effects. It highlights the potential for the manipulation of an external magnetic field in controlling the location and degree of transfection. Levels of transfection were comparable to those obtained with other non-viral vectors but with the key difference that the onset and location of the transfection tissue were under the control of an external magnetic field. While the transfection rates in this study remain relatively low, a range of methods can be applied to enhance transfection efficiency(McBain et al., 2008). These can be based on the

modulation of surface charge and polymer characteristics- or alternatively on the shape of the nanoparticle. To date, this is the first study to transfect endothelium in whole cornea tissue by magnetofection.

It is interesting to note an increase in transfection is seen with higher oscillatory frequencies in NSCs in line with other reports but not in cornea tissue. It is possible that the manipulation of oscillatory frequency could modify depth of transfection in tissue layers rather than affect transfection efficiency itself. The use of magnetofection in ocular tissue requires further exploration. Reassuringly, MNPs are reported as safe and non-toxic (Prow et al., 2008). Future work for use of magnetofection in ocular tissue is abundant. It could extend to treatment of corneal dystrophies, optimization of endothelial cells of donor cornea prior to transplant, magnetofection of localised corneal scar tissue, retinal diseases such as RP, LCA, Stargardt's and trabecular meshwork to facilitate aqueous outflow for glaucoma. The cornea can easily be subjected to external magnetic fields to guide and retain MNPs within a region of interest. The retina may not be as accessible but is still possible as a day-case procedure. Future work into designing a more portable hand-held form of magnet with modifiable oscillatory function would be crucial to its clinical translation.

A number of studies have looked at harnessing galvanotaxis in SCs for therapeutic application in spinal cord injury and CNS disease. As an extension of the brain it seemed logical to expand EF directed migration of SC for ocular use. In chapter 5, NSC directed migration from RGC layer into IPL layer occurred with EF application. The modified Boyden chamber experiment was novel since work surrounding NSC galvanotaxis has mainly been with a 2D electrotactic chamber environment whereby migration is directed along the horizontal axis rather than vertically in a 3D environment as in the retina explant. My work highlights the need to develop better 3D assays as this would be most compatible with an in-vivo environment. In the retina explants, NSC would have needed to migrate through tissue layers and few papers have addressed EF directed NSC migration in a 3D manner, most of which do not use ex-vivo tissue culture. Zhang et al used 3D Matrigel as a model for studying electrotaxis in hiPS (Zhang et al., 2011a). It showed that hiPS could migrate in the gel towards the anode; in the horizontal plane, but migration in the z plane (vertical) also occurred. Z plane movement was not analysed or fully described. Sun et al. developed a polydimethylsiloxane(PDMS)-based microfluidic device to generate uniformly sized bubbles in gelatin by injecting a gelatin solution with nitrogen gas from two different inlets (Sun et al., 2012). These were then collected and cross linked and degassed to form a 3D scaffold. Once again, only horizontal movements were analysed but movement in z dimensions were not described. Meng et al. used organotypic spinal cord cultures, but again describe only horizontal migration and not vertical. Although use of GFP

fluorescence only allows for gross detection of NSC vertical migration in ex-vivo tissue environment, it paves the way for future in-vivo work where EF directed migration can be better assessed(Meng et al., 2012).

In chapter 7, I explored the use of NSC as a vector for BDNF delivery and RGC protection. The advantages of BDNF were two–fold in that it not only reduced RGC dendritic degeneration but also and improved EF directed migration into IPL layer. BDNF alone without EF did not induce migration. Interestingly, Xu et al. also report NSC migration towards CXCL12 only occurred in BDNF pre-treated NSC(Xu and Heilshorn, 2013). The exact mechanism of this BDNF facilitated NSC chemotaxis is unclear. In NSC electrotaxis, several pathways for cathode and anodal migration have been explored; one of which involves the P13K/Akt pathway, of which BDNF can activate via Trk receptors. Indeed, several studies have reported that growth factors are usually necessary for electrotaxis to occur (Meng et al., 2011, Zhao et al., 1996, Wang et al., 2003). Of note, EF induced migration occurred without BDNF in chapter 5, as EGF and FGF-2 is already present in NSC culture media. Meng et al. suggested an important link exists between growth factors, EFs and PI3K/Akt pathway (Meng et al., 2012). They looked at EGF and FGF-2, which were required for electrotaxis to take place. Indeed, they showed an EF-induced asymmetric redistribution of GF receptors in NPCs. It is possible that BDNF presence can enhance the effect of galvanotaxis in NSC, and future studies will need to dissect the mechanism behind this.

In developing NSC electrotaxis for in-vivo work, several factors need to be considered. The point of contact for voltage induction will inevitably give off heat and electrode products and affect the surrounding cell structures. To induce electrotaxis of NSC in the eyeball, the lowest voltage threshold for the shortest duration would need to be defined. Indeed, the introduction of an oscillating EF stimulator for spinal cord injury have already reached phase 1 trial (Shapiro et al., 2005). Transcorneal electrical stimulation in animals and humans have already been reported, although these studies investigated the neuroprotective effects of activating endogenous growth factors and not directed migration of NSC (Ni et al., 2009, Sato et al., 2008, Tao et al., 2016, Ozeki et al., 2013). Regardless, it interesting to note the method of voltage introduction; by bipolar contact lens electrode with an inner and outer ring serving as stimulating electrodes or a microfiber electrode is placed on the cornea after topical anaesthesia followed by electric pulses. Further work into NSC galvanotaxis can apply these methods of EF delivery with reassurance that eventual clinical translation is plausible.

Summary of Future Work:

With successful magnetofection of the cornea, this can be extended to magnetofection of the trabecular meshwork in healthy mouse and also glaucoma mouse-models i.e. DBA/2J mouse in-vivo. Magnetofection of the retina can also be trialled on in-vivo with a BDNF-overexpressing gene and looking at RGC Sholl plots on retina after inducing raised IOP in the mouse.

In the cornea, the endothelium was magnetofected but to a lesser extent when oscillation was increased during magnetofection. There was a suggestion that some stromal cells were magnetofected at higher oscillations, suggesting that perhaps the cells magnetofected were deeper when oscillation was higher. It would be interesting to assess if depth of magnetofection in cornea or even retinal tissue can be controlled with a higher oscillation.

Development of a portable magnet with oscillatory function for magnetofection of the anterior segment and posterior segment could facilitate its clinical translation. Posterior segment magnetofection will require applanation of the device inferotemporal to the limbus for macular magnetofection. Hence, a small portable device would better serve this purpose.

The threshold voltage for NSC migration post intravitreal injection of NSC in-vivo needs to be optimized. EF application in animal models of retinal degeneration of wild type can be introduced via electroacupuncture (retrobulbar needle with voltage application) or transcorneal electrical stimulation. Ideally, a new method should be developed to introduce EF in assessing electric field application in live animals. This is to prevent metal electrodes possibly ionizing electrolytes in tissue and hence inducing a chemical gradient.

The effect of NSC migration with and without BDNF in the absence of EF application also needs to be assessed. Whether BDNF plays a part in galvanotaxis can be explored by looking and recombinant mice with BDNF overexpression and administering intravitreal injections of NSC with or without EF application. Alternatively, experiments with NSC magnetofected without any plasmids can be used to determine if magnetofection itself causes increased migration.

REFERENCES

A study of the safety and efficacy of CNTO2476 in patients with age-related macular degeneration. [Online]. Available: http://clinicaltrials.gov/ct2/show/NCT01226628.

ADAMS, C. F., PICKARD, M. R. & CHARI, D. M. 2013. Magnetic nanoparticle mediated transfection of neural stem cell suspension cultures is enhanced by applied oscillating magnetic fields. *Nanomedicine*.9(6):737-41.

AGUIRRE, A., RIZVI, T. A., RATNER, N. & GALLO, V. 2005. Overexpression of the epidermal growth factor receptor confers migratory properties to nonmigratory postnatal neural progenitors. *J Neurosci,* 25**,** 11092-106.

AKITA, J., TAKAHASHI, M., HOJO, M., NISHIDA, A., HARUTA, M. & HONDA, Y. 2002. Neuronal differentiation of adult rat hippocampus-derived neural stem cells transplanted into embryonic rat explanted retinas with retinoic acid pretreatment. *Brain Res.*8;954(2):286-93.

AL-MAJED, A. A., BRUSHART, T. M. & GORDON, T. 2000. Electrical stimulation accelerates and increases expression of BDNF and TrkB mRNA in regenerating rat femoral motoneurons. *Eur J Neurosci,* 12**,** 4381-90.

ALLEN, G. M., MOGILNER, A. & THERIOT, J. A. 2013. Electrophoresis of cellular membrane components creates the directional cue guiding keratocyte galvanotaxis. *Curr Biol,* 23**,** 560-8.

ALLOCCA, M., DORIA, M., PETRILLO, M., COLELLA, P., GARCIA-HOYOS, M., GIBBS, D., KIM, S. R., MAGUIRE, A., REX, T. S., DI VICINO, U., CUTILLO, L., SPARROW, J. R., WILLIAMS, D. S., BENNETT, J. & AURICCHIO, A. 2008. Serotype-dependent packaging of large genes in adeno-associated viral vectors results in effective gene delivery in mice. *J Clin Invest,* 118**,** 1955-64.

ALTIZER, A. M., MORIARTY, L. J., BELL, S. M., SCHREINER, C. M., SCOTT, W. J. & BORGENS, R. B. 2001. Endogenous electric current is associated with normal development of the vertebrate limb. *Dev Dyn,* 221**,** 391-401.

ANDERSON, D. G., LEVENBERG, S. & LANGER, R. 2004. Nanoliter-scale synthesis of arrayed biomaterials and application to human embryonic stem cells. *Nat Biotechnol,* 22**,** 863-6.

AOKI, H., HARA, A., NAKAGAWA, S., MOTOHASHI, T., HIRANO, M., TAKAHASHI, Y. & KUNISADA, T. 2006. Embryonic stem cells that differentiate into RPE cell precursors in vitro develop into RPE cell monolayers in vivo. *Exp Eye Res;82(2):265-74.*

AOKI, H., HARA, A., NIWA, M., MOTOHASHI, T., SUZUKI, T. & KUNISADA, T. 2008. Transplantation of

cells from eye-like structures differentiated from embryonic stem cells in vitro and in vivo regeneration of retinal ganglion-like cells. *Graefes Arch Clin Exp Ophthalmol,* 246**,** 255-65.

AROCENA, M., ZHAO, M., COLLINSON, J. M. & SONG, B. 2010. A time-lapse and quantitative modelling analysis of neural stem cell motion in the absence of directional cues and in electric fields. *J Neurosci Res,* 88**,** 3267-74.

ASANO Y, E. H. Instructions Chemotaxis and Migration Tool 2.0, ibidi GmbH, Version 1.1.

ASSAWACHANANONT, J., MANDAI, M., OKAMOTO, S., YAMADA, C., EIRAKU, M., YONEMURA, S., SASAI, Y. & TAKAHASHI, M. 2014. Transplantation of embryonic and induced pluripotent stem cell-derived 3D retinal sheets into retinal degenerative mice. *Stem Cell Reports,* 2**,** 662-74.

ATMACA-SONMEZ, P., LI, Y., YAMAUCHI, Y., SCHANIE, C. L., ILDSTAD, S. T., KAPLAN, H. J. & ENZMANN, V. 2006. Systemically transferred hematopoietic stem cells home to the subretinal space and express RPE-65 in a mouse model of retinal pigment epithelium damage. *Exp Eye Res,* 83**,** 1295-302.

Autologous bone marrow-derived stem cells transplantation for retinitis pigmentosa. [Online]. Available: http://clinicaltrials.gov/ct2/show/NCT01068561.

BABONA-PILIPOS, R., POPOVIC, M. R. & MORSHEAD, C. M. 2012. A galvanotaxis assay for analysis of neural precursor cell migration kinetics in an externally applied direct current electric field. *J Vis Exp*;(68):pii:4193

BABONA-PILIPOS, R., Droujinine , I.A., POPOVIC, M. R. & MORSHEAD, C. M. 2011. Adult subependymal neural precursors, but not differentiated cells, undergo rapid cathodal migration in the presence of direct current electric fields. PLos One; 6(8): e23808

BAINBRIDGE, J. W., MEHAT, M. S., SUNDARAM, V., ROBBIE, S. J., BARKER, S. E., RIPAMONTI, C., GEORGIADIS, A., MOWAT, F. M., BEATTIE, S. G., GARDNER, P. J., FEATHERS, K. L., LUONG, V. A., YZER, S., BALAGGAN, K., VISWANATHAN, A., DE RAVEL, T. J., CASTEELS, I., HOLDER, G. E., TYLER, N., FITZKE, F. W., WELEBER, R. G., NARDINI, M., MOORE, A. T., THOMPSON, D. A., PETERSEN-JONES, S. M., MICHAELIDES, M., VAN DEN BORN, L. I., STOCKMAN, A., SMITH, A. J., RUBIN, G. & ALI, R. R. 2015. Long-term effect of gene therapy on Leber's congenital amaurosis. *N Engl J Med,* 372**,** 1887-97.

BAINBRIDGE, J. W., SMITH, A. J., BARKER, S. S., ROBBIE, S., HENDERSON, R., BALAGGAN, K., VISWANATHAN, A., HOLDER, G. E., STOCKMAN, A., TYLER, N., PETERSEN-JONES, S., BHATTACHARYA, S. S., THRASHER, A. J., FITZKE, F. W., CARTER, B. J., RUBIN, G. S., MOORE, A. T. & ALI, R. R. 2008. Effect of gene therapy on visual function in Leber's congenital amaurosis. *N Engl J Med,* 358**,** 2231-9.

BAINBRIDGE, J. W., STEPHENS, C., PARSLEY, K., DEMAISON, C., HALFYARD, A., THRASHER, A. J. & ALI, R. R. 2001. In vivo gene transfer to the mouse eye using an HIV-based lentiviral vector; efficient long-term transduction of corneal endothelium and retinal pigment epithelium. *Gene Ther,* 8**,** 1665-8.

BALLIOS, B. G., COOKE, M. J., DONALDSON, L., COLES, B. L., MORSHEAD, C. M., VAN DER KOOY, D. & SHOICHET, M. S. 2015. A Hyaluronan-Based Injectable Hydrogel Improves the Survival and Integration of Stem Cell Progeny following Transplantation. *Stem Cell Reports,* 4**,** 1031-45.

BALLIOS, B. G., COOKE, M. J., VAN DER KOOY, D. & SHOICHET, M. S. 2010. A hydrogel-based stem cell delivery system to treat retinal degenerative diseases. *Biomaterials,* 31**,** 2555-64.

BALLIOS, B. G., COOKE, M. J., DONALDSON, L., COLES, B. L., MORSHEAD, C. M., VAN DER KOOY, D. & SHOICHET, M. S. 2015. A Hyaluronan-Based Injectable Hydrogel Improves the Survival and Integration of Stem Cell Progeny following Transplantation. *Stem Cell Reports,* 4**,** 1031-45.

BASARAN, E., DEMIREL, M., SIRMAGUL, B. & YAZAN, Y. 2010. Cyclosporine-A incorporated cationic solid lipid nanoparticles for ocular delivery. *J Microencapsul,* 27**,** 37-47.

BAUER, D., LU, M., WASMUTH, S., LI, H., YANG, Y., ROGGENDORF, M., STEUHL, K. P. & HEILIGENHAUS, A. 2006. Immunomodulation by topical particle-mediated administration of cytokine plasmid DNA suppresses herpetic stromal keratitis without impairment of antiviral defense. *Graefes Arch Clin Exp Ophthalmol,* 244**,** 216-25.

BAUER, D., WASMUTH, S., LU, M. & HEILIGENHAUS, A. 2013. Particle-mediated administration of plasmid DNA on corneas of BALB/c mice. *Methods Mol Biol,* 940**,** 215-20.

BECKER, D., BONNESS, V. & MOBBS, P. 1998. Cell coupling in the retina: patterns and purpose. *Cell Biol Int,* 22**,** 781-92.

BELTRAN, W. A. 2008. On the role of CNTF as a potential therapy for retinal degeneration: Dr. Jekyll or Mr. Hyde? *Adv Exp Med Biol,* 613**,** 45-51.

BHATIA, B., SINGHAL, S., LAWRENCE, J. M., KHAW, P. T. & LIMB, G. A. 2009. Distribution of Muller stem cells within the neural retina: evidence for the existence of a ciliary margin-like zone in the adult human eye. *Exp Eye Res,* 89**,** 373-82.

BI, Y. Y., FENG, D. F. & PAN, D. C. 2009. Stem/progenitor cells: a potential source of retina-specific cells for retinal repair. *Neurosci Res;65(3):215-21.*

BINLEY, K. E., NG, W. S., BARDE, Y. A., SONG, B. & MORGAN, J. E. 2016. Brain-derived neurotrophic factor prevents dendritic retraction of adult mouse retinal ganglion cells. *Eur J Neurosci,* 44**,** 2028-39.

BIRCH, D. G., WELEBER, R. G., DUNCAN, J. L., JAFFE, G. J. & TAO, W. 2013. Randomized Trial of Ciliary

Neurotrophic Factor Delivered by Encapsulated Cell Intraocular Implants for Retinitis Pigmentosa. *Am J Ophthalmol*;156(2):283-292.

BLAIR-PARKS, K., WESTON, B. C. & DEAN, D. A. 2002. High-level gene transfer to the cornea using electroporation. *J Gene Med,* 4**,** 92-100.

BORGENS, R. B., JAFFE, L. F. & COHEN, M. J. 1980. Large and persistent electrical currents enter the transected lamprey spinal cord. *Proc Natl Acad Sci U S A,* 77**,** 1209-13.

BORGENS, R. B., TOOMBS, J. P., BREUR, G., WIDMER, W. R., WATERS, D., HARBATH, A. M., MARCH, P. & ADAMS, L. G. 1999. An imposed oscillating electrical field improves the recovery of function in neurologically complete paraplegic dogs. *J Neurotrauma,* 16**,** 639-57.

BOYDEN, S. 1962. The chemotactic effect of mixtures of antibody and antigen on polymorphonuclear leucocytes. *J Exp Med,* 115**,** 453-66.

BUCH, P. K., MACLAREN, R. E., DURAN, Y., BALAGGAN, K. S., MACNEIL, A., SCHLICHTENBREDE, F. C., SMITH, A. J. & ALI, R. R. 2006. In contrast to AAV-mediated Cntf expression, AAV-mediated Gdnf expression enhances gene replacement therapy in rodent models of retinal degeneration. *Mol Ther,* 14**,** 700-9.

BUCHHOLZ, D. E., HIKITA, S. T., ROWLAND, T. J., FRIEDRICH, A. M., HINMAN, C. R., JOHNSON, L. V. & CLEGG, D. O. 2009. Derivation of functional retinal pigmented epithelium from induced pluripotent. *Stem Cells,* 27**,** 2427-34.

BULL, N. D., IRVINE, K. A., FRANKLIN, R. J. & MARTIN, K. R. 2009. Transplanted oligodendrocyte precursor cells reduce neurodegeneration in a model of glaucoma. *Invest Ophthalmol Vis Sci;50(9):4244-53.*

BULL, N. D., JOHNSON, T. V., WELSAPAR, G., DEKORVER, N. W., TOMAREV, S. I. & MARTIN, K. R. 2011. Use of an adult rat retinal explant model for screening of potential retinal ganglion cell neuroprotective therapies. *Invest Ophthalmol Vis Sci;52(6):3309-20.*

BUNCE, C. & WORMALD, R. 2006. Leading causes of certification for blindness and partial sight in England & Wales. *BMC Public Health.* England.

CAFFE, A. R., AHUJA, P., HOLMQVIST, B., AZADI, S., FORSELL, J., HOLMQVIST, I., SODERPALM, A. K. & VAN VEEN, T. 2001. Mouse retina explants after long-term culture in serum free medium. *J Chem Neuroanat.*

CAI, X., CONLEY, S. M., NASH, Z., FLIESLER, S. J., COOPER, M. J. & NAASH, M. I. 2010. Gene delivery to mitotic and postmitotic photoreceptors via compacted DNA nanoparticles results in improved phenotype in a mouse model of retinitis pigmentosa. *Faseb j,* 24**,** 1178-91.

CAMPOCHIARO, P. A., NGUYEN, Q. D., SHAH, S. M., KLEIN, M. L., HOLZ, E., FRANK, R. N., SAPERSTEIN, D. A., GUPTA, A., STOUT, J. T., MACKO, J., DIBARTOLOMEO, R. & WEI, L. L. 2006. Adenoviral vector-delivered pigment epithelium-derived factor for neovascular age-related macular degeneration: results of a phase I clinical trial. *Hum Gene Ther,* 17**,** 167-76.

CARR, A. J., VUGLER, A. A., HIKITA, S. T., LAWRENCE, J. M., GIAS, C., CHEN, L. L., BUCHHOLZ, D. E., AHMADO, A., SEMO, M., SMART, M. J., HASAN, S., DA CRUZ, L., JOHNSON, L. V., CLEGG, D. O. & COFFEY, P. J. 2009. Protective effects of human iPS-derived retinal pigment epithelium cell. *PLoS One;4(12):e8152*

CASTANHEIRA, P., TORQUETTI, L., NEHEMY, M. B. & GOES, A. M. 2008. Retinal incorporation and differentiation of mesenchymal stem cells intravitreally injected in the injured retina of rats. *Arq Bras Oftalmol,* 71**,** 644-50.

CAYOUETTE, M., BEHN, D., SENDTNER, M., LACHAPELLE, P. & GRAVEL, C. 1998. Intraocular gene transfer of ciliary neurotrophic factor prevents death and increases responsiveness of rod photoreceptors in the retinal degeneration slow mouse. *J Neurosci,* 18**,** 9282-93.

CHACKO, D. M., DAS, A. V., ZHAO, X., JAMES, J., BHATTACHARYA, S. & AHMAD, I. 2003. Transplantation of ocular stem cells: the role of injury in incorporation and differentiation of grafted cells in the retina. *Vision Res,* 43**,** 937-46.

CHANG, H. F., LEE, Y. S., TANG, T. K. & CHENG, J. Y. 2016. Pulsed DC Electric Field-Induced Differentiation of Cortical Neural Precursor Cells. *PLoS One;*(11):e0158133.

CHEN, M., CHEN, Q., SUN, X., SHEN, W., LIU, B., ZHONG, X., LENG, Y., LI, C., ZHANG, W., CHAI, F., HUANG, B., GAO, Q., XIANG, A. P., ZHUO, Y. & GE, J. 2010. Generation of retinal ganglion-like cells from reprogrammed mouse fibroblasts. *Invest Ophthalmol Vis Sci.*;51(11):5970-8

CHENG, I., GITHENS, M., SMITH, R. L., JOHNSTON, T. R., PARK, D. Y., STAUFF, M. P., SALARI, N., TILESTON, K. R. & KHARAZI, A. I. 2015. Local versus distal transplantation of human neural stem cells following chronic spinal cord injury. *Spine J.*;16(6):764-769.

CHUNG, J. K., PARK, T. K., OHN, Y. H., PARK, S. K. & HONG, D. S. 2011. Modulation of retinal wound healing by systemically administered bone marrow-derived mesenchymal stem cells. *Korean J Ophthalmol,* 25**,** 268-74.

CICERO, S. A., JOHNSON, D., REYNTJENS, S., FRASE, S., CONNELL, S., CHOW, L. M., BAKER, S. J., SORRENTINO, B. P. & DYER, M. A. 2009. Cells previously identified as retinal stem cells are pigmented ciliary epithelial cells. *Proc Natl Acad Sci U S A,* 106**,** 6685-90.

Clinical trial for gene therapy for Leber Congenital Amaurosis caused by RPE65 mutations [Online]. Available: http://clinicaltrials.gov/ct2/show/NCT00821340 [Accessed 12 April 2013].

COLES, B. L., ANGENIEUX, B., INOUE, T., DEL RIO-TSONIS, K., SPENCE, J. R., MCINNES, R. R., ARSENIJEVIC, Y. & VAN DER KOOY, D. 2004. Facile isolation and the characterization of human retinal stem cells. *Proc Natl Acad Sci U S A,* 101**,** 15772-7.

DAHLMANN-NOOR, A., VIJAY, S., JAYARAM, H., LIMB, A. & KHAW, P. T. 2010. Current approaches and future prospects for stem cell rescue and regeneration of the retina and optic nerve. *Can J Ophthalmol;45(4):333-41.*

DAS, S. K., TUCKER, I. G., HILL, D. J. & GANGULY, N. 1995. Evaluation of poly(isobutylcyanoacrylate) nanoparticles for mucoadhesive ocular drug delivery. I. Effect of formulation variables on physicochemical characteristics of nanoparticles. *Pharm Res,* 12**,** 534-40.

DEN HOLLANDER, A. I., ROEPMAN, R., KOENEKOOP, R. K. & CREMERS, F. P. 2008. Leber congenital amaurosis: genes, proteins and disease mechanisms. *Prog Retin Eye Res.*

DI POLO, A., AIGNER, L. J., DUNN, R. J., BRAY, G. M. & AGUAYO, A. J. 1998. Prolonged delivery of brain-derived neurotrophic factor by adenovirus-infected Muller cells temporarily rescues injured retinal ganglion cells. *Proc Natl Acad Sci U S A.,* 95**,** 3978-83.

DOBSON, J. 2006. Gene therapy progress and prospects: magnetic nanoparticle-based gene delivery. *Gene Ther,* 13**,** 283-7.

DOUGLAS-ESCOBAR, M., ROSSIGNOL, C., STEINDLER, D., ZHENG, T. & WEISS, M. D. 2012. Neurotrophin-induced migration and neuronal differentiation of multipotent astrocytic stem cells in vitro. *PLoS One,* 7**,** e51706.

DURAIRAJ, C., KADAM, R. S., CHANDLER, J. W., HUTCHERSON, S. L. & KOMPELLA, U. B. 2010. Nanosized dendritic polyguanidilyated translocators for enhanced solubility, permeability, and delivery of gatifloxacin. *Invest Ophthalmol Vis Sci,* 51**,** 5804-16.

DURBEC, P., FRANCESCHINI, I., LAZARINI, F. & DUBOIS-DALCQ, M. 2008. In vitro migration assays of neural stem cells. *Methods Mol Biol,* 438**,** 213-25.

EIRAKU, M., TAKATA, N., ISHIBASHI, H., KAWADA, M., SAKAKURA, E., OKUDA, S., SEKIGUCHI, K., ADACHI, T. & SASAI, Y. 2011. Self-organizing optic-cup morphogenesis in three-dimensional culture. *Nature;472(7341:51-6.*

EVANS, M. J. & KAUFMAN, M. H. 1981. Establishment in culture of pluripotential cells from mouse embryos. *Nature,* 292**,** 154-6.

FAKTOROVICH, E. G., STEINBERG, R. H., YASUMURA, D., MATTHES, M. T. & LAVAIL, M. M. 1990. Photoreceptor degeneration in inherited retinal dystrophy delayed by basic fibroblast growth factor.

Nature, 347**,** 83-6.

FARBOUD, B., NUCCITELLI, R., SCHWAB, I. R. & ISSEROFF, R. R. 2000. DC electric fields induce rapid directional migration in cultured human corneal epithelial cells. *Exp Eye Res,* 70**,** 667-73.

FENG, J. F., LIU, J., ZHANG, X. Z., ZHANG, L., JIANG, J. Y., NOLTA, J. & ZHAO, M. 2012. Guided migration of neural stem cells derived from human embryonic stem cells by an electric field. *Stem Cells,* 30**,** 349-55.

FENG, L., CHEN, H., YI, J., TROY, J. B., ZHANG, H. F. & LIU, X. 2016. Long-Term Protection of Retinal Ganglion Cells and Visual Function by Brain-Derived Neurotrophic Factor in Mice With Ocular Hypertension. *Invest Ophthalmol Vis Sci,* 57**,** 3793-802.

FLACHSBARTH, K., KRUSZEWSKI, K., JUNG, G., JANKOWIAK, W., RIECKEN, K., WAGENFELD, L., RICHARD, G., FEHSE, B. & BARTSCH, U. 2014. Neural stem cell-based intraocular administration of ciliary neurotrophic factor attenuates the loss of axotomized ganglion cells in adult mice. *Invest Ophthalmol Vis Sci,* 55**,** 7029-39.

FOURIKI, A., CLEMENTS, M. A., FARROW, N. & DOBSON, J. 2012. Efficient transfection of MG-63 osteoblasts using magnetic nanoparticles and oscillating magnetic fields. *J Tissue Eng Regen Med*;8(3):169-75.

FOXMAN, E. F., KUNKEL, E. J. & BUTCHER, E. C. 1999. Integrating conflicting chemotactic signals. The role of memory in leukocyte navigation. *J Cell Biol,* 147**,** 577-88.

FREITAS, E. R., SANTOS, R. L., LIMA, E. C. & GUILLO, L. A. 2013. Feeder-free culture of human embryonic stem cell line BG01V/hOG using magnetic field-magnetic nanoparticles system. *Biomed Pharmacother,* 67**,** 17-21.

FUCHSLUGER, T. A., JURKUNAS, U., KAZLAUSKAS, A. & DANA, R. 2011. Corneal endothelial cells are protected from apoptosis by gene therapy. *Hum Gene Ther,* 22**,** 549-58.

FUJII, Y., KACHI, S., ITO, A., KAWASUMI, T., HONDA, H. & TERASAKI, H. 2010. Transfer of gene to human retinal pigment epithelial cells using magnetite cationic liposomes. *Br J Ophthalmol,* 94**,** 1074-7.

FUJINO, K., KIM, T. S., NISHIDA, A. T., NAKAGAWA, T., OMORI, K., NAITO, Y. & ITO, J. 2004. Transplantation of neural stem cells into explants of rat inner ear. *Acta Otolaryngol Suppl***,** 31-3.

FUCHSLUGER, T. A., JURKUNAS, U., KAZLAUSKAS, A. & DANA, R. 2011. Corneal endothelial cells are protected from apoptosis by gene therapy. *Hum Gene Ther,* 22**,** 549-58.

GAMM, D. M., WANG, S., LU, B., GIRMAN, S., HOLMES, T., BISCHOFF, N., SHEARER, R. L., SAUVE, Y., CAPOWSKI, E., SVENDSEN, C. N. & LUND, R. D. 2007. Protection of visual functions by human neural

progenitors in a rat model of retinal disease. *PLoS One;* (2)**:** e338.
GARCIA, M. A., MERINO, J. M., FERNANDEZ PINEL, E., QUESADA, A., DE LA VENTA, J., RUIZ GONZALEZ, M. L., CASTRO, G. R., CRESPO, P., LLOPIS, J., GONZALEZ-CALBET, J. M. & HERNANDO, A. 2007. Magnetic properties of ZnO nanoparticles. *Nano Lett,* 7**,** 1489-94.
GASTINGER, M. J., KUNSELMAN, A. R., CONBOY, E. E., BRONSON, S. K. & BARBER, A. J. 2008. Dendrite remodeling and other abnormalities in the retinal ganglion cells of Ins2 Akita diabetic mice. *Invest Ophthalmol Vis Sci,* 49**,** 2635-42.
GENG, X., SUN, T., LI, J. H., ZHAO, N., WANG, Y. & YU, H. L. 2015. Electroacupuncture in the repair of spinal cord injury: inhibiting the Notch signaling pathway and promoting neural stem cell proliferation. *Neural Regen Res,* 10**,** 394-403.

GHAZI, N. G., ABBOUD, E. B., NOWILATY, S. R., ALKURAYA, H., ALHOMMADI, A., CAI, H., HOU, R., DENG, W. T., BOYE, S. L., ALMAGHAMSI, A., AL SAIKHAN, F., AL-DHIBI, H., BIRCH, D., CHUNG, C., COLAK, D., LAVAIL, M. M., VOLLRATH, D., ERGER, K., WANG, W., CONLON, T., ZHANG, K., HAUSWIRTH, W. & ALKURAYA, F. S. 2016. Treatment of retinitis pigmentosa due to MERTK mutations by ocular subretinal injection of adeno-associated virus gene vector: results of a phase I trial. *Hum Genet,* 135**,** 327-43.
GHOSH, A., YUE, Y. & DUAN, D. 2011. Efficient transgene reconstitution with hybrid dual AAV vectors carrying the minimized bridging sequences. *Hum Gene Ther,* 22**,** 77-83.
GILLESPIE, R. L., HALL, G. & BLACK, G. C. 2014. Genetic testing for inherited ocular disease: delivering on the promise at last? *Clin Experiment Ophthalmol,* 42**,** 65-77.

GOLDBERG, J. L. 2016. *NT-501 CNTF Implant for glaucoma: Saftey, Neuroprotection and Neuroenhancement* [Online]. https://clinicaltrials.gov/ct2/show/NCT01408472. [Accessed 7.11.16 2016].
GREGORY-EVANS, K., CHANG, F., HODGES, M. D. & GREGORY-EVANS, C. Y. 2009. Ex vivo gene therapy using intravitreal injection of GDNF-secreting mouse embryonic stem cells in a rat model of retinal degeneration. *Mol Vis.*;15:962-73.

GUERIN, M. B., DONOVAN, M., MCKERNAN, D. P., O'BRIEN, C. J. & COTTER, T. G. 2011. Age-dependent rat retinal ganglion cell susceptibility to apoptotic stimuli: implications for glaucoma. *Clin Experiment Ophthalmol,* 39**,** 243-51.

GUO, Y., CEPURNA, W. O., DYCK, J. A., DOSER, T. A., JOHNSON, E. C. & MORRISON, J. C. 2010. Retinal cell responses to elevated intraocular pressure: a gene array comparison between the whole retina and retinal ganglion cell layer. Invest Ophthalmol Vis Sci, 51, 3003-18.

GUO, D., BI, H., LIU, B., WU, Q., WANG, D. & CUI, Y. 2013. Reactive oxygen species-induced cytotoxic effects of zinc oxide nanoparticles in rat retinal ganglion cells. *Toxicol In Vitro,* 27**,** 731-8.

GUO, Y., CEPURNA, W. O., DYCK, J. A., DOSER, T. A., JOHNSON, E. C. & MORRISON, J. C. 2010. Retinal cell responses to elevated intraocular pressure: a gene array comparison between the whole retina and retinal ganglion cell layer. *Invest Ophthalmol Vis Sci,* 51**,** 3003-18.

GUO, Y., SALOUPIS, P., SHAW, S. J. & RICKMAN, D. W. 2003. Engraftment of adult neural progenitor cells transplanted to rat retina injured by transient ischemia. *Invest Ophthalmol Vis Sci,* 44**,** 3194-201.

GUTIERREZ, H. & DAVIES, A. M. 2007. A fast and accurate procedure for deriving the Sholl profile in quantitative studies of neuronal morphology. *J Neurosci Methods,* 163**,** 24-30.

HAMEL, C. 2006. Retinitis pigmentosa. *Orphanet J Rare Dis.* England.

HAN, Z., CONLEY, S. M., MAKKIA, R., GUO, J., COOPER, M. J. & NAASH, M. I. 2012a. Comparative analysis of DNA nanoparticles and AAVs for ocular gene delivery. *PLoS One;(*7**):** e52189.

HAN, Z., KOIRALA, A., MAKKIA, R., COOPER, M. J. & NAASH, M. I. 2012b. Direct gene transfer with compacted DNA nanoparticles in retinal pigment epithelial cells: expression, repeat delivery and lack of toxicity. *Nanomedicine (Lond),* 7**,** 521-39.

HARPER, M. M., ADAMSON, L., BLITS, B., BUNGE, M. B., GROZDANIC, S. D. & SAKAGUCHI, D. S. 2009. Brain-derived neurotrophic factor released from engineered mesenchymal stem cells attenuates glutamate- and hydrogen peroxide-mediated death of staurosporine-differentiated RGC-5 cells. *Exp Eye Res,* 89**,** 538-48.

HARPER, M. M., GROZDANIC, S. D., BLITS, B., KUEHN, M. H., ZAMZOW, D., BUSS, J. E., KARDON, R. H. & SAKAGUCHI, D. S. 2011. Transplantation of BDNF-secreting mesenchymal stem cells provides neuroprotection in chronically hypertensive rat eyes. *Invest Ophthalmol Vis Sci,* 52**,** 4506-15.

HARRIS, J. R., BROWN, G. A., JORGENSEN, M., KAUSHAL, S., ELLIS, E. A., GRANT, M. B. & SCOTT, E. W. 2006. Bone marrow-derived cells home to and regenerate retinal pigment epithelium after injury. *Invest Ophthalmol Vis Sci,* 47**,** 2108-13.

HARTONG, D. T., BERSON, E. L. & DRYJA, T. P. 2006. Retinitis pigmentosa. *Lancet.* England.

HARUTA, M., SASAI, Y., KAWASAKI, H., AMEMIYA, K., OOTO, S., KITADA, M., SUEMORI, H., NAKATSUJI, N., IDE, C., HONDA, Y. & TAKAHASHI, M. 2004. In vitro and in vivo characterization of pigment epithelial cells differentiated from primate embryonic stem cells. *Invest Ophthalmol Vis Sci,* 45**,** 1020-5.

HE, Z., PIPPARELLI, A., MANISSOLLE, C., ACQUART, S., GARRAUD, O., GAIN, P. & THURET, G. 2010. Ex vivo gene electrotransfer to the endothelium of organ cultured human corneas. *Ophthalmic Res,* 43**,** 43-55.

HIPPALGAONKAR, K., ADELLI, G. R., REPKA, M. A. & MAJUMDAR, S. 2013. Indomethacin-loaded solid lipid nanoparticles for ocular delivery: development, characterization, and in vitro evaluation. *J Ocul Pharmacol Ther,* 29**,** 216-28.

HIRAMI, Y., OSAKADA, F., TAKAHASHI, K., OKITA, K., YAMANAKA, S., IKEDA, H., YOSHIMURA, N. & TAKAHASHI, M. 2009. Generation of retinal cells from mouse and human induced pluripotent stem cells. *Neurosci Lett,* 458**,** 126-31.

HOTARY, K. B. & ROBINSON, K. R. 1992. Evidence of a role for endogenous electrical fields in chick embryo development. *Development,* 114**,** 985-96.

HOTARY, K. B. & ROBINSON, K. R. 1994. Endogenous electrical currents and voltage gradients in Xenopus embryos and the consequences of their disruption. *Dev Biol,* 166**,** 789-800.

HOWDEN, S. E., GORE, A., LI, Z., FUNG, H. L., NISLER, B. S., NIE, J., CHEN, G., MCINTOSH, B. E., GULBRANSON, D. R., DIOL, N. R., TAAPKEN, S. M., VEREIDE, D. T., MONTGOMERY, K. D., ZHANG, K., GAMM, D. M. & THOMSON, J. A. 2011. Genetic correction and analysis of induced pluripotent stem cells from a patient with gyrate atrophy. *Proc Natl Acad Sci U S A.* United States.

HOWELL, G. R., MACALINAO, D. G., SOUSA, G. L., WALDEN, M., SOTO, I., KNEELAND, S. C., BARBAY, J. M., KING, B. L., MARCHANT, J. K., HIBBS, M., STEVENS, B., BARRES, B. A., CLARK, A. F., LIBBY, R. T. & JOHN, S. W. 2011. Molecular clustering identifies complement and endothelin induction as early events in a mouse model of glaucoma. J Clin Invest, 121, 1429-44.

HUANG, Y., LI, Y., CHEN, J., ZHOU, H. & TAN, S. 2015. Electrical Stimulation Elicits Neural Stem Cells Activation: New Perspectives in CNS Repair. *Front Hum Neurosci,* 9**,** 586.

HUO, S. J., LI, Y., RAISMAN, G. & YIN, Z. Q. 2011. Transplanted olfactory ensheathing cells reduce the gliotic injury response of Muller cells in a rat model of retinitis pigmentosa. *Brain Res,* 1382**,** 238-44.

HUO, S. J., LI, Y. C., XIE, J., LI, Y., RAISMAN, G., ZENG, Y. X., HE, J. R., WENG, C. H. & YIN, Z. Q. 2012. Transplanted olfactory ensheathing cells reduce retinal degeneration in Royal College of Surgeons rats. *Curr Eye Res,* 37**,** 749-58.

IKEDA, H., OSAKADA, F., WATANABE, K., MIZUSEKI, K., HARAGUCHI, T., MIYOSHI, H., KAMIYA, D., HONDA, Y., SASAI, N., YOSHIMURA, N., TAKAHASHI, M. & SASAI, Y. 2005. Generation of Rx+/Pax6+ neural retinal precursors from embryonic stem cells. *Proc Natl Acad Sci;102(32):1131-6.*

IBIDI. 2016. *Chemotaxis and Migration Tool Version 1.01*

Visualisation and data analysis of chemotaxis and migration processes based on Image J [Online]. www.ibidi.com/fileadmin/products/software/chemotaxis_tool/IN_XXXXX_CT_Tool_1_01_EN.pdf. [Accessed 20.06.16 2016].
INGVAR, S. 1920. Reaction of cells to the galvanic current in tissue cultures.*Exp Biol Med*;17:198-199.

ISHIKAWA, H., TAKANO, M., MATSUMOTO, N., SAWADA, H., IDE, C., MIMURA, O. & DEZAWA, M. 2005. Effect of GDNF gene transfer into axotomized retinal ganglion cells using in vivo electroporation with a contact lens-type electrode. *Gene Ther,* 12**,** 289-98.

JAFFE, L. F. & STERN, C. D. 1979. Strong electrical currents leave the primitive streak of chick embryos. *Science,* 206**,** 569-71.

JAGATHA, B., DIVYA, M. S., SANALKUMAR, R., INDULEKHA, C. L., VIDYANAND, S., DIVYA, T. S., DAS, A. V. & JAMES, J. 2009. In vitro differentiation of retinal ganglion-like cells from embryonic stem cell derived neural progenitors. *Biochem Biophys Res Commun,* 380**,** 230-5.

JAIN, K., KUMAR, R. S., SOOD, S. & DHYANANDHAN, G. 2013. Betaxolol hydrochloride loaded chitosan nanoparticles for ocular delivery and their anti-glaucoma efficacy. *Curr Drug Deliv*;10(5):493-9.

JAYARAM, H., BECKER, S., EASTLAKE, K., JONES, M. F., CHARTERIS, D. G. & LIMB, G. A. 2014. Optimized feline vitrectomy technique for therapeutic stem cell delivery to the inner retina. *Vet Ophthalmol,* 17**,** 300-4.

JENKINS, S. I., PICKARD, M. R., GRANGER, N. & CHARI, D. M. 2011. Magnetic nanoparticle-mediated gene transfer to oligodendrocyte precursor cell transplant populations is enhanced by magnetofection strategies. *ACS Nano,* 5**,** 6527-38.

JEUN, M., JEOUNG, J. W., MOON, S., KIM, Y. J., LEE, S., PAEK, S. H., CHUNG, K. W., PARK, K. H. & BAE, S. 2011. Engineered superparamagnetic Mn0.5Zn0.5Fe2O4 nanoparticles as a heat shock protein induction agent for ocular neuroprotection in glaucoma. *Biomaterials,* 32**,** 387-94.

JOHNSON, T. V., OGLESBY, E. N., STEINHART, M. R., CONE-KIMBALL, E., JEFFERYS, J. & QUIGLEY, H. A. 2016. Time-Lapse Retinal Ganglion Cell Dendritic Field Degeneration Imaged in Organotypic Retinal Explant Culture. *Invest Ophthalmol Vis Sci,* 57**,** 253-64.

JOHNSON, T. V., BULL, N. D., HUNT, D. P., MARINA, N., TOMAREV, S. I. & MARTIN, K. R. 2010a. Neuroprotective effects of intravitreal mesenchymal stem cell transplantation in experimental glaucoma. *Invest Ophthalmol Vis Sci.51(4):2051-9.*

JOHNSON, T. V., BULL, N. D. & MARTIN, K. R. 2010b. Identification of barriers to retinal engraftment of transplanted stem cells. *Invest Ophthalmol Vis Sci,* 51**,** 960-70.

JOHNSON, T. V. & MARTIN, K. R. 2008. Development and characterization of an adult retinal explant organotypic tissue culture system as an in vitro intraocular stem cell transplantation model. *Invest Ophthalmol Vis Sci,* 49**,** 3503-12.

JONAS, J. B., WITZENS-HARIG, M., ARSENIEV, L. & HO, A. D. 2008. Intravitreal autologous bone marrow-derived mononuclear cell transplantation: a feasibility report. *Acta Ophthalmol,* 86**,** 225-6.

KAMPIK, D., ALI, R. R. & LARKIN, D. F. 2012. Experimental gene transfer to the corneal endothelium. *Exp Eye Res,* 95**,** 54-9.

KAUPER, K., MCGOVERN, C., SHERMAN, S., HEATHERTON, P., RAPOZA, R., STABILA, P., DEAN, B., LEE, A., BORGES, S., BOUCHARD, B. & TAO, W. 2012. Two-year intraocular delivery of ciliary neurotrophic factor by encapsulated cell technology implants in patients with chronic retinal degenerative diseases. *Invest Ophthalmol Vis Sci;53(12):7484-91.*

KALESNYKAS, G., OGLESBY, E. N., ZACK, D. J., CONE, F. E., STEINHART, M. R., TIAN, J., PEASE, M. E. & QUIGLEY, H. A. 2012. Retinal ganglion cell morphology after optic nerve crush and experimental glaucoma. *Invest Ophthalmol Vis Sci,* 53**,** 3847-57.

Kamermans, M., Fahrenfort, I., Schultz, K., Janssen-Bienhold, U., Sjoerdsma, T., Weiler, R., 2001 Hemichannel-mediated inhibition in the outer retina. *Science,* 292,1178-1180.

Kaneko, A., Tachibana, M. 1987 GABA mediates the negative feedback from amacrine to bipolar cells. *Neuroscience Research Supplement,* 6, S239-S252.

KAUR, S. & SINGHAL, B. 2012. When nano meets stem: the impact of nanotechnology in stem cell biology. *J Biosci Bioeng.,* 113**,** 1-4. doi: 10.1016/j.jbiosc.2011.08.024. Epub 2011 Sep 28.

KEUTERS, M. H., ASWENDT, M., TENNSTAEDT, A., WIEDERMANN, D., PIKHOVYCH, A., ROTTHUES, S., FINK, G. R., SCHROETER, M., HOEHN, M. & RUEGER, M. A. 2015. Transcranial direct current stimulation promotes the mobility of engrafted NSCs in the rat brain. *NMR Biomed,* 28**,** 231-9.

KHAN, M. S., VISHAKANTE, G. D. & BATHOOL, A. 2013. Development and characterization of pilocarpine loaded Eudragit nanosuspensions for ocular drug delivery. *J Biomed Nanotechnol,* 9**,** 124-31.

KICIC, A., SHEN, W. Y., WILSON, A. S., CONSTABLE, I. J., ROBERTSON, T. & RAKOCZY, P. E. 2003. Differentiation of marrow stromal cells into photoreceptors in the rat eye. *J Neurosci,* 23**,** 7742-9.

KO, M. L., HU, D. N., RITCH, R., SHARMA, S. C. & CHEN, C. F. 2001. Patterns of retinal ganglion cell survival after brain-derived neurotrophic factor administration in hypertensive eyes of rats. *Neurosci*

Lett., 305**,** 139-42.
KURIMOTO, Y., SHIBUKI, H., KANEKO, Y., ICHIKAWA, M., KUROKAWA, T., TAKAHASHI, M. & YOSHIMURA, N. 2001. Transplantation of adult rat hippocampus-derived neural stem cells into retina injured by transient ischemia. *Neurosci Lett,* 306**,** 57-60.
LAI, Y., YUE, Y. & DUAN, D. 2010. Evidence for the failure of adeno-associated virus serotype 5 to package a viral genome > or = 8.2 kb. *Mol Ther,* 18**,** 75-9.

LAMBA, D. A., GUST, J. & REH, T. A. 2009. Transplantation of human embryonic stem cell-derived photoreceptors restores some visual function in Crx-deficient mice. *Cell Stem Cell.* United States.
LAMBA, D. A., MCUSIC, A., HIRATA, R. K., WANG, P. R., RUSSELL, D. & REH, T. A. 2010b. Generation, purification and transplantation of photoreceptors derived from human induced pluripotent stem cells. *PLoS One*;5:e8763.
LAVAIL, M. M., YASUMURA, D., MATTHES, M. T., LAU-VILLACORTA, C., UNOKI, K., SUNG, C. H. & STEINBERG, R. H. 1998. Protection of mouse photoreceptors by survival factors in retinal degenerations. *Invest Ophthalmol Vis Sci,* 39**,** 592-602.
LAWRENCE, J. M., KEEGAN, D. J., MUIR, E. M., COFFEY, P. J., ROGERS, J. H., WILBY, M. J., FAWCETT, J. W. & LUND, R. D. 2004. Transplantation of Schwann cell line clones secreting GDNF or BDNF into the retinas of dystrophic Royal College of Surgeons rats. *Invest Ophthalmol Vis Sci,* 45**,** 267-74.
LAWRENCE, J. M., SINGHAL, S., BHATIA, B., KEEGAN, D. J., REH, T. A., LUTHERT, P. J., KHAW, P. T. & LIMB, G. A. 2007. MIO-M1 cells and similar muller glial cell lines derived from adult human retina exhibit neural stem cell characteristics. *Stem Cells,* 25**,** 2033-43.
LEAVER, S. G., CUI, Q., PLANT, G. W., ARULPRAGASAM, A., HISHEH, S., VERHAAGEN, J. & HARVEY, A. R. 2006a. AAV-mediated expression of CNTF promotes long-term survival and regeneration of adult rat retinal ganglion cells. *Gene Ther.,* 13**,** 1328-41.
LEAVER, S. G., HARVEY, A. R. & PLANT, G. W. 2006b. Adult olfactory ensheathing glia promote the long-distance growth of adult retinal ganglion cell neurites in vitro. *Glia,* 53**,** 467-76.
LEE, C. H., KIM, E. Y., JEON, K., TAE, J. C., LEE, K. S., KIM, Y. O., JEONG, M. Y., YUN, C. W., JEONG, D. K., CHO, S. K., KIM, J. H., LEE, H. Y., RIU, K. Z., CHO, S. G. & PARK, S. P. 2008. Simple, efficient, and reproducible gene transfection of mouse embryonic stem cells by magnetofection. *Stem Cells Dev,* 17**,** 133-41.

LI, L., GU, W., DU, J., REID, B., DENG, X., LIU, Z., ZONG, Z., WANG, H., YAO, B., YANG, C., YAN, J., ZENG, L., CHALMERS, L., ZHAO, M. & JIANG, J. 2012. Electric fields guide migration of epidermal stem cells and promote skin wound healing. *Wound Repair Regen,* 20**,** 840-51.
LI, N., LI, X. R. & YUAN, J. Q. 2009. Effects of bone-marrow mesenchymal stem cells transplanted into

vitreous cavity of rat injured by ischemia/reperfusion. *Graefes Arch Clin Exp Ophthalmol,* 247**,** 503-14.

LI, Y., RECA, R. G., ATMACA-SONMEZ, P., RATAJCZAK, M. Z., ILDSTAD, S. T., KAPLAN, H. J. & ENZMANN, V. 2006. Retinal pigment epithelium damage enhances expression of chemoattractants and migration of bone marrow-derived stem cells. *Invest Ophthalmol Vis Sci,* 47**,** 1646-52.

LI, Y., SAUVE, Y., LI, D., LUND, R. D. & RAISMAN, G. 2003. Transplanted olfactory ensheathing cells promote regeneration of cut adult rat optic nerve axons. *J Neurosci,* 23**,** 7783-8.

LI, Y., WEISS, M. & YAO, L. 2014. Directed migration of embryonic stem cell-derived neural cells in an applied electric field. *Stem Cell Rev,* 10**,** 653-62.

LI, Z. W., LIU, S., WEINREB, R. N., LINDSEY, J. D., YU, M., LIU, L., YE, C., CUI, Q., YUNG, W. H., PANG, C. P., LAM, D. S. & LEUNG, C. K. 2011. Tracking dendritic shrinkage of retinal ganglion cells after acute elevation of intraocular pressure. *Invest Ophthalmol Vis Sci,* 52**,** 7205-12.

LIAO, H., IRVINE, A. D., MACEWEN, C. J., WEED, K. H., PORTER, L., CORDEN, L. D., GIBSON, A. B., MOORE, J. E., SMITH, F. J., MCLEAN, W. H. & MOORE, C. B. 2011. Development of allele-specific therapeutic siRNA in Meesmann epithelial corneal dystrophy. *PLoS One;* 6**:** e28582.

LIM, J. & DOBSON, J. 2012. Improved transfection of HUVEC and MEF cells using DNA complexes with magnetic nanoparticles in an oscillating field. *J Genet,* 91**,** 223-7.

LIN, F., BALDESSARI, F., GYENGE, C. C., SATO, T., CHAMBERS, R. D., SANTIAGO, J. G. & BUTCHER, E. C. 2008. Lymphocyte electrotaxis in vitro and in vivo. *J Immunol,* 181**,** 2465-71.

LIU, Q. & SONG, B. 2014. Electric field regulated signaling pathways. *Int J Biochem Cell Biol,* 55**,** 264-8.

LIU, Y., GONG, Z., LIU, L. & SUN, H. 2010. Combined effect of olfactory ensheathing cell (OEC) transpl

nerve injury in rats. *Mol Vis,* 16**,** 2903-10.

LONGAIR, M. H., BAKER, D. A. & ARMSTRONG, J. D. 2011. Simple Neurite Tracer: open source software for reconstruction, visualization and analysis of neuronal processes. *Bioinformatics,* 27**,** 2453-4.

LU, B., MALCUIT, C., WANG, S., GIRMAN, S., FRANCIS, P., LEMIEUX, L., LANZA, R. & LUND, R. 2009. Long-term safety and function of RPE from human embryonic stem cells in preclinical models of macular degeneration. *Stem Cells,* 27**,** 2126-35.

LUND, R. D., WANG, S., KLIMANSKAYA, I., HOLMES, T., RAMOS-KELSEY, R., LU, B., GIRMAN, S., BISCHOFF, N., SAUVE, Y. & LANZA, R. 2006. Human embryonic stem cell-derived cells rescue visual function in dystrophic RCS rats. *Cloning Stem Cells,* 8**,** 189-99.

LIAO, H., IRVINE, A. D., MACEWEN, C. J., WEED, K. H., PORTER, L., CORDEN, L. D., GIBSON, A. B., MOORE, J. E., SMITH, F. J., MCLEAN, W. H. & MOORE, C. B. 2011. Development of allele-specific therapeutic siRNA in Meesmann epithelial corneal dystrophy. *PLoS One,* 6**,** e28582.

LIN, F., BALDESSARI, F., GYENGE, C. C., SATO, T., CHAMBERS, R. D., SANTIAGO, J. G. & BUTCHER, E. C. 2008. Lymphocyte electrotaxis in vitro and in vivo. *J Immunol,* 181**,** 2465-71.

MA, J., KABIEL, M., TUCKER, B. A., GE, J. & YOUNG, M. J. 2011. Combining chondroitinase ABC and growth factors promotes the integration of murine retinal progenitor cells transplanted into Rho(-/-) mice. *Mol Vis,* 17**,** 1759-70.

MACHALINSKA, A., KLOS, P., BAUMERT, B., BASKIEWICZ, M., KAWA, M., RUDNICKI, M., LUBINSKI, W., WISZNIEWSKA, B., KARCZEWICZ, D. & MACHALINSKI, B. 2011. Stem Cells are mobilized from the bone marrow into the peripheral circulation in response to retinal pigment epithelium damage--a pathophysiological attempt to induce endogenous regeneration. *Curr Eye Res,* 36**,** 663-72.

MACLAREN, R. E., GROPPE, M., BARNARD, A. R., COTTRIALL, C. L., TOLMACHOVA, T., SEYMOUR, L., CLARK, K. R., DURING, M. J., CREMERS, F. P., BLACK, G. C., LOTERY, A. J., DOWNES, S. M., WEBSTER, A. R. & SEABRA, M. C. 2014. Retinal gene therapy in patients with choroideremia: initial findings from a phase 1/2 clinical trial. *Lancet,* 383**,** 1129-37.

MACLAREN, R. E., PEARSON, R. A., MACNEIL, A., DOUGLAS, R. H., SALT, T. E., AKIMOTO, M., SWAROOP, A., SOWDEN, J. C. & ALI, R. R. 2006. Retinal repair by transplantation of photoreceptor precursors. *Nature,* 444**,** 203-7.

MAH, C., FRAITES, T. J., JR., ZOLOTUKHIN, I., SONG, S., FLOTTE, T. R., DOBSON, J., BATICH, C. & BYRNE, B. J. 2002. Improved method of recombinant AAV2 delivery for systemic targeted gene therapy. *Mol Ther,* 6**,** 106-12.

MANABE, S., KASHII, S., HONDA, Y., YAMAMOTO, R., KATSUKI, H. & AKAIKE, A. 2002. Quantification of axotomized ganglion cell death by explant culture of the rat retina. *Neurosci Lett,* 334**,** 33-6.

MARTIN, G. R. 1981. Isolation of a pluripotent cell line from early mouse embryos cultured in medium conditioned by teratocarcinoma stem cells. *Proc Natl Acad Sci U S A,* 78**,** 7634-8.

MARTIN, K. R., QUIGLEY, H. A., ZACK, D. J., LEVKOVITCH-VERBIN, H., KIELCZEWSKI, J., VALENTA, D., BAUMRIND, L., PEASE, M. E., KLEIN, R. L. & HAUSWIRTH, W. W. 2003. Gene therapy with brain-derived neurotrophic factor as a protection: retinal ganglion cells in a rat glaucoma model. *Invest Ophthalmol Vis Sci.,* 44**,** 4357-65.

MATSUMOTO, T., RAUSKOLB, S., POLACK, M., KLOSE, J., KOLBECK, R., KORTE, M. & BARDE, Y. A. 2008. Biosynthesis and processing of endogenous BDNF: CNS neurons store and secrete BDNF, not pro-BDNF. *Nat Neurosci,* 11**,** 131-3.

MAYER, E. J., HUGHES, E. H., CARTER, D. A. & DICK, A. D. 2003. Nestin positive cells in adult human retina and in epiretinal membranes. *Br J Ophthalmol,* 87**,** 1154-8.
MCBAIN, S. C., YIU, H. H. & DOBSON, J. 2008. Magnetic nanoparticles for gene and drug delivery. Int J Nanomedicine, 3, 169-80.

MCCAIG, C. D., RAJNICEK, A. M., SONG, B. & ZHAO, M. 2005. Controlling cell behavior electrically: current views and future potential. *Physiol Rev,* 85**,** 943-78.
MCCAIG, C. D., SONG, B. & RAJNICEK, A. M. 2009. Electrical dimensions in cell science. *J Cell Sci,* 122**,** 4267-76.
MEIJERING, E., JACOB, M., SARRIA, J. C., STEINER, P., HIRLING, H. & UNSER, M. 2004. Design and validation of a tool for neurite tracing and analysis in fluorescence microscopy images. *Cytometry A,* 58**,** 167-76.

MELLOUGH, C. B., CUI, Q., SPALDING, K. L., SYMONS, N. A., POLLETT, M. A., SNYDER, E. Y., MACKLIS, J. D. & HARVEY, A. R. 2004. Fate of multipotent neural precursor cells transplanted into mouse retina selectively depleted of retinal ganglion cells. *Exp Neurol,* 186**,** 6-19.
MENG, X., LI, W., YOUNG, F., GAO, R., CHALMERS, L., ZHAO, M. & SONG, B. 2012. Electric field-controlled directed migration of neural progenitor cells in 2D and 3D environments. *J Vis Exp*.

MENG, X., AROCENA, M., PENNINGER, J., GAGE, F. H., ZHAO, M. & SONG, B. 2011. PI3K mediated electrotaxis of embryonic and adult neural progenitor cells in the presence of growth factors. Exp Neurol, 227, 210-7.MOTHE, A. J. & TATOR, C. H. 2005. Proliferation, migration, and differentiation of endogenous ependymal region stem/progenitor cells following minimal spinal cord injury in the adult rat. *Neuroscience,* 131**,** 177-87.

MERKLE, F. T., TRAMONTIN, A. D., GARCIA-VERDUGO, J. M. & ALVAREZ-BUYLLA, A. 2004. Radial glia give rise to adult neural stem cells in the subventricular zone. *Proc Natl Acad Sci U S A,* 101**,** 17528-32.
MEYER, J. S., HOWDEN, S. E., WALLACE, K. A., VERHOEVEN, A. D., WRIGHT, L. S., CAPOWSKI, E. E., PINILLA, I., MARTIN, J. M., TIAN, S., STEWART, R., PATTNAIK, B., THOMSON, J. A. & GAMM, D. M. 2011. Optic vesicle-like structures derived from human pluripotent stem cells facilitate a customized approach to retinal disease treatment. *Stem Cells,* 29**,** 1206-18.
MEYER, J. S., SHEARER, R. L., CAPOWSKI, E. E., WRIGHT, L. S., WALLACE, K. A., MCMILLAN, E. L., ZHANG, S. C. & GAMM, D. M. 2009. Modeling early retinal development with human embryonic and induced pluripotent. *Proc Natl Acad Sci U S A,* 106**,** 16698-703.
MILLER, F. R. 1907. Galvanotropism in the crayfish. *J Physiol,* 35**,** 215-29.

MILLER, R. J., BANISADR, G. & BHATTACHARYYA, B. J. 2008. CXCR4 signaling in the regulation of stem cell migration and development. *J Neuroimmunol,* 198**,** 31-8.

MINAMINO, K., ADACHI, Y., YAMADA, H., HIGUCHI, A., SUZUKI, Y., IWASAKI, M., NAKANO, K., KOIKE, Y., MUKAIDE, H., KIRIYAMA, N., SHIGEMATSU, A., MATSUMURA, M. & IKEHARA, S. 2005. Long-term survival of bone marrow-derived retinal nerve cells in the retina. *Neuroreport,* 16**,** 1255-9.

MOE, M. C., KOLBERG, R. S., SANDBERG, C., VIK-MO, E., OLSTORN, H., VARGHESE, M., LANGMOEN, I. A. & NICOLAISSEN, B. 2009. A comparison of epithelial and neural properties in progenitor cells derived from the adult human ciliary body and brain. *Exp Eye Res,* 88**,** 30-8.

MORENO-FLORES, M. T., LIM, F., MARTIN-BERMEJO, M. J., DIAZ-NIDO, J., AVILA, J. & WANDOSELL, F. 2003. Immortalized olfactory ensheathing glia promote axonal regeneration of rat retinal ganglion neurons. *J Neurochem,* 85**,** 861-71.

MORENO-MONTANES, J., SADABA, B., RUZ, V., GOMEZ-GUIU, A., ZARRANZ, J., GONZALEZ, M. V., PANEDA, C. & JIMENEZ, A. I. 2014. Phase I clinical trial of SYL040012, a small interfering RNA targeting beta-adrenergic receptor 2, for lowering intraocular pressure. *Mol Ther,* 22**,** 226-32.

MORITOH, S., TANAKA, K. F., JOUHOU, H., IKENAKA, K. & KOIZUMI, A. 2010. Organotypic tissue culture of adult rodent retina followed by particle-mediated acute gene transfer in vitro. *PLoS One;*5**:** e12917.

MORQUETTE, J. B. & DI POLO, A. 2008. Dendritic and synaptic protection: is it enough to save the retinal ganglion cell body and axon? *J Neuroophthalmol,* 28**,** 144-54.

MOTHE, A. J. & TATOR, C. H. 2005. Proliferation, migration, and differentiation of endogenous ependymal region stem/progenitor cells following minimal spinal cord injury in the adult rat. *Neuroscience,* 131**,** 177-87.

MOYSIDIS, S. N., ALVAREZ-DELFIN, K., PESCHANSKY, V. J., SALERO, E., WEISMAN, A. D., BARTAKOVA, A., RAFFA, G. A., MERKHOFER, R. M., JR., KADOR, K. E., KUNZEVITZKY, N. J. & GOLDBERG, J. L. 2015. Magnetic field-guided cell delivery with nanoparticle-loaded human corneal endothelial cells. *Nanomedicine,* 11**,** 499-509.

MULLER, A., HAUK, T. G. & FISCHER, D. 2007. Astrocyte-derived CNTF switches mature RGCs to a regenerative state following inflammatory stimulation. *Brain,* 130**,** 3308-20.

MYCIELSKA, M. E. & DJAMGOZ, M. B. 2004. Cellular mechanisms of direct-current electric field effects: galvanotaxis and metastatic disease. *J Cell Sci,* 117**,** 1631-9.

NAGAO, M., CAMPBELL, K., BURNS, K., KUAN, C. Y., TRUMPP, A. & NAKAFUKU, M. 2008. Coordinated control of self-renewal and differentiation of neural stem cells by Myc and the p19ARF-p53 pathway. *J Cell Biol,* 183**,** 1243-57.

NAKAGAWA, M., KOYANAGI, M., TANABE, K., TAKAHASHI, K., ICHISAKA, T., AOI, T., OKITA, K., MOCHIDUKI, Y., TAKIZAWA, N. & YAMANAKA, S. 2008. Generation of induced pluripotent stem cells without Myc from mouse and human. *Nat Biotechnol,* 26**,** 101-6.

NAKAZAWA, T., TAMAI, M. & MORI, N. 2002. Brain-derived neurotrophic factor prevents axotomized retinal ganglion cell death through MAPK and PI3K signaling pathways. *Invest Ophthalmol Vis Sci,* 43**,** 3319-26.

NGEN, E. J., WANG, L., KATO, Y., KRISHNAMACHARY, B., ZHU, W., GANDHI, N., SMITH, B., ARMOUR, M., WONG, J., GABRIELSON, K. & ARTEMOV, D. 2015. Imaging transplanted stem cells in real time using an MRI dual-contrast method. *Sci Rep,* 5**,** 13628.

NGUYEN, T. H., MURAKAMI, A., FUJIKI, K. & KANAI, A. 2002. Transferrin-polyethylenimine conjugate, FuGENE6 and TransIT-LT as nonviral vectors for gene transfer to the corneal endothelium. *Jpn J Ophthalmol,* 46**,** 140-6.

NI, Y. Q., GAN, D. K., XU, H. D., XU, G. Z. & DA, C. D. 2009. Neuroprotective effect of transcorneal electrical stimulation on light-induced photoreceptor degeneration. Exp Neurol;219(2):439-52.

NISHIDA, A., TAKAHASHI, M., TANIHARA, H., NAKANO, I., TAKAHASHI, J. B., MIZOGUCHI, A., IDE, C. & HONDA, Y. 2000. Incorporation and differentiation of hippocampus-derived neural stem cells transplanted in injured adult rat retina. *Invest Ophthalmol Vis Sci,* 41**,** 4268-74.

NOWAK, J. Z. 2006. Age-related macular degeneration (AMD): pathogenesis and therapy. *Pharmacol Rep,* 58**,** 353-63.

NUCCITELLI, R. 2003. Endogenous electric fields in embryos during development, regeneration and wound healing. *Radiat Prot Dosimetry,* 106**,** 375-83.

OHLEMACHER, S. K., SRIDHAR, A., XIAO, Y., HOCHSTETLER, A. E., SARFARAZI, M., CUMMINS, T. R. & MEYER, J. S. 2016. Stepwise Differentiation of Retinal Ganglion Cells from Human Pluripotent Stem Cells Enables Analysis of Glaucomatous Neurodegeneration. *Stem Cells,* 34**,** 1553-62.

OHMIYA, M., SHUDAI, T., NITTA, A., NOMOTO, H., FURUKAWA, Y. & FURUKAWA, S. 2002. Brain-derived neurotrophic factor alters cell migration of particular progenitors in the developing mouse cerebral cortex. *Neurosci Lett,* 317**,** 21-4.

OKANO, H., OGAWA, Y., NAKAMURA, M., KANEKO, S., IWANAMI, A. & TOYAMA, Y. 2003. Transplantation of neural stem cells into the spinal cord after injury. *Semin Cell Dev Biol; 14(3):191-8.*

ONG, J. M. & DA CRUZ, L. 2012. A review and update on the current status of stem cell therapy and the retina. *Br Med Bull,* 102**,** 133-46.

OREFICE, L. L., WATERHOUSE, E. G., PARTRIDGE, J. G., LALCHANDANI, R. R., VICINI, S. & XU, B. 2013. Distinct roles for somatically and dendritically synthesized brain-derived neurotrophic factor in morphogenesis of dendritic spines. *J Neurosci,* 33**,** 11618-32.

OSAKADA, F., IKEDA, H., SASAI, Y. & TAKAHASHI, M. 2009. Stepwise differentiation of pluripotent stem cells into retinal cells. *Nat Protoc,* 4**,** 811-24.

OTANI, A., DORRELL, M. I., KINDER, K., MORENO, S. K., NUSINOWITZ, S., BANIN, E., HECKENLIVELY, J. & FRIEDLANDER, M. 2004. Rescue of retinal degeneration by intravitreally injected adult bone marrow-derived lineage-negative hematopoietic stem cells. *J Clin Invest,* 114**,** 765-74.

OUREDNIK, J., OUREDNIK, V., LYNCH, W. P., SCHACHNER, M. & SNYDER, E. Y. 2002. Neural stem cells display an inherent mechanism for rescuing dysfunctional neurons. *Nat Biotechnol,* 20**,** 1103-10.

OZEKI, N., SHINODA, K., OHDE, H., ISHIDA, S. & TSUBOTA, K. 2013. Improvement of visual acuity after transcorneal electrical stimulation in case of Best vitelliform macular dystrophy. Graefes Arch Clin Exp Ophthalmol, 251, 1867-70.

PAGAR, K. P. & VAVIA, P. R. 2013. Poly[LA-(Glc-Leu)] copolymer as a carrier for ocular delivery of ciprofloxacin: formulation, characterization and in vivo biocompatibility study. *Ther Deliv,* 4**,** 553-65.

PAKULSKA, M. M., BALLIOS, B. G. & SHOICHET, M. S. 2012. Injectable hydrogels for central nervous system therapy. *Biomed Mater;*7(2):024101.

PAPADOULAS, N.G., DEDOUSSIS G.V., SPANAKOS G., GRITZAPIS. A.D., BAXEVANIS C.N., PAPAMICHAIL M., 1994. An improved fluoresence assay for the determination of lymphocyte-mediated cytotoxicity using flow cytometry. *J Immunol Methods*, 28, 177(1-2), 101-11.

PARAMESWARAN, S., BALASUBRAMANIAN, S., BABAI, N., QIU, F., EUDY, J. D., THORESON, W. B. & AHMAD, I. 2010. Induced pluripotent stem cells generate both retinal ganglion cells and photoreceptors: therapeutic implications in degenerative changes in glaucoma and age-related macular degeneration. *Stem Cells,* 28**,** 695-703.

PARK, H. Y., KIM, J. H., SUN KIM, H. & PARK, C. K. 2012. Stem cell-based delivery of brain-derived neurotrophic factor gene in the rat retina. *Brain Res,* 1469**,** 10-23.

PATEL, N. & POO, M. M. 1982. Orientation of neurite growth by extracellular electric fields. *J*

Neurosci, 2**,** 483-96.

PEARSON, R. A., BARBER, A. C., RIZZI, M., HIPPERT, C., XUE, T., WEST, E. L., DURAN, Y., SMITH, A. J., CHUANG, J. Z., AZAM, S. A., LUHMANN, U. F., BENUCCI, A., SUNG, C. H., BAINBRIDGE, J. W., CARANDINI, M., YAU, K. W., SOWDEN, J. C. & ALI, R. R. 2012. Restoration of vision after transplantation of photoreceptors. *Nature,* 485**,** 99-103.

Phasel/IIa study of SAR422459 in patients with Stargardt's macular degeneration [Online]. https://clinicaltrials.gov/ct2/show/NCT01367444. [Accessed 19.11.15 2015].

PEASE, M. E., ZACK, D. J., BERLINICKE, C., BLOOM, K., CONE, F., WANG, Y., KLEIN, R. L., HAUSWIRTH, W. W. & QUIGLEY, H. A. 2009. Effect of CNTF on retinal ganglion cell survival in experimental glaucoma. *Invest Ophthalmol Vis Sci,* 50**,** 2194-200.

PEPPERELL, E. E. & WATT, S. M. 2013. A novel application for a 3-dimensional timelapse assay that distinguishes chemotactic from chemokinetic responses of hematopoietic CD133(+) stem/progenitor cells. *Stem Cell Res,* 11**,** 707-20.

PEREZ, M. T. & CAMINOS, E. 1995. Expression of brain-derived neurotrophic factor and of its functional receptor in neonatal and adult rat retina. *Neurosci Lett,* 183**,** 96-9.

PICKARD, M. R., ADAMS, C. F., BARRAUD, P. & CHARI, D. M. 2015. Using magnetic nanoparticles for gene transfer to neural stem cells: stem cell propagation method influences outcomes. *J Funct Biomater,* 6**,** 259-76.

PICKARD, M. & CHARI, D. 2010. Enhancement of magnetic nanoparticle-mediated gene transfer to astrocytes by 'magnetofection': effects of static and oscillating fields. *Nanomedicine (Lond),* 5**,** 217-32.

PICKARD, M. R., BARRAUD, P. & CHARI, D. M. 2011. The transfection of multipotent neural precursor/stem cell transplant populations with magnetic nanoparticles. *Biomaterials,* 32**,** 2274-84.

PLANK, C., SCHILLINGER, U., SCHERER, F., BERGEMANN, C., REMY, J. S., KROTZ, F., ANTON, M., LAUSIER, J. & ROSENECKER, J. 2003. The magnetofection method: using magnetic force to enhance gene delivery. *Biol Chem,* 384**,** 737-47.

PLANK, C., ZELPHATI, O. & MYKHAYLYK, O. 2011. Magnetically enhanced nucleic acid delivery. Ten years of magnetofection-progress and prospects. *Adv Drug Deliv Rev,* 63**,** 1300-31.

PROW, T. W., BHUTTO, I., KIM, S. Y., GREBE, R., MERGES, C., MCLEOD, D. S., UNO, K., MENNON, M., RODRIGUEZ, L., LEONG, K. & LUTTY, G. A. 2008. Ocular nanoparticle toxicity and transfection of the retina and retinal pigment epithelium. *Nanomedicine,* 4**,** 340-9.

PULLAR, C. E., ISSEROFF, R. R. & NUCCITELLI, R. 2001. Cyclic AMP-dependent protein kinase A plays a role in the directed migration of human keratinocytes in a DC electric field. *Cell Motil Cytoskeleton,* 50**,** 207-17.

QU, J., MATSOUAKA, R., BETENSKY, R. A., HYMAN, B. T. & GROSSKREUTZ, C. L. 2012. Calcineurin activation causes retinal ganglion cell degeneration. *Mol Vis,* 18**,** 2828-38.

QUIGLEY, H. A. & BROMAN, A. T. 2006. The number of people with glaucoma worldwide in 2010 and 2020. *Br J Ophthalmol,* 90**,** 262-7.

RADTKE, N. D., ARAMANT, R. B., PETRY, H. M., GREEN, P. T., PIDWELL, D. J. & SEILER, M. J. 2008. Vision improvement in retinal degeneration patients by implantation of retina together with retinal pigment epithelium. *Am J Ophthalmol.*;146(2):172-182.

RADTKE, N. D., SEILER, M. J., ARAMANT, R. B., PETRY, H. M. & PIDWELL, D. J. 2002. Transplantation of intact sheets of fetal neural retina with its retinal pigment. *Am J Ophthalmol,* 133**,** 544-50.

RAJNICEK, A. M., GOW, N. A. & MCCAIG, C. D. 1992. Electric field-induced orientation of rat hippocampal neurones in vitro. *Exp Physiol,* 77**,** 229-32.

RAJU, H. B., HU, Y., PADGETT, K. R., RODRIGUEZ, J. E. & GOLDBERG, J. L. 2012. Investigation of nanoparticles using magnetic resonance imaging after intravitreal injection. *Clin Experiment Ophthalmol,* 40**,** 100-7.

RAJU, H. B., HU, Y., VEDULA, A., DUBOVY, S. R. & GOLDBERG, J. L. 2011. Evaluation of magnetic micro- and nanoparticle toxicity to ocular tissues. *PLoS One,* 6**,** e17452.

REH, T. A. & LEVINE, E. M. 1998. Multipotential stem cells and progenitors in the vertebrate retina. *J Neurobiol,* 36**,** 206-20.

RIECK, S., ZIMMERMANN, K. & WENZEL, D. 2013. Transduction of Murine Embryonic Stem Cells by Magnetic Nanoparticle-Assisted Lentiviral Gene Transfer. *Methods Mol Biol*.;1058:89-96.

RNIB. 2002. The cost of sight loss in the UK: Campaign report 23.

RODGER, J., DRUMMOND, E. S., HELLSTROM, M., ROBERTSON, D. & HARVEY, A. R. 2012. Long-term gene therapy causes transgene-specific changes in the morphology of regenerating retinal ganglion cells. *PLoS One;*7:e31061.

ROISEN, F. J., KLUEBER, K. M., LU, C. L., HATCHER, L. M., DOZIER, A., SHIELDS, C. B. & MAGUIRE, S. 2001. Adult human olfactory stem cells. *Brain Res,* 890**,** 11-22.

ROSENFELD, P. J., BROWN, D. M., HEIER, J. S., BOYER, D. S., KAISER, P. K., CHUNG, C. Y. & KIM, R. Y. 2006. Ranibizumab for neovascular age-related macular degeneration. *N Engl J Med.*;355(4):1419-31.

RUAN, J., SHEN, J., WANG, Z., JI, J., SONG, H., WANG, K., LIU, B., LI, J. & CUI, D. 2011. Efficient preparation and labeling of human induced pluripotent stem cells by nanotechnology. *Int J*

Nanomedicine, 6**,** 425-35.

SAPET, C., LAURENT, N., DE CHEVIGNY, A., LE GOURRIEREC, L., BERTOSIO, E., ZELPHATI, O. & BECLIN, C. 2011. High transfection efficiency of neural stem cells with magnetofection. *Biotechniques,* 50**,** 187-9.

SAPET, C., PELLEGRINO, C., LAURENT, N., SICARD, F. & ZELPHATI, O. 2012. Magnetic nanoparticles enhance adenovirus transduction in vitro and in vivo. *Pharm Res,* 29**,** 1203-18.

SAPIEHA, P. S., PELTIER, M., RENDAHL, K. G., MANNING, W. C. & DI POLO, A. 2003. Fibroblast growth factor-2 gene delivery stimulates axon growth by adult retinal ganglion cells after acute optic nerve injury. *Mol Cell Neurosci,* 24**,** 656-72.

*SATO, T., FUJIKADO, T., MORIMOTO, T., MATSUSHITA, K., HARADA, T. & TANO, Y. 2008. Effect of electrical stimulation on IGF-1 transcription by L-type calcium channels in cultured retinal Muller cells. Jpn J Ophthalmol, 52**,** 217-23.*

Safety and tolerability of MA09-hRPE cells in patients with Stargardt's Macular Dystrophy (SMD) [Online]. Available: http://clinicaltrials.gov/ct2/show/NCT0162559. [Accessed 12 April 2013.

Safety and tolerability of sub-retinal transplantation of h-ESC derived RPE(MA09-nRPE) cells in patients with advanced Dry Age Related Macular Degeneration (Dry AMD). [Online]. Available: http://clinicaltrials.gov/ct2/show/NCT01344993.

Safety and tolerability of sub-retinal transplantation of human embryonic stem cell derived retinal pigmented epithelial (hESC-RPE) cells in patients with Stargardt's Macular Dystrophy (SMD). [Online]. Available: http://clinicaltrials.gov/ct2/show/NCT01469832 [Accessed 12 April 2013].

SCHERER, F., ANTON, M., SCHILLINGER, U., HENKE, J., BERGEMANN, C., KRUGER, A., GANSBACHER, B. & PLANK, C. 2002. Magnetofection: enhancing and targeting gene delivery by magnetic force in vitro and in vivo. *Gene Ther,* 9**,** 102-9.

SCHLICHTENBREDE, F. C., MACNEIL, A., BAINBRIDGE, J. W., TSCHERNUTTER, M., THRASHER, A. J., SMITH, A. J. & ALI, R. R. 2003. Intraocular gene delivery of ciliary neurotrophic factor results in significant loss of retinal function in normal mice and in the Prph2Rd2/Rd2 model of retinal degeneration. *Gene Ther,* 10**,** 523-7.

SCHLICHTENBREDE, F. C., MITTMANN, W., RENSCH, F., VOM HAGEN, F., JONAS, J. B. & EULER, T. 2009. Toxicity assessment of intravitreal triamcinolone and bevacizumab in a retinal explant mouse model using two-photon microscopy. *Invest Ophthalmol Vis Sci,* 50**,** 5880-7.

SCHMITZ, S. K., HJORTH, J. J., JOEMAI, R. M., WIJNTJES, R., EIJGENRAAM, S., DE BRUIJN, P., GEORGIOU, C., DE JONG, A. P., VAN OOYEN, A., VERHAGE, M., CORNELISSE, L. N., TOONEN, R. F. & VELDKAMP, W. J. 2011. Automated analysis of neuronal morphology, synapse number and synaptic

recruitment. *J Neurosci Methods,* 195**,** 185-93.

SCHWARTZ, S. D., HUBSCHMAN, J. P., HEILWELL, G., FRANCO-CARDENAS, V., PAN, C. K., OSTRICK, R. M., MICKUNAS, E., GAY, R., KLIMANSKAYA, I. & LANZA, R. 2012. Embryonic stem cell trials for macular degeneration: a preliminary report. *Lancet.*;379(9817):713-20.

SEMMLING, V., LUKACS-KORNEK, V., THAISS, C. A., QUAST, T., HOCHHEISER, K., PANZER, U., ROSSJOHN, J., PERLMUTTER, P., CAO, J., GODFREY, D. I., SAVAGE, P. B., KNOLLE, P. A., KOLANUS, W., FORSTER, I. & KURTS, C. 2010. Alternative cross-priming through CCL17-CCR4-mediated attraction of CTLs toward NKT cell-licensed DCs. *Nat Immunol,* 11**,** 313-20.

SHAPIRO, S., BORGENS, R., PASCUZZI, R., ROOS, K., GROFF, M., PURVINES, S., RODGERS, R. B., HAGY, S. & NELSON, P. 2005. Oscillating field stimulation for complete spinal cord injury in humans: a phase 1 trial. *J Neurosurg Spine,* 2**,** 3-10.

SHARMA, A., GHOSH, A., HANSEN, E. T., NEWMAN, J. M. & MOHAN, R. R. 2010a. Transduction efficiency of AAV 2/6, 2/8 and 2/9 vectors for delivering genes in human corneal fibroblasts. *Brain Res Bull,* 81**,** 273-8.

SHARMA, A., TOVEY, J. C., GHOSH, A. & MOHAN, R. R. 2010b. AAV serotype influences gene transfer in corneal stroma in vivo. *Exp Eye Res,* 91**,** 440-8.

SHIH, Y. Y., MUIR, E. R., LI, G., DE LA GARZA, B. H. & DUONG, T. Q. 2012. High-resolution 3D MR microangiography of the rat ocular circulation. *Radiology,* 264**,** 234-41.

SHOLL, D. A. 1953. Dendritic organization in the neurons of the visual and motor cortices of the cat. *J Anat,* 87**,** 387-406.

SCHLICHTENBREDE, F. C., MITTMANN, W., RENSCH, F., VOM HAGEN, F., JONAS, J. B. & EULER, T. 2009. Toxicity assessment of intravitreal triamcinolone and bevacizumab in a retinal explant mouse model using two-photon microscopy. *Invest Ophthalmol Vis Sci,* 50**,** 5880-7.

SINGHAL, S., LAWRENCE, J. M., BHATIA, B., ELLIS, J. S., KWAN, A. S., MACNEIL, A., LUTHERT, P. J., FAWCETT, J. W., PEREZ, M. T., KHAW, P. T. & LIMB, G. A. 2008. Chondroitin sulfate proteoglycans and microglia prevent migration and integration of grafted Muller stem cells into degenerating retina. *Stem Cells,* 26**,** 1074-82.

SINGHAL, S., LAWRENCE, J. M., SALT, T. E., KHAW, P. T. & LIMB, G. A. 2010. Triamcinolone attenuates macrophage/microglia accumulation associated with NMDA-induced RGC death and facilitates survival of Muller stem cell grafts. *Exp Eye Res,* 90**,** 308-15.

SIQUEIRA, R. C., MESSIAS, A., VOLTARELLI, J. C., SCOTT, I. U. & JORGE, R. 2011. Intravitreal injection of autologous bone marrow-derived mononuclear cells for hereditary retinal dystrophy: a phase I

trial. *Retina,* 31**,** 1207-14.

SIQUEIRA, R. C., VOLTARELLI, J. C., MESSIAS, A. M. & JORGE, R. 2010. Possible mechanisms of retinal function recovery with the use of cell therapy with bone marrow-derived stem cells. *Arq Bras Oftalmol,* 73**,** 474-9.

SLUCH, V. M., DAVIS, C. H., RANGANATHAN, V., KERR, J. M., KRICK, K., MARTIN, R., BERLINICKE, C. A., MARSH-ARMSTRONG, N., DIAMOND, J. S., MAO, H. Q. & ZACK, D. J. 2015. Differentiation of human ESCs to retinal ganglion cells using a CRISPR engineered reporter cell line. *Sci Rep;*5**:**16595.

SMITH, I. O., LIU, X. H., SMITH, L. A. & MA, P. X. 2009. Nanostructured polymer scaffolds for tissue engineering and regenerative medicine. *Wiley Interdiscip Rev Nanomed Nanobiotechnol,* 1**,** 226-36.

SNELL, RS, LEMP MA. 1998. Clinical anatomy of the eye. *Blackwell Publishing,* 177-181.

SONG, B., GU, Y., PU, J., REID, B., ZHAO, Z. & ZHAO, M. 2007. Application of direct current electric fields to cells and tissues in vitro and modulation of wound electric field in vivo. *Nat Protoc,* 2**,** 1479-89.

SONG, B., ZHAO, M., FORRESTER, J. & MCCAIG, C. 2004. Nerve regeneration and wound healing are stimulated and directed by an endogenous electrical field in vivo. *J Cell Sci,* 117**,** 4681-90.

SONIGRA, R. J., BRIGHTON, P. C., JACOBY, J., HALL, S. & WIGLEY, C. B. 1999. Adult rat olfactory nerve ensheathing cells are effective promoters of adult central nervous system neurite outgrowth in coculture. *Glia,* 25**,** 256-69.

SONODA, S., TACHIBANA, K., UCHINO, E., OKUBO, A., YAMAMOTO, M., SAKODA, K., HISATOMI, T., SONODA, K. H., NEGISHI, Y., IZUMI, Y., TAKAO, S. & SAKAMOTO, T. 2006. Gene transfer to corneal epithelium and keratocytes mediated by ultrasound with microbubbles. *Invest Ophthalmol Vis Sci,* 47**,** 558-64.

STADTFELD, M., NAGAYA, M., UTIKAL, J., WEIR, G. & HOCHEDLINGER, K. 2008. Induced pluripotent stem cells generated without viral integration. *Science,* 322**,** 945-9.

STOCCHINO, A., REPETTO, R. & CAFFERATA, C. 2007. Eye rotation induced dynamics of a Newtonian fluid within the vitreous cavity: the effect of the chamber shape. *Phys Med Biol,* 52**,** 2021-34.

STRATEN, G., SCHMEER, C., KRETZ, A., GERHARDT, E., KUGLER, S., SCHULZ, J. B., GRAVEL, C., BAHR, M. & ISENMANN, S. 2002. Potential synergistic protection of retinal ganglion cells from axotomy-induced apoptosis by adenoviral administration of glial cell line-derived neurotrophic factor and X-chromosome-linked inhibitor of apoptosis. *Neurobiol Dis,* 11**,** 123-33.

SUBRAMANIAN, M., LIM, J. & DOBSON, J. 2013. Enhanced nanomagnetic gene transfection of human prenatal cardiac progenitor cells and adult cardiomyocytes. *PLoS One,* 8**,** e69812.

Sub-retinal transplantation of hESC derived RPE (MA09-hRPE) cells in Stargardt's Macular Dystrophy [Online]. Available: http://clinicaltrials.gov/ct2/show/NCT01345006 [Accessed 12 April 2013.

SULIK, G. L., SOONG, H. K., CHANG, P. C., PARKINSON, W. C., ELNER, S. G. & ELNER, V. M. 1992. Effects of steady electric fields on human retinal pigment epithelial cell orientation and migration in culture. *Acta Ophthalmol (Copenh),* 70**,** 115-22.

*SUN, Y. S., PENG, S. W., LIN, K. H. & CHENG, J. Y. 2*012. Electrotaxis of lung cancer cells in ordered three-dimensional scaffolds*. Biomicrofluidics, 6**,** 14102-1410214.*

SUN, W., LI, N. & HE, S. 2002. Large-scale morphological survey of mouse retinal ganglion cells. *J Comp Neurol,* 451**,** 115-26.

TAKAHASHI, K., TANABE, K., OHNUKI, M., NARITA, M., ICHISAKA, T., TOMODA, K. & YAMANAKA, S. 2007. Induction of pluripotent stem cells from adult human fibroblasts by defined. *Cell,* 131**,** 861-72.

TAKAHASHI, M., PALMER, T. D., TAKAHASHI, J. & GAGE, F. H. 1998. Widespread integration and survival of adult-derived neural progenitor cells in the developing optic retina. *Mol Cell Neurosci.* ;12(6):340-8.

TAN, A. R., ALEGRE-AGUARON, E., O'CONNELL, G. D., VANDENBERG, C. D., AARON, R. K., VUNJAK-NOVAKOVIC, G., CHLOE BULINSKI, J., ATESHIAN, G. A. & HUNG, C. T. 2015. Passage-dependent relationship between mesenchymal stem cell mobilization and chondrogenic potential. *Osteoarthritis Cartilage,* 23**,** 319-27.

TANDON, N., GOH, B., MARSANO, A., CHAO, P. H., MONTOURI-SORRENTINO, C., GIMBLE, J. & VUNJAK-NOVAKOVIC, G. 2009. Alignment and elongation of human adipose-derived stem cells in response to direct-current electrical stimulation. *Conf Proc IEEE Eng Med Biol Soc,* 2009**,** 6517-21.

TAO, W., WEN, R., GODDARD, M. B., SHERMAN, S. D., O'ROURKE, P. J., STABILA, P. F., BELL, W. J., DEAN, B. J., KAUPER, K. A., BUDZ, V. A., TSIARAS, W. G., ACLAND, G. M., PEARCE-KELLING, S., LATIES, A. M. & AGUIRRE, G. D. 2002. Encapsulated cell-based delivery of CNTF reduces photoreceptor degeneration in animal models of retinitis pigmentosa. Invest Ophthalmol Vis Sci, 43**,** 3292-8.

TAO, Y., CHEN, T., LIU, B., WANG, L. Q., PENG, G. H., QIN, L. M., YAN, Z. J. & HUANG, Y. F. 2016. The transcorneal electrical stimulation as a novel therapeutic strategy against retinal and optic neuropathy: a review of experimental and clinical trials. *Int J Ophthalmol, 9**,** 914-9.*

TENG, Y. D., YU, D., ROPPER, A. E., LI, J., KABATAS, S., WAKEMAN, D. R., WANG, J., SULLIVAN, M. P., REDMOND, D. E., JR., LANGER, R., SNYDER, E. Y. & SIDMAN, R. L. 2011. Functional multipotency of stem cells: a conceptual review of neurotrophic factor-based evidence and its role in translational research. *Curr Neuropharmacol,* 9**,** 574-85.

TESTA, F., MAGUIRE, A. M., ROSSI, S., PIERCE, E. A., MELILLO, P., MARSHALL, K., BANFI, S., SURACE, E. M., SUN, J., ACERRA, C., WRIGHT, J. F., WELLMAN, J., HIGH, K. A., AURICCHIO, A., BENNETT, J. & SIMON Virus in Patients with Leber Congenital Amaurosis Type 2. *Ophthalmology*;120(6):1283-91.

THANOS, S. 1991. Specific transcellular carbocyanine-labelling of rat retinal microglia during injury-induced neuronal degeneration. *Neurosci Lett,* 127**,** 108-12.

THOMSON, J. A., ITSKOVITZ-ELDOR, J., SHAPIRO, S. S., WAKNITZ, M. A., SWIERGIEL, J. J., MARSHALL, V. S. & JONES, J. M. 1998. Embryonic stem cell lines derived from human blastocysts. *Science,* 282**,** 1145-7.

THOREK, D. L., CHEN, A. K., CZUPRYNA, J. & TSOURKAS, A. 2006. Superparamagnetic iron oxide nanoparticle probes for molecular imaging. *Ann Biomed Eng,* 34**,** 23-38.

THRIVIKRAMAN, G., MADRAS, G. & BASU, B. 2014. Intermittent electrical stimuli for guidance of human mesenchymal stem cell lineage commitment towards neural-like cells on electroconductive substrates. *Biomaterials,* 35**,** 6219-35.

THANOS, S. 1991. Specific transcellular carbocyanine-labelling of rat retinal microglia during injury-induced neuronal degeneration. *Neurosci Lett,* 127**,** 108-12.

THOREK, D. L., CHEN, A. K., CZUPRYNA, J. & TSOURKAS, A. 2006. Superparamagnetic iron oxide nanoparticle probes for molecular imaging. *Ann Biomed Eng,* 34**,** 23-38.

TIBBETTS, M. D., SAMUEL, M. A., CHANG, T. S. & HO, A. C. 2012. Stem cell therapy for retinal disease. *Curr Opin Ophthalmol,* 23**,** 226-34.

TOMITA, M., ADACHI, Y., YAMADA, H., TAKAHASHI, K., KIUCHI, K., OYAIZU, H., IKEBUKURO, K., KANEDA, H., MATSUMURA, M. & IKEHARA, S. 2002. Bone marrow-derived stem cells can differentiate into retinal cells in injured rat retina. *Stem Cells,* 20**,** 279-83.

TOMITA, M., LAVIK, E., KLASSEN, H., ZAHIR, T., LANGER, R. & YOUNG, M. J. 2005. Biodegradable polymer composite grafts promote the survival and differentiation of retinal progenitor cells. *Stem Cells,* 23**,** 1579-88.

TUSZYNSKI, M. H. 2007. Nerve growth factor gene delivery: animal models to clinical trials. *Dev Neurobiol,* 67**,** 1204-15.

VAN ADEL, B. A., ARNOLD, J. M., PHIPPS, J., DOERING, L. C. & BALL, A. K. 2005. Ciliary neurotrophic factor protects retinal ganglion cells from axotomy-induced apoptosis via modulation of retinal glia in vivo. *J Neurobiol,* 63**,** 215-34.

VAN ADEL, B. A., KOSTIC, C., DEGLON, N., BALL, A. K. & ARSENIJEVIC, Y. 2003. Delivery of ciliary neurotrophic factor via lentiviral-mediated transfer protects axotomized retinal ganglion cells for an extended period of time. *Hum Gene Ther,* 14**,** 103-15.

VENTURA, C., CAVALLINI, C., BIANCHI, F. & CANTONI, S. 2008. Stem cells and cardiovascular repair: a role for natural and synthetic molecules harboring differentiating and paracrine logics. *Cardiovasc Hematol Agents Med Chem,* 6**,** 60-8.

VENUGOPALAN, P., WANG, Y., NGUYEN, T., HUANG, A., MULLER, K. J. & GOLDBERG, J. L. 2016. Transplanted neurons integrate into adult retinas and respond to light. *Nat Commun,* 7**,** 10472.

*WANG, E., ZHAO, M., FORRESTER, J. V. & MCCAIG, C. D. 2003. Bi-directional migration of lens epithelial cells in a physiological electrical field. Exp Eye Res, 76**,** 29-37.*

WANG, H. C., BROWN, J., ALAYON, H. & STUCK, B. E. 2010a. Transplantation of quantum dot-labelled bone marrow-derived stem cells into the vitreous of mice with laser-induced retinal injury: survival, integration and differentiation. *Vision Res,* 50**,** 665-73.

WANG, S., LU, B., GIRMAN, S., DUAN, J., MCFARLAND, T., ZHANG, Q. S., GROMPE, M., ADAMUS, G., APPUKUTTAN, B. & LUND, R. 2010b. Non-invasive stem cell therapy in a rat model for retinal degeneration and vascular pathology. *PLoS One,* 5**,** e9200.

WARFVINGE, K., KAMME, C., ENGLUND, U. & WICTORIN, K. 2001. Retinal integration of grafts of brain-derived precursor cell lines implanted subretinally into adult, normal rats. *Exp Neurol,* 169**,** 1-12.

WELEBER, R. G., PENNESI, M. E., WILSON, D. J., KAUSHAL, S., ERKER, L. R., JENSEN, L., MCBRIDE, M. T., FLOTTE, T. R., HUMPHRIES, M., CALCEDO, R., HAUSWIRTH, W. W., CHULAY, J. D. & STOUT, J. T. 2016. Results at 2 Years after Gene Therapy for RPE65-Deficient Leber Congenital Amaurosis and Severe Early-Childhood-Onset Retinal Dystrophy. *Ophthalmology,* 123**,** 1606-20.

WEST, E. L., PEARSON, R. A., DURAN, Y., GONZALEZ-CORDERO, A., MACLAREN, R. E., SMITH, A. J., SOWDEN, J. C. & ALI, R. R. 2012. Manipulation of the recipient retinal environment by ectopic expression of neurotrophic growth factors can improve transplanted photoreceptor integration and survival. *Cell Transplant;21(5):871-87.*

WEY, A. & KNOEPFLER, P. S. 2010. c-myc and N-myc promote active stem cell metabolism and cycling as architects of the developing brain. *Oncotarget,* 1**,** 120-30.

WIDERA, D., HOLTKAMP, W., ENTSCHLADEN, F., NIGGEMANN, B., ZANKER, K., KALTSCHMIDT, B. & KALTSCHMIDT, C. 2004. MCP-1 induces migration of adult neural stem cells. *Eur J Cell Biol,* 83**,** 381-7.

WILLIAMS, P. A., MORGAN, J. E. & VOTRUBA, M. 2010. Opa1 deficiency in a mouse model of dominant optic atrophy leads to retinal ganglion cell dendropathy. *Brain,* 133**,** 2942-51.

WIDERA, D., HOLTKAMP, W., ENTSCHLADEN, F., NIGGEMANN, B., ZANKER, K., KALTSCHMIDT, B. & KALTSCHMIDT, C. 2004. MCP-1 induces migration of adult neural stem cells. *Eur J Cell Biol,* 83**,** 381-7.

WINSTEAD, W., MARSHALL, C. T., LU, C. L., KLUEBER, K. M. & ROISEN, F. J. 2005. Endoscopic biopsy

of human olfactory epithelium as a source of progenitor cells. *Am J Rhinol,* 19**,** 83-90.

WOOD, J. P., PLUNKETT, M., PREVIN, V., CHIDLOW, G. & CASSON, R. J. 2011. Nanosecond pulse lasers for retinal applications. *Lasers Surg Med,* 43**,** 499-510.

www.addgene.org [Online]. [Accessed 17.04.2014].

WU, M. M., FAN, D. G., TADMORI, I., YANG, H., FURMAN, M., JIAO, X. Y., YOUNG, W., SUN, D. & YOU, S. W. 2010. Death of axotomized retinal ganglion cells delayed after intraoptic nerve transplantation of olfactory ensheathing cells in adult rats. *Cell Transplant,* 19**,** 159-66.

WU, W., LI, J., WU, L., WANG, B., WANG, Z., XU, Q. & XIN, H. 2013. Ophthalmic Delivery of Brinzolamide by Liquid Crystalline Nanoparticles: In Vitro and In Vivo Evaluation. *AAPS PharmSciTech*;14(3):1063-71.

XIAN, B., ZHANG, Y., PENG, Y., HUANG, J., LI, W., WANG, W., ZHANG, M., LI, K., ZHANG, H., ZHAO, M., LIU, X. & HUANG, B. 2016. Adult Human Peripheral Blood Mononuclear Cells Are Capable of Producing Neurocyte or Photoreceptor-Like Cells That Survive in Mouse Eyes After Preinduction With Neonatal Retina. *Stem Cells Transl Med*.jil25.pii:sctm.20175-0395[EPub ahead of print].

XU, H. & HEILSHORN, S. C. 2013. Microfluidic investigation of BDNF-enhanced neural stem cell chemotaxis in CXCL12 gradients. *Small,* 9**,** 585-95.

XU, Y., GAO, C., LI, X., HE, Y., ZHOU, L., PANG, G. & SUN, S. 2013. In vitro antifungal activity of silver nanoparticles against ocular pathogenic filamentous fungi. *J Ocul Pharmacol Ther,* 29**,** 270-4.

YAN, X., HAN, J., ZHANG, Z., WANG, J., CHENG, Q., GAO, K., NI, Y. & WANG, Y. 2009. Lung cancer A549 cells migrate directionally in DC electric fields with polarized and activated EGFRs. *Bioelectromagnetics,* 30**,** 29-35.

YANAI, A., HAFELI, U. O., METCALFE, A. L., SOEMA, P., ADDO, L., GREGORY-EVANS, C. Y., PO, K., SHAN, X., MORITZ, O. L. & GREGORY-EVANS, K. 2012. Focused magnetic stem cell targeting to the retina using superparamagnetic iron oxide nanoparticles. *Cell Transplant,* 21**,** 1137-48.

YAO, L., SHANLEY, L., MCCAIG, C. & ZHAO, M. 2008. Small applied electric fields guide migration of hippocampal neurons. *J Cell Physiol,* 216**,** 527-35.

YOUNG, M. J., RAY, J., WHITELEY, S. J., KLASSEN, H. & GAGE, F. H. 2000. Neuronal differentiation and morphological integration of hippocampal progenitor cells transplanted to the retina of immature and mature dystrophic rats. *Mol Cell Neurosci,* 16**,** 197-205.

YU, J., VODYANIK, M. A., SMUGA-OTTO, K., ANTOSIEWICZ-BOURGET, J., FRANE, J. L., TIAN, S., NIE, J., JONSDOTTIR, G. A., RUOTTI, V., STEWART, R., SLUKVIN, II & THOMSON, J. A. 2007. Induced pluripotent stem cell lines derived from human somatic cells. *Science,* 318**,** 1917-20.

ZANTL, R. & HORN, E. 2011. Chemotaxis of slow migrating mammalian cells analysed by video

microscopy. *Methods Mol Biol,* 769**,** 191-203.

ZHANG, J., CALAFIORE, M., ZENG, Q., ZHANG, X., HUANG, Y., LI, R. A., DENG, W. & ZHAO, M. 2011. Electrically guiding migration of human induced pluripotent stem cells. Stem Cell Rev, 7, 987-96.

ZHANG, K., HOPKINS, J. J., HEIER, J. S., BIRCH, D. G., HALPERIN, L. S., ALBINI, T. A., BROWN, D. M., JAFFE, G. J., TAO, W. & WILLIAMS, G. A. 2011b. Ciliary neurotrophic factor delivered by encapsulated cell intraocular implants for treatment of geographic atrophy in age-related macular degeneration. *Proc Natl Acad Sci U S A,* 108**,** 6241-5.

ZHANG, S. S., FU, X. Y. & BARNSTABLE, C. J. 2002. Tissue culture studies of retinal development. *Methods,* 28**,** 439-47.

ZHANG, Y. & WANG, W. 2010. Effects of bone marrow mesenchymal stem cell transplantation on light-damaged retina. *Invest Ophthalmol Vis Sci,* 51**,** 3742-8.

ZHANG, R. P., WANG, L. J., HE, S., XIE, J. & LI, J. D. 2016. Effects of Magnetically Guided, SPIO-Labeled, and Neurotrophin-3 Gene-Modified Bone Mesenchymal Stem Cells in a Rat Model of Spinal Cord Injury. *Stem Cells Int,* 2016**,** 2018474.

ZHAO, M., AGIUS-FERNANDEZ, A., FORRESTER, J. V. & MCCAIG, C. D. 1996. Orientation and directed migration of cultured corneal epithelial cells in small electric fields are serum dependent. *J Cell Sci, 109 (Pt 6), 1405-14.*

ZHAO, H., STEIGER, A., NOHNER, M. & YE, H. 2015. Specific Intensity Direct Current (DC) Electric Field Improves Neural Stem Cell Migration and Enhances Differentiation towards betaIII-Tubulin+ Neurons. *PLoS One;*10**:**e0129625.

ZHAO, M., CHALMERS, L., CAO, L., VIEIRA, A. C., MANNIS, M. & REID, B. 2012a. Electrical signaling in control of ocular cell behaviors. *Prog Retin Eye Res,* 31**,** 65-88.

ZHAO, M., DICK, A., FORRESTER, J. V. & MCCAIG, C. D. 1999. Electric field-directed cell motility involves up-regulated expression and asymmetric redistribution of the epidermal growth factor receptors and is enhanced by fibronectin and laminin. *Mol Biol Cell,* 10**,** 1259-76.

ZHAO, M., SONG, B., PU, J., WADA, T., REID, B., TAI, G., WANG, F., GUO, A., WALCZYSKO, P., GU, Y., SASAKI, T., SUZUKI, A., FORRESTER, J. V., BOURNE, H. R., DEVREOTES, P. N., MCCAIG, C. D. & PENNINGER, J. M. 2006. Electrical signals control wound healing through phosphatidylinositol-3-OH kinase-gamma and PTEN. *Nature,* 442**,** 457-60.

ZHAO, Z., QIN, L., REID, B., PU, J., HARA, T. & ZHAO, M. 2012b. Directing migration of endothelial progenitor cells with applied DC electric fields. *Stem Cell Res,* 8**,** 38-48.

ZHOU, X. M., SUN, J. B., YUAN, H. P., WU, D. L., ZHOU, X. R., SUN, D. W., LI, H. Y., SHAO, Z. B. &

ZHANG, Z. R. 2009a. A rat model for studying neural stem cell transplantation. *Acta Pharmacol Sin,* 30**,** 1496-504.

ZHOU, X. M., SUN, J. B., YUAN, H. P., WU, D. L., ZHOU, X. R., SUN, D. W., LI, H. Y., SHAO, Z. B. & ZHANG, Z. R. 2009. A rat model for studying neural stem cell transplantation. *Acta Pharmacol Sin,* 30**,** 1496-504.

ZUBERI, M., LIU-SNYDER, P., UL HAQUE, A., PORTERFIELD, D. M. & BORGENS, R. B. 2008. Large naturally-produced electric currents and voltage traverse damaged mammalian spinal cord. *J Biol Eng,* 2**,** 17.